AD-A167 989 SATELLITE APPLICATIONS INFORMATION NOTES OCTOBER 1975 - DECEMBER 1978(U) AIR WEATHER SERVICE SCOTT AFB IL AUG 79 AWS/TN-79/003 1/4

UNCLASSIFIED F/G 4/2 NL

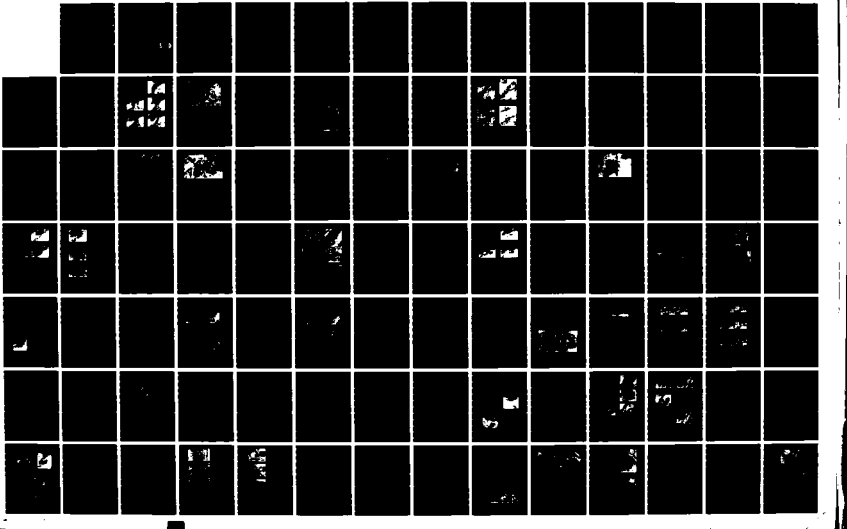

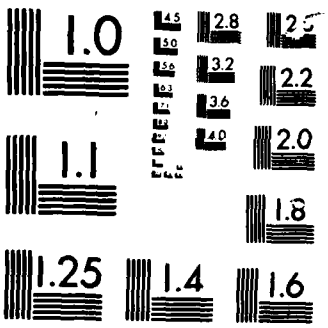

MICROCOPY CHART

(2)

AWS/TN-79/003

SATELLITE APPLICATIONS INFORMATION NOTES OCTOBER 1975 – DECEMBER 1978

PREPARED BY
NATIONAL ENVIRONMENTAL SATELLITE SERVICE
AND
NATIONAL WEATHER SERVICE

INCORPORATES CHANGE 1

AUGUST 1979

AIR WEATHER SERVICE (MAC)
Scott AFB, Illinois 62225

REVIEW AND APPROVAL STATEMENT

This publication approved for public release. There is no objection to unlimited distribution of this document to the public at large, or by the Defense Documentation Center (DDC) to the National Technical Information Service (NTIS).

This technical publication has been reviewed and is approved for publication.

GEORGE TANIGUCHI
Asst Ch, Forecasting Svc Div
Directorate of Aerospace Services
Reviewing Officer

FOR THE COMMANDER

GARY D. ATKINSON, Colonel, USAF
DCS/Aerospace Sciences
Air Weather Service

DEPARTMENT OF THE AIR FORCE

REPLY TO ATTN OF: DNTS (MSgt Bailey, 4741)

SUBJECT: Change 1 to AWS/TN-79-003

1. Remove the following pages:

   a. Satellite Applications Information Note (SAIN) 76/11, pages 5 and 6.

   b. SAIN 76/19, pages 2, 3, 4, and SAIN 76/20, page 1.

   c. SAIN 77/10, page 5, and SAIN 77/11, page 1.

   d. SAIN 77/18 pages 2 and 3.

2. Insert new pages listed in attachments.

JAMES C. MARSHALL, Lt Col, USAF
Ch, Forecasting Services Division
Directorate of Aerospace Services

4 Atch
1. Pages 5 and 6
2. Pages 2, 3, 4, and 1
3. Pages 5 and 1
4. Pages 2 and 3

SECURITY CLASSIFICATION OF THIS PAGE (When Data Entered)

REPORT DOCUMENTATION PAGE		READ INSTRUCTIONS BEFORE COMPLETING FORM
1. REPORT NUMBER	2. GOVT ACCESSION NO.	3. RECIPIENT'S CATALOG NUMBER
4. TITLE (and Subtitle) Collection of National Weather Service/National Environmental Satellite Service Satellite Applications Information Notes		5. TYPE OF REPORT & PERIOD COVERED Final 6. PERFORMING ORG. REPORT NUMBER
7. AUTHOR(s) Dept of Commerce National Weather Service/ National Environmental Satellite Service		8. CONTRACT OR GRANT NUMBER(s)
9. PERFORMING ORGANIZATION NAME AND ADDRESS Air Weather Service/DNT Scott AFB IL 62225		10. PROGRAM ELEMENT, PROJECT, TASK AREA & WORK UNIT NUMBERS
11. CONTROLLING OFFICE NAME AND ADDRESS AWS/DNT Scott AFB IL 62225		12. REPORT DATE August 1979 13. NUMBER OF PAGES
14. MONITORING AGENCY NAME & ADDRESS(if different from Controlling Office)		15. SECURITY CLASS. (of this report) Unclassified 15a. DECLASSIFICATION DOWNGRADING SCHEDULE

16. DISTRIBUTION STATEMENT (of this Report)

Approved for public release; distribution unlimited.

17. DISTRIBUTION STATEMENT (of the abstract entered in Block 20, if different from Report)

18. SUPPLEMENTARY NOTES

Incorporates Change 1, undated.

19. KEY WORDS (Continue on reverse side if necessary and identify by block number)

Meteorological satellites; Wind;
Visible, infrared imagery; Ocean thermal features;
Satellite data; Synoptic features;
Storm systems;
Severe weather;

20. ABSTRACT (Continue on reverse side if necessary and identify by block number)

Publication contains a complete collection of the Satellite Applications Information Notes published by the National Environmental Satellite Service from Oct 1975 to Dec 1978. The Notes discuss identification of local terrain effects, case studies of synoptic situations, and uncommon cloud features, cloud pattern interpretations which deal with the practical applications of satellite data.

DD FORM 1 JAN 73 1473

UNCLASSIFIED

SECURITY CLASSIFICATION OF THIS PAGE (When Data Entered)

FOREWARD

This publication contains a complete collection of the Satellite Applications Information Notes prepared mostly by members of the National Environmental Satellite Service (NESS) from October 1975 through December 1978. Two articles were authored by National Weather Service (NWS) members.

The articles in this report cover a wide range of topics dealing with identification of local terrain effects, case studies of synoptic situations and severe weather, uncommon cloud features, cloud pattern interpretations, etc., which deals with the practical applications of satellite data. Geographical coverage of topics range from Hawaii to the east coast of continental U. S. and the Atlantic. The notes are designed by NESS to primarily provide rapid dissemination of operationally useful satellite data applications techniques to NWS forecasters. It may be used as a companion text to AWSTR 212, "Application of Meteorological Satellite Data in Analysis and Forecasting" and AWSTR 74-250, "DMSP User's Guide."

Headquarters Air Weather Service extends its gratitude to the personnel of the Applications Group, National Environmental Satellite Service for making the original manuscripts available for publication.

Table of Contents

Table of Contents Cont'd

* 2/77 not published.

Table of Contents Cont'd

Table of Contents Cont'd

SATELLITE APPLICATIONS INFORMATION NOTE 10/75-1

ATLANTIC AND EASTERN PACIFIC TROPICAL WEATHER SYSTEMS AS SEEN FROM SATELLITE

B. MAX MAYFIELD

NESS Satellite Field Services Station, Miami, Fla. 33124

Figure 1 is a 4-km resolution visible spectrum picture taken at 1730 GMT 24 August 1975 from the Synchronous Meteorological Satellite No. 1 (SMS-1). Several interesting tropical weather systems are seen in various stages of development.

The most intense weather system on the picture is Hurricane Ilsa at A, but this one still picture hardly does justice to its long history of development. The first view from SMS-1 of what was to become Ilsa appeared on 6 August, as a weak disturbance moved off the coast of Africa. Its cloud pattern crossed the Atlantic at low latitudes and then moved westward across the northern portion of South America. This disturbance appeared as an impressive mass of convection as it emerged into the southwest Caribbean Sea, but again development was hindered when the system went over the land mass of Central America. Next, this disturbance emerged into the eastern Pacific as a bright area of convection and eventually developed into Hurricane Ilsa which had a well defined eye at the time this picture was taken. Intensity estimates of tropical cyclones are routinely made by the National Environmental Satellite Service using the Dvorak (1975) technique.

The tropical depression at B has a similar history. This cloud system first came off the African coast on 9 August and was easily followed across the Atlantic and Caribbean, including one period just east of the Lesser Antilles when the system took on the appearance of Frank's (1968) "inverted V." The system became disorganized after crossing Central America, and only slowly developed into the tropical depression seen in Figure 1. This depression continued to develop in the eastern Pacific and eventually became Hurricane Jewel.

The tropical distrubance at C was a relatively short-lived blowup of convective activity which never showed enough organization to define a cloud system center.

Another tropical depression is located at D. The first clue to the existence of this system appeared as a northward bulge on the ITCZ near the west coast of Africa on 16 August. As it moved westward across the Atlantic it maintained excellent continuity. Although this depression looks unimpressive in Figure 1 as far as convective activity is concerned, a cloud system center can be defined with the assistance of the curved low cloud lines in the western semicircle. This depression later developed into Hurricane Caroline and eventually made landfall on the northern Gulf coast of Mexico.

Yet another African disturbance is seen in the central Atlantic at E. It has the appearance of an "inverted V" with its axis along 51W. This system moved westward across the Atlantic without any significant development.

One last tropical system is suggested by the northward bulge in the ITCZ at F. As this system moved across the Atlantic it became much better defined with an apparent vortex visible in the low clouds on several days. It was accompanied by an increase in convective activity as it moved through the Caribbean.

In summary, Figure 1 reveals several tropical weather systems in a variety of stages of development. Continuous coverage by geostationary satellite has permitted a closer view of the life cycles and journeys of these systems. Of particular interest is the development of eastern Pacific storms from disturbances which appear to have an origin over Africa.

REFERENCES

Dvorak, V. F., 1975: "Tropical cyclone intensity analysis and forecasting from satellite imagery", Mon. Wea. Rev., 103, 420-430.

Frank, N., 1968: "The 'inverted V' cloud pattern - an easterly wave?", Mon. Wea. Rev., 97, 130-140.

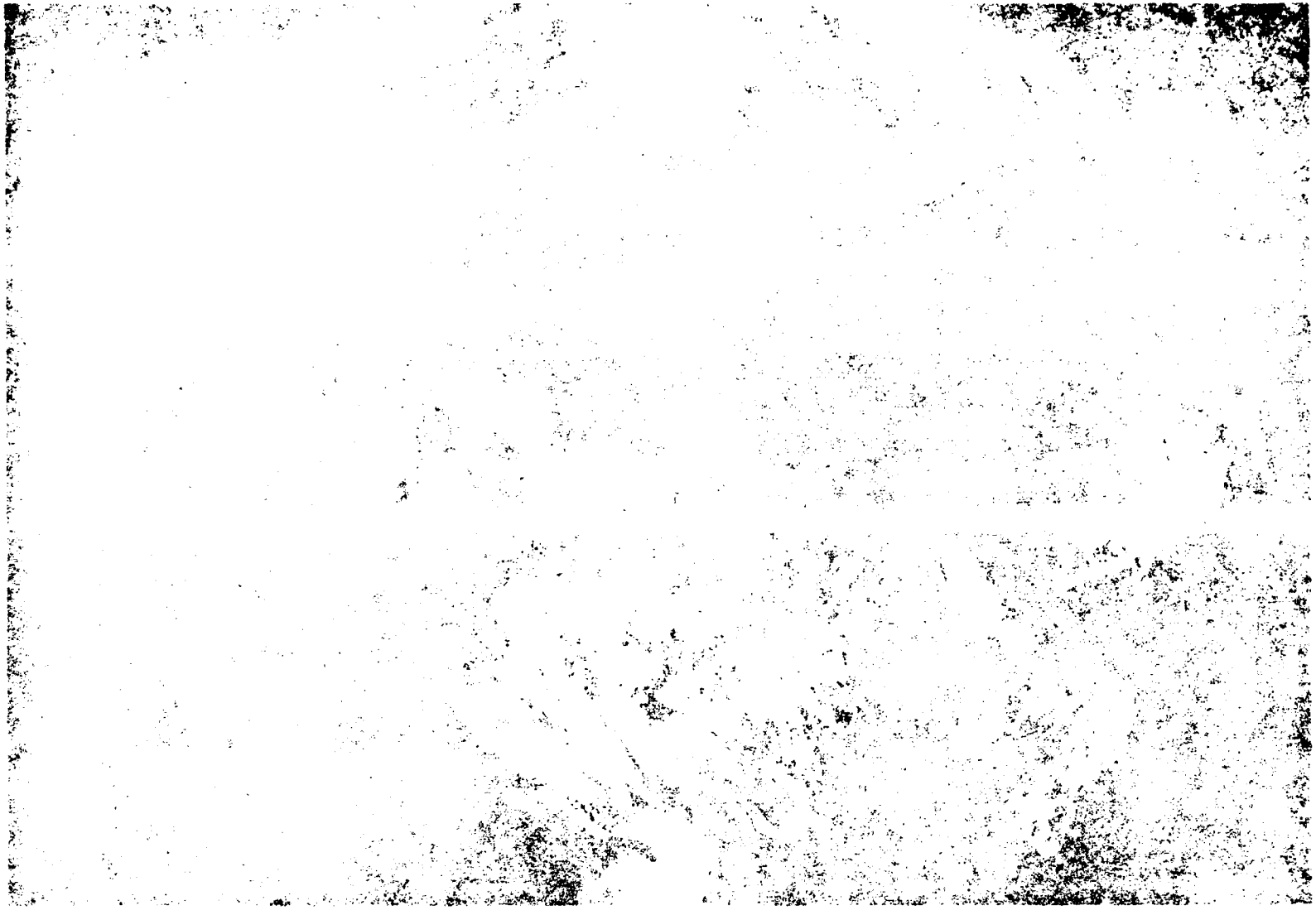

Fig. 1. SMS-1 visible spectrum picture with 4 km resolution taken at 1730 GMT 24 August 1975.

SATELLITE APPLICATIONS INFORMATION NOTE 10/75-2

HEAVY RAINS ALONG THE EAST COAST
September 23-24, 1975

Frances C. Parmenter

Heavy rains deluged the East Coast during the week of September 23rd. Newspaper and TV reports "blamed" hurricane ELOISE for the rains but in essence, a cut-off 300 mb low in the southern Plains and strong ridge just off the Atlantic Coast, plus the remains of ELOISE set up a strong southerly flow from both the Gulf of Mexico and Coastal Atlantic that acted as a covergence mechanism at the surface and horizontal export mechanism at mid-tropospheric levels.

On Tuesday, September 23, 0000GMT, a stationary front was analyzed from Cape Hatteras southward through central Georgia then westward into the Gulf of Mexico along the north side of ELOISE. Rain was occurring from the Gulf to Pennsylvania. At 300 mb a cut-off low was located on the Oklahoma/Arkansas border with strong 50 kt southerly flow over the mid-Atlantic States. Two forecasting problems were apparent: the first concerned the landfall of hurricane ELOISE and second, the heavy precipitation and flashflooding that would occur in the northern states. Initial QPF guidance showed a bullseye of heavy precipitation, greater than 4", prognosticated northeastward along the mountains and located along the Tennessee, North Carolina and Virginia Borders by 1200Z, September 24, (Figure 1).

Figure 2 shows the hurricane and extensive area of middle and high cloudiness over the Eastern U.S. The cut-off low (L) is cloud-free and the axis of the southern wind maximum, at 300 mb, lies along the cirrus edge from Louisiana to New England. Of particular interest are the convective cells (M) that appeared to break off from an upper level cold low that had tracked across the Atlantic. These convective clusters continued to be generated over the Gulf Stream waters and moved northward with the 40-kt 500-mb flow.

Landfall of ELOISE occurred near dawn. During this period the cut-off low drifted southward increasing the southerly flow along the Appalachians. A band of cirrus (N, Figure 3) developed along the zone of maximum windshear in the upper level trough, and middle level clouds, signifying mid-tropospheric vortex development, appeared in northeastern Arkansas. Strong onshore flow and upslope motion reinforced the production of convection in the near mountain areas of the Eastern States. The convective clusters (M) had moved northward to the North Carolina Coast at this time and had reached inland over the Carolinas to Virginia by 1700GMT, Figure 7.

Subsequent views, at 2330GMT 23 September, 0630 and 1130GMT 24 September, Figures 4, 5, and 6 show that the top level remnants of ELOISE (E) became caught up in the strong southerly flow and had dissipated over the New England states by 1130GMT. Heavy precipitation occurred along its path, but the heaviest rains continued, primarily east of the mountains (M), as moist, unstable tropical air continued northward from the Gulf.

Formation of a cloud pattern (L) with the cut-off low continued throughout this period. Moisture from the tropical system never appeared to become involved with this system.

The severe weather that occurred with ELOISE late on September 23, was located along the long "feeder band" (J, Figure 7). It developed when this moisture-laden convective band moved into northern Georgia where skies had been clear and surface heating was maximum (J, Figure 4).

5

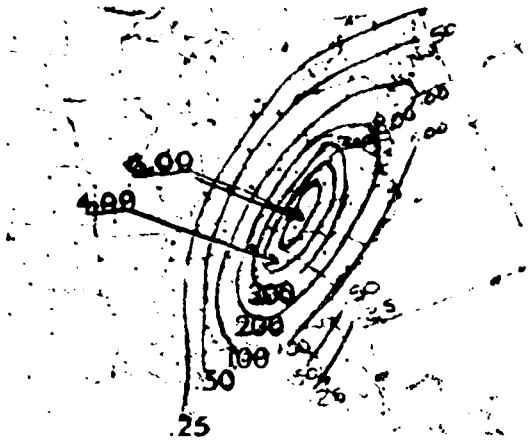

Fig 1 24 Hr QPF for Day 2 ending 12Z 24 Sep 75

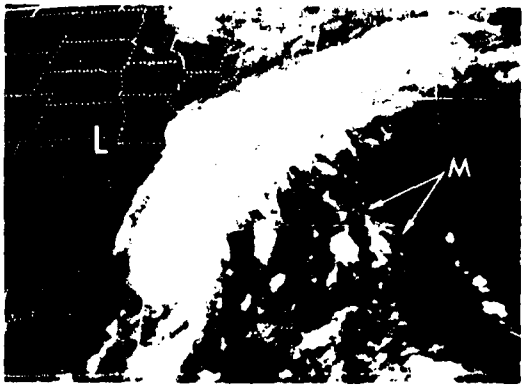

Fig 2 SMS-1 IR 0100Z 23 Sep 75

Fig 3 SMS-1 IR 1030Z 23 Sep 75

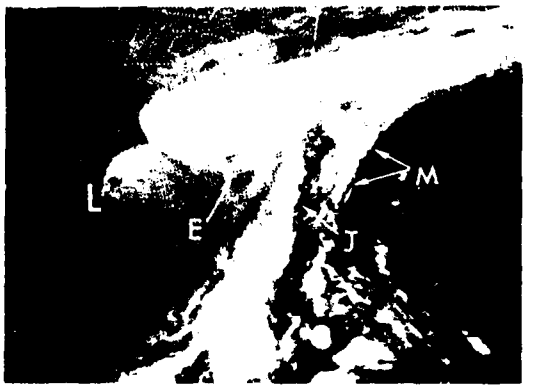

Fig 4 SMS-1 IR 2330Z 23 Sep 75

Fig 5 SMS-1 IR 0630Z 24 Sep 75

Fig 6 SMS-1 IR 1130Z 24 Sep 75

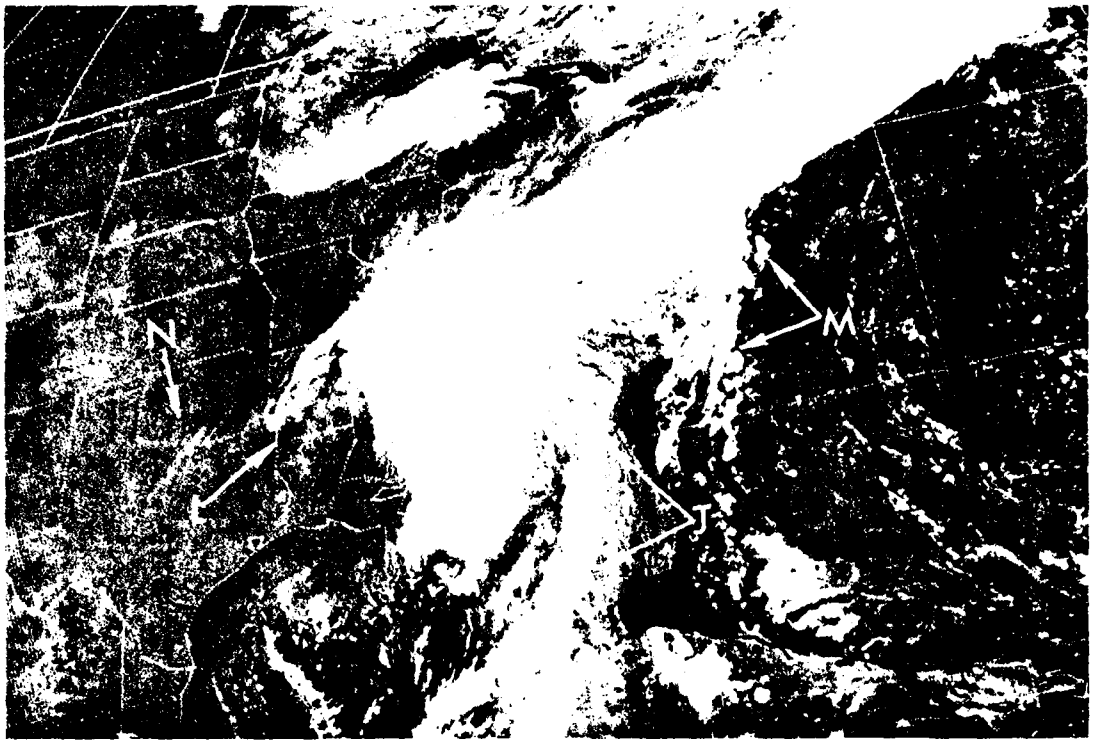

Fig 7 SMS-1 1-mile resolution VIS
17002 23 Sep 75

SATELLITE APPLICATIONS INFORMATION NOTE 10/75-3

DISTINGUISHING FOG FROM STRATUS ON SATELLITE PICTURES

James J. Gurka

The SMS-1 1/2-mile resolution visible picture of the eastern U.S. from 1400Z on September 28, 1975, illustrates two situations in which fog can be identified on satellite pictures.

In many cases it is impossible to distinguish fog from stratus on satellite imagery. To date, there are two primary clues which can be used on the visible pictures: (1) if a deck of low clouds is moving, it is probably stratus rather than fog, and (2) if the low cloud is restricted to valleys or bounded by low level terrain features, fog is more likely than stratus.

With the 1/2-mile resolution visible SMS pictures, another clue is now available in some situations. When valleys are filled with fog they frequently show up on 1/2-mile resolution pictures as narrow lines which are brighter than adjacent fog or low clouds. This is reasonable since the fog should be deeper over a valley if the fog has a fairly uniform top as illustrated in Figure 1. In most cases, infrared pictures show that the temperature of the tops of fog and stratus is very uniform, indicating a uniform height of the fog top.

This effect can be seen on Figure 2, where the fog over the river valleys at A, B, and C is brighter than the surrounding cloud. Fog can also be seen at D, E, and F where the cloud is restricted to the valleys.

Surrounding the valleys at A, B, and C, no definite conclusion can be drawn from the satellite picture as to whether the clouds are fog or stratus or a mixture of both, but fog would be more likely adjacent to valleys that are filled with fog than near valleys that are fog-free.

Furthermore, rivers beneath areas of thin stratus sometimes show up as lines which are darker than the surrounding cloud since the rivers have a lower albedo than the surrounding terrain. If the stratus is thin enough, the brightness of the cloud top depends not only on the light reflected by the cloud itself but also that reflected by the surface below.

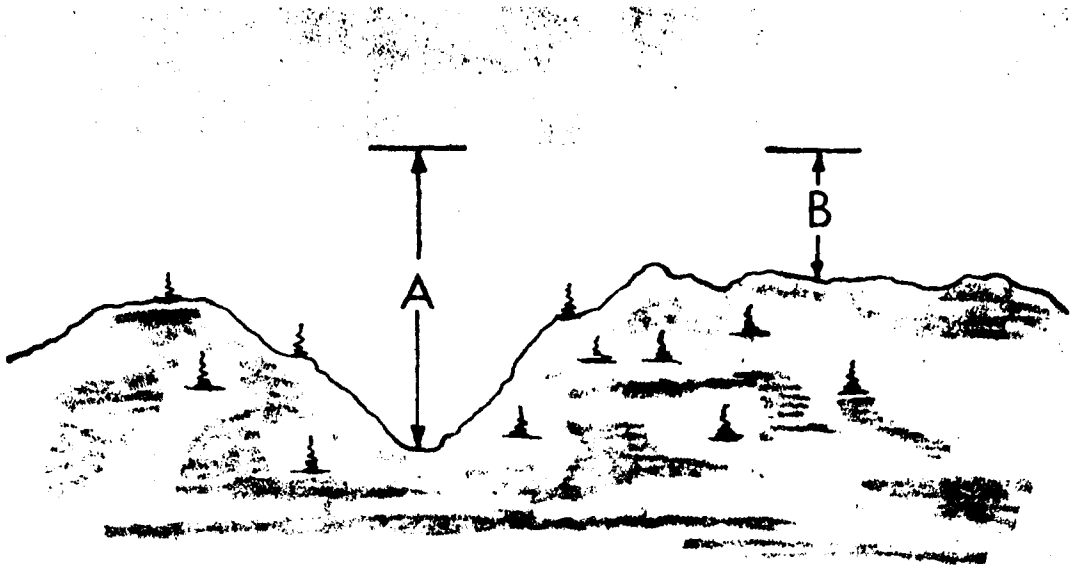

Fig 1. Cloud thickness greater in valley at A than at B.

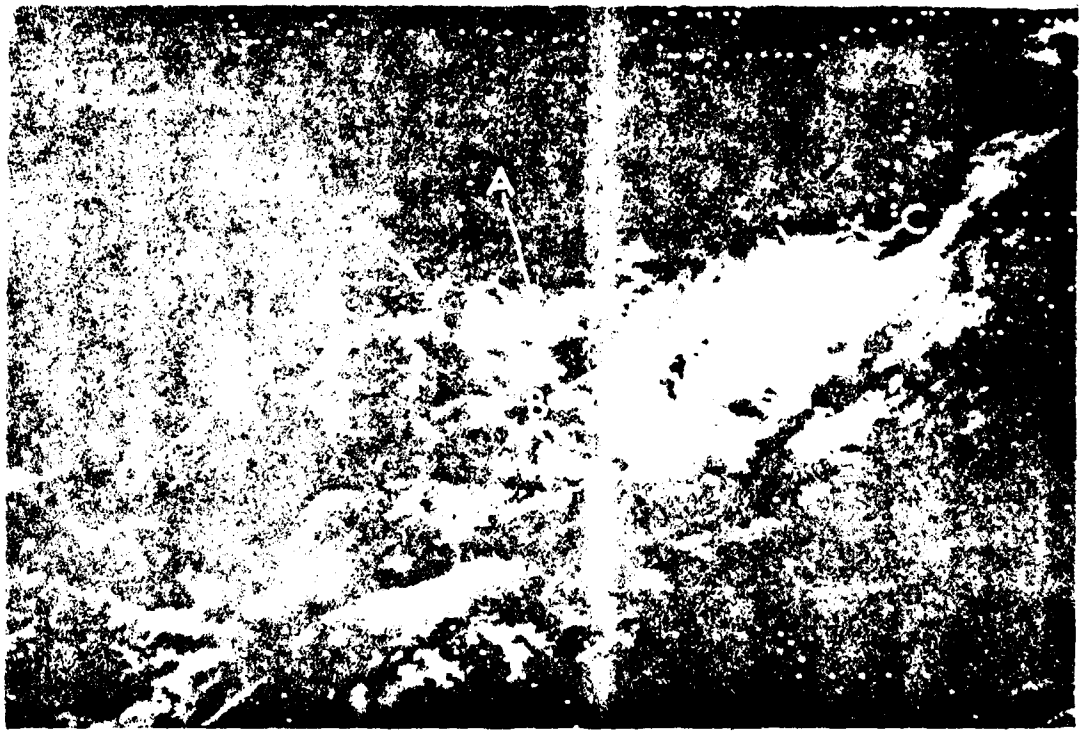

Fig 2. SMS 1 ½ mile resolution visible, 1400GMT 28 Sep 75

SATELLITE APPLICATIONS INFORMATION NOTE 11/75-1

LOW LEVEL CIRCULATION SYSTEMS IN THE EASTERLIES

R. Weldon
Applications Group, NESS

There is a large variation in the weather which occurs within the frontal/baroclinic zone on the east side of a major trough in the westerlies. In addition to such factors as geography, season of the year, time of the day, and atmospheric stability, which affect the type and amount of weather, much of the variation can be attributed to short wave disturbances or vorticity maxima moving in the westerlies around or across the trough onto the east side. The SMS satellite data have enabled us to identify and follow such systems of quite small wave lengths and rapid motion. Frequently, however, the weather of the frontal zone - and in advance of it - is significantly influenced by systems moving within the easterlies around the south side of the anticyclone which is east of the trough. There are at least three specific types of systems in this category; they generally approach the frontal zone from the southeast quadrant turning to a more northward track as they come around the southwest side of the anticyclone. One of these three types of systems in the easterlies is illustrated in the SMS-1 pictures of Oct. 31 thru Nov. 3, 1975, as follows.

When a storm in the westerlies moves over a relatively warm ocean surface, the region of strong low level cold advection behind the cold front is usually covered by very distinct lines of cumulus clouds - as seen on the IR and VIS SMS-1 photos of Oct. 31, 1975, just off the U.S. east coast (Figures 1 and 2). Near their upwind end, the lines are very thin and generally parallel to the low level flow direction. Further downwind, the lines contain larger cells, and have become deformed by shear; here they are no longer parallel to the low level wind direction.

As the region of strong cold advection moves eastward behind the storm, the clouds forming the original distinct lines enter the anticyclonic flow of the approaching high pressure system. During this phase, the lines will usually deteriorate into large cells or wide bands of stratocumulus. Such a configuration is illustrated on the IR and VIS pictures of the following day Nov. 1, 1975 (See Figures 3 and 4). The stratocumulus cells or bands will usually persist and move southwestward, then westward, south of the surface anticyclone. Often, during the winter season off the U.S. east coast, large cumulus lines will be formed by cold advection over the bays along the middle Atlantic coast. These will maintain their identity as large stratocumulus

bands, and will move south - then westward, onto the coast of Florida or South Carolina as large patches of stratocumulus and increased low level moisture.

On other occasions, such as illustrated on the 3rd day of this sequence for November 2nd (Figures 5 and 6), very large patches of stratocumulus with relatively cloud-free areas in between will be formed. Note the large patches of warm cloudiness on the IR photo - Figure 5. On the visible photo for the same time (Figure 6), the patches can be seen to contain small cumulus lines and areas of stratiform clouds arranged into organized patterns. When observed on time lapse movie loops, each of the patches can be seen to form a small circulation system. The motion of the cumulus clouds revealed a positive vorticity maximum associated with cyclonic shear in the easterly flow. During the time of the picture, the systems were maintaining their identity and propagating westward. The subsequent 24 hour movement was near 5 degrees of longitude - a rate of just over 10 knots.

Figure 7 shows the same group of systems on 1 mile resolution visible data for the next day - Nov. 3, 1975. Again, cloud motions on the movie loops showed the characteristic cyclonic twist in the cumulus cloud groups, as is associated with positive vorticity maxima. Also seen on the photograph - and in motion on the movie loop - is a layer of stratiform clouds moving with anticyclonic motion. These are associated with each cumulus cloud system and are identified by arrows on Figure 7. The stratiform outflow layer with the system approaching the South Carolina coast was near the 700mb surface (as identified on the Charleston sounding at 00Z, Nov. 4).

Although each of these small circulation systems caused cloudiness and rainshowers as they moved onto the coast, the ones over the Atlantic did not enter the frontal zone of the storm over the central U.S. One small low level system shown on these pictures did enter the frontal zone. This can be seen on Figures 5 and 6, just west of Cuba and north of the Yucatan Peninsula. That small cloud system - in its phase shown on the pictures - is very similar to those over the Atlantic; however, its origin was different and was associated with one of the other two types of systems mentioned. This system moved northwestward across the Gulf of Mexico. It can be seen on Figure 7 on the next day (identified by the letter "A") as it forms a comma shape while entering the frontal zone of the storm over the central U.S. Subsequent to the picture time (Figure 7) this system developed deep convection and moved northeastward along the frontal zone. When systems of the same origin as those over the Atlantic enter a frontal zone, they behave very similarly as the one over the Gulf.

In subsequent articles of this series, I will discuss the other two types of systems mentioned.

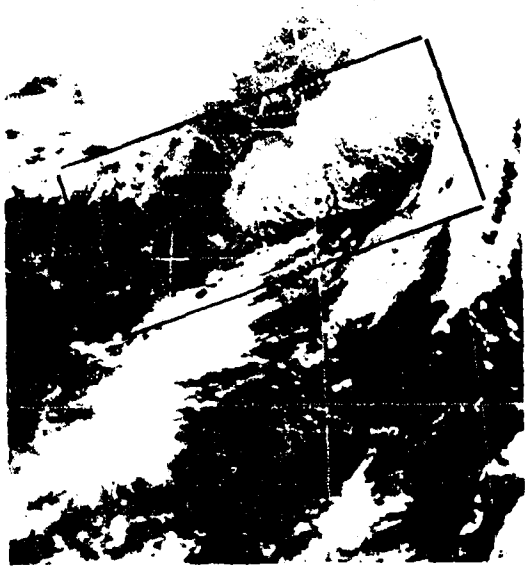

Fig. 1 SMS-1 IR 1700GMT 31 Oct 75

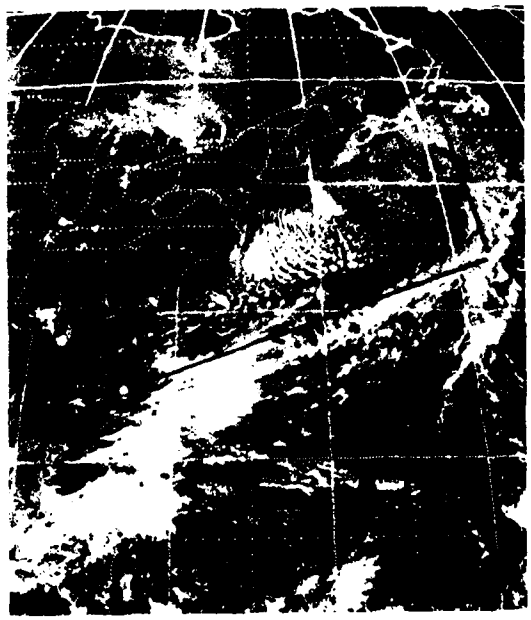

Fig. 2 SMS-1 VIS 1800GMT 31 Oct 75
2-Mile Resolution

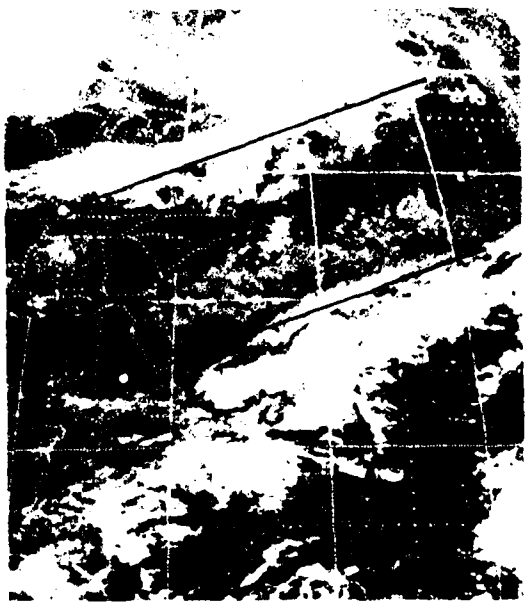

Fig. 3 SMS-1 IR 1830GMT 01 Nov 75

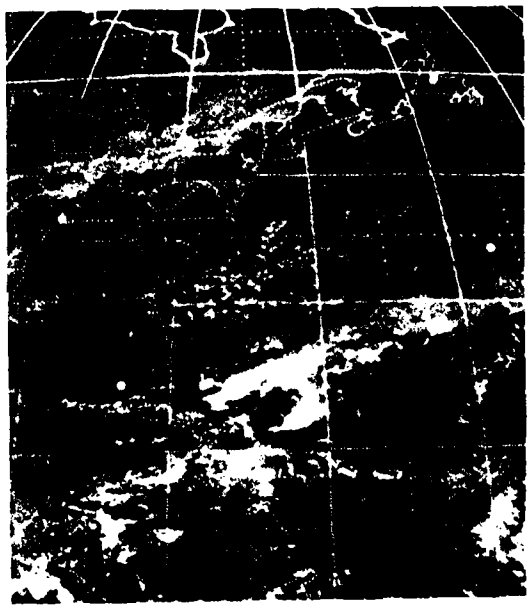

Fig. 4 SMS-1 VIS 1800GMT 01 Nov 75
2-Mile Resolution

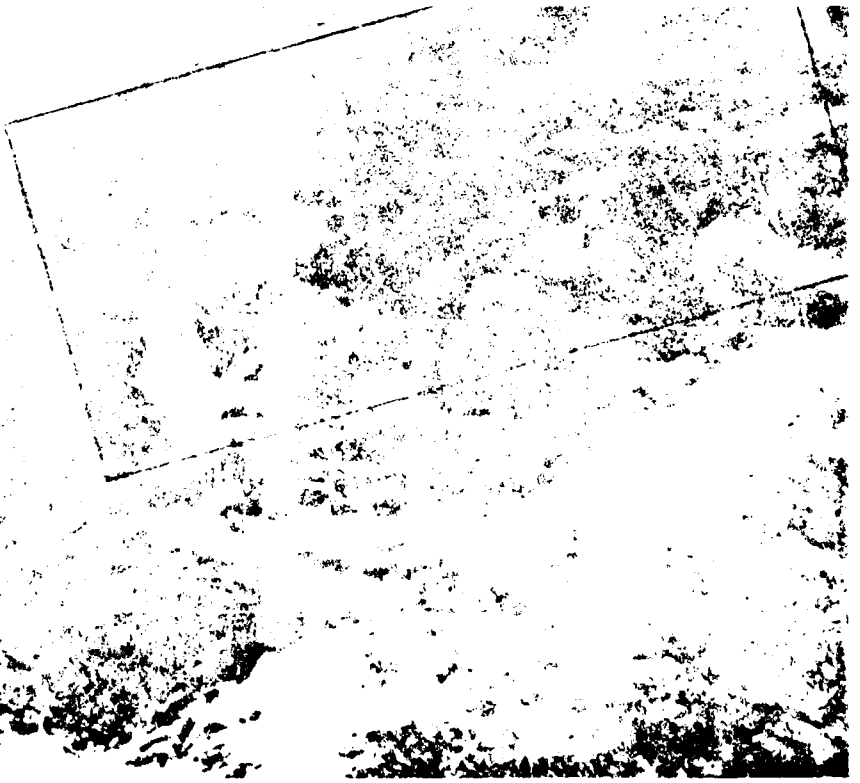

SATELLITE APPLICATIONS INFORMATION NOTE 11/75-2

THE DEVELOPMENT OF TROPICAL STORM "HALLIE"

Vernon F. Dvorak
Applications Group, National Environmental Satellite Service, Washington, D.C. 20233

Tropical storm HALLIE was named at 2200Z on October 26, 1975, while off the east coast of Florida. The storm subsequently moved northeastward passing east of the outer banks of North Carolina with a Coast Guard lightship located offshore about 60 miles south of Wilmington reporting sustained winds up to 58 mph. The storm began to weaken early on the 27th as it accelerated rapidly northeastward.

Tropical storms like HALLIE form in this region during the early summer and late fall. They form east of troughs aloft (cut-off lows) which bring energy from the Westerlies southward into the subtropics at this time of the year. It is also common to have a weakening cold front in the vicinity of the formation. Although this type of storm development is relatively common off the coast of Florida and the Carolinas, little is currently known that explains or predicts the phenomenon. The accompanying satellite pictures are intended to shed some light on this problem.

Daily visible satellite pictures taken at 16Z or 17Z from October 21, to 28 are shown in the figures. The first three pictures, October 21-23, have the 12Z NMC surface (black lines) and 300 mb (white lines) analyses superimposed on the picture imagery. The 12Z 300 mb analyses is shown on the October 24-26 pictures.

The conventional data shows a cut-off low at 300 mb dropping south to southern Florida with a surface trough containing a front to the east of it. On the succeeding days, the data indicates that the low aloft moves eastward and weakens as the surface wave intensifies into a low pressure center that moves westward north of the low aloft. The actual positions of the 300 mb and surface low centers (and hence their interaction) cannot be determined from these data.

The satellite view of HALLIE's formation shows an area of deep-layer cumulus convection increasing in size and taking on a "comma" configuration. This cloud pattern in different sizes and orientations is common to most cyclonic development. This particular comma can be viewed as a structure containing two curved bands (or lines) of convective clouds and cirrus; one oriented east-west where the front is analyzed on October 22, and the other to the south of it oriented north-south. Indications of a lower tropospheric circulation became evident south of the western half of the east-west band on the 22nd becoming more obvious on the 23rd and showing an easily recognizable inverted comma pattern on the 24th. The earlier indications of this low and middle level vorticity are more easily detected in visible movie loops and high resolution pictures than it is in the pictures shown here. The development of vorticity in the lower troposphere begins, where

bands, and will move south - then westward, onto the coast of Florida or South Carolina as large patches of stratocumulus and increased low level moisture.

On other occasions, such as illustrated on the 3rd day of this sequence for November 2nd (Figures 5 and 6), very large patches of stratocumulus with relatively cloud-free areas in between will be formed. Note the large patches of warm cloudiness on the IR photo - Figure 5. On the visible photo for the same time (Figure 6), the patches can be seen to contain small cumulus lines and areas of stratiform clouds arranged into organized patterns. When observed on time lapse movie loops, each of the patches can be seen to form a small circulation system. The motion of the cumulus clouds revealed a positive vorticity maximum associated with cyclonic shear in the easterly flow. During the time of the picture, the systems were maintaining their identity and propagating westward. The subsequent 24 hour movement was near 5 degrees of longitude - a rate of just over 10 knots.

Figure 7 shows the same group of systems on 1 mile resolution visible data for the next day - Nov. 3, 1975. Again, cloud motions on the movie loops showed the characteristic cyclonic twist in the cumulus cloud groups, as is associated with positive vorticity maxima. Also seen on the photograph - and in motion on the movie loop - is a layer of stratiform clouds moving with anticyclonic motion. These are associated with each cumulus cloud system and are identified by arrows on Figure 7. The stratiform outflow layer with the system approaching the South Carolina coast was near the 700mb surface (as identified on the Charleston sounding at 00Z, Nov. 4).

Although each of these small circulation systems caused cloudiness and rainshowers as they moved onto the coast, the ones over the Atlantic did not enter the frontal zone of the storm over the central U.S. One small low level system shown on these pictures did enter the frontal zone. This can be seen on Figures 5 and 6, just west of Cuba and north of the Yucatan Peninsula. That small cloud system - in its phase shown on the pictures - is very similar to those over the Atlantic; however, its origin was different and was associated with one of the other two types of systems mentioned. This system moved northwestward across the Gulf of Mexico. It can be seen on Figure 7 on the next day (identified by the letter "A") as it forms a comma shape while entering the frontal zone of the storm over the central U.S. Subsequent to the picture time (Figure 7) this system developed deep convection and moved northeastward along the frontal zone. When systems of the same origin as those over the Atlantic enter a frontal zone, they behave very similarly as the one over the Gulf.

In subsequent articles of this series, I will discuss the other two types of systems mentioned.

15


16
960
16


960
12
960

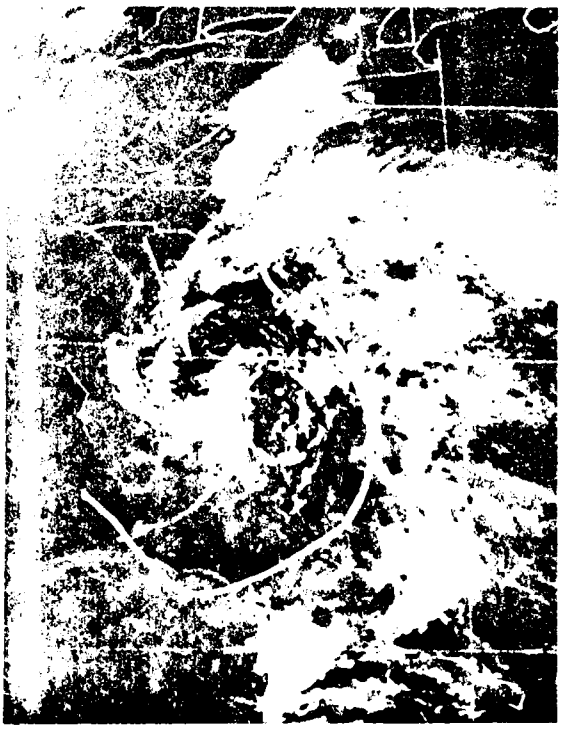

1600GMT 25 OCT 75

1800GMT 26 OCT 75

1700GMT 25 OCT 75

2000GMT 25 OCT 75

SATELLITE APPLICATIONS INFORMATION NOTE 11/75-3

A COMPARISON OF VISIBLE AND INFRARED VIEWS FROM SMS-2 OF THE REMNANTS OF TROPICAL STORM GEORGETTE

John P. Kearns
Honolulu Satellite Field Services Station

The post-tropical depression stage of what briefly had been Tropical Storm Georgette is shown in the 2-km resolution visible imagery from SMS-2 taken at 2318GMT, August 16, 1975 (Figure 1). The center (G) of the delicate vortex was taken about 250 miles from the island of Hawaii (H) at about 16°N, 146°W.

The fine cells of the north semicircle imply surface winds of about 25 knots, which agrees with ship observations. A plume of cirrus from cumulonimbus activity at (I) obscures some of these lower clouds. While there are fewer clouds in the south semicircle, enough are present to reveal southerly and westerly movements when the corresponding film loop is viewed.

The last bulletin on this tropical depression had been issued for August 16, at 0600GMT, when the system was located near 16°N, 130°W. Visible and infrared satellite pictures for the next 65 hours show clearly that the system was maintaining itself while moving westward nearly a thousand miles.

It is not unusual for such Eastern Pacific disturbances of less than tropical depression intensity to approach the Hawaiian Islands. They are of concern to forecasters since even though they might not present a high wind hazard at this stage, they do threaten heavy rain and flooding. A more alarming possibility is that of regeneration to the tropical depression stage, or even higher.

Figure 2 shows the SMS-2 infrared picture with 8-km resolution of the same area 20 1/2 hours later, at 1949GMT, August 17. The high clouds have increased in areal extent. Somewhat disturbing to the forecaster, the shape of this area, expecially the hook-shaped cloud configurations (L and M) along the western edge, suggests a vortex (G?) centered just east of the bright cloud mass (N). It might be inferred that "ex-Georgette" has re-intensified and that it has begun a northward movement.

Figure 3, which like Figure 1 is a 2-km resolution visible picture, was obtained one-half hour after Figure 2, at 2019GMT, August 17. The system obviously has not regenerated; rather, the low level circulation has continued on its prior course and is now at (G), near 15°N, 151°W, some 300 miles from the pseudo-circulation (G?) indicated in Figure 2.

The low level vortex maintained its identity for at least another 27 hours and continued moving west southwest, passing about 200 miles south of the island of Hawaii.

Misinterpretation of a satellite picture is of itself not so unusual, but Figure 2 demonstrates a rather high order of deceptiveness. Certain properties of weak tropical disturbances make them particularly poor subjects for standard infrared representation. It happens in this case that the incompatibility of subject and method produces both concealment and misdirection -- precisely the fundamentals of stage magic.

The low level cloud elements outlining the vortex which is so obvious in Figures 1 and 3 are concealed in the infrared of Figure 2 by their own warmth and fineness. These warm clouds are near the temperature of the underlying sea surface and their detection (G, Figure 2) is difficult. The small warm clouds here are as effectively hidden as a dark gray thread in front of a black curtain.

Misdirection is also present in this example. As frequently happens, a cumulonimbus has formed not too far from the center of the vortex. The tops of CBs and their attendant cirrus blow-offs are cold and appear bright white in standard IR imagery. The high clouds of Figure 1 became part of the anticyclonic flow east of a col between two upper level lows, and in time formed the shape which so dominates Figure 2. The size and brightness of this area capture the analyst's eye, and the apparent vortex demands his attention. But perhaps most importantly, since a strong upper level outdraft is one of the significant symptoms of regeneration that a concerned forecaster would be looking for, the analyst's apprehensions are misled, as well. Thus this illustrates the importance of continuity afforded by synchronous satellite data over and above the once or twice-a-day polar orbiting data.

Fortunately, no false alarms were issued here -- partly because high resolution visible pictures were obtained before such a step would have been necessary. However, visible pictures are unavailable at night so that an analyst must keep in mind that warm clouds may not be well displayed by standard IR pictures, and that even those enhanced to emphasize warm clouds may miss delicate features because of the relatively poor resolution of SMS-2 infrared imagery.

Of additional interest are the organized bands of trade wind strato-cumulus such as (C, Figure 1) that pass over the islands and produce rain. As the vortex propagated southwestward toward the Hawaiian islands, the north-easterly flow increased thus aiding the arrival of precipitation on the following day. Rainfall also increased significantly on Hawaii during the passage of the vortex.

The satellite data in Figure 1 also show the near daily persistance of cloud plumes downwind of the Island chain. Strong trade wind flow from the northeast becomes deflected by the island obstacles. Downwind the deflected air forms vorticies or long cloud streamers. The largest plume or streamer (D) extends westward from Hawaii and much smaller streamers extend from Oahu and Kauai (E and F).

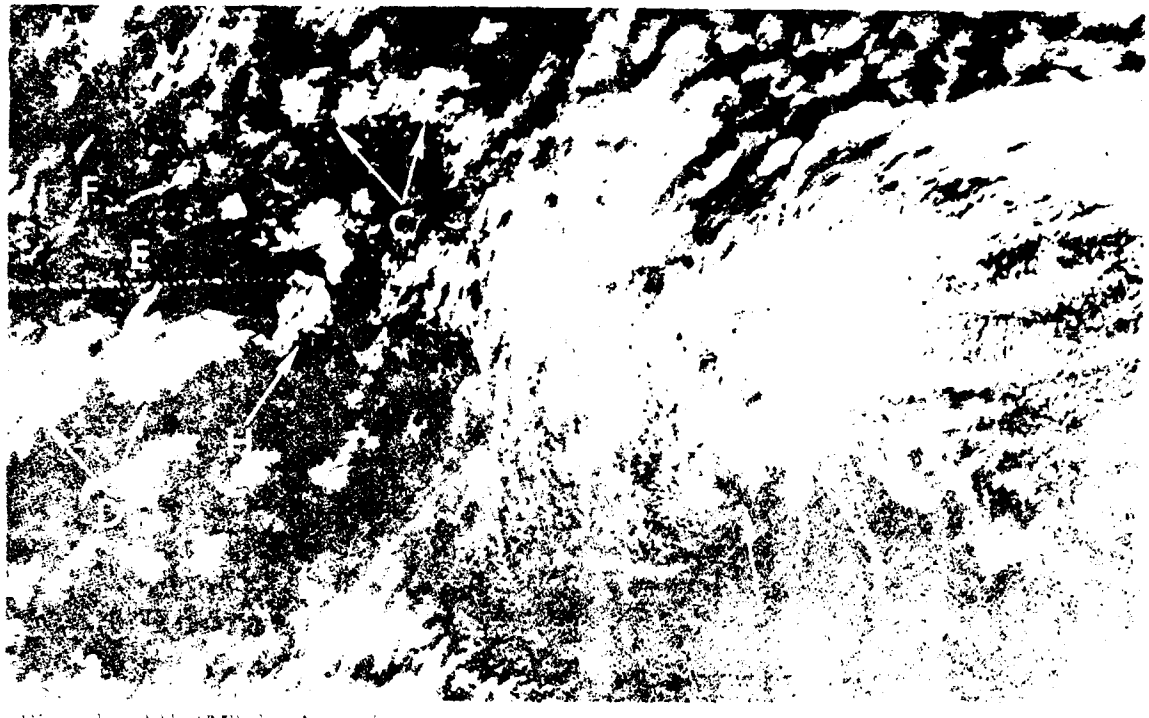

Fig. 1 2315GMT 16 Aug 75

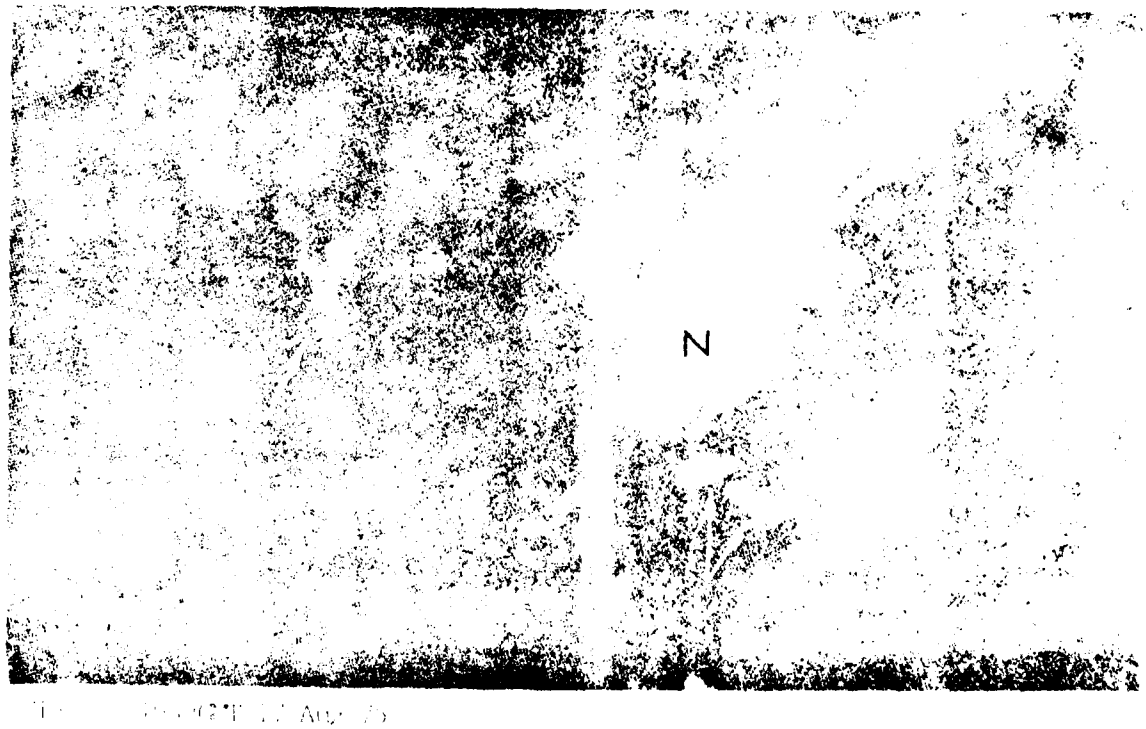

Fig. 2 0102GMT 17 Aug 75

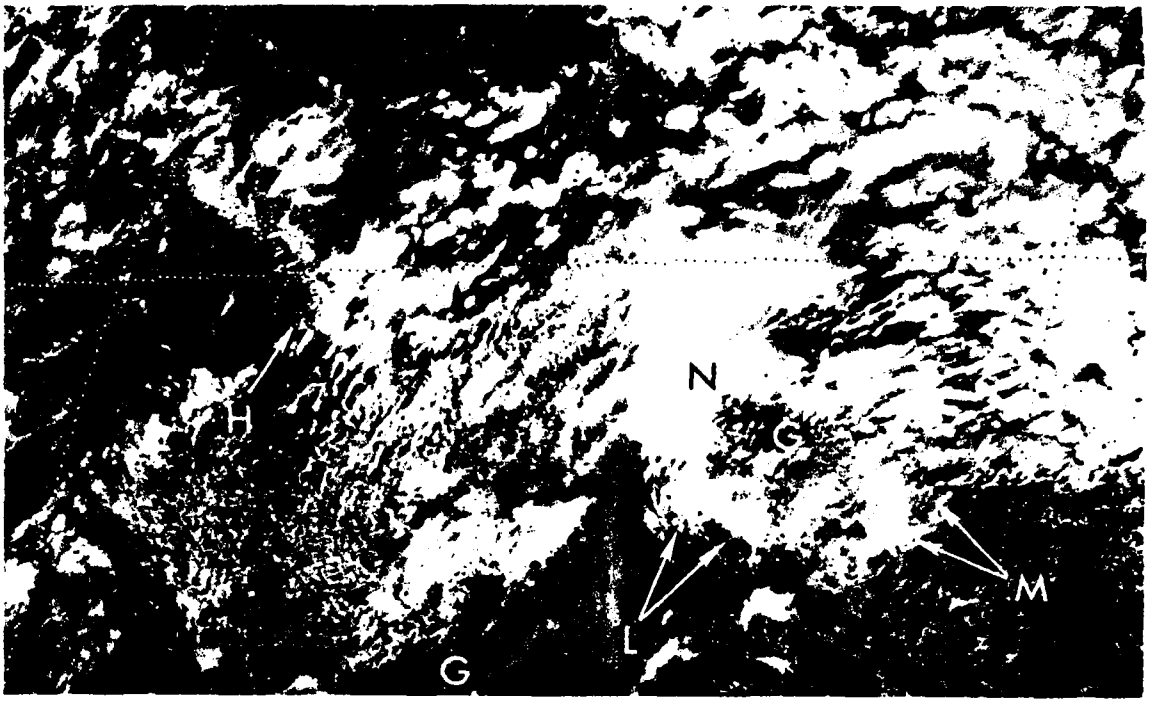

Fig. 3 2019GMT 17 Aug 75

National Weather Service/National Environmental Satellite Service
SATELLITE APPLICATIONS INFORMATION NOTE 12/75-1

FOG DISSIPATION IN THE VICINITY OF THE CHESAPEAKE BAY

Carl E. Weiss and James J. Gurka
NOAA/NESS, Applications Group

Forecasting the dissipation of fog in the vicinity of the Chesapeake Bay is one of the more difficult tasks faced by the marine forecasters at the Washington, D.C. WSFO. This problem is compounded by the differences in terrain over which the fog lies. An example of Bay area fog dissipation is illustrated by a sequence of 1-km SMS-1 visible imagery for November 9, 1975.

The 1500 GMT surface analysis, Figure 1, shows a weak cold front stretching from the New England coast westward through New York state and the southern Great Lakes. A ridge of high pressure also extended westward from the Atlantic over the middle Atlantic coast. Winds over the entire Bay region were generally light, less than five knots and temperatures ranged from the low to middle 60's. The 1530 GMT 1-km SMS-1 visible picture, Figure 2, shows an extensive area of fog covering southern New Jersey, the eastern half of Maryland and most of eastern Virginia and the coastal waters. Within the fog area, the land masses of Cape May, the Delmarva Peninsula and the western shore of the Bay (A) are readily identifiable by their brightness.

In this situation, anticipating the dissipation of the fog was made even more difficult because the fog was present over both land and water. The forecasting problem should be separated into two parts, dissipation over the land areas and dissipation over the water. Gurka (1974) demonstrated that over land, fog areas of minimum brightness on visible satellite imagery are usually the first to dissipate while the brightest fog areas persist the longest. In Figure 2, an area of minimum brightness over the Delmarva can be seen at (B). This area should be forecast to clear sooner than the brighter fog areas.

Forecasting fog dissipation over the cool waters of the Chesapeake Bay is an exceedingly difficult task. With light winds and water temperatures reported in the upper 50's to the middle 60's, the low-level air was cooled and moisture was added so that the fog was continually being reformed. Therefore, the satellite based fog dissipation forecasting techniques used over land cannot be employed successfully for fog over water. All that can be said is that in general, fog over water should persist longer than fog over adjacent land areas.

By 1700 GMT, the 1-km imagery, Figure 3, shows the fog over the Delmarva Peninsula has begun to dissipate (C). This area of dissipation closely matches the area of minimum brightness (B) shown in Figure 2. Fog can be seen to persist over the cooler river, bay, and ocean waters (D). The surface winds at this time became southwesterly, averaging about five knots. Temperatures remained in the low 60's where the dense fog persisted, but climbed to 68°F at Salisbury, Md. (SBY), and 66°F at Andrews Air Force Base (ADW) where the dissipation has started.

The 1-km visible imagery at 1900 GMT, Figure 4, shows most of the Delmarva Peninsula and the western shore of the Bay to be fog-free (E), while dense fog remained over the Bay proper and coastal waters (F). By this time, the winds turned more southerly and increased to near ten knots near the coast, but continued about five knots farther inland. The turn to more southerly flow favored fog persistence over the Bay where the air had a long trajectory over the water. Cumulus clouds (G) developed in response to surface heating over land areas where the fog had dissipated. 1900 GMT temperatures ranged from 74°F at Salisbury, Md. (SBY) and 71°F at Ft. Meade, Md. (FME) under abundant sunshine to 61°F at Dover, Del. (DOV) and 64°F at Patuxent, Md. (NHK) under a thick fog blanket.

REFERENCE

Gurka, J. J., 1974: "Using satellite data for forecasting fog and stratus dissipation", Preprint Volume, Fifth Conference on Weather Forecasting and Analysis, March 4-7, 1974, 54-57.

23

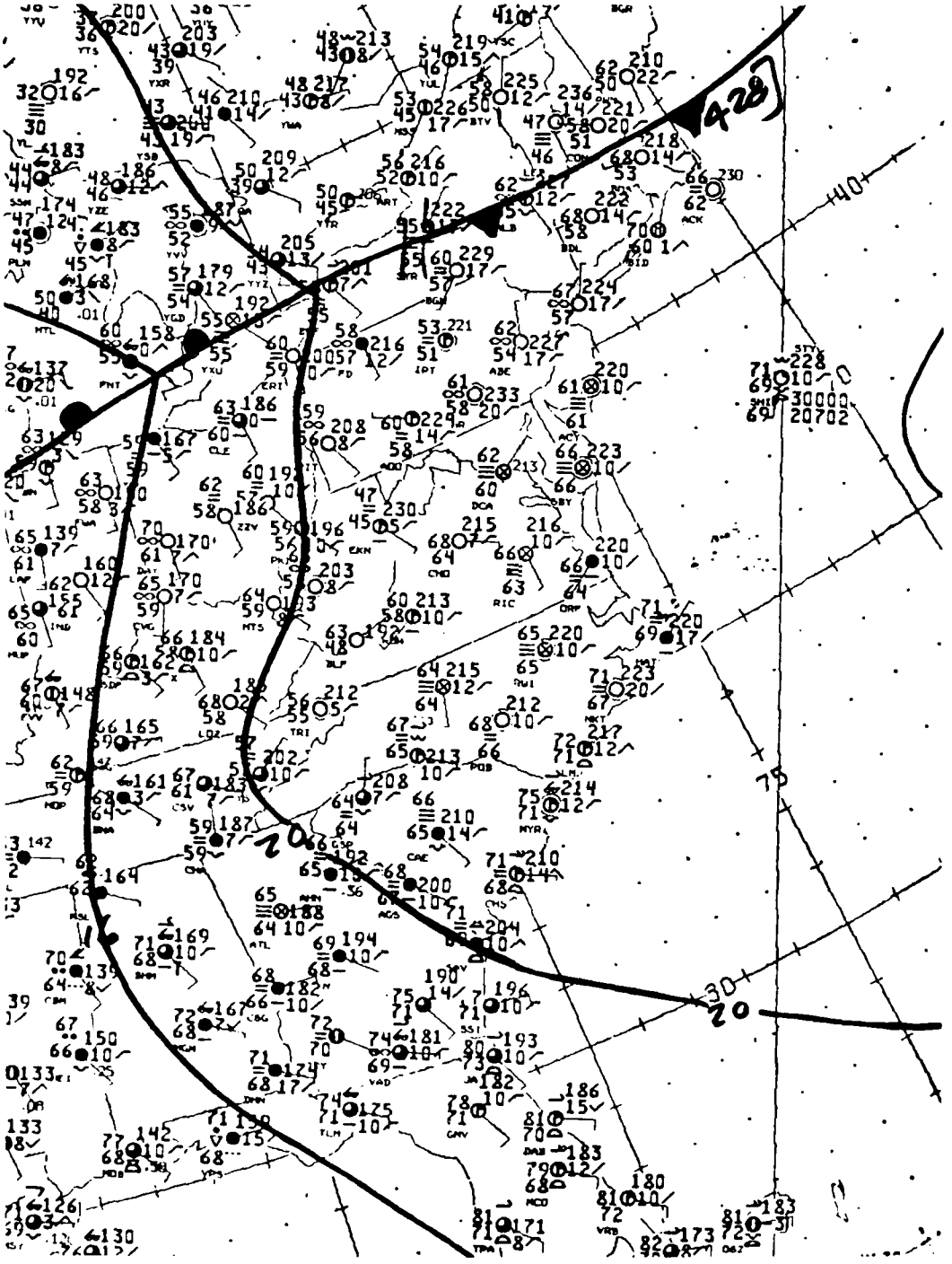

Fig 1. 1500GMT Surface Analysis, 9 November 1975.

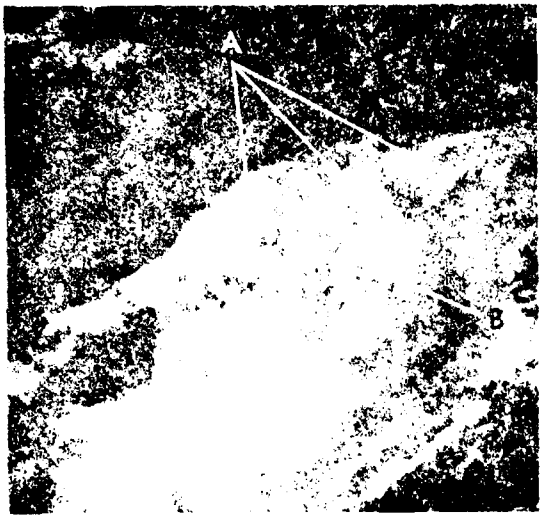

Fig. 2. SMS-1 1-km visible imagery [illegible] November 1975.

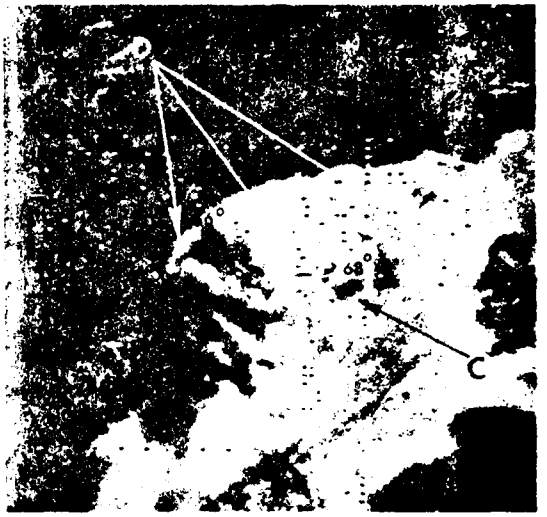

Fig. 3. SMS-1 1-km visible imagery 1700GMT, 9 November 1975.

Fig. 4. SMS-1 1-km visible imagery [illegible] 9 November 1975.

[illegible] The automatically implanted grid on the 1700 GMT picture in Figure 3 is placed about 10 miles too far east. On the 1900 GMT picture in Figure 4, the grid is about 30-40 miles east of the correct location.

National Weather Service/National Environmental Satellite Service
SATELLITE APPLICATIONS INFORMATION NOTE 12/75-2

INTEGRATION OF SATELLITE IMAGERY WITH THE SURFACE ANALYSIS CHART

John A. Ernst
NOAA/NESS, Satellite Field Services Station, Washington, D.C. 20233

The NWS forecaster continuously evaluates and melds informational data from a multitude of diverse sources. One such data source, real-time infrared (IR) imagery obtained from meteorological satellites, can be of material benefit to the forecaster (numerical imagery in the form of computer-enhanced IR images will be on-line in the near future.) When there are conflicting, missing, or incomplete conventional data, the satellite picture with its overall view often furnishes the decisive input to the formulation of an accurate diagnosis or successful forecast. The following is a brief discussion outlining one approach to integration of this satellite IP imagery with the surface analysis chart.

Figures 1a. and 1b. are time concurrent at 07/0000 GMT November 1975, and represent portions of the SMS-1 Equivalent IR DB5 sector, and the NMC Surface Analysis Chart. Figure 1a. has been annotated with some key features that led the SFSS/DCA duty meteorologist to suspect the presence of a surface trough over the Gulf Coast states.

An upper level cyclonic circulation center appears just east of MKC. The associated flow pattern, indicated by the streaming cirrus, is shown with smooth continuous arrows. A dashed line, representing the axis of the trough aloft (TROAL), is extended to near the bottom inflection point. Lack of moisture in the trough's southern and western portions makes exact placement somewhat arbitrary but still operationally useful. In this case the characteristic "comma-cloud" shape of the PVA area is quite elongated stretching from Mississippi to Illinois (sketched-in). Note (over western Tennessee) that the northern half of the cloud has become merged with clouds along its eastern edge.

The preceding is a typical description of an organized upper level system that in most cases has some surface or lower level reflection. Upon further examination of the appearance of numerous bright, white "flaring" areas (A, B, C, D, E) of possible convective activity are noted. The spatial organization suggests the presence of a weather band often associated with surface troughs, convergence lines and/or prefrontal squall lines. Slightly to the west of the convective area, a line configuration does seem to appear and is shown by a dotted line.

At the surface there are some indications of trough formation that correlate well with the satellite IR image. On Figure 1b., a grouping of stations are revealed (encircled by dashed line) that reported precipitation ranging from

light continuous rain at Mobile, Alabama (MOB) to heavy rainshowers at Memphis, Tennessee (MEM). The spatial grouping of the stations is notably similar in appearance to that seen in the satellite IR picture, suggesting the presence of a weather band.

The surface wind regime, although light in speed, does contain several significant variations in reported wind direction. Several station-pairs reported 20 degree or more wind directional difference.

At 07/0050 GMT (prior to receipt of the NMC 0000 GMT Surface Analysis Chart) the SFSS/DCA duty meteorologist discussed the 0000 GMT satellite IR picture with meteorologists of NESS's Analysis Branch who coordinated with NMC. The 0200 GMT Satellite Interpretation Message (SIM) issued by the Washington SFSS noted the presence of the surface trough. NMC's Surface Analysis Chart contained a trough in close proximity to that position suggested by the satellite pictures.

27

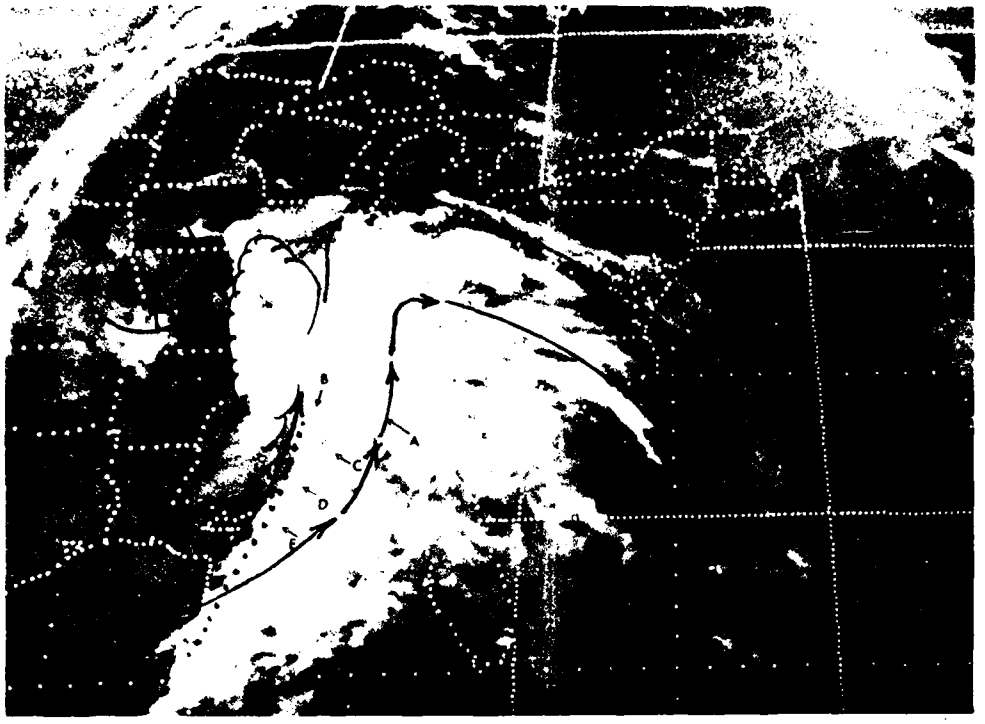

Figure 1a. SMS 1 Equivalent IR
DS 5 Sector, 0000 GMT, November 7, 1975.

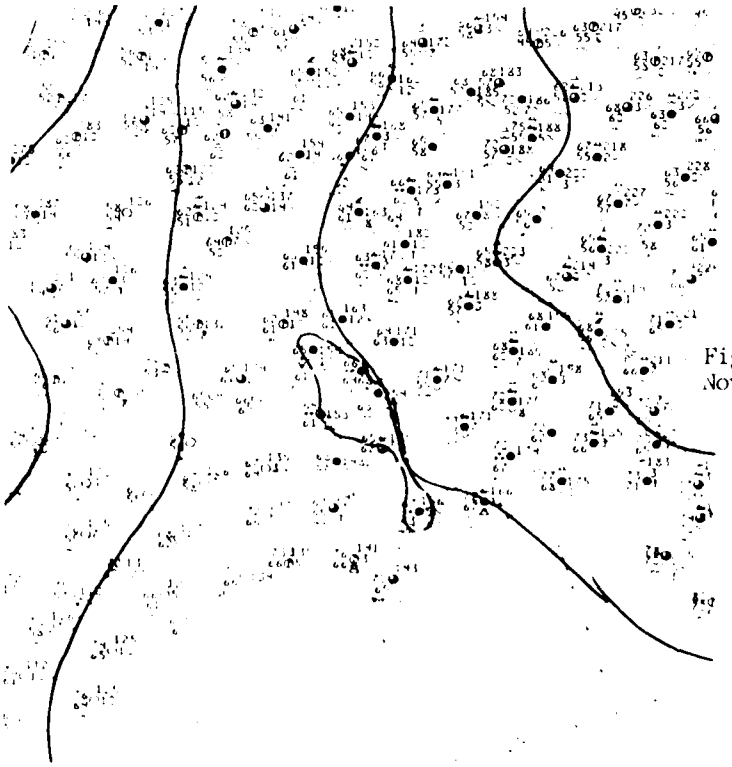

Figure 1b. NMC Surface Analysis, 0000 GMT
November 7, 1975

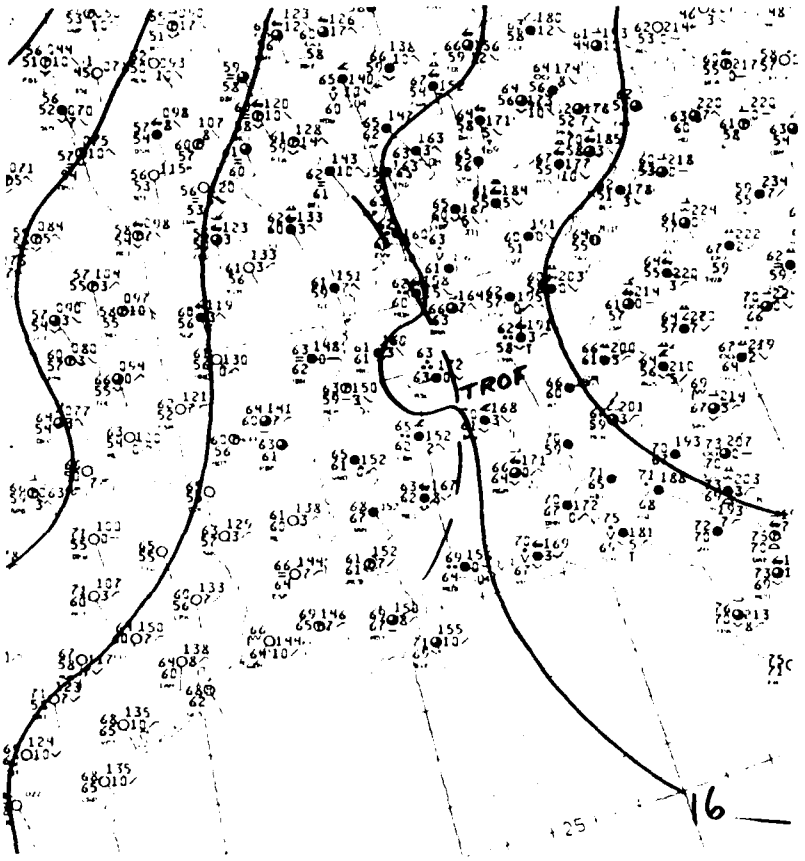

Figure 2. NMC Surface Analysis, 0300 GMT November 7, 1975.

29

National Weather Service/National Environmental Satellite Service
SATELLITE APPLICATIONS INFORMATION NOTE 12/75-3

INFRARED IMAGERY USED FOR TRACKING THE 26 NOVEMBER SNOWSTORM

Roderick A. Scofield
Applications Group, NESS

Heavy snow fell over much of Kansas and Missouri during 25 and 26 November 1975. The infrared (IR) imagery was particularly useful in tracking the upper air disturbance responsible for the heaviest snow that was deposited over Missouri on 26 November.

The 500-mb LFM analysis for 26 November 0000GMT, Figure 1, shows vorticity centers over the Oklahoma Panhandle and Four Corners area. Also, the 300-mb jet axis is indicated stretching from Utah eastward into Oklahoma then to southern Ohio.

On 26 November, 0000GMT, the satellite data in Figure 2 show an elongated east/west area of cloudiness stretching from western Kansas eastward into Missouri. The cloudiness in western Kansas and Nebraska at (C) was associated with the upper level trough in the northern plains. In addition, the clouds to the east at (A) were associated with the positive vorticity advection (PVA) ahead of the vorticity center in the Oklahoma Panhandle. Passage of this easternmost system deposited snow over eastern Kansas with lighter amounts over Missouri. The heaviest snowfall over Missouri occurred with the disturbance located in the Four Corners area. Clouds associated with this disturbance are located at (B). Their configuration is influenced by the presence of mountainous terrain.

During the next 12 hours the vorticity center over the Four Corners area intensified and moved southeastward to the Texas Panhandle, Figure 3. The vorticity center over the Oklahoma Panhandle moved northwestward and weakened and the 300-mb jet axis became more sharply curved.

The IR pictures at 0600GMT and 1100GMT, Figures 4 and 5, respectively, give continuity on the progress of the upper air disturbance at (B). Note that the cloudiness, originally associated with the vorticity center in Oklahoma becomes less distinct over the upper midwest and Ohio Valley at (A) as the new system deepens over the Texas Panhandle. Cloudiness in Nebraska and Iowa at (C) associated with the 500-mb low appears to maintain itself as a distinct and separate system during this period. By 1100GMT, heavy snow had begun in western Missouri as the disturbance at (B) intensified and took on the familiar "S-shaped" pattern which is best related to the middle and upper level baroclinic zone and jet stream. Intensification of this upper air disturbance occurred in the cold air on the cyclonic shear side

of this jet in an area of PVA and upper air divergence. At the surface, this upper air development was reflected as an inverted trough located from eastern Kansas to a weak low near the upper coastal plains of Texas.

Six-hour precipitation amounts, ending at 1200GMT, 26 November, Figure 6, indicate that significant precipitation fell in Kansas and western Missouri. Most of this precipitation occurred with the cloudiness associated with PVA and indicated by (A) in the previous IR pictures.

Continued development of the upper air disturbance at (B) can be tracked in the IR pictures for 1330GMT, 1700GMT, and 2100GMT (Figures 7, 8, and 9, respectively). The clouds associated with the upper air disturbance assume a more "comma-shape" configuration through the period. In this case, the sharp anticyclonic back edge of the comma at (E) separates the areas of moderate and heavy snow to the east and lighter snow to the west. The clouds at (C) appear to move southeastward in response to the movement of the 500-mb low. Thunderstorms at (T) develop as the surface low in southwest Louisiana intensified and moved northeastward along the trough axis.

The six-hour observations of precipitation ending at 1800GMT, 26 November, and 0000GMT, 27 November, are presented in Figures 10 and 11, respectively. Most of this precipitation fell as snow in Missouri producing up to 10 inches in St. Louis. Note in Figure 10 that the thunderstorm activity near Lake Charles, Louisiana, produced 2.70 inches of rain in a six-hour period.

Interpretation of the infrared imagery in Figures 7, 8, and 9 suggested that the 500-mb low was moving southeastward and deepening. The 0000GMT LFM1 analysis on 27 November, Figure 12, verifies this interpretation by showing a deepened 500-mb low over northwest Missouri with a negative-tilted trough.

31

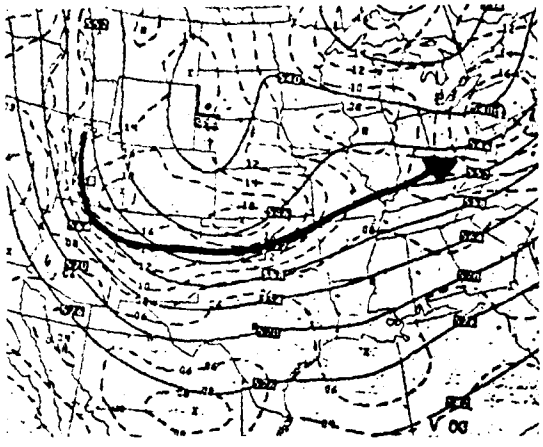

Fig. 1. -- LFM Anal. 0000GMT 26 Nov. 75.

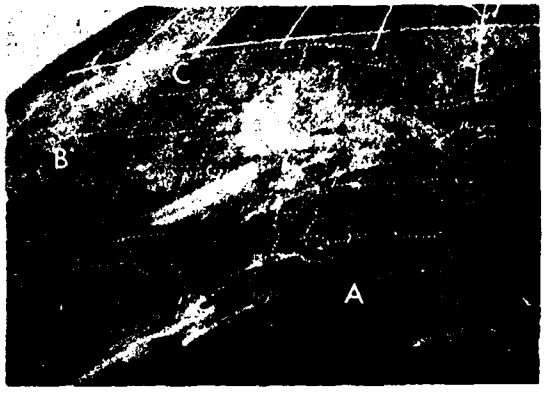

Fig. 4.-- SMS-1 IR 0600GMT 26 Nov. 75.

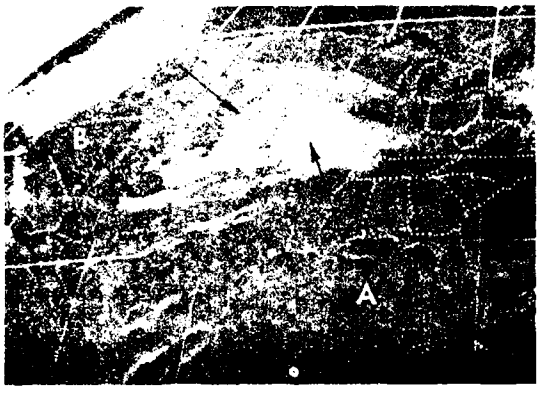

Fig. 2. -- SMS-1 IR 0000GMT 26 Nov. 75.

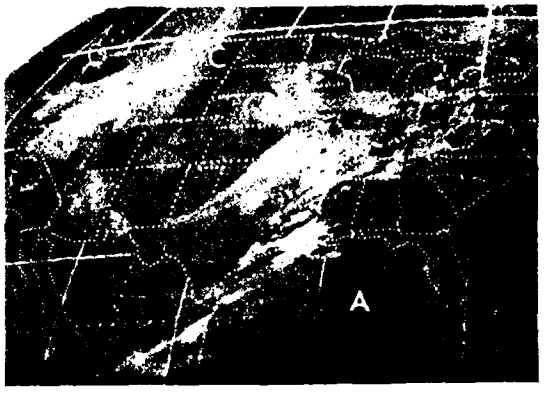

Fig. 5.-- SMS-1 IR 1100GMT 26 Nov. 75.

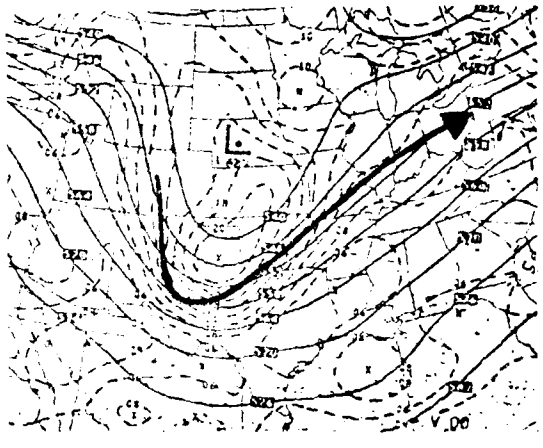

Fig. 3. -- LFM Anal. 1200GMT 26 Nov. 75.

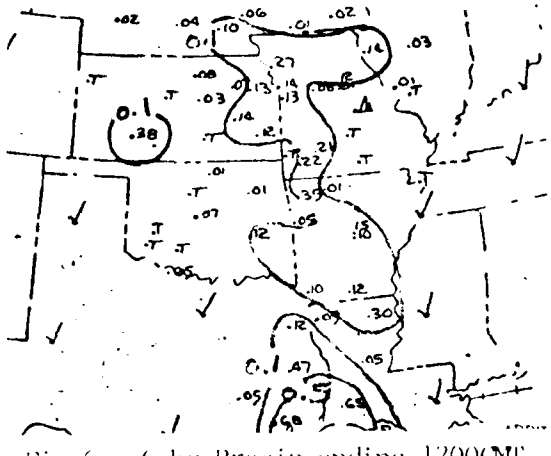

Fig. 6. -- 6-hr Precip ending 1200GMT 26 Nov. 75.

32

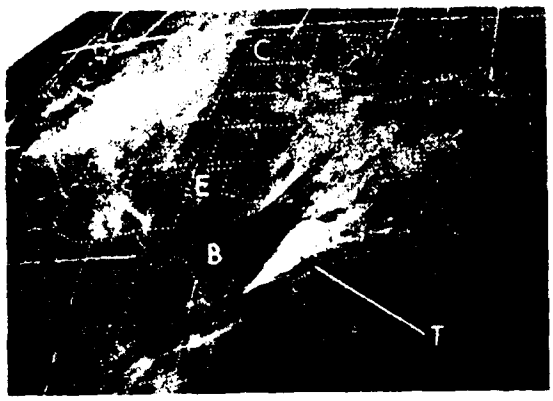

Fig. 7.--SMS-1 IR 1330GMT 26 Nov. 75.

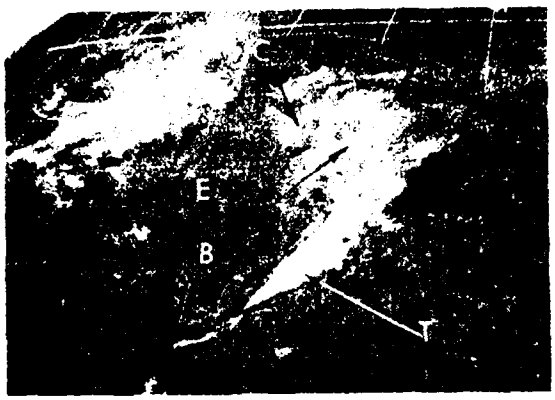

Fig. 8.--SMS-1 IR 1700GMT 26 Nov. 75.

Fig. 9.--SMS-1 IR 2100GMT 26 Nov. 75.

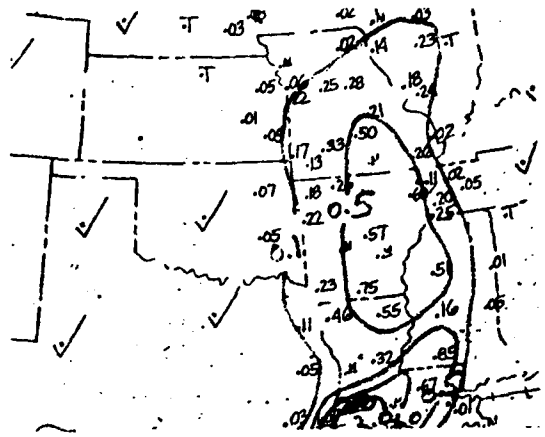

Fig. 10.--6-hr Precip. ending 1800GMT 26 Nov. 75.

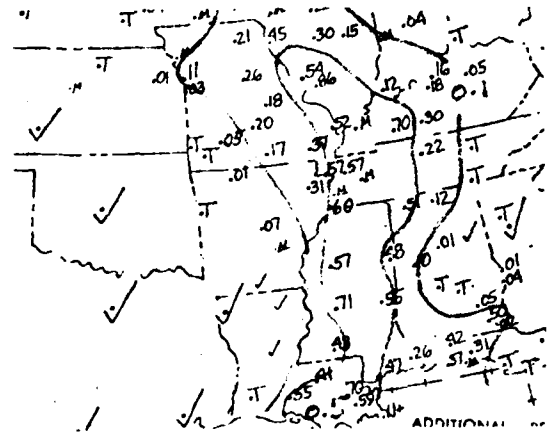

Fig. 11.--6-hr Precip. ending 0000GMT 27 Nov. 75.

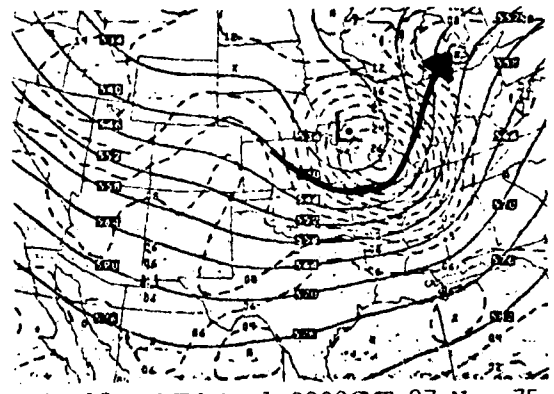

Fig. 12.--LFM Anal. 0000GMT 27 Nov. 75.

33

U.S. DEPARTMENT OF COMMERCE

National Weather Service/National Environmental Satellite Service
SATELLITE APPLICATIONS INFORMATION NOTE 1/76-1

A DECEMBER COLD FRONT AT THE HAWAIIAN ISLANDS

H. McClure Johnson
NOAA/NESS/Applications Group, Washington, D.C. 20233

When a cold front is approaching the Hawaiian Islands in the winter season, a set of seemingly simple, related, and basic questions is usually asked: (1) Where is the front? (2) Will it pass any or all of the islands? (3) When will it pass? and (4) What weather will it bring? These are questions of practical importance, and of real interest to weather-watching islanders as well as to professional forecasters. The problem is rendered more difficult and interesting by the empirical fact that many such fronts approach closely but do not pass, or do not seem to pass. Some are so modified or otherwise weakened after several days of generally southward progress over mid-pacific waters, that little happens or changes when they pass.

The cold front which approached the islands on December 8, 1975, did definitely pass the island of Oahu. Detailed data from this site sheds some light on the nature of the meteorological problem and provides answers to the above set of questions.

A section from the NMC surface chart for 0000GMT December 9, 1975, Figure 1, shows the surface position of the frontal surface to be a little east of Oahu and just west of Molokai. The labeled dashed lines indicate other operational positions (from Oahu) of the front at the times indicated. (The Oahu 0000GMT line is in quite good agreement with the NMC line.)

Figure 2, a 1 km resolution visible view, illustrates the frontal conditions about the Hawaiian Islands at 0015GMT December 9, 1975. The major islands are indicated by the letters: K - Kauai, O - Oahu, M - Maui, H - Hawaii. A letter S indicates the approximate position of the ship JJDT (see Figure 1.) The line A-A' indicates the position of the primary cumulus line that represents a local maximum of vertical development and showers, and provides a good estimate of the surface front position (between Oahu and Molokai) at this time. A comparable "prefrontal" line lies further east, at P-P' with similar lines appearing in and near the frontal zone, especially northeast of the island. This multiple cumulus-line structure is a common analysis (and forecast) problem with such older fronts. Usually, as here, the most prominent line near the leading edge of the frontal zone relates best to the surface position of the front as determined by conventional means with relatively good data. This line is usually a distinct narrow, but conspicuously long maximum of cumulus convection. Several hundred miles southwest of the islands (near N) this line changes into a net-like array of convective cumulus cells. Much stratiform middle cloudiness can be seen along

the length of the frontal zone major band, and is a major component of it. It lies mainly northwest of the surface front position, and is reported by the ship at (S), and extends as far northwest as Kauai. A middle-cloud plume (E) streams northeastward from Kauai's central mountain mass. A meso-scale organized convective system can be seen near and north of Oahu (O). It has a convective line (B) which runs northeastward and then curves back southwestward over Oahu. A middle-cloud layer (D) lies to the north and an associated cloud minimum or subsidence (G) area bounds it on the west and southwest. This minor, component, comma-cloud system, with middle-cloud "head" and cumulus line "tail", soon moved off northeastward. Its passage brought the second period of light showers to Oahu (see Figure 3.)

Further to the northwest the cold advection cumulus field is well shown as near C. Figure 2b depicts some of these features schematically.

Figure 3 shows the hourly winds, the light shower events, and hourly temperatures at the airport station, Oahu. As the complex convective frontal zone cloud system arrived, a slight drop in the temperature occurred (2000GMT), showers began at 2100GMT, and light west winds prevailed (except immediately after the first shower.) Then as the second cumulus band passed, a little before 0000GMT, the winds veered becoming NW at 10-15 knots, and appreciable cold air advection commenced, resulting in the substantially lowered minimum night temperatures observed from 1400 to 1700GMT. The pressure dropped from 1012.5 mb at 2000GMT to 1009.4 mb at 0000GMT, then remained fairly steady for the next 24 hours.

Figures 2 and 3, together, illustrate the fact that the convective cumulus cloud system of the forewardmost part of the frontal surface (including that part called the surface front) was at least 50 nm in width, and contained significant and active substructure. The surface front as a very narrow intersection line is an idealization. The real surface front, a relative discontinuity and a narrow zone of large gradients and marked changes, began its passage by Oahu at a time near 2000GMT, and was passing at the time of the shower event of 2200-2300GMT (just before Figure 2), and was clearly by 0100 or 0200GMT December 9, after which the post-frontal cold air advection was distinct but of moderate intensity. This rather moderate cold front did pass, but little troublesome weather was experienced.

Figure 4, an enhanced infrared view about 12 hours prior to frontal passage at Oahu, shows the frontal zone major cloud band as a well defined synoptic scale feature and clearly west of Kauai.

Figure 5, the corresponding view about 12 hours after frontal passage at Oahu, shows the middle cloud over Maui and the leading edge and convective line at the island of Hawaii.

35

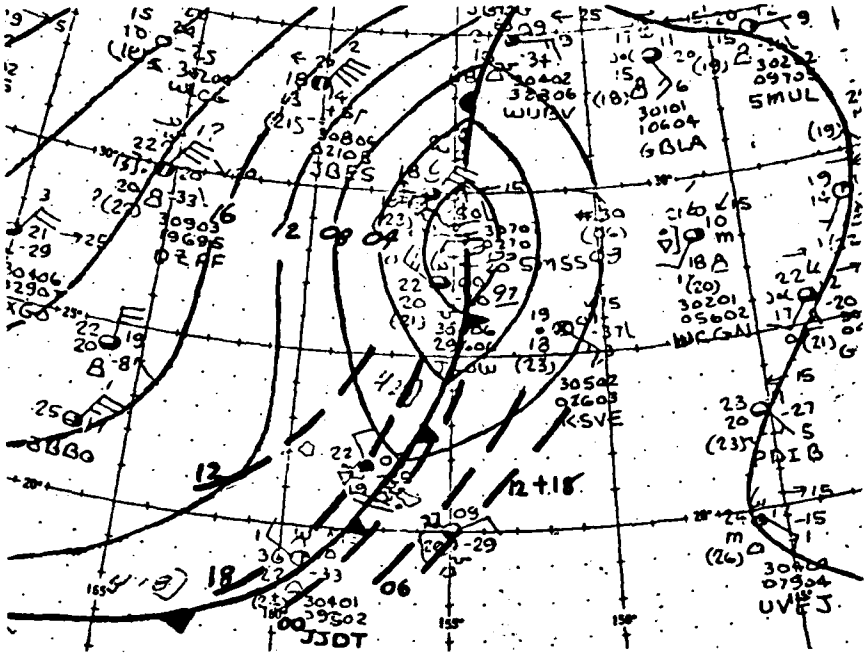

Figure 1. NMC Surface Chart, 0000GMT, 9 Dec 1975.

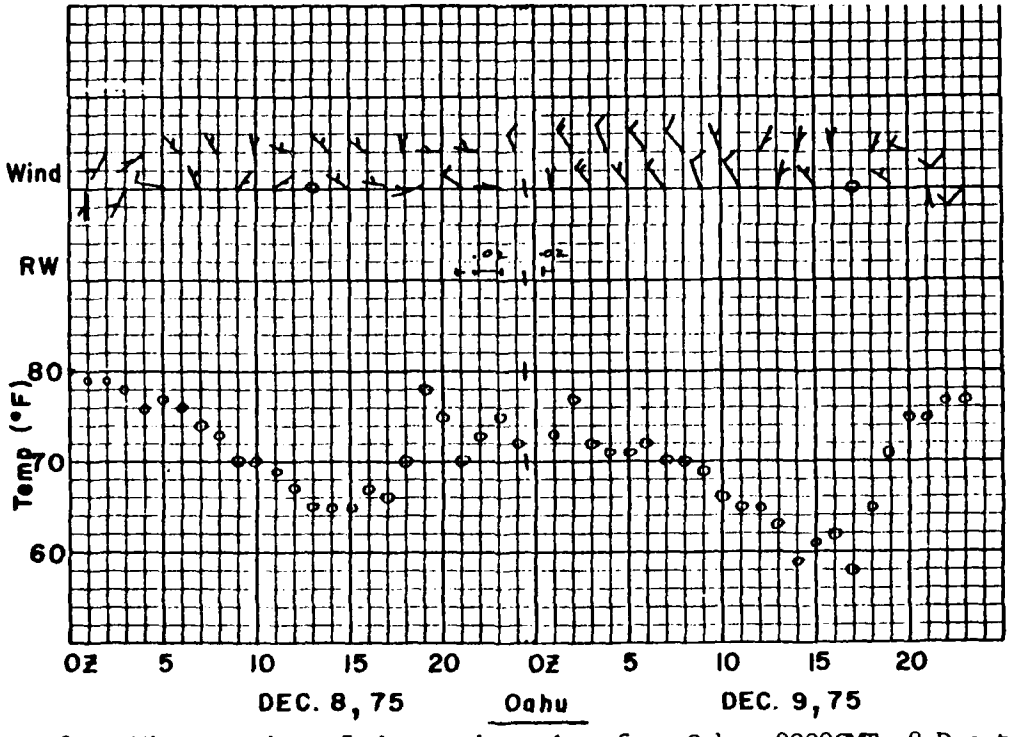

Figure 3. Time section of observed weather from Oahu, 0000GMT, 8 Dec to 0000GMT, 10 Dec 1975. Top row: hourly winds even hours, second row: odd hours, third row: precipitation events, fourth row: hourly temperatures.

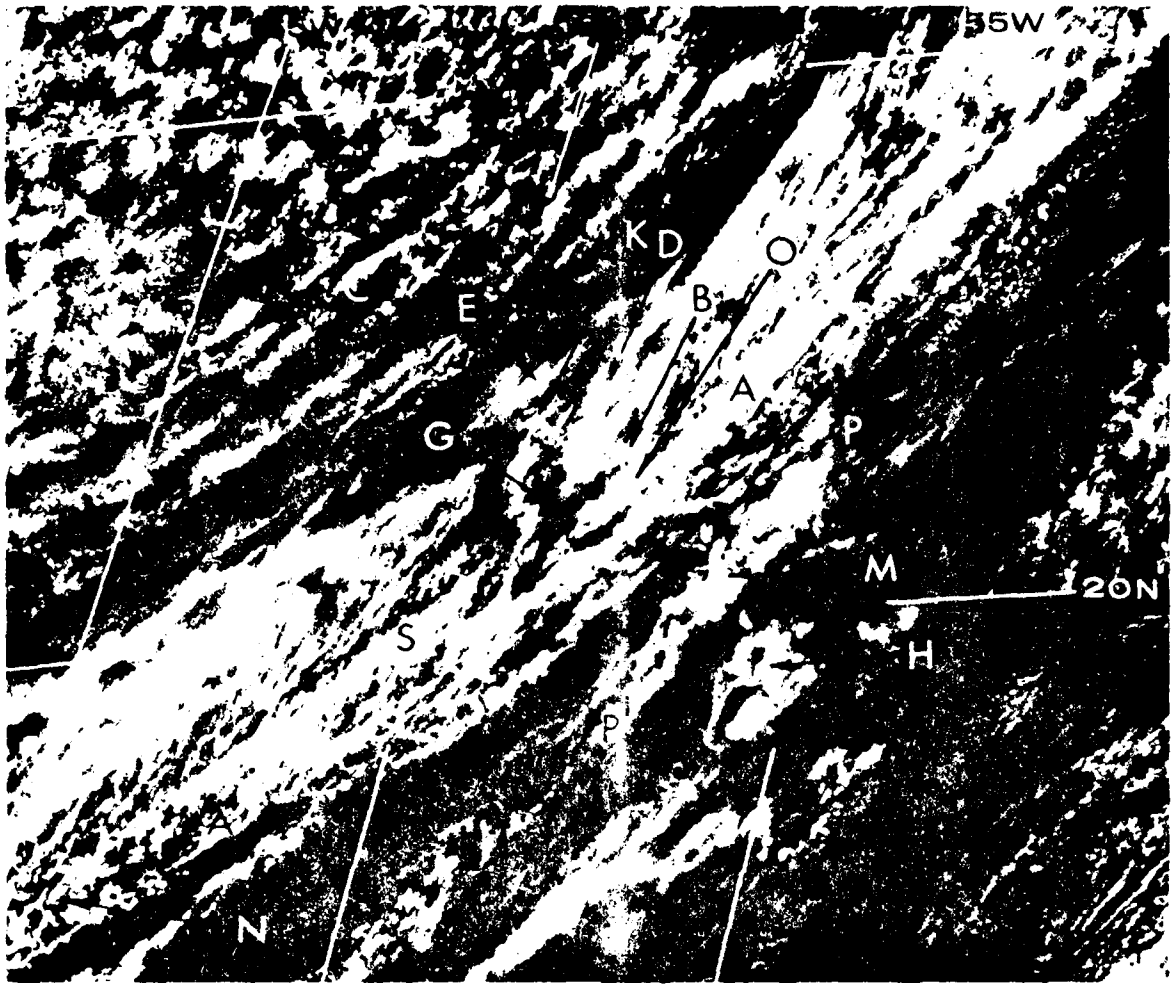

Figure 2a. SMS-2 1 km Visible Data, 0015GMT, 9 Dec 1975.

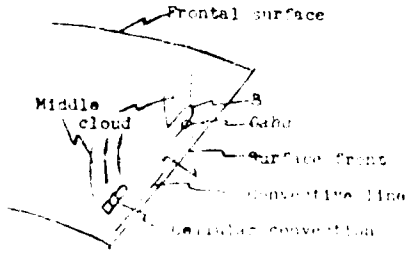

Fig. 2b. Schematic of the Frontal Cloud Zone

Fig. 4. SMS-2 8 km Infrared Data, 1145GMT 8 Dec 1975.

Fig. 5. SMS-2 8 km Infrared Data, 1145GMT 9 Dec 1975.

U.S. DEPARTMENT OF COMMERCE

National Weather Service/National Environmental Satellite Service
SATELLITE APPLICATIONS INFORMATION NOTE 1/76-2

MIDWEST SEVERE WEATHER OUTBREAK OF DEC. 13-14, 1975

Melvin D. Mathews and Edward C. Johnston
Satellite Field Services Station, Kansas City, MO

During the late night and early morning hours of Saturday and Sunday, December 13 - 14, 1975, a series of severe thunderstorms developed over portions of the midwest ... unusual for time of day as well as time of year. The activity occurred along the trailing end of a remarkably well defined vorticity comma cloud that developed over the central Plains and moved rapidly northeastward toward the upper Great Lakes. A brief sequence of related events follows.

A moderate amplitude long-wave trough extended N-S over the intermountain region with a series of short waves rotating through it. At midday on December 13, one such short wave near the Arizona - New Mexico border was moving eastward at 20-25 knots. An upstream vorticity maximum over central Oregon was plunging southeastward at 30-35 knots. With the ever decreasing wave length thus implied, we expected the short wave in the southern Rockies to accelerate northeastward. This in fact occurred later in the day. The upstream vorticity center, which by then had dropped into central Nevada, was ejecting the short wave northeastward out of the southern Rockies as illustrated by the barotropic vorticity analysis for 14/00Z (Fig. 1).

The short-wave trough was moving at a speed of near 60 knots by 02Z, when the comma cloud began to take shape over western Kansas (K, Fig. 2). By this time, the southern branch of the polar jet (A) was discernible in the infrared imagery along a line from Dodge City (DDC) to Huron, S.D. (HON) to International Falls, Minn. (INL). The subtropical jet (B) extended along a line from Abilene, Tex. (ABI) to Tulsa, OK to Louisville, KY (SDF) (both superimposed on Fig. 2). Note the obvious diffluent zone between the jets downstream from the developing comma tail.

Conventional data at 850mb for 00Z showed a moist tongue with dew points greater than 8°C extending from the Texas - Louisiana Gulf coast area northward through central and eastern Kansas, western Missouri and southern Iowa. A portion of this moist tongue, dark gray in the IR imagery, can be seen between the jet stream cloudiness northeastward from N, Fig. 2. As the leading edge of PVA moved over the low level moist field, a squall line developed just to the right of the polar jet.

The comma cloud (K) continued to develop and race northeastward across the midwest (Figs. 3 and 4). Radar indicated tops to 46,000 feet in the tail of the comma which produced severe weather between 02Z and 11Z on December 14.

Reports included 4 tornadoes, 14 occurrences of gusts in excess of 50 knots, wind damage, and hail up to golf ball size from south central Kansas to eastern Iowa. All of the severe weather occurred in the upper diffluent zone between the two jets. The 0735Z radar summary chart (Fig. 5) depicts the strongest activity as well as the valid weather watches issued by the National Severe Storms Forecast Center.

We seldom observe a vorticity comma cloud system over land which is as well organized as the one discussed here. We believe the compact and well defined nature of this cloud system implies a concentration of positive vorticity advection (strong upward vertical motion), and thus is indicative of the severity of this thunderstorm outbreak.

37

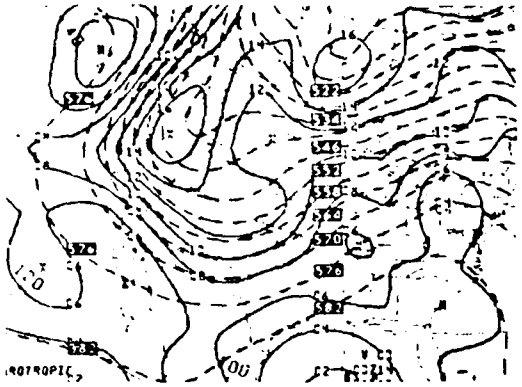

Fig. 1 Barotropic
00Z 14 Dec. 75

Fig. 2 SMS-1 IR 02Z
14 Dec. 75

Fig. 3 SMS-1 IR 05Z
14 Dec. 75

Fig. 4 SMS-1 IR 08Z
14 Dec. 75

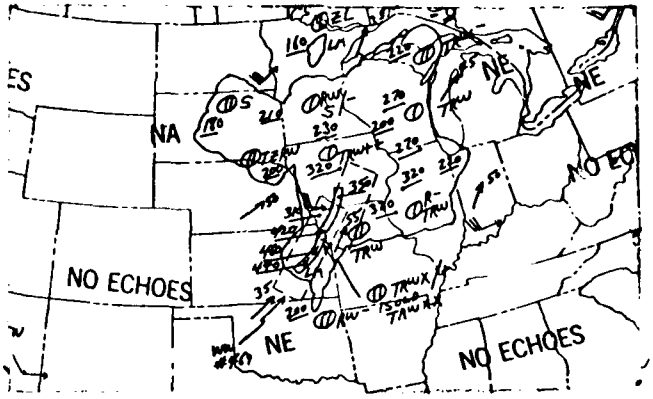

Fig. 5 Radar Summary
0735Z 14 Dec. 75

40

U.S. DEPARTMENT OF COMMERCE

National Weather Service/National Environmental Satellite Service
SATELLITE APPLICATIONS INFORMATION NOTE 2/76-1

UNUSUAL TROPICAL DEVELOPMENT FROM A MID PACIFIC COLD LOW

Donald R. Cochran

NESS, Satellite Field Services Station
Honolulu, Hawaii

Tropical storms in Hawaiian waters (between 140° - 180°W) are rare. Non-tropical vortices deserving of gale warnings are more frequent. Central Pacific Hurricane Center records for 25 years show few tropical storm tracks extending north of 25°N and none north of 35°N. Nevertheless, Figure 1A shows the track of a remarkable storm. It began as a cold low, developed down to the surface, and became a probable hurricane -- all well north of the Hawaiian Islands.

In the SMS-2 picture taken at 0048 GMT 31 August 1975, the parent cold low (near A on Figure 1B) was located some 1500 km northeast of Honolulu. Satellite data and aireps both indicated that the system was a typical upper cyclone which normally migrates westward along the east Pacific trough. Using the Hebert-Poteat (HP) (1975) system (a new technique designed to mesh with the Dvorak (1975) system), the Honolulu Satellite Field Services Station (SFSS) "classified" this cold low at 25 to 30 knots. At 00 GMT, 01 September, the low was centered near A on Figure 2A. (The shallow vortex visible southeast of A was later absorbed by the developing storm.) By 00 GMT, 02 September (Figure 2B), the low had assumed the characteristic double banded configuration of a well-developed vortex. A 35- to 40-knot wind estimate was required by the HP system, and a simultaneous application of the Dvorak system indicated similar results. Continued growth occurred so that by early morning on the 2nd convection near the circulation center had increased substantially and had become more isolated. These two key characteristics foretold an incipient tropical storm.

By 03 September 00 GMT (Figure 2C) the system was clearly a tropical cyclone, with a small central dense overcast (CDO) warranting a more than 50-knot intensity estimate (T3.0 trending toward T3.5) on the Dvorak scale. Late that evening the infrared imagery from SMS-2 hinted at the formation of an eye. Next morning, configuration in the form of the 2018 GMT NOAA 4 view (Figure 2D) could not be mistaken. Analysts gaped at the classic round eye -- a probable hurricane -- and at 40° north! Using the approximate 1/2 degree of latitude distance by which the center of the eye was imbedded from the nearest edge of the CDO along with the technique's other components, a Dvorak wind estimate of 65 knots or greater was warranted. Since the pictures later on September 3 indicated that the storm was becoming involved with the adjacent frontal clouds, analysts hoped for quick corroboration

from ship data. Perhaps fortuitously, support for the satellite data finally arrived. At 04 September 00 GMT a ship which apparently (and no doubt inadvertently) passed near the eye of this tight storm reported 45-knot winds. Located some 90 km WSW of the storm's center and heading west, this ship's barometer read 1003.2 mb at 04/00 GMT with a three hour tendency of +13.5 mb, suggesting a pressure under 990 mb near 2100 GMT. Using Holliday's ('969) well-known graphical composite of the various hurricane wind/pressure equations a speed of about 65 knots is obtained from the 990 pressure. Additional ship reports at 0600 GMT continued to confirm the storm's fury. A ship about 200 km SSE reported the highest ship winds during the sequence: 190 degrees at 55 knots. On into the evening this small but dangerous storm tracked rapidly northeastward. Before dawn she had lost most tropical characteristics, and was enmeshed in the extensive frontal cloudiness and strong southwesterlies ahead of the upper trough.

SUMMARY AND CONCLUSION

This note reports what may have been the first formation of a hurricane north of the Hawaiian Islands, or, as is more likely, the first such observed case. Dr. Neil Frank, Director of the National Hurricane Center, has stated (1975) that the ultimate measure of an analysis or forecast technique is its ability to handle the "rare" event, e.g., the explosively deepening hurricane. In this storm, the Hebert-Poteat and Dvorak systems seem to have handled a similar rarity quite well. This case again demonstrates that real-time, high resolution satellite imagery, meaningfully integrated into the man-machine mix, can make a significant contribution toward indentification and eventual solution of complex meteorological forecast and warning problems.

REFERENCES

Dvorak, V. F., May 1975: "Tropical Cyclone Intensity Analysis and Forecasting from Satellite Imagery", Monthly Weather Review, Vol. 103, No. 5, pp. 420-430.

Frank, N. F., January 1975: Verbal Comments at the NOAA Hurricane Conference, Miami, Florida.

Herbert, P. J. & Poteat, K. O., June 1975: "A Satellite Classification Technique for Subtropical Cyclones", Proceedings of Tenth Conference on Hurricanes and Tropical Meteorology, Key Biscayne, Florida.

Holliday, C. N., May 1969: "On the Maximum Sustained Winds Occurring in Atlantic Hurricanes", ESSA Technical Memorandum WBTM-SR-45, 6 pages.

(An expanded version of this note has been submitted for publication in the Monthly Weather Review.)

42

A. Track of Storm, 31 August-5 September 1975, 0000 GMT Positions

B. SMS-2 Visual 2-km Resolution, 0048 GMT 31 August 1975

FIGURE 1 Pg. 3

A. SMS-2 Visual 2 km, 0048 GMT 01 Sep 75

B. SMS-2 Visual 2 km, 2348 GMT 01 Sep 75

C. SMS-2 Visual 2 km, 2348 GMT 02 Sep 75

D. NOAA-4 Visual 1 km, 2018 GMT 03 Sep 75

FIGURE 2

U.S. DEPARTMENT OF COMMERCE

National Weather Service/National Environmental Satellite Service
SATELLITE APPLICATIONS INFORMATION NOTE 2/76-2

VERTICAL WIND SHEAR vs. UPPER FLOW AS REVEALED BY CIRRUS PLUMES - January 26, 1976

Edward C. Johnston
SFSS, Kansas City, Missouri

Frequently, the wind direction at high levels is approximated on satellite pictures by the orientation of cirrus blow-offs from cumulonimbus tops. However, such an assumption is not always valid. A good example of this phenomenon occurred on the morning of January 26, 1976.

At 1230Z, a line of thunderstorms extended southwestward from the Florida Panhandle into the Gulf of Mexico, as depicted by the radar summary chart in Fig. 1. Note the cell movement within the line, averaging 50-55 knots toward the northeast.

At this time, the upper level flow pattern revealed a rather pronounced meridional trough extending from Minnesota southward across Texas, with predominantly west to southwesterly flow over the Gulf of Mexico. The corresponding 200mb chart (Fig. 2) shows winds along the Gulf coast blowing from 250° to 265°, decreasing from 130 knots over Brownsville to 45 knots at Tampa. One might expect to see cirrus blowing off the tops of the cumulonimbus in the Gulf toward the east-northeast. But the 13Z picture shows the orientation of the cirrus streaks toward the southeast (Fig. 3).

This is an example of the important role that vertical wind shear plays in the orientation of the cirrus plumes in the picture. A vector representation of the mean flow through the convective layer and at cirrus levels illustrates this relationship (Fig. 4). Notice the shear between the mean cell movement, from about 225° at 50 knots, and the 200mb average flow in that area, 260° at around 70 knots. We have drawn the vectors tail to tail from those directions with lengths proportional to speeds (Vectors A and B in Fig. 4). The resultant wind shear is toward the southeast, as represented by Vector C. This explains the orientation of cirrus blow-offs in Fig. 3.

Examples such as this are not frequently observed, but do occur in varying degrees from time to time. The purpose of this brief discussion is to illustrate the importance of recognizing that the cirrus will align itself along the vertical shear wind vector, rather than the flow at cirrus levels. Many times the shear wind will agree fairly well with the upper flow; but not always, as illustrated here.

Ref: ESSA Technical Report NESC 51, March, 1974; pp. 4-D-1 & 2.

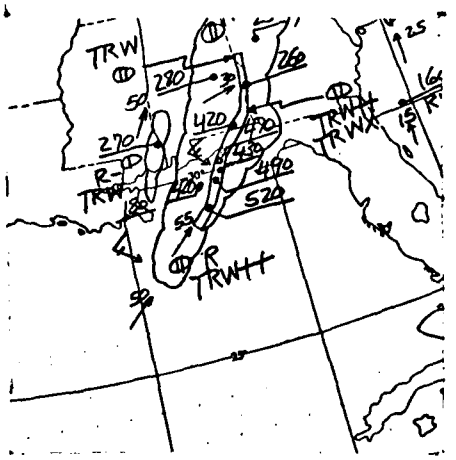

FIG. 1: RADAR SUMMARY CHART
1235Z, 26 JAN 76

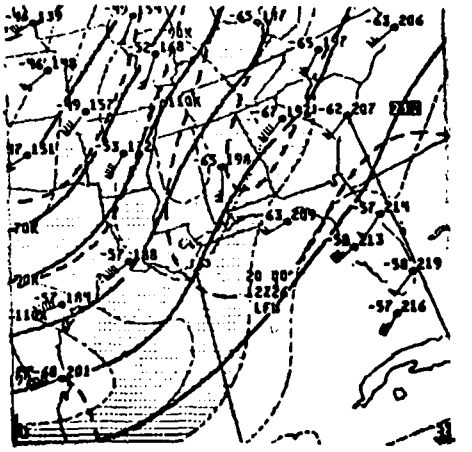

FIG. 2: 200mb ANALYSIS
1200Z, 26 JAN 76

FIG. 3: GOES-1 IR
1300Z, 26 JAN 76

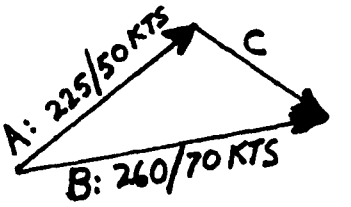

FIG. 4: VECTOR REPRESENTATION
OF VERTICAL SHEAR

U.S. DEPARTMENT OF COMMERCE

National Weather Service/National Environmental Satellite Service
SATELLITE APPLICATIONS INFORMATION NOTE 3/76-1

USING SATELLITE DATA AS AN AID TO FORECASTING FOG AND STRATUS FORMATION

James Gurka
Applications Group, NESS

Although fog and stratus are frequently observed in the Gulf and central plains states during the fall, winter, and spring when the low-level flow is from the Gulf of Mexico, it nevertheless remains a difficult forecasting problem. Now, enhanced IR satellite pictures can provide the forecaster with a new tool for forecasting the extent of warm air advection fog and stratus formation.

Frequently, areas where fog and stratus are most likely to form will appear as relatively dark areas on satellite pictures that are taken a few hours after sunset. These dark areas are normally found downwind from a moisture source, such as the Gulf of Mexico, and as noted by Parmenter (1), appear to outline the boundary of relatively moist air in the lower levels of the atmosphere. This boundary can be monitored and used as an estimate of the extent of fog and stratus formation during the night.

Of course, the extent of the moist air at the surface can be located with surface dew points. The satellite, however, has much higher resolution than the surface observation network. Furthermore, the moisture will frequently move into an area above the surface so that it does not show up on the surface reports.

On October 27, 1975 at 0200 GMT (Fig. 1), the boundary of warmer temperatures can be seen at A and B. The general pattern corresponds roughly to the area of higher dew points on (Fig. 2.) Although the moist air appears to extend into southeastern Nebraska, on the 0200 GMT picture, the dew point at Lincoln Nebraska is only 31, and those in eastern Kansas are in the mid 40's, suggesting that the moist air in southeast Nebraska is above the surface. From the ceiling and visibility chart (Fig. 3), it can be seen that there are no low clouds reported in Nebraska, Kansas, or Oklahoma at 0200 GMT. There is some stratus reported in east central and southeast Texas (C, Fig. 1).

Using the moisture pattern implied from the 0200 GMT picture, stratus formation would be expected in extreme southeast Nebraska, central Kansas, excluding the extreme eastern and western portions of the state, most of Oklahoma, except the western panhandle and extreme eastern portions, and most of Texas except the panhandle and extreme western portions. On the 1331 GMT visible picture (Fig. 6), the pattern of fog and stratus (A and B) is very similar to the moisture pattern implied from the 0200 GMT IR picture. The low clouds did not extend as far west as expected in Kansas or in the Oklahoma panhandle, as some dryer air had moved in from the west shortly before sunrise.

The area of low clouds in Arkansas (seen in Fig. 6) spread northward from an extensive area of low clouds that extended eastward to the Appalachians at 1000 GMT (C on Fig. 4). For cases such as this, where the darker area on the IR imagery indicates a low cloud boundary rather than a moisture boundary, the cloud edge is typically more well defined than the latter; but at times it is difficult to distinguish between the two. During the night, most fog and stratus, with the exception of post cold frontal stratus, appears warmer than the surrounding land areas, while fog and stratus in the daytime almost always appears colder than the surrounding land areas, which are quickly heated. In cases where the cloud edge moves into a relatively dry area, the satellite pictures can still be an aid for short range forecasting by simply making it possible to locate the position of the cloud boundaries at one half hour intervals.

However, in forecasting fog formation or any other meteorological phenomena, the satellite data cannot be used exclusively, but is simply an additional tool to be used with all the available conventional data to aid in the short range forecast. For example, chinook warming over the central plains can have a very similar appearance to an area of high moisture content. Therefore, the cause of the warmer temperatures should first be determined from the surface charts. Also, deep river valleys almost always appear warmer than the surrounding terrain at night, and should not be confused with a moisture maximum.

In summary, the pattern of relatively high moisture content in the lower levels of the atmosphere can frequently be determined from the early evening (0200 - 0300 GMT) enhanced IR satellite pictures. This information can then be used as an aid to forecasting extent of the formation of warm air advection fog and stratus during the night.

Reference: (1) Parmenter, Frances C., 1976: Low-level Moisture Intrustion from Infrared Imagery, Monthly Weather Review, Vol. 104, pp. 100-104.

48

Fig 1. SMS-1 4X4 enhanced IR imagery 0200GMT, 27 Oct 75.

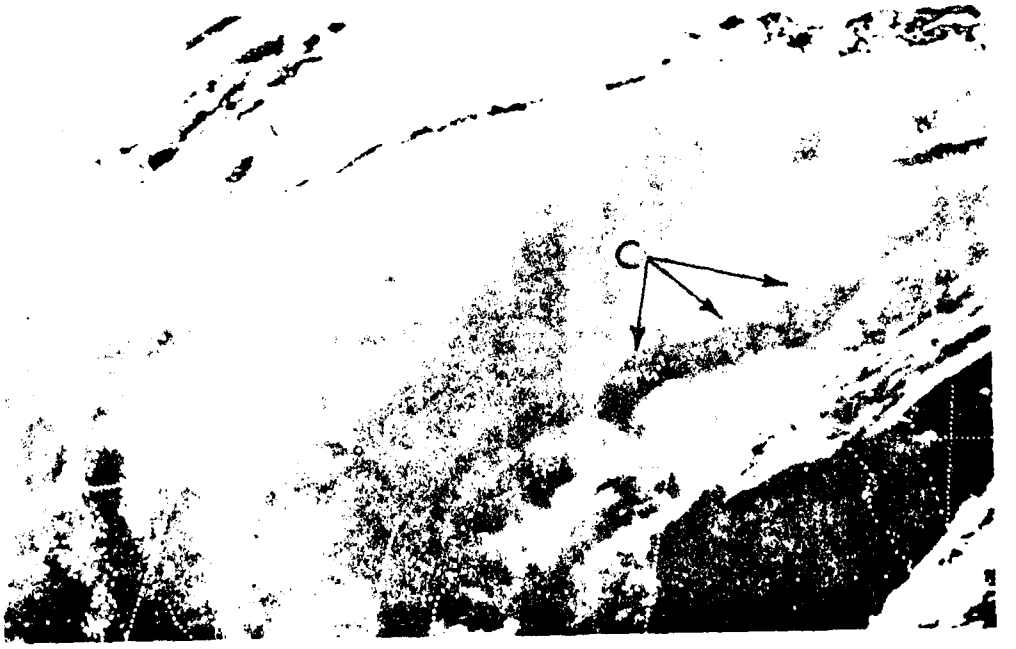

Fig 4. SMS-1 4X4 enhanced IR imagery 1000GMT, 27 Oct 75.

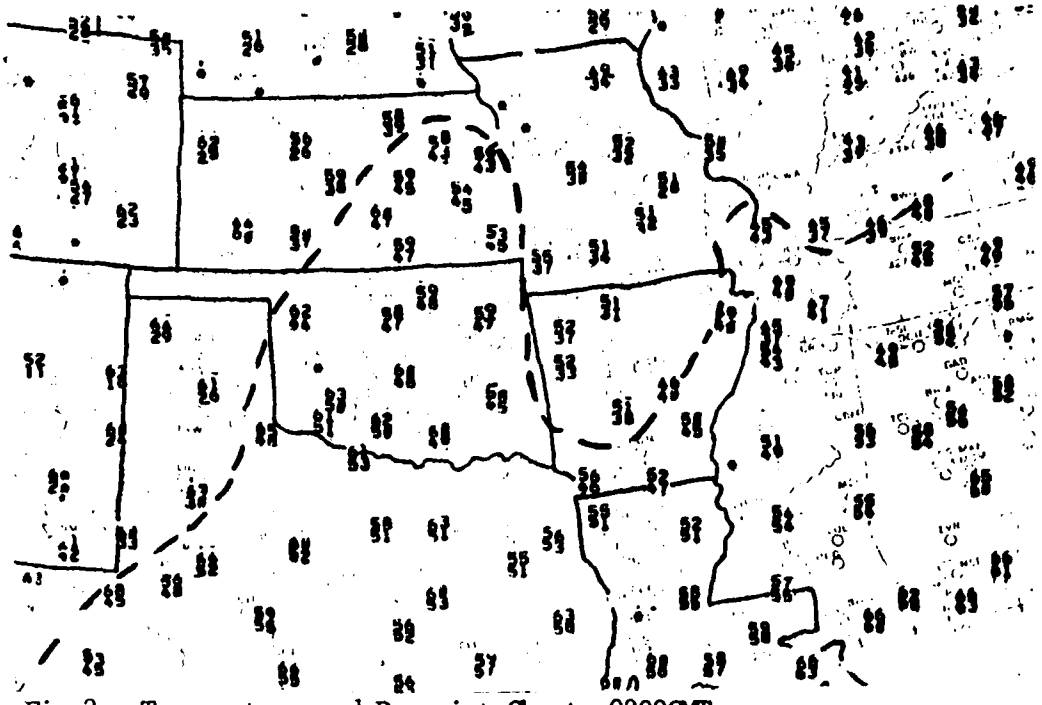

Fig 2. Temperature and Dewpoint Chart, 0200GMT, 27 Oct 75. Dashed line is 40°F dewpoint isopleth.

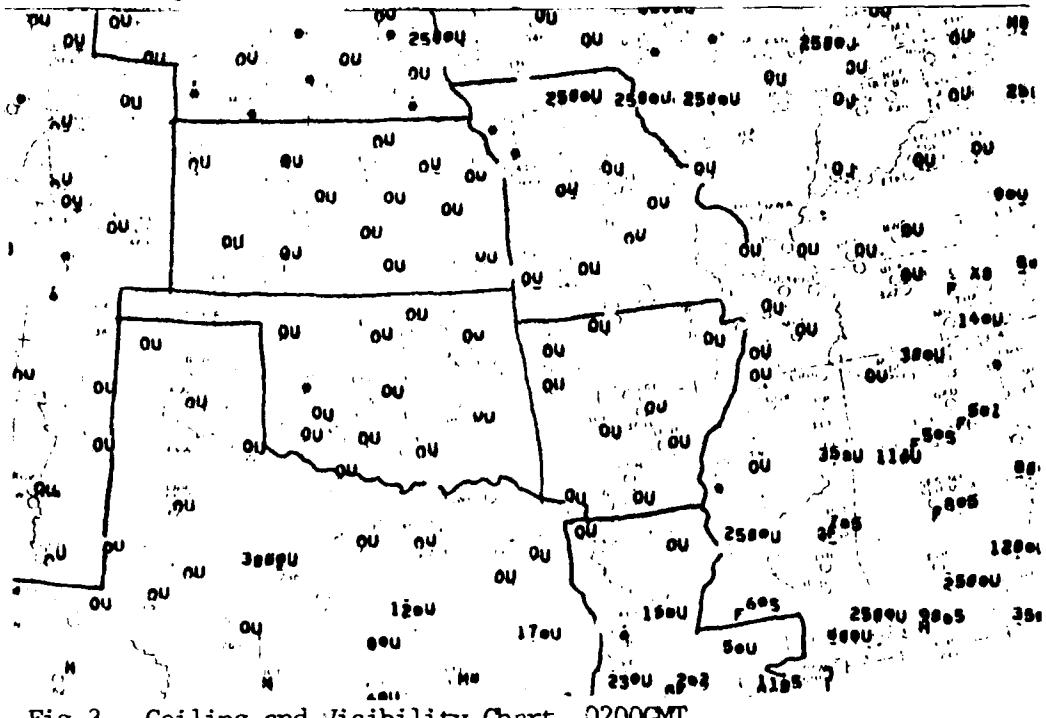

Fig 3. Ceiling and Visibility Chart, 0200GMT, 27 Oct 75. 0 indicates no ceiling, U indicates no obstruction to visibility.

Fig 5. SMS-1 4X4 enhanced IR imagery
1100GMT, 27 Oct 75.

Fig 6. SMS-1 1 km visible imagery
1331GMT, 27 OCT 75.

U.S. DEPARTMENT OF COMMERCE

National Weather Service/National Environmental Satellite Service
SATELLITE APPLICATIONS INFORMATION NOTE 3/76-2

A NEAR-STATIONARY GULF OF ALASKA LOW--
ITS EFFECT ON WEATHER IN THE PACIFIC NORTHWEST

Frances C. Parmenter
Applications Group/NESS

During the last week of February, the northwestern U.S. experienced the passage of a number of rain/snow producing sub-synoptic systems that formed and rotated around a large Gulf of Alaska low. Some of these systems came onshore and moved eastward; others were channeled northwestward along the rugged coastline back towards the Aleutians. The data for February 26 are presented. A time section of weather from three stations: Astoria (AST) and Pendleton (PDT), Oregon, and Missoula (MSO), Montana, which represent coastal, plains, and mountain environments, is also included for this day.

The initial surface analysis at 0000GMT, February 26 (Fig. 1), showed two surface lows north of 50°N. These were indicated by the two cloud vortices (L and L') in the visible (2245GMT) and IR (2345GMT) images (Figs. 2 and 3). The visible data shows a remarkably large number of organized cloud systems within this large cyclonic flow. For example, a number of old vortices that have completed a circuit about the low, can be seen in a cyclonic arc from (L' to J).

East of (L') is the cloud band (M) associated with the analyzed Canadian cold front. A well organized comma-shaped cloud pattern (N) lies ahead of the surface trough near 130°W while a smaller cloud mass (N') appears at the apex of the wave on the southernmost front.

Looking upwind, a number of equally impressive cloud patterns can be seen. Movie loops showed a low-level circulation with the comma pattern at (O) and lesser rotation with the system (P to P'); IR data located two additional areas (Q and R) as incipient stages of comma cloud development. The succeeding series of pictures show the ensuing trajectories and developments. What is of particular interest is the behavior of the cloud systems (N, N' O and P-P') and their effect on the weather at AST, PDT, and MSO (indicated by dots on Fig. 3). A time section showing altimeter, winds and weather at these stations appears in Fig. 4.

Initially (0000GMT), precipitation was occurring along the coast with showers on the mountains near PDT and light rain at MSO. The 0245GMT data (Fig. 5) shows a general eastward movement of all the systems during the intervening three hours with some important changes evident in the

small scale features. Note that the cloudiness associated with the surface wave (N') has a distinct comma shape with colder tops along the northern side. The clouds at (P') have caught up and increased the convection near the comma tail of (O) and appear to be advancing eastward faster than the cloudiness (P) north of 45°N, thus suggesting a significant speed shear at low levels.

By 0645GMT (Fig. 6), the organized cloudiness with the northward moving wave (N') has become broken by the terrain into a number of east/west bands. The upwind cloud systems (O, P) continue to show little eastward movement north of 45°N, while the southern portions continue to move NNE resulting in the re-orientation of this convection into a more zonal configuration. Pressures have st rted to fall rapidly in Oregon although surface winds remain easterly (Fig. 4). Based on the movements extrapolated from this satellite data, precipitation would be expected, once again, along the coast accompanied by a change to southerly winds at increased speeds. At MSO, precipitation would also be expected as the remnants of the wave (N') move across the initial cloud band (N). This can be seen in the short period fluctuation of winds, fall in pressure, and increasing snow shower activity from 0600GMT.

By 1100GMT, light but continuous snow was reported at MSO. A look at the 1145GMT data (Fig. 7), shows that this precipitation originated from the orographically produced cirrus and alto-stratus cloudiness that frequently forms in areas of PVA. During this period another system (S) moved from California into southern Oregon. Note that the cloudiness at (P') has become more organized and still poses a threat to the Oregon coast. Winds have changed from light southerly to SW, gusting to 23 knots at AST.

The 1345GMT data (Fig. 8) shows that the cloudiness marking the approaching vortex (P') had increased in areal coverage, but no precipitation was reported at AST. A slight northeastward movement of the cloud band (N) during this period saw the end of snow at MSO.

Falling pressure and snow showers mark the approach of the next system (S), (Fig. 9) into Idaho and Montana. Snow showers continued over the higher terrain near PDT along the comma tail. Only a brief period of distant snow showers was reported with the cloudiness (P') at AST.

In the last view (Fig. 10), the system (P') and (S) can still be located. Note the bright anticyclonically shaped cirrus in Idaho and Montana. Ice crystals from this cirrus plume appear to effectively seed the underlying stable cloudiness producing continuous light to moderate snow throughout the area.

In the mountainous region of the western U.S. where light ranges are treated, close monitoring of satellite imagery and local weather trends as are those presented here allow the forecaster to better understand the occurrence of intermittent precipitation events. Enhanced IR imagery can further detail the observations by indicating the active areas of approaching system.

ESSA: The title of Note 3/76-1 should read "Using Satellite Data As An Aid to Forecasting Fog and Stratus Formation; paragraph 2, page 1, line 3...upwind should be downwind.

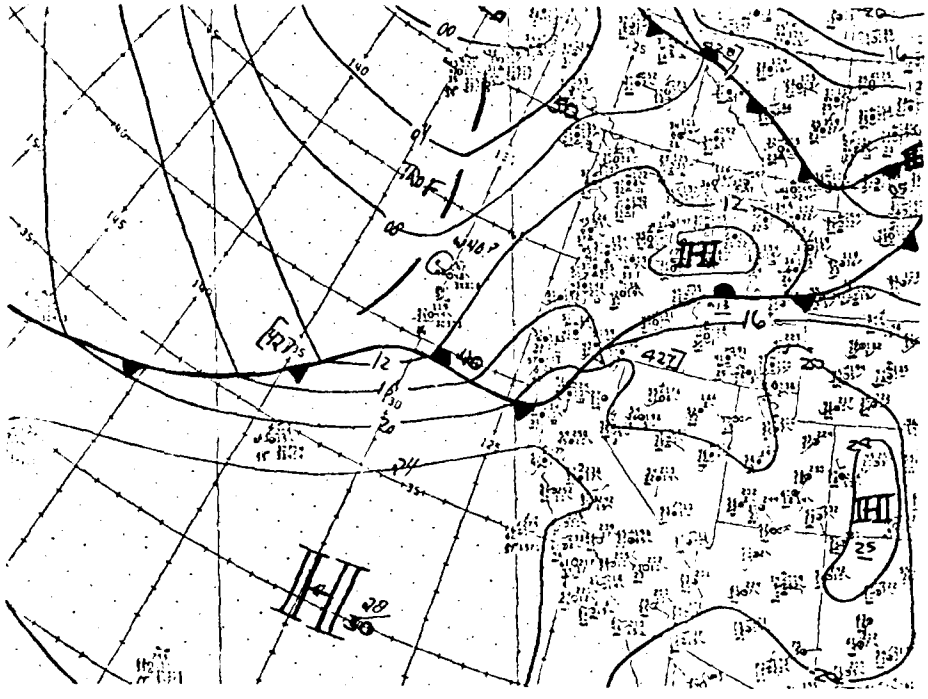

Figure 1. Surface Analysis, 0000 GMT
26 February 1976.

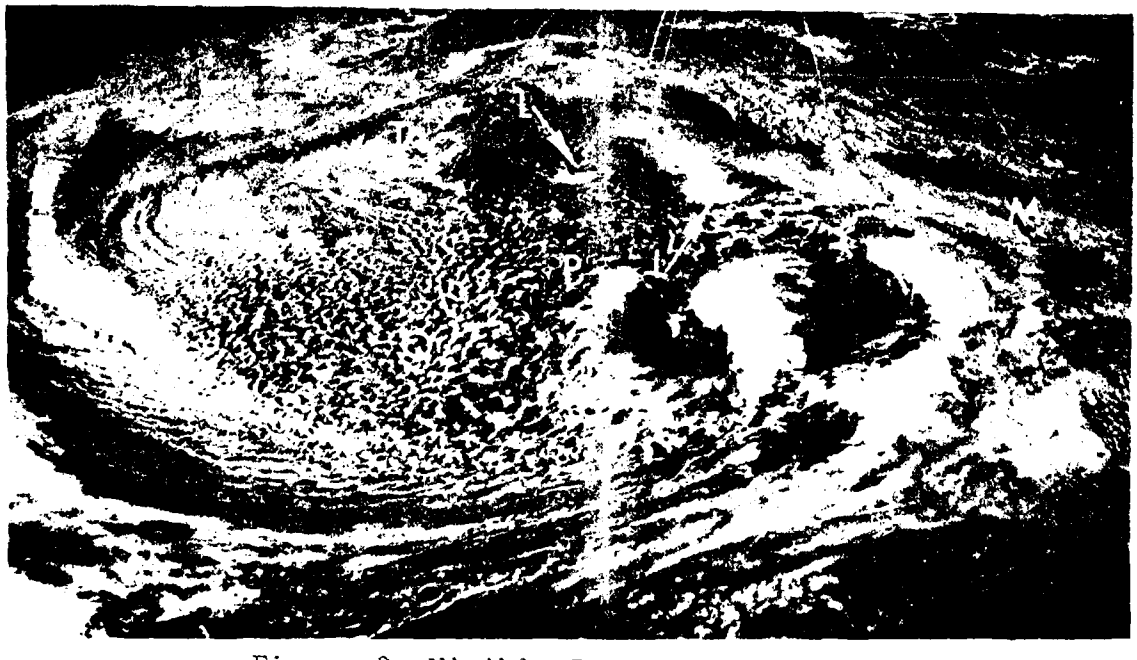

Figure 2. Visible Imagery SMS-2
2245 GMT, 25 February 1976.

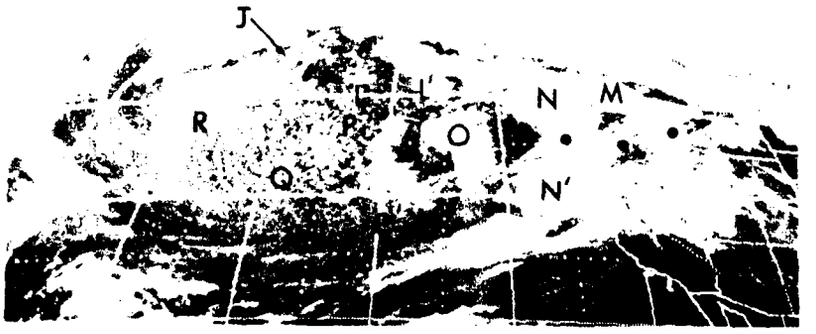

Figure 3. Infrared Imagery SMS-2
2345 GMT, 25 February 1976.

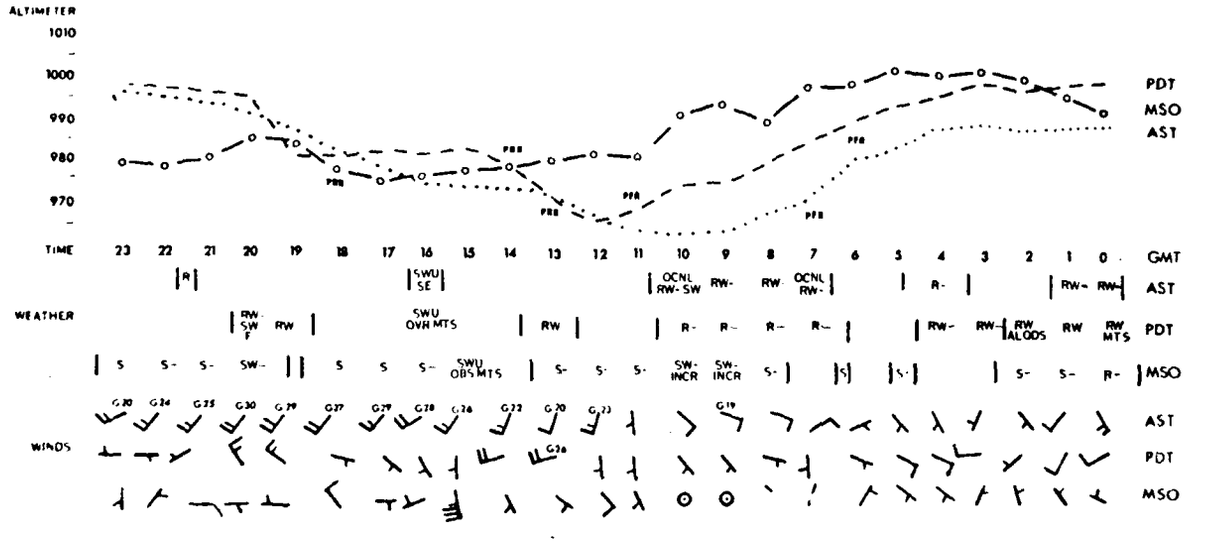

Figure 4. Time section (increasing from right to left) of altimeter, weather and winds at three stations: Astoria (AST), and Pendleton (PDT), Oregon, and Missoula, Montana for 26 February 1976.

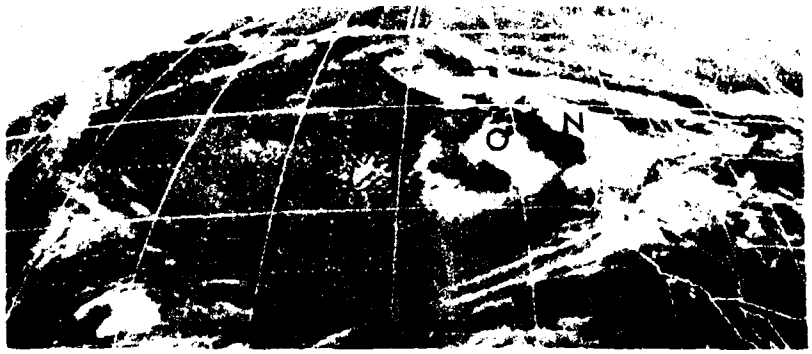

Figure 5. Infrared Imagery SMS-2, 0245 GMT 26 February 1976.

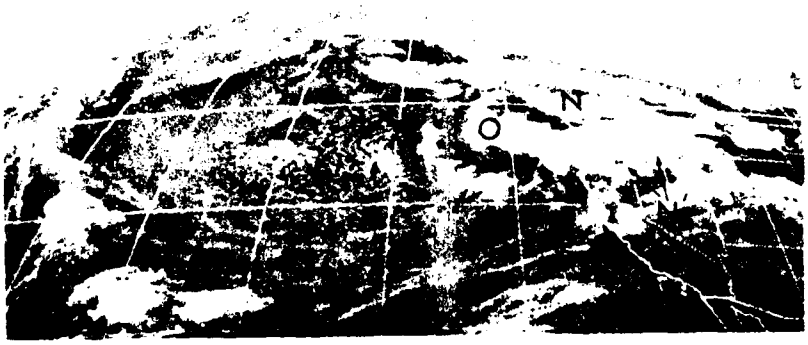

Figure 6. Infrared Imagery SMS-2, 0645 GMT 26 February 1976.

Figure 7. Infrared Imagery SMS-2, 1145 GMT 26 February 1976.

57

Figure 8. Infrared Imagery SMS-2,1345 GMT
26 February 1976.

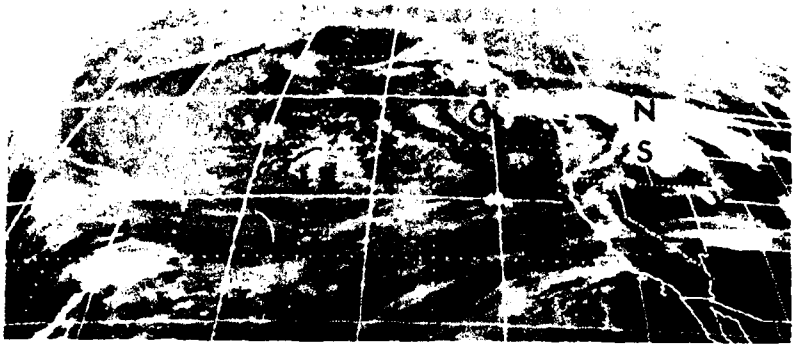

Figure 9. Infrared Imagery SMS-2, 1545 GMT
26 February 1976.

Figure 10. Infrared Imagery SMS-2, 1745 GMT
26 February 1976.

U.S. DEPARTMENT OF COMMERCE

National Weather Service/National Environmental Satellite Service
SATELLITE APPLICATIONS INFORMATION NOTE 76/7*

OCEAN THERMAL FEATURES AS SEEN FROM GOES-1

Stephen R. Baig
Satellite Field Services Station, Miami, FL

The National Weather Service has recently introduced a "Gulf Stream Wall Bulletin" as an adjunct to regular East Coast weather broadcasts for mariners. The bulletin provides the location of the western edge (cyclonic edge) of the Gulf Stream.

The National Environmental Satellite Service makes input to this product with thermal infrared data from both the NOAA-4 (polar orbiting) and GOES-1 (geostationary) satellites. This note will describe some of the Miami SFSS experience with GOES-1 from the marine viewpoint.

There can be little doubt that for non-spatially limiting features, imagery from a geostationary satellite is much preferable to that from a polar orbiting satellite, at least where there are no features to provide easy registration of latitude and longitude.

The second and perhaps most important advantage of the GOES-1 data is that it provides an image every half-hour instead of every twelve hours of the entire Gulf Stream region. Ocean features do not move with speeds which would require images more often than once every few days, were it not for the overlying clouds. When a few hours of GOES-1 imagery are used to prepare an animated movie the data seem to come alive! Small cloud-free areas move along with the air flow, revealing the positions of thermal features in the nearly stationary water below. The satellite analyst's eye persistence integrates this information, allowing the thermal features in the water to be described with a continuous contour.

The images used for the preparation of the animated movies are "enhanced" to better display the weak thermal gradients found in the ocean. NESS oceanographers have prepared a number of different enhancements for various parts of the ocean. For the Gulf Stream and adjacent waters the most useful enhancement currently available is labeled "S" (The type of enhancement displayed in a GOES image is indicated in the picture header.) A description of the S-curve enhancement is included in the "Enhancement Kit" available at all WSFO's.

It is expected that, as more interest is generated within the marine community, the marine forecasts will be asked to supply not only the Gulf Stream Wall Bulletin but also more detailed information about

---

* We've been asked by subscribers to number the notes serially for each calendar year. So far in 1976 we've distributed 2 Information Notes in each of the first 3 months and this one in April for a total of 7.

thermal features in smaller areas, and the changes features undergo after the Bulletin has been issued. Indeed, the increased number of observations provided by GOES-1 imagery already has shown us a higher variability in the Gulf Stream position than had been generally recognized.

Occasionally the cloud conspires to clearly reveal large portions of the oceans. An example is shown in Figure 1. The Gulf Stream system is well defined from near the Georgia coastal zone downstream to a position south of Nova Scotia. A series of small edge waves can be seen along the cyclonic edge.

Southeast of Cape Hatteras a pool of cool water is nearly surrounded by a warm band. Two well defined warm eddies can easily be seen in the slope water between the cyclonic edge and Nova Scotia. Data from recent research cruises into similar eddies shows that the water is uniformly warm right to the bottom of such eddies, (Apel & Byrne). Many such features can be tracked from day-to-day.

In the Gulf of Mexico a good portion of the Eastern Gulf Loop Current is visible. This water bulges into the Gulf and then breaks off, forming a gigantic warm eddy. The process repeats on an annual cycle (Maul, 1975). Knowledge of the extent and position of the features described above are of immense value to merchant shipping as well as fisheries interests.

In the Eastern Pacific two patches of cold water can be seen extending out from the shore. One, near 16N98W, is the result of the classic Tehuantepecer, cold air being funneled through the mountain pass of the Isthmus of Tehuantepec. The second patch extends seaward from near 12N86W. In this case air is funneled over the Lake Managua region. These low level jets cause a seaward displacement of the usually warm surface water and brings colder deep water to the surface. In both areas the marine forecaster can therefore infer the direction and relative magnitude of the low level winds. Note also that the wind stress curls the cold water to the right.

It should be noted that only a few hours before this GOES image was made the entire Gulf Stream system was covered by cloud. A few hours after this iamge was made, cloud again obscured the Gulf Stream. By monitoring the images on a 30-minute schedule the marine forecaster can request ocean enhanced images timed to provide him with a maximum of information. By contacting the oceanographer or hydrologist at the NESS/SFSS serving him the marine forecaster can obtain other information which will be useful in his forecast speciality.

Figure 2 shows the analysis made from the movie loop prepared using a series of images including figure 1. These loops are analyzed every day at Miami. On Tuesdays a final weekly analysis is prepared, on

66

tracing paper, using Tuesday's data. If a portion of the area is obscured, then data from Monday is used, and so on. In this way the latest available data is included in the final weekly analysis. If an area is obscured for more than one week, no data is shown on the analysis. By hanging the most recent analysis over those of the previous weeks, changes can easily be seen and data from previous weeks used to estimate positions in the breaks in the most recent analysis.

REFERENCES

Apel, J. and Byrne, M., Personal Communication.

Maul, G. A., "An Evaluation of the Use of the Earth Resources Technology Satellite for Observing Ocean Current Boundaries in the Gulf Stream System', NOAA Tech Report, ERL 335-AOML 18, 1975.

61

Figure 1. GOES -1 Enhanced IR (S-Curve) showing oceanographic features at 0300 GMT, 28 February 1976.

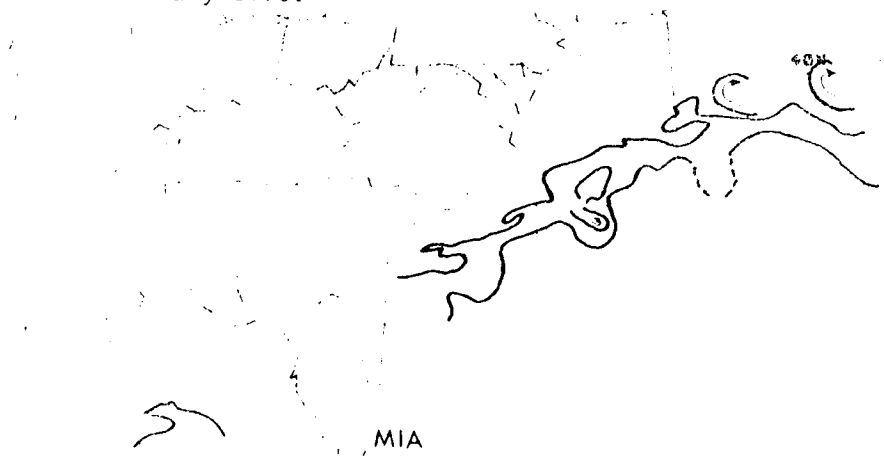

Figure 2. Gulf Stream and Loop Current analysis derived from data in Figure 1.

64

U.S. DEPARTMENT OF COMMERCE

National Weather Service/National Environmental Satellite Service
SATELLITE APPLICATIONS INFORMATION NOTE 76/8

THE EAST COAST WINTER STORM, 1-2 FEBRUARY 1976, A CASE STUDY

Richard M. Clark
NOAA/NESS, Satellite field Services Station
Washington, D.C. 20233

This storm produced the first significant snowfall of the winter season in the Washington, D.C. area. Although only one inch of snow was officially reported at Washington National Airport (DCA), strong winds and plunging temperatures, which accompanied the passage of a cold front after the storm passed to the northeast of DCA, whirled the snow into near blizzard conditions that made driving hazardous and closed most schools. The purpose of this paper is twofold: First, the origin of the storm is unique in that it can be traced from over southern Baja, CA as an upper level cold-core low. Secondly, as the storm moved from the Gulf of Mexico up the east coast the night of 2 February 1976, the author, who was on duty in the Washington SFSS, had an opportunity to observe, compare, and comment on the relative merits or disadvantages of three different enhancement curves of GOES-1 infrared (IR) imagery. The first of the three curves was the Z curve which was developed for general purpose meteorological use with the full disk IR. This curve is primarily used for film loop production by the Satellite Field Services Station and the NESS Satellite Winds Group. It also is forwarded via GOES Fax to NWS WSFOs, supported by the Washington SFSS, who desire receipt of alternate visible-infrared images on the Washington one mile resolution sector (DB-5). During the nighttime hours it is alternated (every other image) with an IR image having one of 12 different enhancement curves currently being tested and improved by NWS Field Forecast Offices and the Washington SFSS. As seen in Figure 1, temperatures from 56.8°C will appear as black areas on the satellite images with the Z curve. Enhancement is applied to lower warm clouds (Segment 2) and high level, cold clouds (Segments 4 & 5), while a slope factor of 1 is applied to middle level clouds (Segment 3). The G curve was enhancing the IR images as the storm was in the Washington SFSS area of responsibility (Figure 2). The objective of this display is to enhance both for fog/stratus (Segment 2) and convection with one curve (Segments 4 - 8). Segment 3 of this curve ranges from -3.2°C to -21.7°C. This wide, black buffer zone is an attempt to differentiate between the warm and cold ends of the curve. As seen on later images, a considerable area of data was blacked out by the black buffer zone but this was primarily with clear skies after the storm had passed, so was of little consequence. On the positive side, Segments 5 & 6 showed middle clouds and lower cirrus while Segments 7 & 8 clearly depicted convective areas. The third enhancement curve being monitored was the

M curve (Figure 3). This curve was set into one of the Washington SFSS floaters. The primary purpose is to enhance convective activity by using an alternating gray shade step-function format for the coldest temperatures. All data warmer than -32°C are displayed linearly (Segment 2) but with a steeper than normal slope factor of 1 to produce some enhancement. Convective areas stand out well, especially Segments 5, 6, & 7, and they are easy to interpret.

The author first noticed a well defined comma-shaped circulation of middle and high clouds south of El Paso, TX over Chihauhau, Mexico on the early 30 January 1976 IR film loop. A vorticity center was drifting to the southeast and by 00Z 31 January appeared to be just south of Laredo, TX. After the storm passed the Washington area, a call to the NWS San Antonio Forecast Office (WSFO) revealed that they had been monitoring this system earlier on the Kansas City SFSS KB-8 sector from the NESS SMS-2 satellite. San Antonio WSFO provided Figures 4 and 5 for this study. Both images are enhanced IR with the Z curve. Figure 4 is the 2215Z, 28 January image which shows the early stages of development of the system. The bright clouds over lower Baja, the Gulf of California, and Mexico, depicted as "Ci:, are high, cold cirrus moving in the direction of the arrow. By 0115Z, 31 January (Figure 5) the upper level cloud shield has increased with the leading edge extending eastward over the Gulf of Mexico, again depicted as "Ci". Cloud cover had increased with the familiar comma shape, indicative of positive vorticity, with the center of rotation near notation "O". This center correlates well with the National Meteorological Center (NMC) 300 MB Analysis at 0000Z, 31 January which placed a closed low southwest of Laredo, TX (Figure 6). The corresponding Surface Chart (Figure 7) had a weak surface low near Tucumcari, NM with variable middle and high clouds over the area. 24 hours later, at 00Z, 01 February, a surface low with closed circulation was centered over Louisiana (Figure 8). By 1500Z, 01 February, NMC had placed the apex of an open wave frontal system near Tallahassee, FL (Figure 9). Aloft, a north to south trough of low pressure extended to all levels from a low over James Bay in the north to over New Orleans in the south (Figures 10, 11, and 12). Positive vorticity was being advected rapidly to the east as seen on the NMC Barotropic Chart (Figure 13). The 1500Z, 01 February, Visible 1 mile resolution GOES-1 image (Figure 14) correlates well the position of the open wave as seen on Figure 9. A line of thunderstorms is along and ahead of the frontal position over the Gulf and north across Florida and over central Georgia. Dense cirrus overcast covers most of South Carolina and the eastern half of Georgia. Rain is falling over Georgia, the Carolinas, and Virginia with snow showers over New England and Central Pennsylvania. An opportunity to compare the enhanced G and M curves with one of the last visible images before darkness covered the East Coast was at 2130Z. By this time the open wave was over Augusta, GA (Figure 15) and the trailing cold front had crossed the Florida Peninsula and paralleled 80°W offshore. Comparing the 2130Z Visible (Figure 16) with the 2130Z enhanced M curve (Figure 17), and the 2100Z enhanced G curve (Figure 18), an important feature on each of the three images is the north/south

64

trailing, or western edge of the dense cirrus shield which extends from over Roanoke, VA south to Columbia, SC, then offshore north of Savannah, GA. These stations are indicated by R, C, and S on the 3 satellite images. A wedge of cold, dry air has moved in behind the frontal zone causing skies to clear over coastal areas of Georgia and the Gulf Coast states to the west. The M curve enhanced IR (Figure 17) also shows the sharp break over the Carolinas between the warm lower clouds to the west and the higher colder clouds to the east. The location of the offshore thunderstorms, as indicated by the symbols on the visible image, are fairly easy to locate because of low sun angle. However, some cells are undoubtedly lost in the dense cirrus overcast which covers the offshore area north to southern Delmarva. The M curve shows a good correlation between known convective areas and Segment 6 (black) and Segment 7 (white). For example, the black area of Figure 17, along the North Carolina coast, northeast of Cape Fear, was being tracked by Wilmington (ILM) radar. Unfortunately, Hatteras radar was inoperative during this time period. The author has depicted the dark gray areas (Segment 5) over the Carolinas as indicative of towering cumulus (Code 3) since moderate rain was reported through this area. The G curve (Figure 18) correlates well with the M curve in depicting thunderstorm areas. This is especially true of areas 1, 2, 3, and 4. Individual cells and clusters of cells appear to protrude above the black (Segment 7) areas. The white, hazy appearance (Segment 8) of the image over the black areas is cirrus blowoff from overshooting CB tops. On later images this cirrus is seen being pushed to the northeast by strong southwesterly flow. The disadvantage of this curve is the large areas of data blocked out by the buffer zone (Segment 3) which saturates the image with black. Some of these buffer areas are indicated on Figure 18 as "B".

The next series of images shows the rapid northeast movement of the storm but more dramatically shown is the intensification of offshore convection ahead of, and along, the trailing cold front. As seen on Figure 19, at 0300Z, 03 February, the surface low was centered over eastern North Carolina. The 0300Z enhanced IR with Z curve, (Figure 20) shows a large area of convection north of 35°N and between 70°W with scattered cells to the south ahead of the cold front. Figure 21, with the 0330Z M curve, shows a very large increase in the areas covered by the black, Segment 6, and white, Segment 7. Figure 22, with the 0330Z G curve, shows a similar areal coverage of Segment 8 (white), when compared with the M curve area of temperatures colder than -52°C, or the combined areas of Segments 5, 6, and 7. Of interest on Figures 20,21, and 22, are the enhanced clouds over central North Carolina and southcentral Virginia. This represents an area of positive vorticity advection (PVA) which moved over the Carolinas with the upper-level trough. Its center is seen over Louisiana on Figure 13. This is what the satellite meteorologists normally look for when viewing the IR movie loops - positive vorticity advecting over an area at mid-tropospheric levels. PV centers are usually best defined on IR imagery as middle-level alto clouds as opposed to higher,

65

colder cirrus clouds. As such they are warmer than cirrus clouds and appear darker than cirrus on the IR image with Z curve, yet brighter than lower, warmer clouds. Tracking the vorticity induced clouds gives the field meteorologists an opportunity to compare the NMC 5 panel Barotropic and Baroclinic models and LFM packages to the actual speed and direction of vorticity and moisture advection.

Also of interest on this series of images is the rapid movement to the northeast of the trailing or western edge of the high cirrus cloud shield noted on Figures 16, 17, and 18. The trailing edge now extends from over Norfolk, VA northwest to near Charlottesville, VA representing a speed of approximately 65 knots to the northeast. It was near the same time as this series of images that Patuxent River radar started painting buildups east of the Delmarva Peninsula. These cells moved northeast and were off the 125 nm remote scope by 0445Z. The storm continued to move rapidly up the east coast and by 1500Z, 02 February, had deepened to 958 mb and was centered over Maine (Figure 23). During the night the M curve was dropped from the imagery. However, the 1400Z enhanced IR with Z curve (Figure 24) depicted the offshore frontal position with a line of CB ahead of the cold front. Cold, bright cirrus tops are also seen over the Gulf of St. Lawrence and northern New Brunswick with the upper level vorticity center (PVA) near Portland, ME. Cold, dry air follows the surface position of the front and a dry slot is seen northeast of Maine over New Brunswick. Behind the front to the coast is predominately broken to overcast low clouds. A dry slot is also seen in the offshore low clouds from near Bar Harbour, ME south to 35°N. Skies over Virginia and the southeast states are mostly clear. The 1500Z enhanced G curve image (Figure 25) correlates both the existence of the line of CB ahead of the cold front and the two dry zones described from Figure 24. The black buffer zone B again appears over Virginia and North Carolina.

In summary, although based on a limited number of images, it appears that the M curve is superior to both the Z and G curves for routine, operational use. Convective cells on enhanced Z curve imagery may be hidden or difficult to locate when embedded in multi-layered cloud shields. Also, the M curve with 5 step-boundaries to provide temperature contours for quantitative height determination does a good job of differentiating warm, low clouds from middle level clouds as well as showing convective areas. The G curve may be superior to the M curve for showing individual thunderstorms or clusters of convection. However, the large areas of data blacked-out by the buffer zone on this curve may discourage its routine use by forecasters.

Editor's Note

Since the writing of this paper, a modification has been made to the M curve. The new M curve incorporates the same slope factors 1, 2, and 3 as the Z curve (Figure 1); maintains Segments 3, 4, 5, and 6 of the M curve (Figure 3); and incorporates a slope similar to that of the G curve (Figure 2) at the coldest end. This new M curve should therefore be able to handle most of the enhancement needs for routine satellite meteorology analysis.

66

LIST OF FIGURES

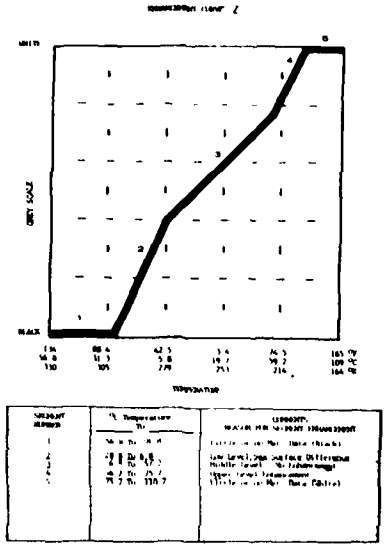

Fig. 1 Enhancement Curve Z

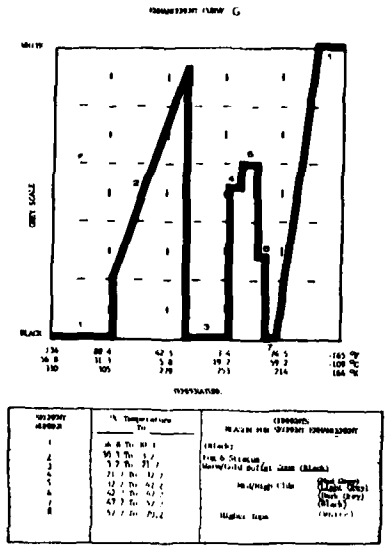

Fig. 2 Enhancement Curve G

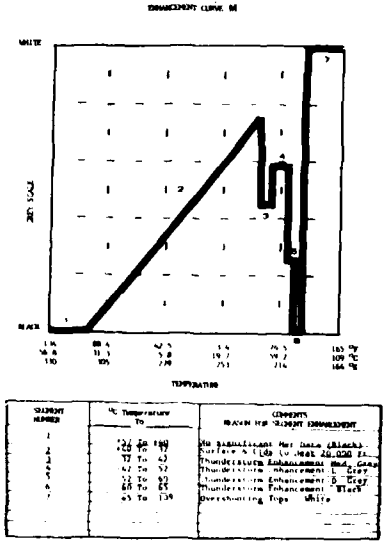

Fig. 3 Enhancement Curve M

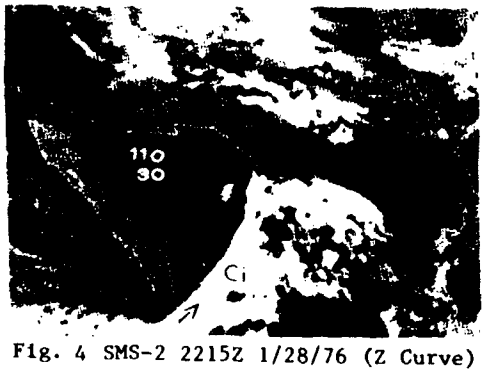

Fig. 4 SMS-2 2215Z 1/28/76 (Z Curve)

Fig. 5 SMS-2 0115Z 1/31/76 (Z Curve)

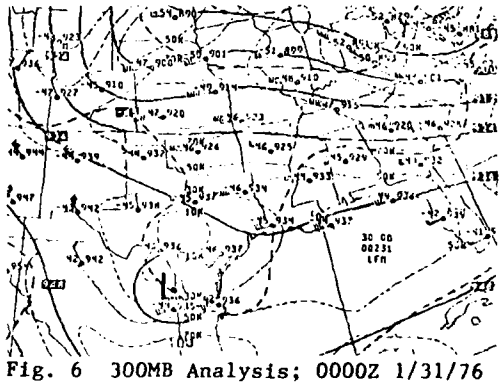

Fig. 6 300MB Analysis; 0000Z 1/31/76

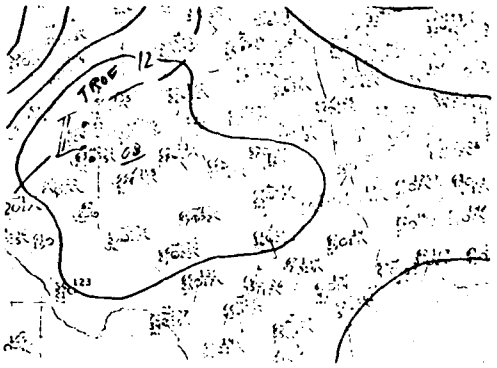

Fig. 7 Sfc. Analysis; 000Z 1/31/76

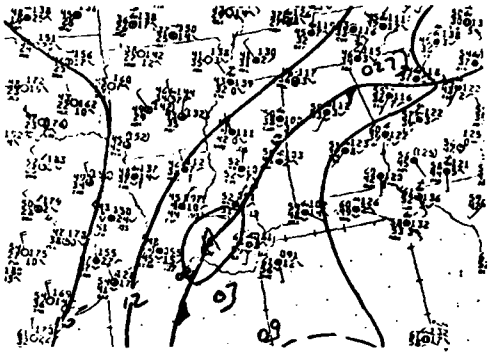

Fig. 8 Sfc. Analysis: 0000Z 2/1/76

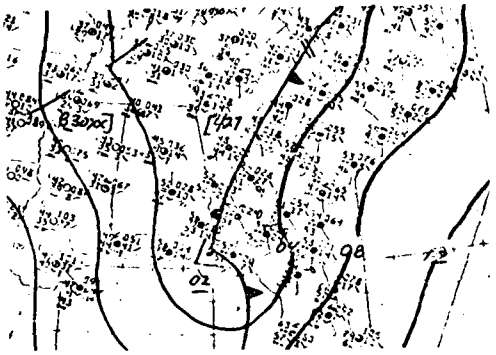

Fig. 9 Sfc. Analysis: 1500Z 2/1/76

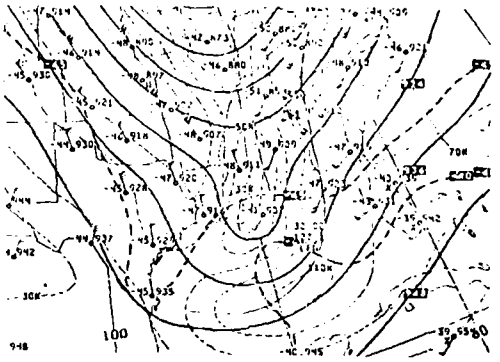

Fig. 10 300MB Analysis: 1200Z 2/1/76

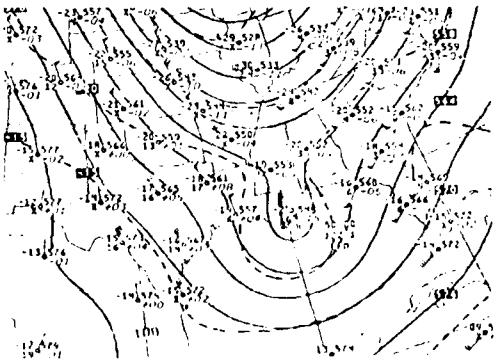

Fig. 11 500MB Analysis: 1200Z 2/1/76

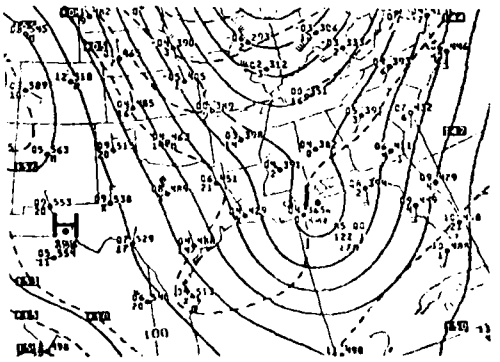

Fig. 12 850MB Analysis: 1200Z 2/1/76

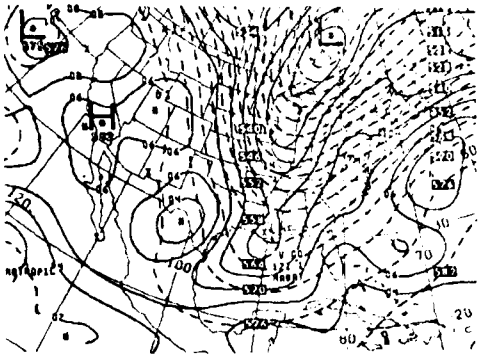

Fig. 13 BATROP Anal: 1200Z 2/1/76

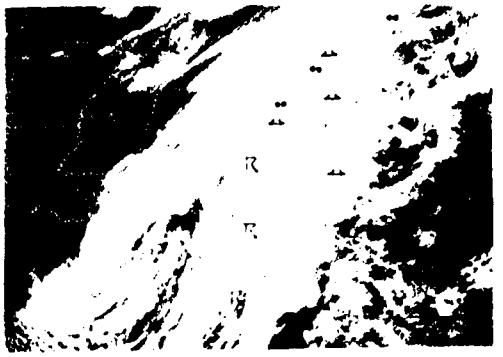

Fig. 14 GOES-1 Visible: 1500Z 2/1/76

Fig. 15 Sfc. Analysis: 2100Z 2/1/76

Fig. 16 GOES-1 Visible: 2130Z 2/1/76

Fig. 17 GOES-1 IR (M Curve) 2130Z 2/1/76

Fig. 18 GOES-1 IR (G Curve) 2100Z 2/1/76

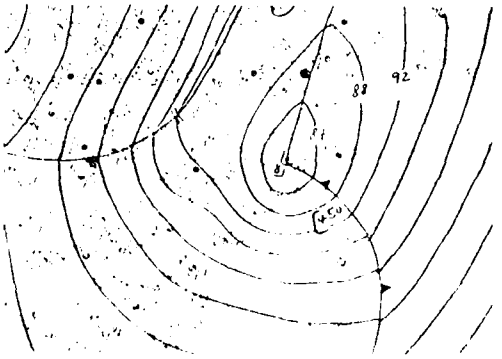

Fig. 19 Sfc. Analysis: 0300Z 2/2/76

Fig. 20 GOES-1 IR (Z Curve) 0300Z 2/2/76

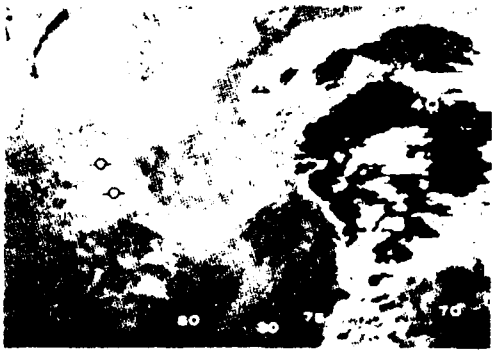

Fig. 21 GOES-1 IR (M Curve) 0330Z 2/2/76

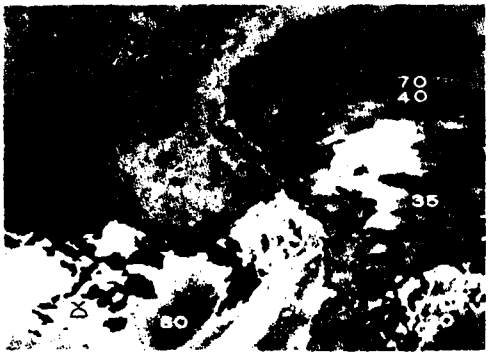

Fig. 22 GOES-1 IR (G Curve) 0330Z 2/2/76

Fig. 23 Sfc. Analysis: 1500Z 2/2/76

Fig. 24 GOES-1 IR (Z Curve) 1400Z 2/2/76

Fig. 25 GOES-1 IR (G Curve) 1500Z 2/2/76

U.S. DEPARTMENT OF COMMERCE

National Weather Service/National Environmental Satellite Service
SATELLITE APPLICATIONS INFORMATION NOTE 76/9

CONVECTIVE TRIGGER MECHANISM AS VIEWED BY GOES-1

Edward C. Johnston
Satellite Field Services Station, Kansas City, MO

During the early morning hours of Tuesday, March 24, 1976, a significant upper air feature was detected in the satellite imagery which rather strongly influenced the surface weather over parts of the central U.S. later in the day. A brief explanation follows.

At 07Z on the 24th, an upper trough extended southward from a vorticity center north northeast of Williston, North Dakota to the northwestern corner of New Mexico. The trough was translating eastward at 30-35 knots, in good agreement with the interpolated barotropic position and speed. However, shortly thereafter, a spiraling cloud configuration (V Fig. 1) appeared along the Nebraska - South Dakota border. Though none of the prog packages showed evidence of this system, a definite cloud rotation could be seen near Valentine, Nebraska on the movie loop at 09Z. This feature was moving eastward at 35-40 knots and accelerating, with indication of a subsequent turn toward the northeast. Positive vorticity advection (PVA) ahead of the poorly defined vorticity comma tail helped trigger convective development (T Fig. 2) along the 850mb thermal ridge from northern Oklahoma to eastern Iowa in advance of the surface frontal system. By 13Z (Fig. 2) the center had accelerated to near 50 knots and had moved into southwestern Minnesota, with an associated short wave trough through western Iowa.

It was learned later that WSFO Milwaukee, Wisconsin (indicated by (o) Fig. 2 and 3) had updated their morning state forecast to include a chance of thundershowers during the day over most sections. Surface conditions were not particularly favorable for convective development at the time, as temperatures were in the 40's with dew points in the low 30's. Later conversation with the WSFO revealed that the revised forecast was based on the possibility of a short wave coming out ahead of the mean trough, and that the final decision was influenced by the satellite interpretation message which called attention to this impulse.

By 1630Z (Fig. 3) the vorticity center (V) had moved into northwestern Wisconsin. Strong PVA ahead of the associated short wave was generating convective activity (T) over Wisconsin, verifying the earlier updated forecast.

This is one of several cases observed this spring in which significant PVA has been one of the more important factors in generating convection. The presence of this impulse, which was not detected by the 00Z March 24 vorticity progs, was obviously a major contributor to the convective development that occurred on this particular morning.

73

Fig. 1: GOES-1 4x4 IR
09Z, 3-24-76

Fig. 2: GOES-1 4x4 IR
13Z, 3-24-76

Fig. 3: GOES-1 2 MI VIS
1630Z, 3-24-76

U.S. DEPARTMENT OF COMMERCE

National Weather Service/National Environmental Satellite Service
SATELLITE APPLICATIONS INFORMATION NOTE 76/10

TECHNICAL ATTACHMENT

BRIEF ANALYSIS OF AN ARC CLOUD AND ITS EFFECTS ON A NEARBY THUNDERSTORM

Daniel L. Smith
WSFO, Birmingham, Alabama

Since the introduction of routine GOES Imagery there has been increasing awareness and documentation of arc clouds* and effects associated with them. Unfortunately, little of this documentation has originated from the field and there may remain some doubt whether features of this scale can be incorporated into our forecast and warning procedures - even when recognized in the imagery. The present report concerns the occurrence of an arc cloud which was unusual (to the author) in two respects. First, the arc cloud was observed in IR imagery at night. This is unusual because the cloud is a low level and relatively warm feature. Second, the major effect of the cloud appears to have been enhancement of an existing thunderstorm. Usually we try to anticipate where an arc cloud may induce new development.

The accompanying figures show the sequence of events in East Texas during the early evening of March 25, 1976. From 0000 to 0230 GMT enhanced (curve MB) and unenhanced IR images are shown and at hourly intervals the corresponding MDR(1) data are included for comparison. In the MDR plots Dallas (D) and Tyler (T) are indicated to serve as reference points. At 2330 (all times GMT) the last visual image of the day shows an arc cloud emanating from an eastward-moving group of intense thunderstorms in the vicinity of Shreveport. The arc cloud is moving westward. In all photographs, the arc is just at the point of the arrow - it was very faint in the original images and in the process of reproduction may be difficult to observe.

Between 2330 and 0030 the arc cloud propagated westward toward the group of thunderstorms southwest of Dallas. MDR data and satellite images suggest that these thunderstorms moved very little during this hour. Based on imagery available at 0030 we anticipated at that time that within an hour these thunderstorms would intensify rapidly along the eastern edge of the cloud mass. Since our main concern is far from East Texas, we had no way of knowing whether this expectation was reasonable in light of additional conventional data or whether the previous state of events supported this estimate. The passage of the arc cloud at Tyler

---

*"Arc cloud" is a misnomer but use of the term will be continued here. Actually, the miniature cold air mass which originates from a thunderstorm, of which the arc cloud is only (sometimes) a visible manifestation, is the meteorological feature of interest.

(1)Manually Digitized Radar

might have been seen in conventional surface data but in this case was probably obscured by the thunderstorms themselves. It could not be seen in the hourly observations which may mean only that the scale of the phenomenon is too small.

At 0100 the arc cloud appears to have just passed under the eastern edge of the thunderstorm cloud area. The satellite picture is ungridded at 0130 but the arc cloud can be seen extending northward from the top of the cloud area. At 0130 the MDR data shows an eastward movement (or development) of the thunderstorms although intense echoes (MDR 8) are still located southwest of Dallas. The MDR 8 values near Tyler do not seem to agree with the satellite photo. These MDR squares are well beyond the effective range of the Stephenville radar and the MDR values are based on intensity estimates. (The echoes were noted as TRWU in the body of the radar SD report.)

Part of the arc is still visible at 0200 and the enhanced IR image clearly shows that our expectation was verified - whether or not the arc cloud was the cause. The sketch beside the 0200 picture shows the outlines of the thunderstorm cloud areas at 0100 and 0200. The highest cloud tops are shaded. A similar superimposition at 0000 and 0100 would show little change during that hour - especially with regard to the location of the highest tops. The rapid eastward shift of the strongest thunderstorms can also be seen by comparing the 0130 and 0230 MDR plots. Note particularly the very strong and intense echoes south and southwest of Dallas at 0230.

How such an expectation might be translated into a useful forecast is another matter. It might take the form of a special statement such as,

> ...there are indications that this storm will increase rapidly in intensity within the next hour in the vicinity of ..., etc.

As a final note, it is interesting to observe in the 0230 picture the boundary of the moist air in West Central Texas. The dry line separates the lighter (drier) and darker (moist) areas of the picture. (Notice in the 2330 visible picture that this area is generally cloudless.) It was along the dry line, at about the point marked by the arrow, that the thunderstorm group subsequently affected by the arc cloud first formed about mid-afternoon.

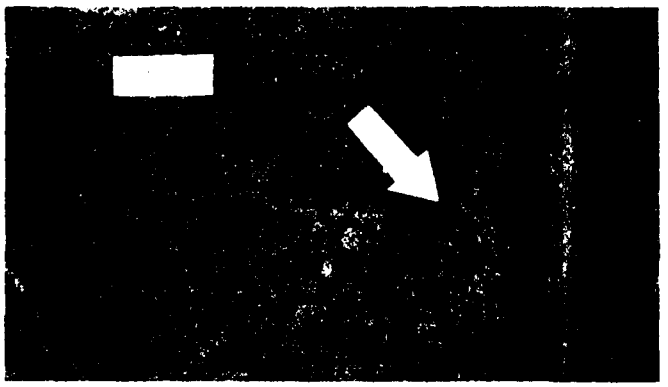

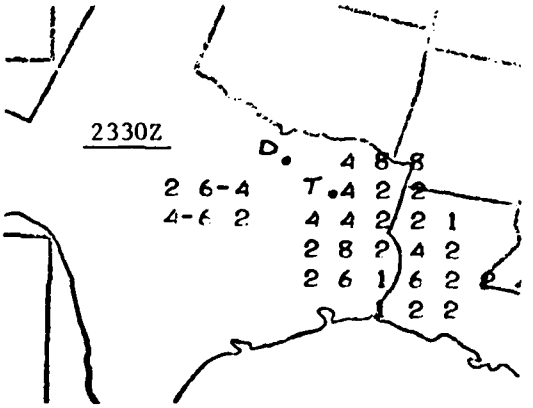
2330Z
D
T
2 6-4
4-6 2

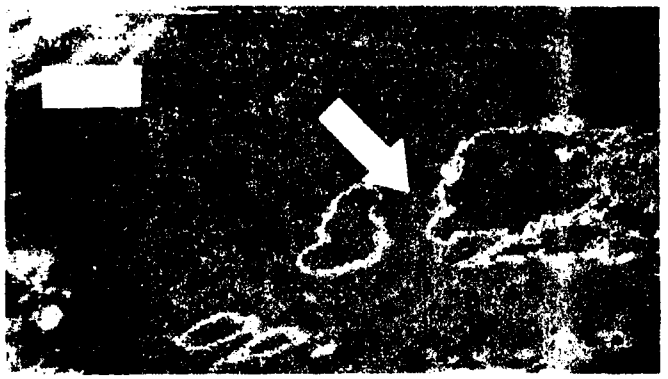

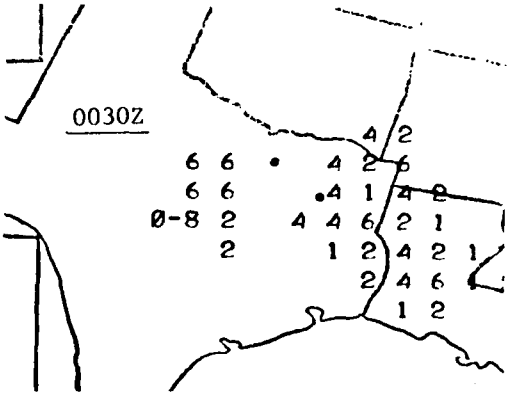
0030Z
6 6
6 6
0-8 2
2

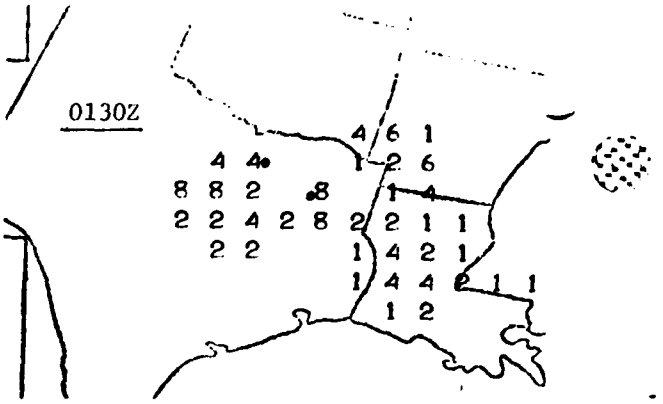
0130Z

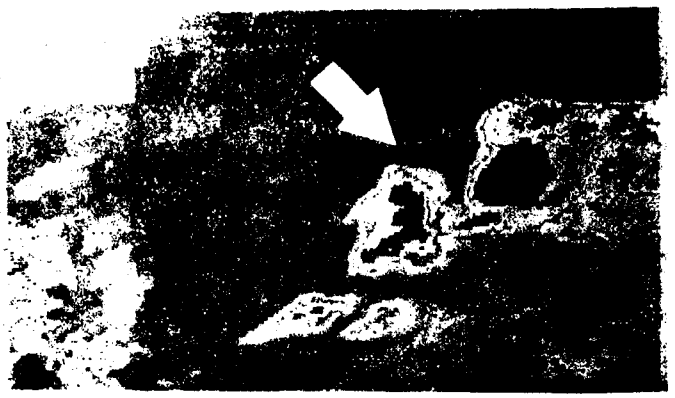

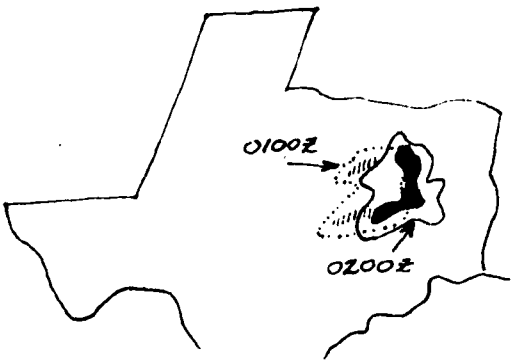
0100Z
0200Z

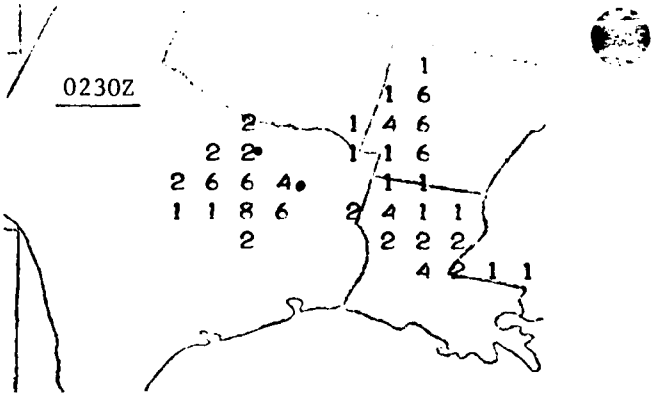
0230Z

U.S. DEPARTMENT OF COMMERCE

National Weather Service/National Environmental Satellite Service
SATELLITE APPLICATIONS INFORMATION NOTE 76/11

HIGH LEVEL PVA IMPULSE IS INTENSIFIED BY LOW-LEVEL OLD FRONTAL OCCLUSION

David L. Cohen
National Environmental Satellite Service, San Francisco

On April 12, 1976, a positive vorticity advection (referred to as PVA) impulse moved over a weak, old frontal occlusion off the southern California coast. When the two systems were in phase they intensified each other, and this in turn caused moderate rain over southern California later that day. This paper gives a brief history of how a high level and a low level system developed separately, then later came into phase and intensified, and how this kind of development could be anticipated by using satellite data. The first set of pictures show the systems about 24 hours before they came into phase.

12Z, April 11, 1976

The general synoptic scale flow pattern that prevailed over the eastern north Pacific throughout this episode was shown on the 500 mb chart for 12Z, April 11 (Fig. 1). A broad long wave ridge had its axis along 155°W. A sharp trough-line was quasi-stationary just off the west coast along 127°W.

The SMS-2 IR picture for 12Z, April 11 (Fig. 2) clearly shows the positions of the two systems.

The low level system (A, Fig. 2) was an old frontal occlusion with its back edge near 13°N, 134°W drifting east southeastward about 25 knots. Two days earlier it broke off a quasi-stationary mid-Pacific front near 45°N, 160°W and since then had been drifting east southeastward. It is significant that the old occlusion did maintain its organization as it moved through an area of general subsidence between the long wave ridge line and the sharp trough line.

The fact that this old occlusion did maintain its organization could be verified by examining the IR enhancement curve "H" that was available at the San Francisco SFSS during this period. Curve "H" is a three step IR enhancement curve. The first step goes from black to white between 36°C and 0°C; the second step goes from black to white between 0°C and -52°C; the third step goes from black to white between -52°C and -82°C. As the old occlusion drifted east southeastward, the coldest cloud top temperatures were in the second step of curve "H", that is between 0°C and -52°C. The old occlusion is shown (A, Fig. 3) as it appeared on curve "H" at 12Z, April 11, 1976.

The high level system (B, Figs. 2 and 3) was a PVA impulse near 47°N, 148°W at 12Z, April 11. This PVA impulse could first be seen at 12Z April 10, near 43°N, 165°W. Being a high level system, it first moved northeastward over the long wave ridge line near 155°W, then dropped east southeastward at about 50 knots towards the sharp trough line. Like the old occlusion, the PVA impulse maintained its organization quite well in an area of general subsidence.

00Z, April 12, 1976

Now the stage was set for the PVA impulse to move over the old occlusion. The back edge of the old occlusion was near 30°N, 130°W (A, Fig. 4) and had changed its movement to just slightly south of due east at 15 to 20 knots. The PVA impulse was near 40°N 133°W (B, Fig. 4) and still moving east southeastward 50 knots. Since the PVA impulse was moving in an almost straight line; its vorticity was due mostly to the shear term in the vorticity equation.

12Z, April 12, 1976

The PVA impulse was on top of the northern part of the old occlusion with the back edge of both along 125°W (A and B, Fig. 5). As the PVA impulse reached the base of the sharp trough (Fig. 1), more of its vorticity was due to the twisting term in the vorticity equation.

00Z, April 13, 1976

The dramatic result of the PVA impulse and the old occlusion coming into phase could be clearly seen at 00Z, April 13. The two systems had "merged" and greatly intensified just off the southern California coast. A new vorticity center had formed near Point Conception (A, Fig. 6). As the main PVA impulse slowed off the coast, cirrus clouds moving out ahead of it were over southeast California and western Arizona (B, Fig. 6). During the next 24 hours, the system off the coast moved inland and brought between 1/4 and 1/2 inch of rain to much of the southern California coastal area.

It is quite likely that the PVA impulse would have undergone some intensification at the base of the trough even without the presence of the old occlusion, but this intensification would not have been as great. The presence of the old occlusion also pinpointed the exact area where the intensification would take place.

Separately, both the PVA impulse or the old occlusion could probably have passed through southern California and caused little or no precipitation. It was the coming into phase of the two that gave the total system far more impact then the sum of both its separate parts.

8

The purpose of this paper is to show how useful the SMS-2 satellite can be for tracking and anticipating the "merger" of a high level and a low level system. Using the satellite, it should be possible to forecast whether a weak front will pass through an area almost dry, or if it will receive a sudden input of upper level support and pass through the same area quite wet.

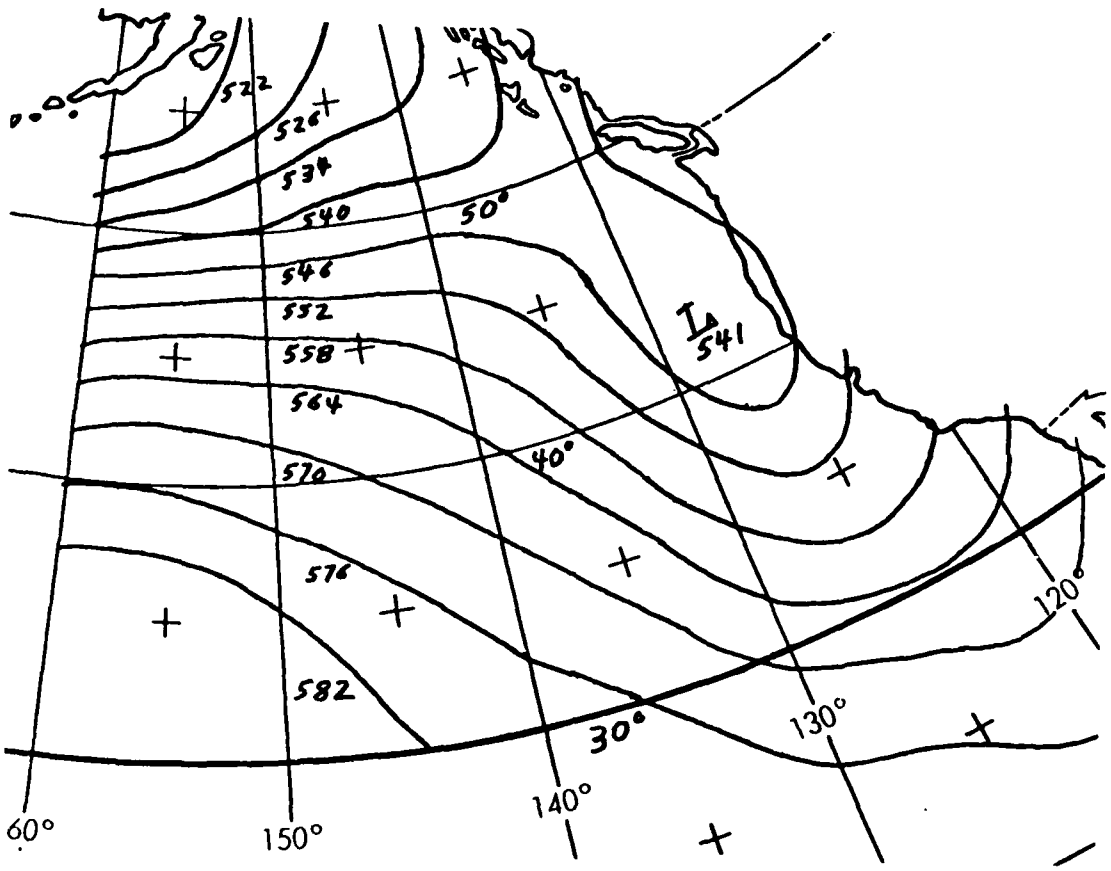

Figure-1 500mb Analysis, 1200 GMT,11April 1976

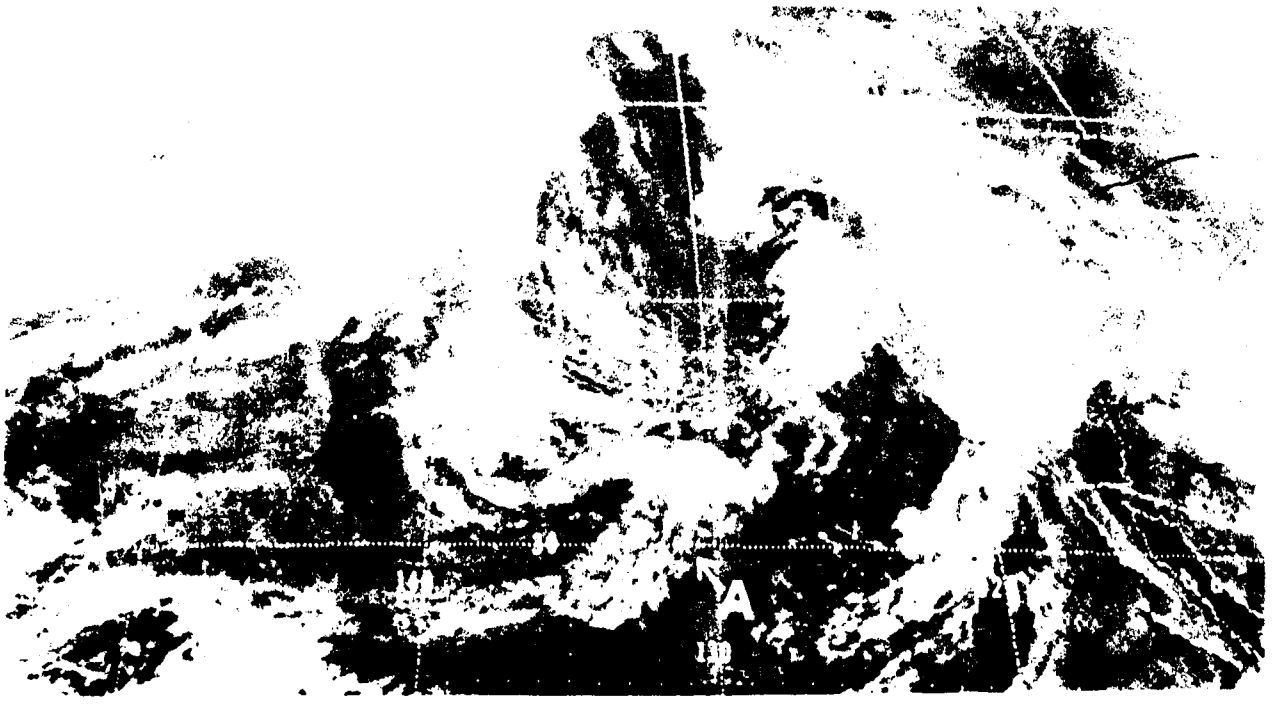

Figure 2 SMS-2 Infrared, 1200GMT, 11 April 1976

82

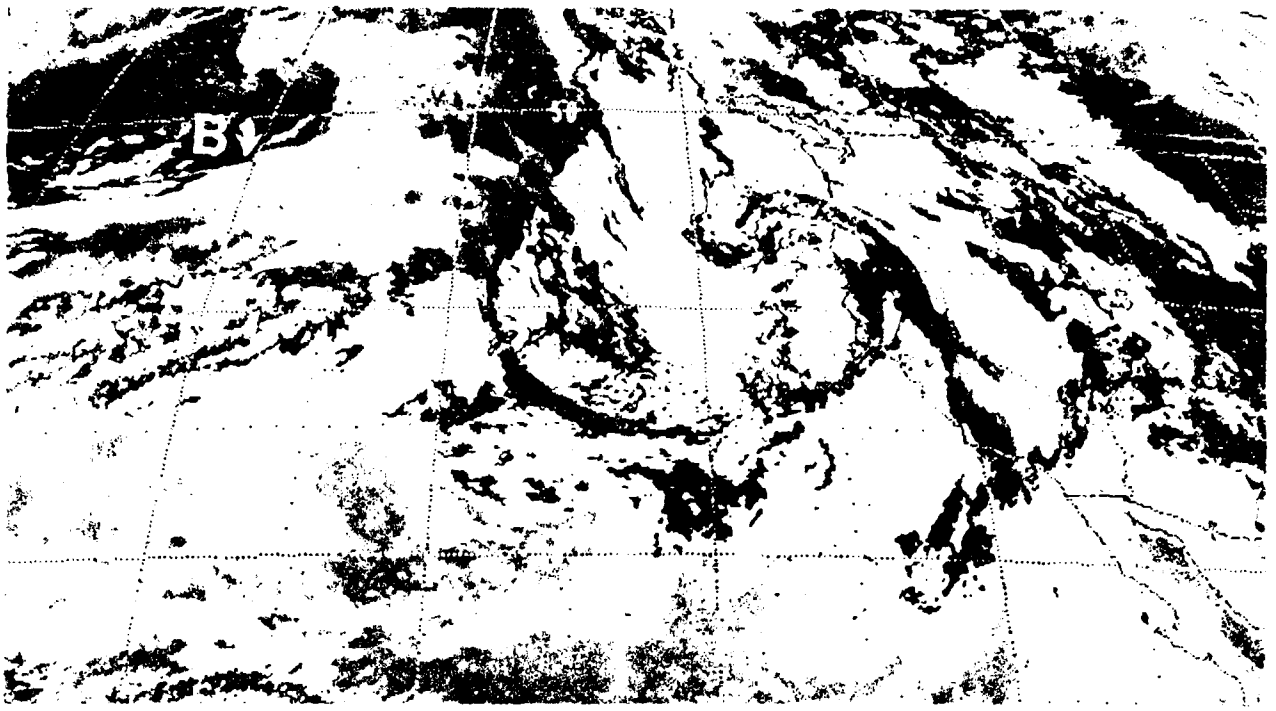

Figure 3 SMS-2 Infrared H-curve, 1200GMT, 11 April 1976

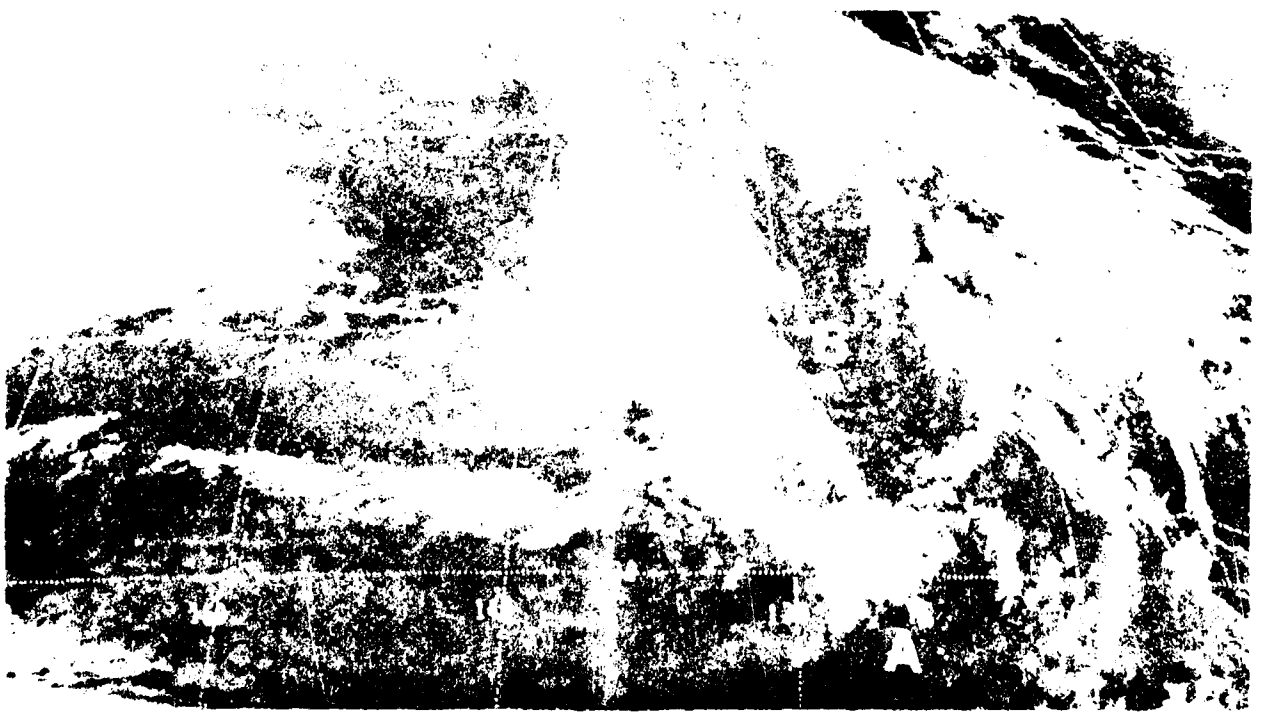

Figure 4 SMS-2 Infrared, 0000GMT, 12 April 1976

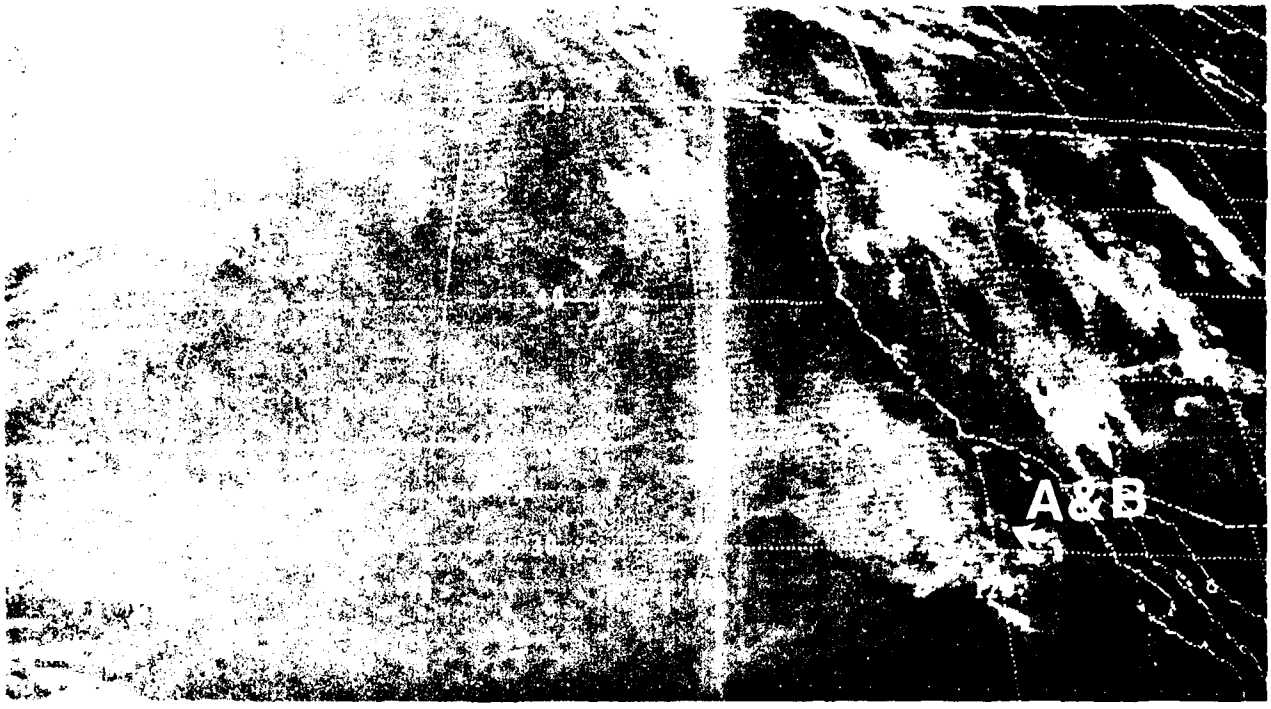

Figure 5 SMS-2 Infrared, 1200GMT, 12 April 1976

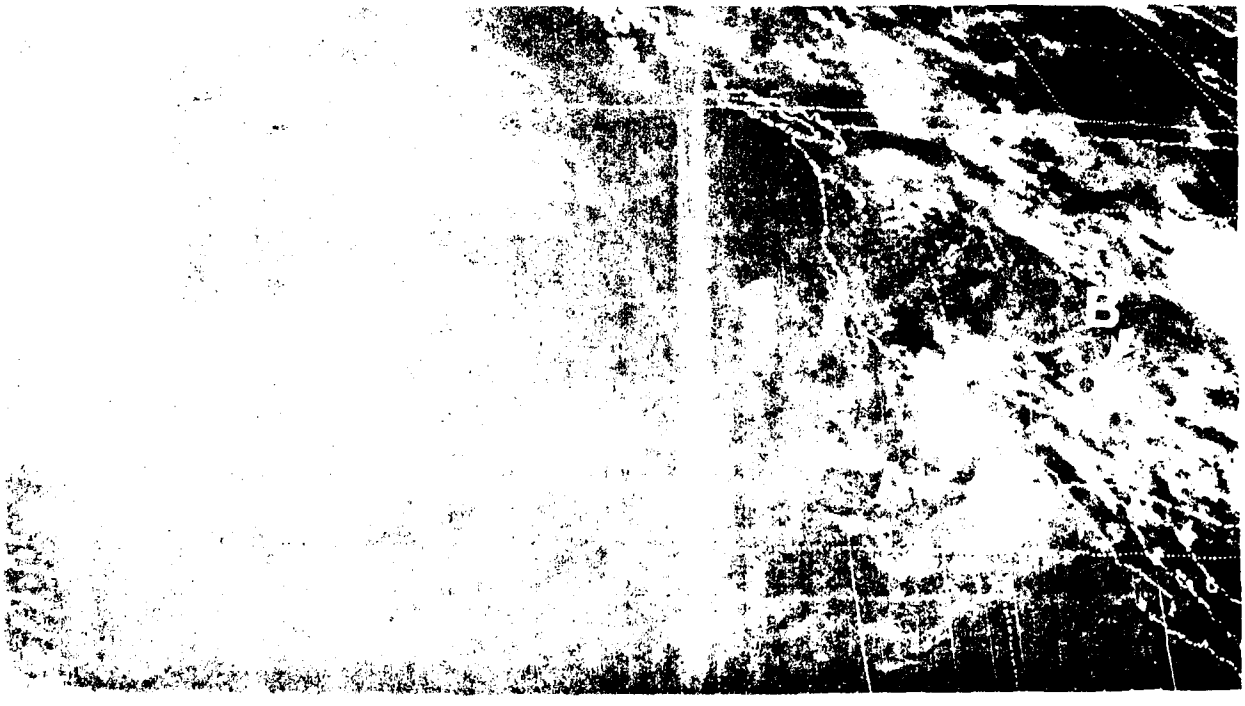

[illegible], 1200 GMT, 13 April 1976

U.S. DEPARTMENT OF COMMERCE

National Weather Service/National Environmental Satellite Service
SATELLITE APPLICATIONS INFORMATION NOTE 76/12

AN EXAMPLE OF DRY LINE CONVECTIVE DEVELOPMENT "THE OMAHA TORNADO"

Joseph A. Miller
Satellite Field Services Station, Kansas City, Missouri

Satellite Imagery presented a "birds eye" view of intense thunderstorm development on May 6, 1975, as a well defined dry line moved eastward over the Plains.

There were other meteorological factors at work in conjunction with the dry line development which meshed together to produce the Omaha tornado; however, for the sake of brevity, the sequence of satellite pictures depicting the actual dry line development will be presented as an entity devoid of charts and figures.

Briefly, some of the other meteorological factors are here presented. Most important was an old surface boundary formed by previous thunderstorm activity. Across the boundary a wind, temperature and dew point discontinuity developed as rain-cooled air "back doored" into northwest Missouri and extreme eastern Nebraska. Figure 1, a visual one-mile resolution picture taken at 2045 GMT shows this boundary as a line of clouds (A) extending from southeast Missouri to northwest Missouri and then disappearing beneath the cirrus "blowoffs" in extreme southeast Nebraska. The geographical location of this old boundary, with respect to the squall line(s) easing in from the west, was probably a prime factor in concentrating the maximum low level convergence near the intersection of the two lines -- in the Omaha area. Figure 2 is an ungridded visual 1/2 mile resolution picture taken at 2100Z with synoptic surface reports superimposed (Omaha (O) is circled). Note the location of low surface convergence and temperature-dew point discontinuities in this view. Also, it appears that the low level moist tongue was squeezed and funneled into the Omaha area by the old boundary to the east and the approaching dry line to the west. An unstable air mass, the location and configuration of the high level jet structure, PVA, etc., were other segments of the total picture, however, let's look at this series of two-mile resolution IR pictures with the concept that here is pristine dry line development.

1501Z FIG. 3 Low level cumulus clouds, in the moist air, can be seen as a long grey shadow (D) from central South Dakota southward through eastern Nebraska into north central Texas. The sharp western edge correlates to the dormant dry line. Note the line of thunderstorms (B) from southeast Missouri to western Iowa.

85

1600Z FIG. 4 The sharp western edge of the low clouds (dry line (D)) is still plainly visible and has edged slowly eastward during the past hour. The line is beginning to come to life as the first hint of developing convection can be seen over south central South Dakota (E) and along the central portion of the Kansas and Oklahoma border (C).

1700Z FIG. 5 Dry line (D) has moved further east and is "lighting up" along a good portion of its length. South Dakota thunderstorm tops are pluming off to the northeast with the prevailing upper flow. The Kansas and Oklahoma activity continues to increase in intensity and convection has started to form in eastern Nebraska.

1730Z FIG. 6 In just 30 minutes, activity has shown a marked increase. The entire eastward moving dry line commences to explode as it begins to encounter the deeper moisture gradient along the western side of the moist tongue axis.

2100Z FIG. 7 This print was taken approximately 33 minutes prior to the Omaha tornado. Very heavy thunderstorm activity can be seen from the Dakotas to northwest Oklahoma. The main squall line is near the western edge of the bright clouds with cirrus blowoffs to the east and northeast of the line. Note also, several large thunderstorms (F) over eastern Texas. This activity is just east of the dry line near the intersection of the sub-tropical jetstream, as evidenced by the high clouds from the Texas Big Bend northeastward, and the low level moist tongue.

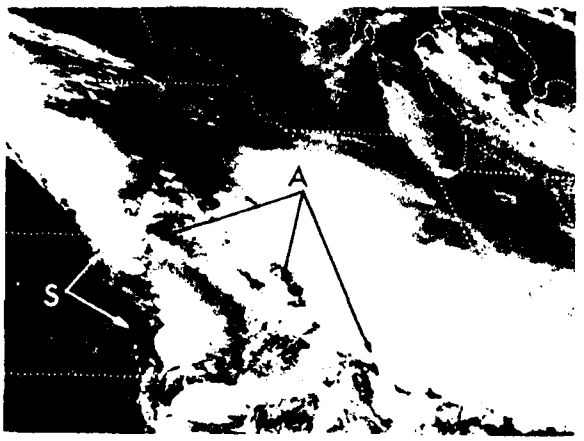

FIG. 1 SMS-2 VIS 2045Z
6 MAY 1975

FIG. 2 SMS-2 VIS 2100Z
6 MAY 197)
2100Z SFC REPORTS SUPERIMPOSED

87

AD-A167 989 SATELLITE APPLICATIONS INFORMATION NOTES OCTOBER 1975 - DECEMBER 1978(U) AIR WEATHER SERVICE SCOTT AFB IL AUG 79 AWS/TN-79/003 2/4

UNCLASSIFIED F/G 4/2 NL

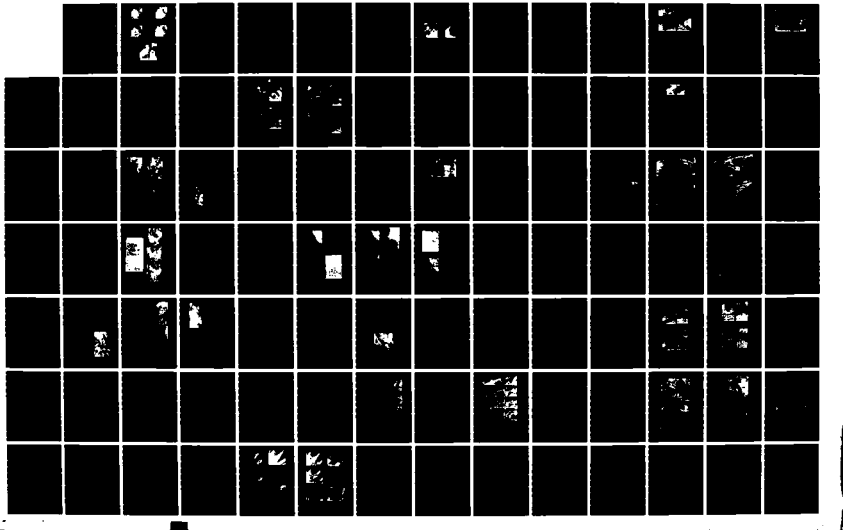

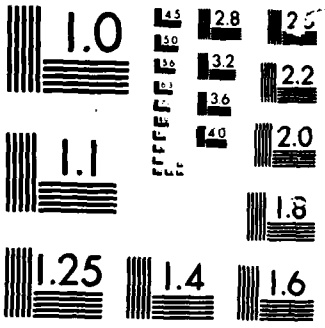

MICROCOPY CHART

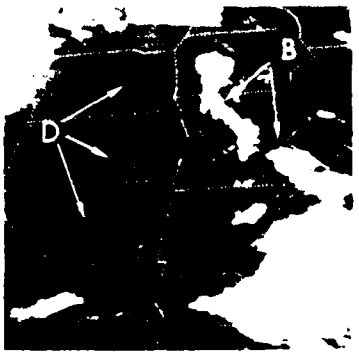

FIG. 3 SMS-1 IR 1501Z
6 MAY 1975

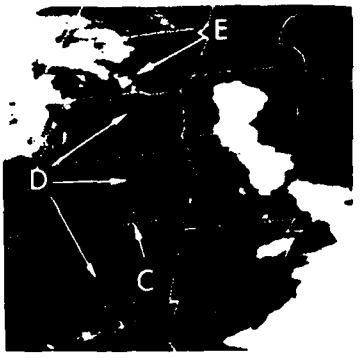

FIG. 4 SMS-1 IR 1600Z
6 MAY 1975

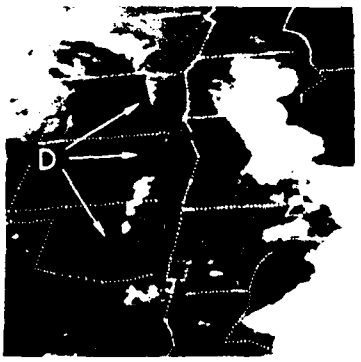

FIG. 5 SMS-1 IR 1700Z
6 MAY 1975

FIG. 6 SMS-I IR 1730Z
6 MAY 1975

FIG. 7 SMS-1 IR 2100Z
6 MAY 1975

U.S. DEPARTMENT OF COMMERCE

National Weather Service/National Environmental Satellite Service
SATELLITE APPLICATIONS INFORMATION NOTE 76/13

A LIMITATION TO THE ENHANCED IR DATA

Brian E. Heckman
Satellite Field Services Station, Kansas City, Missori

One of the immediate benefits realized with enhanced IR (EIR) data (when using certain look-up curves) has been the elimination of the dense cirrus shield frequently observed with convective activity on regular IR data. EIR data received at 30 minute intervals provides a new dimension in weather analysis to field users. This new dimension is a vertically structured temperature profile of cloud patterns and is especially useful in the analysis of convective activity. Extensive work in the enhancement of NOAA IR data has been conducted since 1974, at the SFO SFSS with excellent results.

EIR data was transmitted on an experimental basis to the SFSS's between June 1975, and January 1976. Comparisons were made between these data and radar data to determine how the satellite imagery could be used to monitor thunderstorm activity.

Experience to date indicates trends of intensity and movement of convective areas is best afforded by the M_B (Figure 1) or similar curve. Convection is well highlighted by segments 4-8 (Figure 1) on the enhanced image. We have found that the time rate of change, as determined from an EIR sequence of building convection, to be somewhat analogous to intensity trends noted by the Video Integrator and Processor (VIP) on the WSR-57 radar. This allows the forecaster to relate changes in cloud top temperature as sensed by the satellite to changes in intensity as indicated by radar.

Even though enhanced data provides a new means of observing convection, certain limitations exist. Several cases have been documented in which two areas of convection appeared similar on the Radar Summary Chart (intensity, areal extent and maximum cell tops), but appeared significantly different on the EIR data. A detailed investigation was made to determine the cause of this difference. Our approach was to examine conditions at the tropopause since, in general, the upper extent of convective growth is near this level.

Cloud top temperatures are a function of the environmental air temperature. Each shade of grey in the EIR image corresponds to a known temperature interval. Therefore, if a cloud is displayed in the imagery as a particular grey shade, the cloud particles must exist at that level where the atmospheric temperature is within the temperature range assigned to that shade of grey. (This assumes that the cloud particles in question radiate as approximate black bodies).

Assume, for instance, the tropopause temperature was near -55°C and the enhanced curve displays as black those cloud particles whose temperature is between -59°C and -62°C (segment 7, Figure 1). In this situation, black would not appear on the EIR image since cloud particles which have these temperatures do not exist in the atmosphere at this location (assuming the convection did not penetrate the tropopause).

Based on a number of cases studied, it appears likely that the manner in which active convection is enhanced (number of segments displayed) is heavily dependent upon the tropopause temperatures. Evidence supporting this conclusion is illustrated in the following discussion of a case study.

The Radar Summary Chart for 0135Z April 7, 1976, Figure 2a, depicted a scattered area of TRW++ from north central Kansas to central Nebraska. Maximum cell tops ranged from 30,000-40,000 feet. The scattered area of TRW+ and TRWXX located in south Texas at 0135Z April 8, 1976, (Figure 2b) was of similar intensity and height.

Figures 3a and 3b are the enhanced images using the M_B look-up curve for display of these convective areas. It's obvious the activity in 3a is much more accentuated than in 3b. Note only the first three grey shades are displayed in 3b while all shades plus some lighter shades inside the black region (temperatures $\leq$ -63°C, segment 8) are displayed in 3a. This gives the impression that the thunderstorms in 3a are stronger. Response from field forecasters indicates that significant weight is placed upon the appearance (the number of grey shade contours present) of the EIR data when judging convective strength. If this technique was applied in this case, the activity shown in Figure 3b would rate lower than that shown in 3a. Two tornadoes and several reports of large hail occurred on the 8th, while only thunder was reported on the 7th.

Figures 4a and 4b show tropopause temperatures taken from NSSFC's Jet and Tropopause Chart for 0000Z April 7 and 8, respectively. Figure 4a depicts a cold termal pool aloft over the northern Plains with temperatures in the -60°C to -62°C range near the Kansas-Nebraska convection. In the area of maximum tops, the observed temperatures correspond fairly well with those represented in the EIR. The small amount of grey within the black suggests the spacecraft sensor is detecting cloud particles in the lower end of segment 8 (Figure 1).

It is interesting to compare this situation with the enhanced depiction of the activity in the vicinity of a warm thermal ridge aloft over central Texas (Figure 5b). Temperatures over the convection near Austin are substantially warmer than those observed 24 hours previously over Kansas and Nebraska. Again, there is reasonable agreement between observed tropopause temperatures (over area of maximum cloud tops) and the temperature range of the third grey shade (segment 6, Figure 1).

40

This case brings to light how two areas of convection which appear similar on the Radar Summary Chart can be displayed significantly different by the same enhancement curve. Even with intense thunderstorm activity (accompanied by severe weather reports), the enhanced data can appear very flat and unaccentuated. It is suggested that the tropopause temperature overlaying the convection greatly affects the enhanced display.

The look-up curves constructed for enhancement of convection have been changed (GOES Imagery Enhancement Kit, Amendment #3) so that a family of curves are available to field users. This variety of curves is made so that all displays of convection, regardless of the curve, will exhibit convection in a similar manner (all curves are now similar to M_B curve). The only portion of each curve modified is the colder portion which has been adjusted for varying tropopause temperatures. Use of this family of curves should provide greater flexibility in selecting a curve corresponding to existing or anticipated tropopause temperatures. Also, all convection, regardless of season or synoptic situation, can be judged by somewhat of a common denominator, i.e., the number of grey shades displayed and amount of accentuation present.

This case study illustrates one of the limitations encountered when a single curve is used in the enhancement of convection. A possible solution to this problem has been provided. In conclusion, knowledge of existing tropopause temperatures by field forecasters contributes to a better understanding of enhanced displays of convective activity.

Reference:
(1) GOES Imagery Enhancement Information Kit, FSD, NESS, 1976.

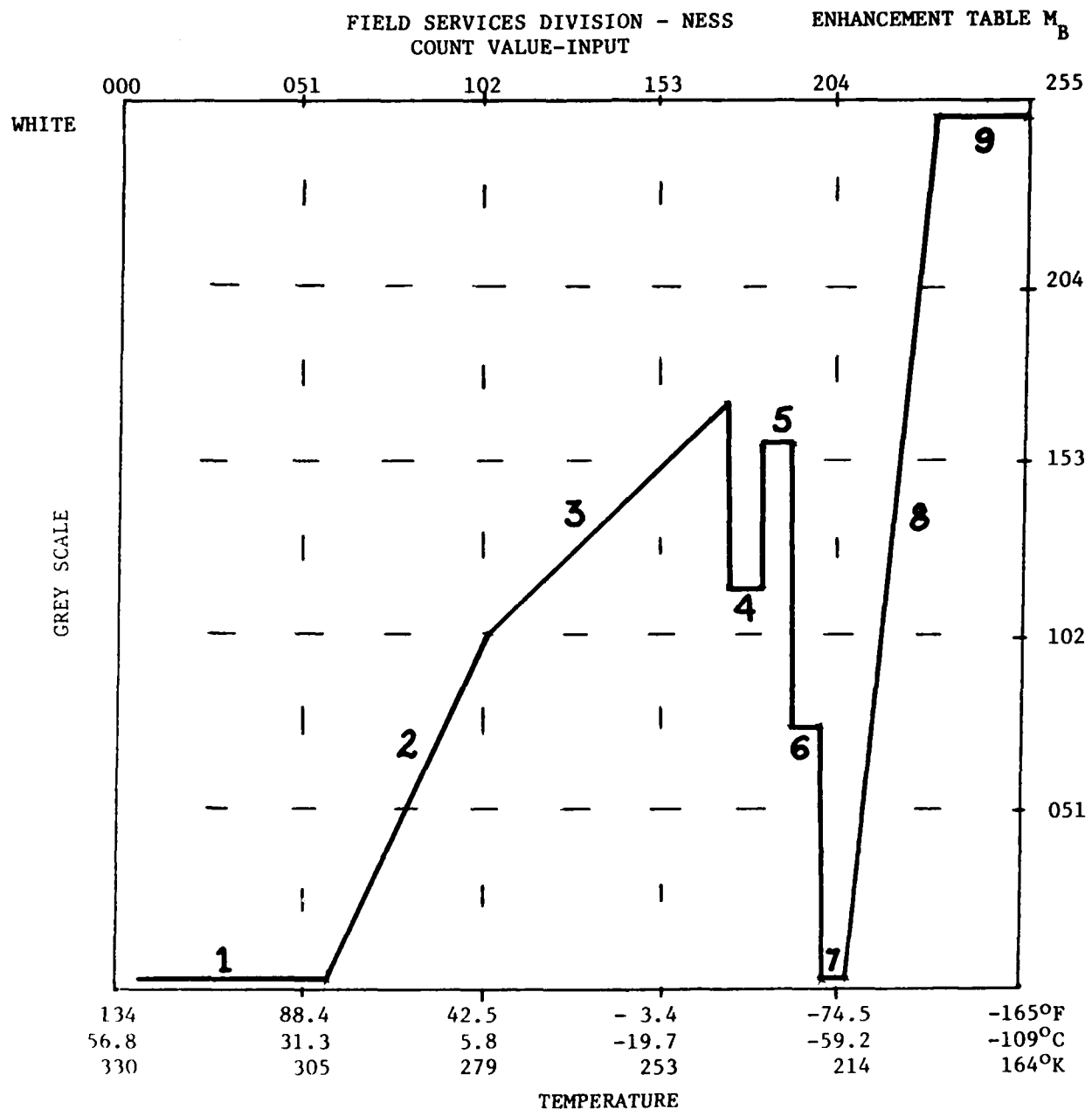

SEGMENT NUMBER	°C TEMPERATURE TO	COMMENTS REASON FOR SEGEMENT ENHANCEMENT
1	+58.8 To +28.2	Little or no useful Met Data (Black)
2	+28.8 To + 6.8	Low Level/Sea Surface Difference
3	+ 6.8 To -31.2	Middle Level - No Enhancement
4	-32.2 To -41.2	First Level Contour (Med Grey)
5	-42.2 To -52.2	Thunderstorm (Light Grey)
6	-53.2 To -58.2	Enhancement (Dark Grey
7	-59.2 To -62.2	(Black)
8	-63.2 To -80.2	Overshooting Tops Enhancement
9	-80.2 To -109.0	(White)

FIGURE 1

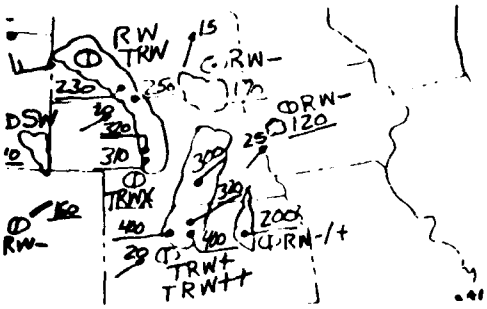

Figure 2a-Radar Summary Chart
0135Z 7 April 1976

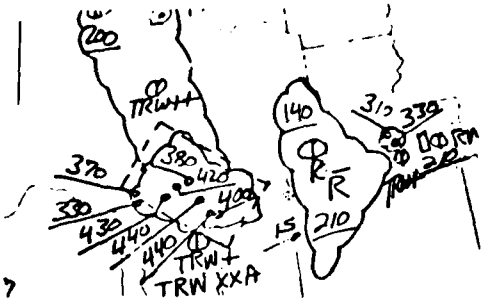

Figure 2b-Radar Summary Chart
0135Z 8 April 1976

Figure 3a-Mb Enhanced IR
0100Z 7 April 1976

Figure 3b-Mb Enhanced IR
0100Z 8 April 1976

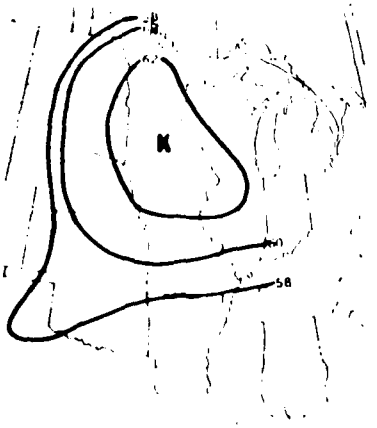

Figure 4a-Tropopause Temperatures
(- °C) 00Z 7 April 1976

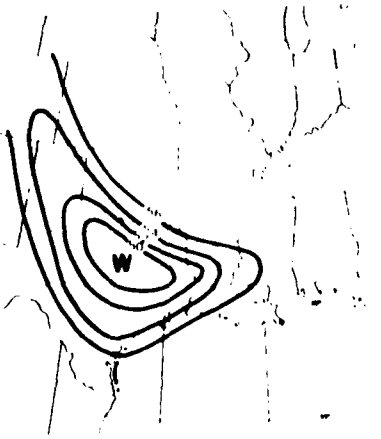

Figure 4b-Tropopause Temperatures
(- °C) 00Z 8 April 1976

U.S. DEPARTMENT OF COMMERCE

National Weather Service/National Environmental Satellite Service
SATELLITE APPLICATIONS INFORMATION NOTE 76/14

DIURNAL VARIATION IN THE WAVELENGTH OF LEE STANDING WAVES

Carl E. Weiss
Applications Group, NESS

Low-level standing lee waves are frequently observed during the winter and spring downwind from the Appalachians. The vertical motions which establish and alter such a wave pattern are of interest to most light aircraft and glider pilots. Changes in the lee wave pattern reflect variations in thermal stability and tropospheric winds. The 1 km visible imagery for April 27, 1976 illustrates a situation in which wavelength changes were observed during the day.

Scorer (1949, 1953, 1954) has demonstrated that the wavelength of lee standing waves is a function of both the wind speed and stability, with the former being more critical. Short wavelengths are found with light winds and strong stability and longer wavelengths are found with stronger winds and weaker stability. Fritz (1965), using Corby's (1957) observational results along with TIROS visible imagery, observed a similar relationship between wavelength and wind speed and stability.

The 1 km visible imagery for 1330GMT on April 27, 1976, Figure 1, shows an extensive area of mountain wave cloudiness (A-A') stretching from central Pennsylvania into southwestern Virginia. This wave cloud pattern developed within a stratocumulus deck extending southward from the Great Lakes. This cloudiness was located in the region of northwesterly flow behind a large storm over the Canadian Maritime Provinces, Figure 2. The stratocumulus terminated abruptly where the low-level flow changed from cyclonic to anticyclonic curvature. A more cellular or convective pattern is present in the stratocumulus field north of Lake Erie and in portions of Ohio and Pennsylvania (B).

The surface and 850mb analyses at 1200GMT, Figures 2 and 3, show a trough extending westward from the low center across northern New England into the Great Lake states. At 850mb, a pool of cooler air extended from Michigan into Ohio and Pennsylvania. The enhanced convection (B, Figure 1) appears to be located in this cooler, less stable air aloft, with snow showers being reported in this area.

The 1200GMT sounding from Dulles Airport, Virginia (IAD), Figure 4, suggests that the stratocumulus layer was shallow with cloud tops occurring at 864mb (~1400m), the base of a strong subsidence inversion. Wind speeds below the inversion averaged 20 knots and ranged from 31 to 34 knots just

beneath the inversion, increasing to 8 knots at the surface and 15 knots at 820 mb. The strongest winds were found just above the average mountain ridge elevation. Winds in the lower layers were from the northwest, perpendicular to the ridges of the Appalachians. Adiabatic conditions were present below the inversion in the wind-mixed lower layers.

By late afternoon, 2035GMT, the wavelength of the lee wave clouds (A, Figure 5) had increased markedly in Virginia and West Virginia. Part of this increase in wavelength can be attributed to the diurnal destablization that occurred due to daytime surface heating and stronger lower-level winds.

At this time, the stratocummulus south of the Great Lakes had become generally more convective with the most cellular clouds (B) stretching from eastern Ohio into Pennsylvania, West Virginia and extreme western Maryland. This convective area moved southeastward during the day. Mountain waves of even longer wavelength (C) are visible in the area where the enhanced convective cloudiness had entered the standing wave train. Along the northern portion of this area (D), over southwestern Pennsylvania, the added instability coupled with somewhat lower terrain had almost completely destroyed the wave pattern. The southern edge of the stratocumulus through northern Virginia and extreme southern West Virginia continued to mark the boundary between cyclonic and anticylonic surface flow.

The synoptic situation at 0000GMT on April 28, had not changed significantly from the earlier map. The gradient flow remained west northwesterly at both the surface and at 850mb. The area of enhanced convection continued to accompany the cooler temperatures found in the 850mb trough (Figure 6). Snow showers, reported earlier in Ohio and Pennsylvania, had ceased by this time.

By 0000GMT, the low-level inversion had lifted to 828mb (~1700m) and had weakened considerably at IAD (Figure 7). The average wind velocity below the inversion had increased to 27 knots during the day. The weakening of the inversion or the destabilization of the lowest layers can be attributed to advection of cooler air aloft and solar heating of the surface layers.

In summary, the meteorological conditions on the morning of April 27, 1976, favored the formation of lee standing wave clouds over the Middle Atlantic region. An increase in the wavelength of these wave clouds reflected a gradual decrease in the atmospheric stability and an increase in the wavelength of these wave clouds reflected a gradual decrease in the atmospheric stability and an increase in the low-level winds.

75

REFERENCES

Corby, G. A., 1957: "Preliminary study of atmospheric waves using radiosonde data," Quart. J. Roy. Meteor. Soc., 83, p. 49-60.

Fritz, S., 1965: "The significance of mountain lee waves as seen from satellite pictures," J. Appl. Meteor., 4, p. 31-37.

Scorer, R. S.,1949: "Theory of waves in the lee of mountains," Quart. J. Roy. Meteor. Soc., 75, 41 pp.

----------, 1953: "Theory of airflow over mountains: II - The flow over a ridge," Quart. J. Roy. Meteor. Soc., 79, 70 pp.

----------, 1954: "Theory of airflow over mountains: III - Airstream characteristics," Quart. J. Roy. Meteor. Soc., 80, 417 pp.

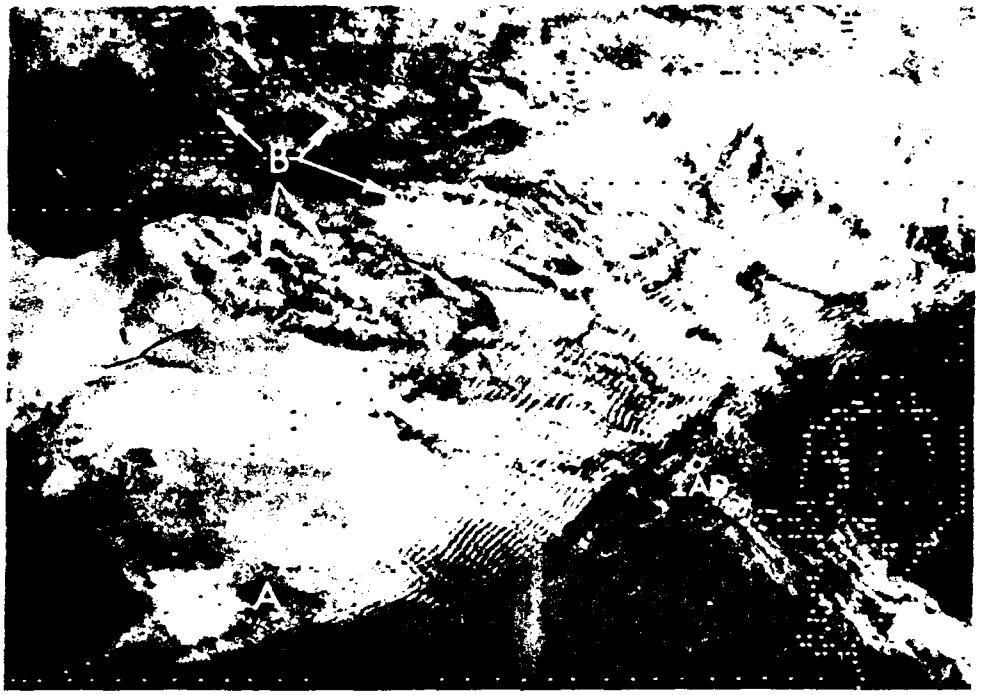

Fig. 1: GOES-1 1 km Visible Imagery 1330GMT, 27 April 1976.

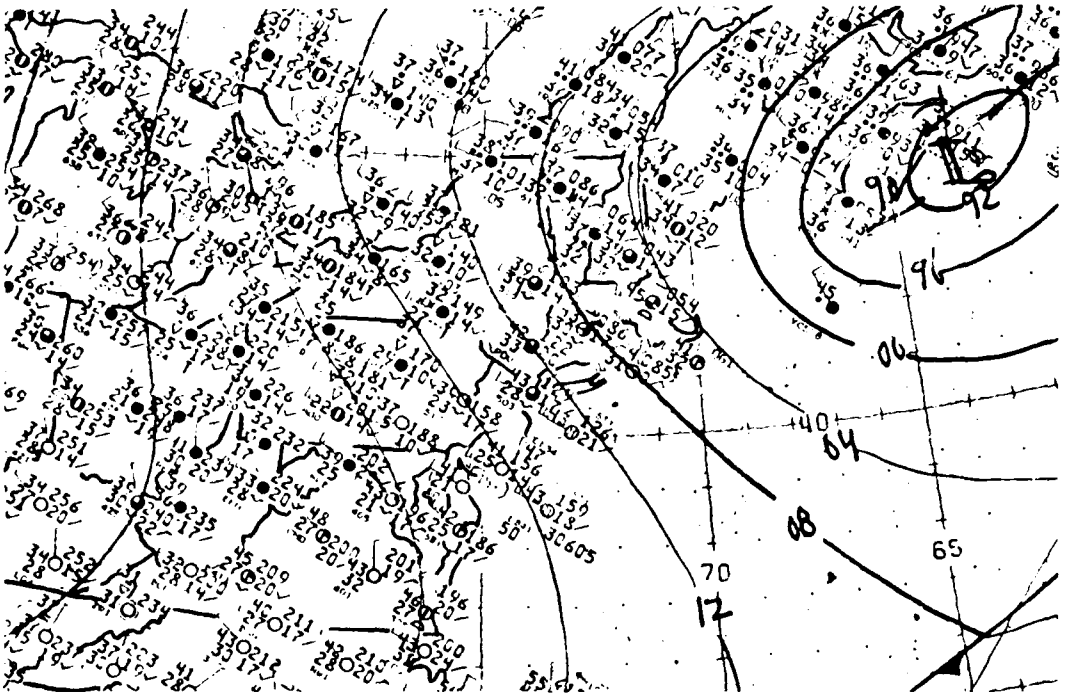

Fig. 2: 1200GMT Surface Analysis, 27 April 1976.

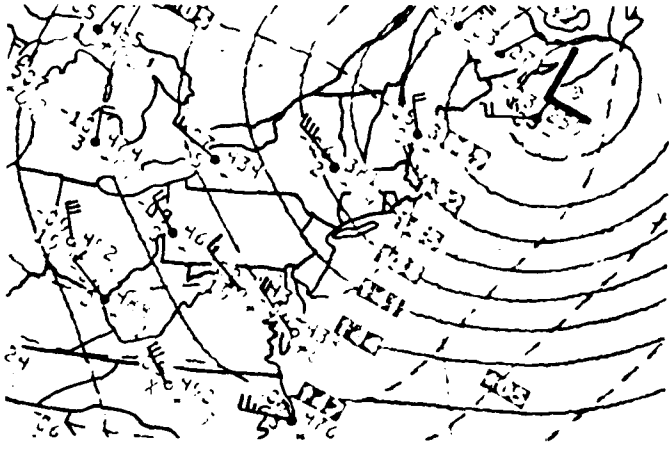

Fig. 3: 1200GMT 850mb Analysis, 27 April 1976.

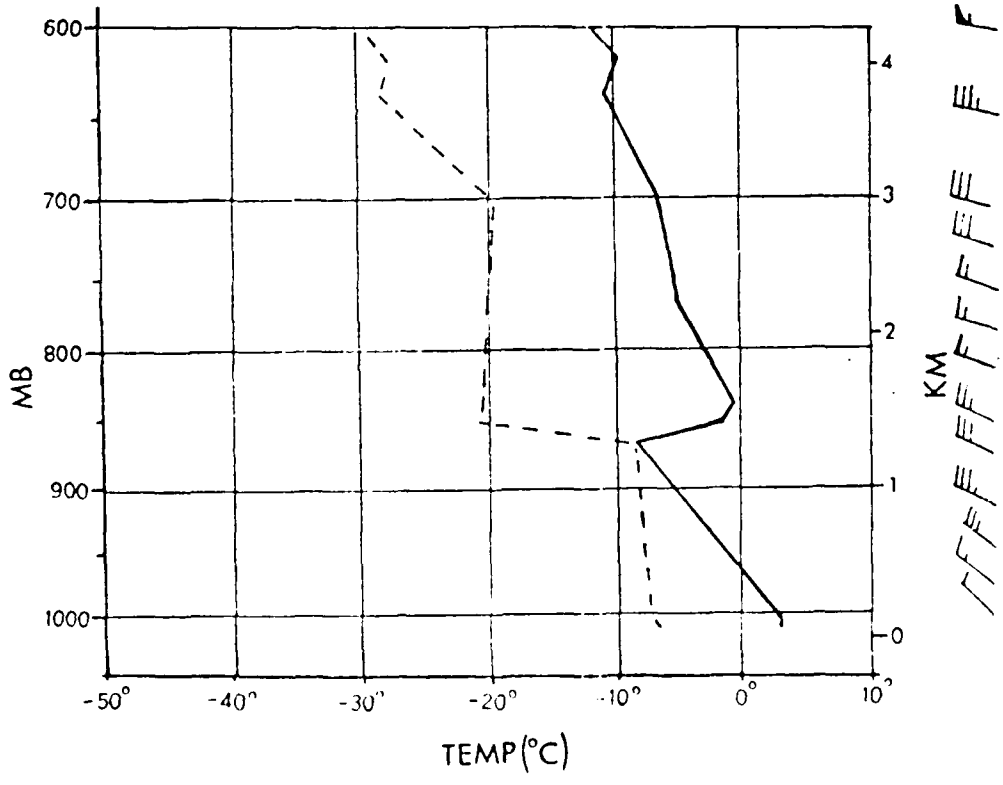

Fig. 4: 1200GMT Sounding, from Dulles (IAD), 27 April 1976.

Fig. 5: GOES-1 1km Visible Imagery 2035GMT, 27 April 1976.

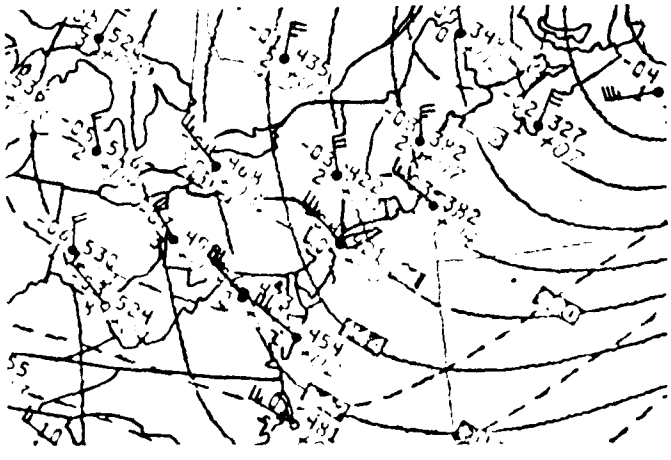

Fig. 6: 0000GMT 850mb Analysis, 28 April 1976.

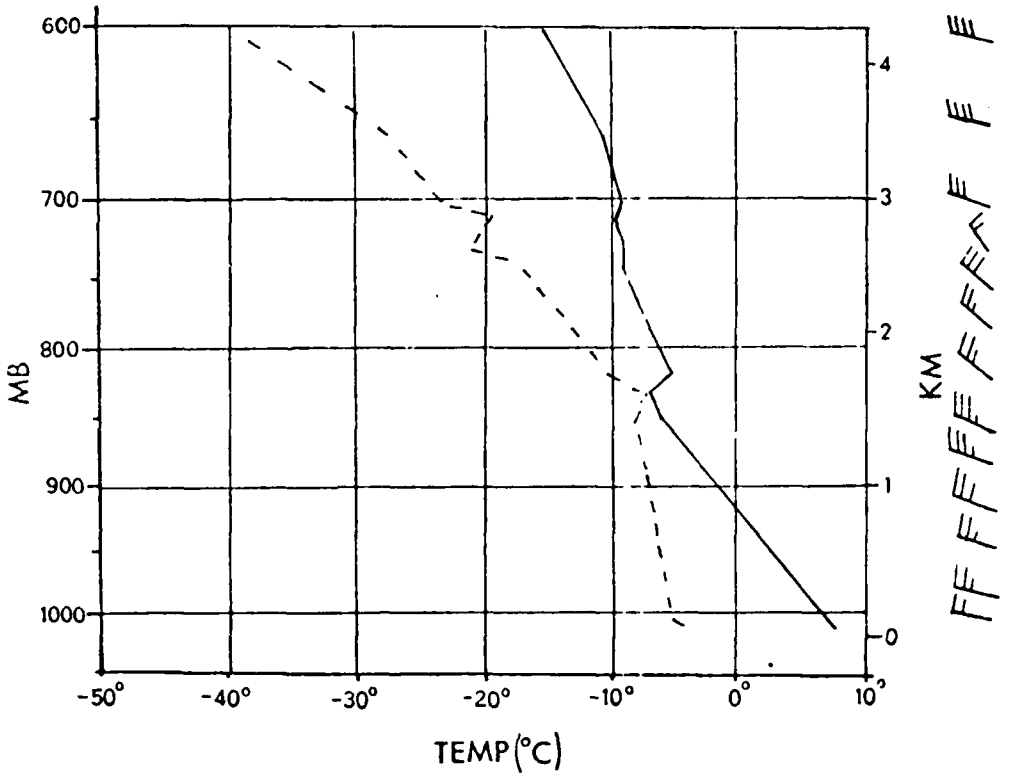

Fig. 7: 0000GMT Sounding from Dulles (IAD), 28 April 1976.

U.S. DEPARTMENT OF COMMERCE

National Weather Service/National Environmental Satellite Service
SATELLITE APPLICATIONS INFORMATION NOTE 76/15

THE USE OF GOES 1 km RESOLUTION IMAGERY IN HELPING PINPOINT TORNADO ACTIVITY

James F. W. Purdom
Applications Group, NESS, Washington, D.C. 20233

The isolation of areas within a severe weather watch where intense tornado activity should be expected to develop is one of the real problems facing the field forecaster. For many years, an accurate and timely mesoscale surface analysis was one of the most important tools available to the forecaster in locating these areas. This was because surface reports were the only observations of sufficient density, in both space and time, to identify mesoscale weather systems. The most important information to be gained from an analysis of this type is the location of areas of stronger surface wind convergence and thermodynamic instability and how they change with time. This type analysis, however, is a laborious one with many mesoscale systems going undetected due to the lack of a reporting station at the right place at the right time. Additionally, when a mesoscale surface analysis is of most value to the forecaster, he is normally too busy to do more than take a cursory glance at the currently available teletype data, or NMC surface chart.

The same type reasoning used to make a mesoscale surface analysis also holds when using GOES imagery in severe weather forecasting. Changes in thermodynamic instability can be inferred by observing cloud types and their change with time. Many important areas of low level moisture covergence appear as organized convective lines in the satellite imagery long before the first thunderstorm associated with this covergence forms. Other important boundaries, such as those bounding the thunderstorm mesoscale high are often readily detectable as arc cloud in the imagery. One of the more important things which satellite imagery has repeatedly shown is that the merger or intersection of these convective cloud lines and arcs with another boundary, such as a front, dry line, or other convective line almost always locates a point for intense thunderstorm development. In fact, for at least one type of intense tornado, convective-scale interaction in this form seems to be an absolute requirement. The following example, from May 25, 1976, will be used to show how satellite imagery might be used to isolate an area with a high probability of intense tornado activity.

May 25th was an ideal day for tornadoes in Texas. The 1800 GMT NMC surface analysis, Figure 1, shows a stationary front across the central portion of the state; the dry line in southwest Texas was just beginning to move eastward. Inspection of the 1 km resolution GOES picture for 1800 GMT, Figure 2, shows a large thunderstorm area along the stationary

front at A. This thunderstorm area was moving to the southeast along the front and as we will see, it played a key role in determining where the tornadoes would be later in the day. By the 1900 GMT GOES picture, Figure 3, the arc cloud boundary (B, C) produced by the thunderstorm complex at A was easily detectable. The important area of the arc is along its western end, where it will be interacting with the stationary frontal boundary and the dry line; attention should be focused there for tornado activity. At 1900 GMT, a scan of the teletype would have shown that the arc had moved to the south of Abilene, Texas (ABI) where the wind had shifted from 210^{0} at 8 knots to 90^{0} at 13 knots. Note the enhanced convective activity forming where the arc and frontal boundary are merging (D). By 1945 GMT, Figure 4, a large thunderstorm complex has formed at the intersection point D. The arc cloud is readily detected merging into the area. For point warning purposes, all attention should be focused on that storm area.

Figure 5 is the GOES picture for 2045 GMT with Abilene, Texas located at the X. The following severe weather was reported in the Abilene area:

1. 2045 GMT, tornado 14 NNW ABI, 5 homes damaged;

2. 2053 GMT, tornado 10 N ABI;

3. 2120 GMT, tornado 14 E ABI, farm homes damaged;

4. 2130 GMT, tornado 7 NNE ABI, 12 homes damaged.

In this example, the arc cloud merged with a stationary frontal boundary helping create the needed conditions for tornadic thunderstorm development. Similar results would have occurred if the arc had interacted with the dry line. Thus, the use of satellite imagery in the early location of boundaries and subsequent determination of important interaction points can greatly aid the forecaster in his mesoscale assessment of the convective situation at hand.

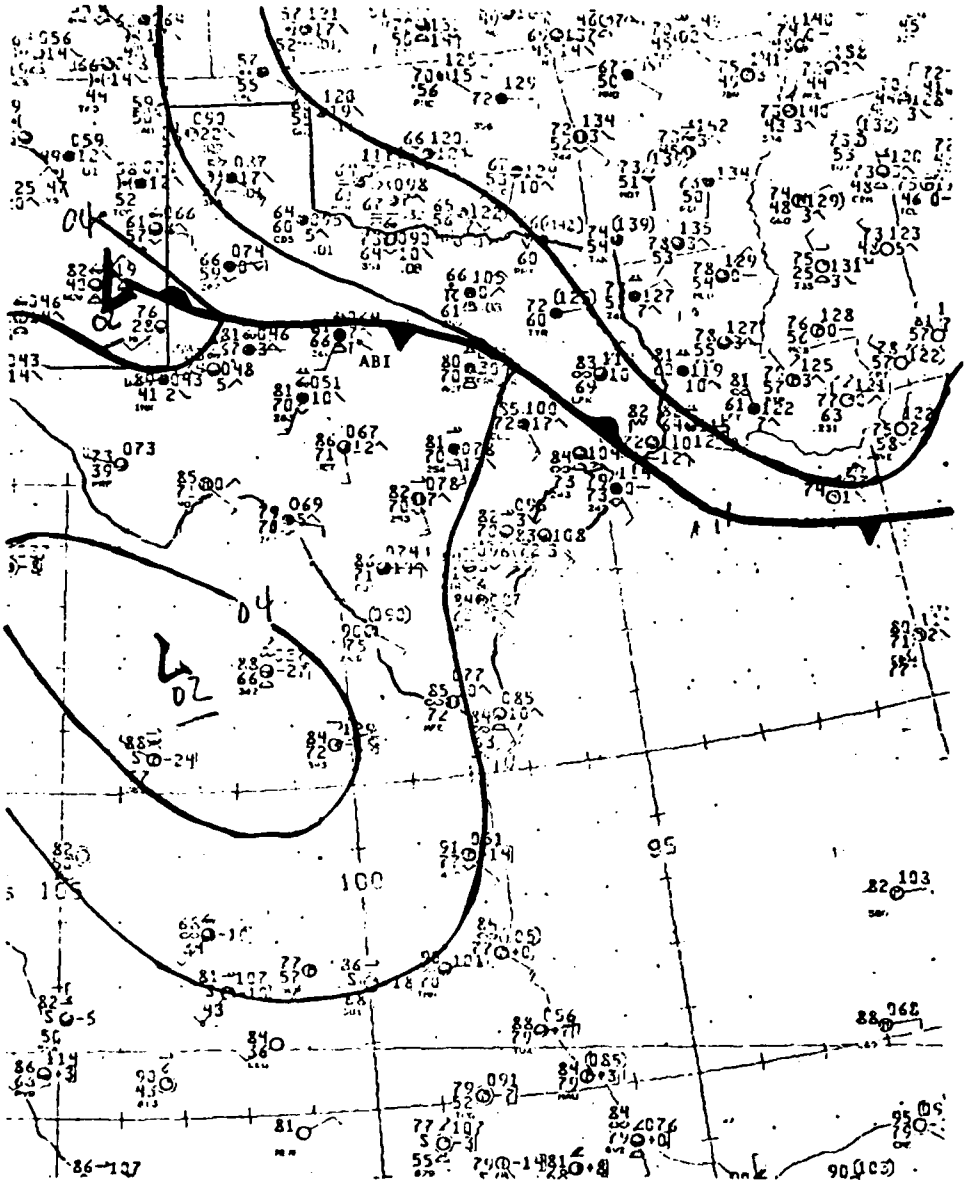

Figure 1. Surface Analysis, 1800 GMT, 25 May 1976

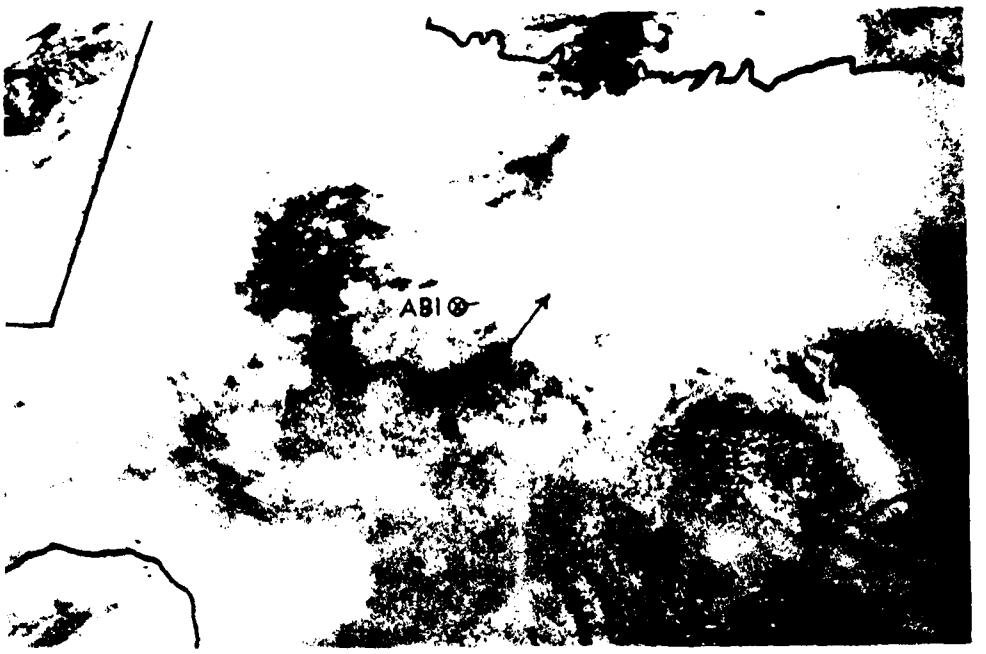

Figure 2. GOES-1, Visible (1 KM) data taken at 1800GMT 25 May 1976.

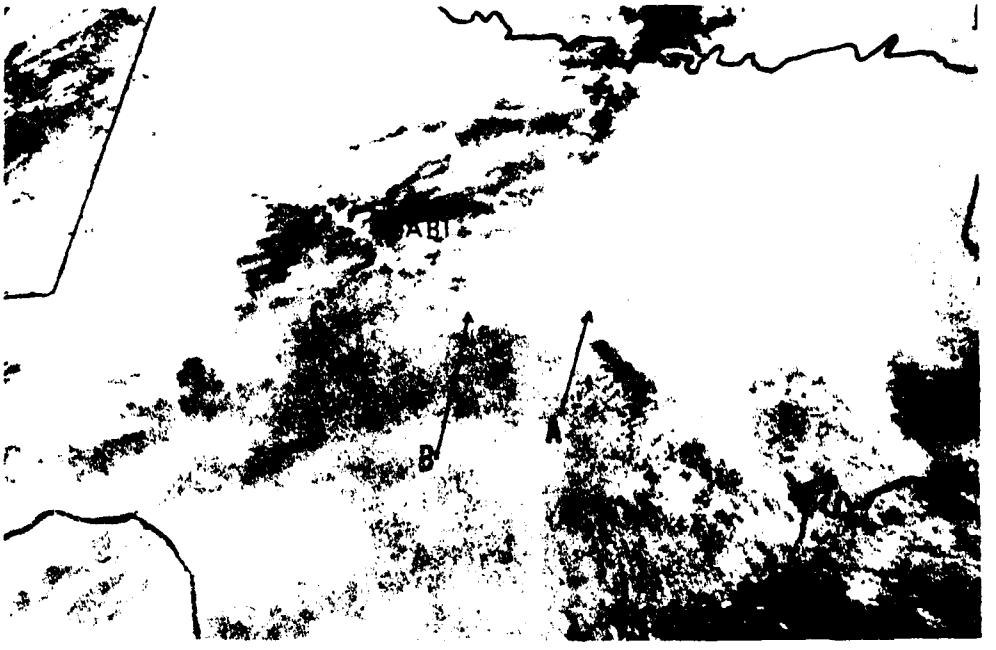

Figure 3. GOES-1, Visible (1 KM) data taken at 1900GMT 25 May 1976.

Figure 4. GOES-1, Visible (1 KM) data taken at 1945GMT 25 May 1976.

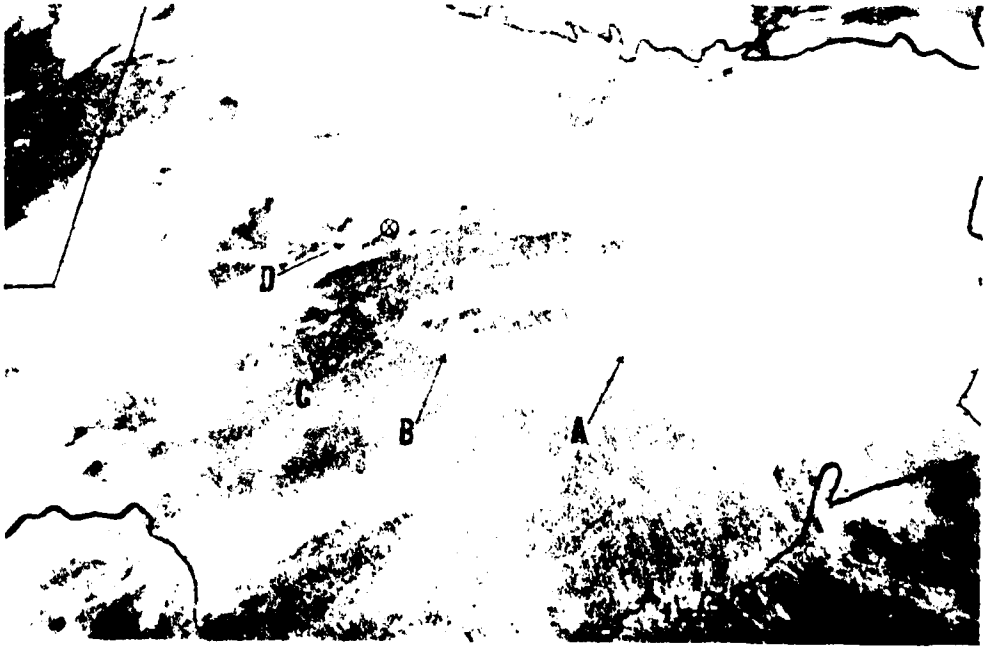

Figure 5. GOES-1, Visible (1KM) data taken at 2045 GMT 25 May 1976

DEPARTMENT OF COMMERCE

National Weather Service/National Environmental Satellite Service
SATELLITE APPLICATIONS INFORMATION NOTE 76/16

HOW CAN DISTANCES ON GOES PICTURES BE MEASURED MORE ACCURATELY?

John D. Thomas
NOAA, NESS, Satellite Field Services Station, Washington, D.C.

Have you noticed that weather systems seem to move eastward faster on satellite pictures than the other data would indicate? This discrepancy may be a result of the procedure used to measure distance on the pictures. The standard method seems to be to measure distance on the pictures the same way as on weather maps: transfer the distance to a latitude scale, at the same latitude as the segment being measured; a technique that works on weather maps, because they are projections of the earth which are designed so that the distance scale is the same in all directions from a specific point. But the grid on GOES pictures is designed only to fit the view of the earth from outer space. The distance scale is not the same in all directions from any given point, because of the earth's curvature.

The 60 n.mi. per degree of latitude technique is accurate on GOES pictures only for measurements in a north or south direction. In addition one other condition must be met: The latitude scale that is used must either be near the segment being measured or near the mirror image of that point on the other side of the longitude of the satellite subpoint. For example: The latitude scale is the same at 40°N 85°W and 40°N 65°W for GOES-1, which is located at 75°W.

This method applied to east or west cloud motions on GOES-1 pictures can lead to large errors, especially in New England where the earth's curvature causes distances to appear to be compressed much more from south to north than from east to west. For example: When measuring the distance across the state of Maine (at 45°N) on a map projection and rotating that distance to the perpendicular, it measures approximately 2.8° of latitude, or about 168 n.mi. (Figure 1). This is comparable to the distance obtained from a Rand McNally Atlas. If this same distance is measured by using the same technique on a GOES-1 picture it becomes approximately 4.2° of latitude, or about 249 n.mi. (Figure 2), an error of 48 percent! The error is less over the rest of the U.S., but is significant (20 percent to 50 percent) throughout the Eastern Region.

An accurate measurement of the distance between two points on a GOES picture can be made by transferring the points to a standard map, if the points can be transferred accurately. In many situations,

especially over the ocean, this may be the best way to proceed. But, what about those times when the points cannot be accurately transferred because they are not near geographical features on the picture or the grid?

East or west distances can be measured accurately on GOES pictures by using the longitude scales on them. The number of miles per degree of longitude is a function of latitude. The following table is provided to measure the miles-per-degree at various latitudes on GOES-1 satellite pictures.

Latitude (degrees)	n.mi. per degree of longitude
20	56
25	54
30	52
35	49
40	46
45	43
50	39
55	35
60	30

For the greatest accuracy, measure the degrees of longitude in the same geographical area as the segment being measured. Again, for example: The measured distance across Maine at 45°N on the satellite picture (Figure 2) is approximately 3.9° longitude. Using the table above: $3.9^{o} \times \frac{43 \text{ n.mi.}}{1^{o}} = 167.7$ n.mi. -- the same as the map measurements.

However, the latitude and longitude lines are left out of the satellite grids over the U.S. It turns out that, over the eastern U.S., the error is very small if a longitude scale over southeast Canada, the Gulf of Mexico, or just off the East Coast is used instead. It must be remembered though, that the number of miles-per-degree of longitude that is used must correspond to the latitude where the longitude scale is located on the picture.

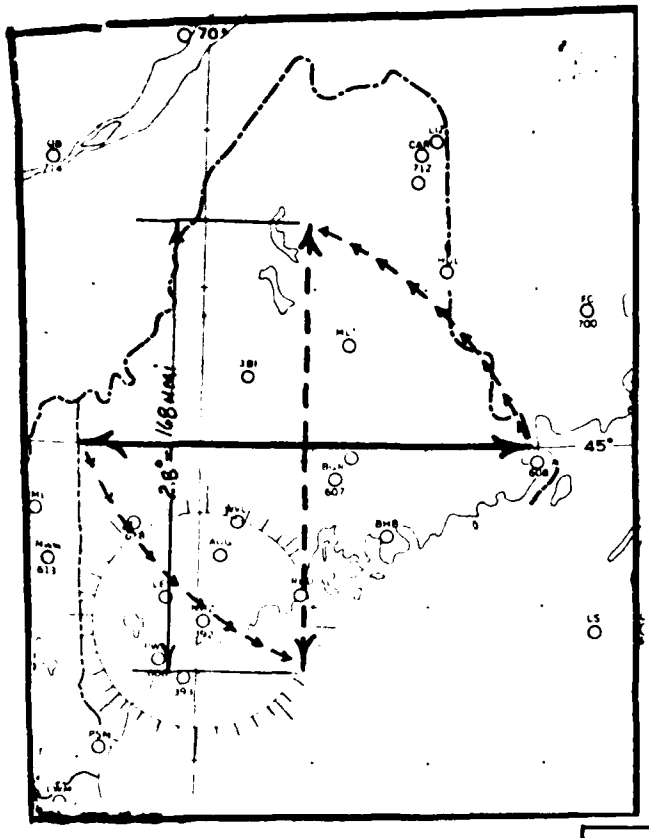

Figure 1. Distance across Maine at 45°N rotated to the perpendicular on a map.

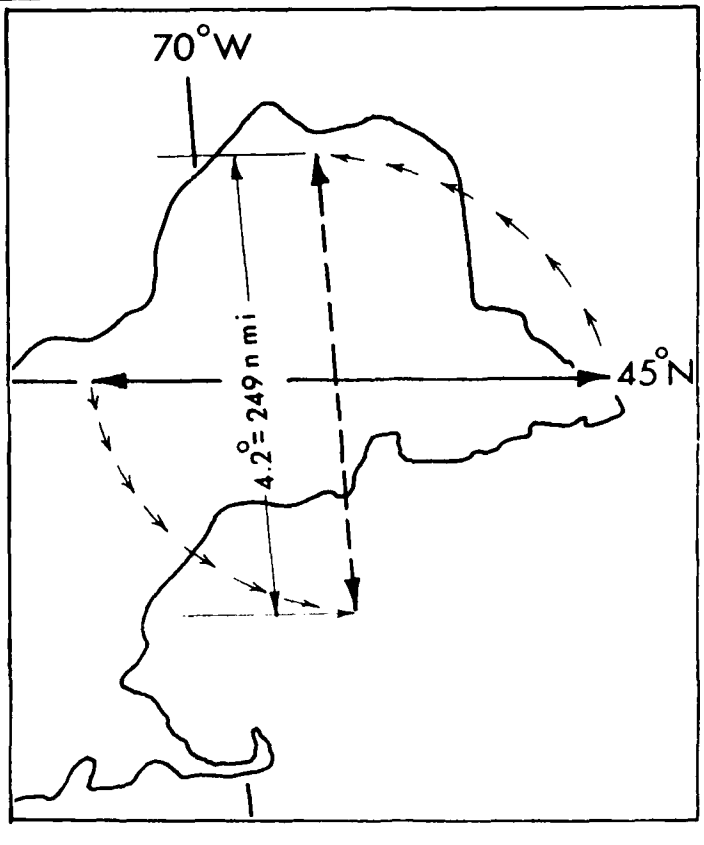

Figure 2. Distance across Maine at 45°N rotated to the perpendicular on a satellite picture.

U.S. DEPARTMENT OF COMMERCE

National Weather Service/National Environmental Satellite Service
SATELLITE APPLICATIONS INFORMATION NOTE 76/17

ESTIMATION OF RAINFALL FROM SATELLITE IMAGERY

Vincent J. Oliver and Roderick A. Scofield

NOAA/NESS Applications Group
Washington, D.C. 20233

1. INTRODUCTION

Since the launch of our first satellite in 1960, there has been continued interest and progress on the use of these weather satellites for the determination of rainfall. One of the earliest studies was by Mae Lethbridge (1967) at Pennsylvania State University who compared the local rainfall with the combination of image brightness and infrared (IR) temperature. Later Eric Barrett (1970, 1973) of Bristol University, England, did a series of studies on monthly rainfall estimates in which he developed statistical methods of estimating rainfall from nephanalyses and later from the actual pictures. Most of this work was designed to determine where rain had fallen; however, his latest works concern the use of satellite data for the prediction of rain.

During the past five years with the advent of better satellite data and the availability of digitized data, more detailed quantitative studies have been conducted using computers, color displays of intensity levels, and concentrated ground truth data. Martin, Stout and Sikdar (1975), University of Wisconsin, Martin and Scherer (1973), Simpson and Woodley (1971) and Griffith et al. (1976), ERL, Miami, were pioneers in this effort. We are now at the point where given the high quality digitized satellite pictures, the processing equipment, and time, reasonably accurate estimate of precipitation can be made.

Hydrologists, working on current operational problems for river or lake management, have frequently asked the following questions: (1) How can we use the satellite data to determine total watershed rainfall quickly enough to be of use in the day-to-day operation of a dam or spillway system? and (2) Where have rains occurred in the past hour heavy enough to cause flashflooding? Using ideas gleaned from the above research plus much experimentation, Walt Follansbee (1973) has attempted to find answers to these two questions using satellite data taken during the afternoon part of the day. Follansbee developed a technique for estimating the 24-hour rainfall in tropical or semi-tropical land areas by judiciously combining the amounts of different types of clouds over the area of concern. A statistical technique was developed which gave useful rainfall averages for areas the size of a small state (about three degrees square). Subsequently, Follansbee and Oliver (1975) developed a modification to this method for use with the evening (9PM) IR satellite data which became available after the afternoon data was discontinued.

Recently, Follansbee in an as yet unpublished manuscript, has developed a technique for estimating rainfall from winter storms anywhere in the world using the twice-per-day satellite pictures now routinely available. Follansbee combines the use of satellite imagery with the normal frequency and amount of precipitation to obtain a rainfall estimate based on the amount and type of cloudiness. Values from zero to several hundred percent of normal are obtained using this technique.

This present study of quantitative precipitation is an attempt to utilize much of the research done previously in conjunction with the development of new IR picture enhancing techniques. The Applications Group of NESS has been using these enhancing techniques to make thunderstorm rainfall estimates more quantitatively processable.

The new IR picture presentation (which we call picture enhancement) makes use of an analog equivalent of a look-up table by which the temperatures and the picture gray-scale can be modified to give us the ability to determine the temperature (or height) of the tops of clouds from the imagery received every half-hour. By using a nearly linear relationship between temperature and brightness (dark for warm and white for cold) up to the thin cirrus level, we obtain the usual cloud pictures everyone has become familiar with, then by contouring the colder temperatures with various shades of gray, we see the tops of thunderstorms and the distribution of the anvil material accompanying these storms. As one might expect, the highest and coldest clouds form where the thunderstorms are most vigorous and the rain heaviest, which taper off downwind as the anvil material blows away from its origin over the updraft.

2. A SCHEME FOR USING ENHANCED IR IMAGERY IN RAINFALL ESTIMATION

As an initial effort for testing the feasibility of enhanced IR imagery in rainfall estimation, the following simple procedure was devised for summer convection in the middle

latitudes. Using enhanced IR imagery as shown in Figure 1, we see seven distinct gray shades. Each shade was assigned a number with "1" (dark gray) representing the warmest and "7" (whitest) those clouds with the coldest tops. The following gray shades were evaluated as follows:

dark gray (warmest - +17 to -2°C)	= 1
light gray (-3 to -23°C)	= 2
white (-24 to -43°C)	= 3
dark gray (-44 to -58°C)	= 4
light gray (-59 to -63°C)	= 5
blackest (-64 to -68°C)	= 6
whitest (coldest - below -68°C)	= 7

Utilizing the above scale, digital IR values were obtained for a 6-hour period (every half-hour) between 0000GMT and 0600GMT on 26 August. Then these digital IR values were summed (for the 6-hour period), analyzed, and compared with the 6-hour precipitation ending at 0600GMT. This comparison is shown in Figure 2 with 500 mb winds for 0000GMT depicted. Since 12 enhanced IR pictures were employed in this case study, the maximum cumulative digital IR value possible was 84. The maximum cumulative IR values of the convective system were located and a dashed line was drawn approximating the axis of the digital IR pattern passing through this maximum. This dashed line separated approximately that portion upwind from the IR maximum and that portion downwind. In this case, the southern two-thirds of Missouri was in the upwind portion while the northern one-third was in the downwind portion. The upwind and downwind portion of the convective system can be determined directly from the imagery pattern in Figure 1 by using the shape of the individual anvils to determine the wind direction.

It can be observed in both Figures 1 and 2 that the largest gradient in the enhanced IR imagery and in the cumulative digital IR values occurred in the upwind portion of the convective system. Also, this upwind portion was where the most significant precipitation occurred. The enhanced IR imagery in Figure 1 shows the cumulonimbus anvil cirrus blowing off downstream. This cirrus contributed to the rather large digital IR values located in northeast Missouri, southeast Iowa, and northwest Illinois, downwind from the active thunderstorms. Six-hour precipitation amounts were generally less than 0.2 inches in this area.

Correlations were computed between the cumulative digital IR values and the observed 6-hour precipitation. These correlations were computed for the entire convective system (upwind and downwind portion) and for the upwind portion alone.

For the entire convective system, the correlation between the observed 6-hour precipitation and the cumulative digital IR values was 0.63. However, when data from only the upwind portion of the convective system was considered, the correlation increased to 0.88. A simple regression equation was obtained in the upwind portion of the convective system between the cumulative digital IR values and the observed 6-hour precipitation. This equation was generated from the data in the upwind portion of the convective system and is given by:

$$P = 0.0185E, \text{ where}$$

P = observed 6-hour precipitation and E = cumulative 6-hour digital IR values.

The results from using the above equation are presented in Figure 3. In the Figure, the 6-hour rainfall estimates are plotted and analyzed for 0000-0600GMT, 26 August 1975. The observed 6-hour precipitation amounts ending at 0600GMT are plotted and analyzed in Figure 4. In both Figures, the upwind and downwind portions of the convective system are indicated by the dashed line. In the upwind portion of the convective system, the analyses of the 6-hour rainfall estimate and observed 6-hour precipitation are comparable. In addition, rainfall was generally overestimated in the periphery of the convective system. Downwind from the center line, the rainfall estimates were not usable. This was expected since that sector represented the blown off anvil area.

3. SUMMARY

In this paper, a simple scheme for estimating rainfall was developed for summer convection in the middle latitudes. Since this simple scheme gave usable results for six-hour rainfall estimation, it appears worthwhile to make a more exact system by enlarging the data sample and incorporating the following already demonstrated improvements:

a. Use only the upwind portion of each cumulonimbus cell for the rain estimates.

b. Weight the rapid expansion period of anvil growth much greater than the decay period.

c. Use Simpson and Woodley's results to give greater weight to merging cumulonimbus cells.

The scheme should also be a function of the synoptic situation and local effects. These above improvements plus an increasing ability to produce digitally enhanced pictures with greater temperature resolution and more precise slicing in the anvil areas suggest that hydrologic applications of satellite imagery can become of great value in the near future.

NOTE: This paper appears in the preprint volumes from both the Sixth Conference on Weather Forecasting and Analysis, May 10-14, 1976, Albany, New York and the Conference on Hydro-Meteorology, April 20-23, 1976, Ft. Worth, Texas.

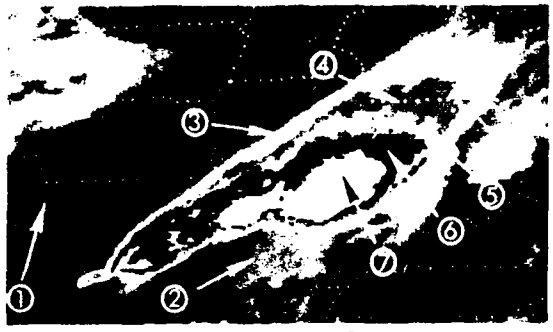

Figure 1. SMS-1 Enhanced IR, 8 km resolution, 0300GMT, 26 August 1975.

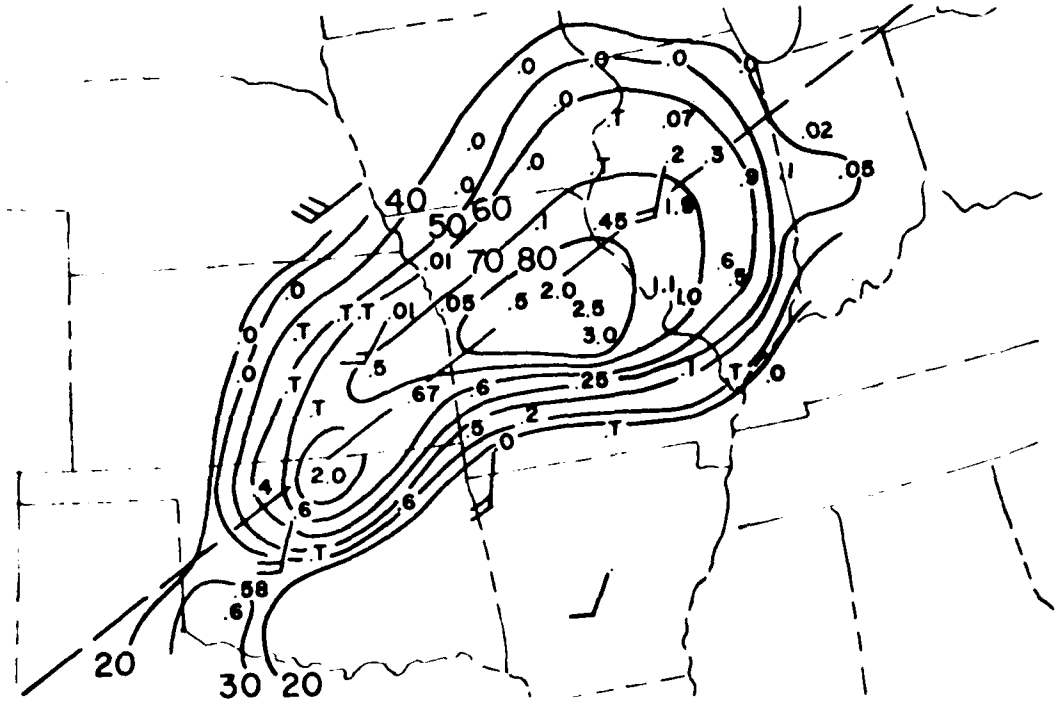

Figure 2. Six-hour precipitation amounts (plotted) and cumulative six-hour digital IR isopleths for 0000-0600GMT, 26 August 1975. 500 mb winds for 0000GMT are also indicated. Dashed line separates upwind and downwind portion of convective system.

ERRATA: SAT APP INFO NOTE 76/14
P.2, para 3, line 1 -- "stratocumulus" vice "stratocummulus".

P.2, last para, lines 4 & 5 -- delete last half of line 4 beginning with "and" and all of line 5.

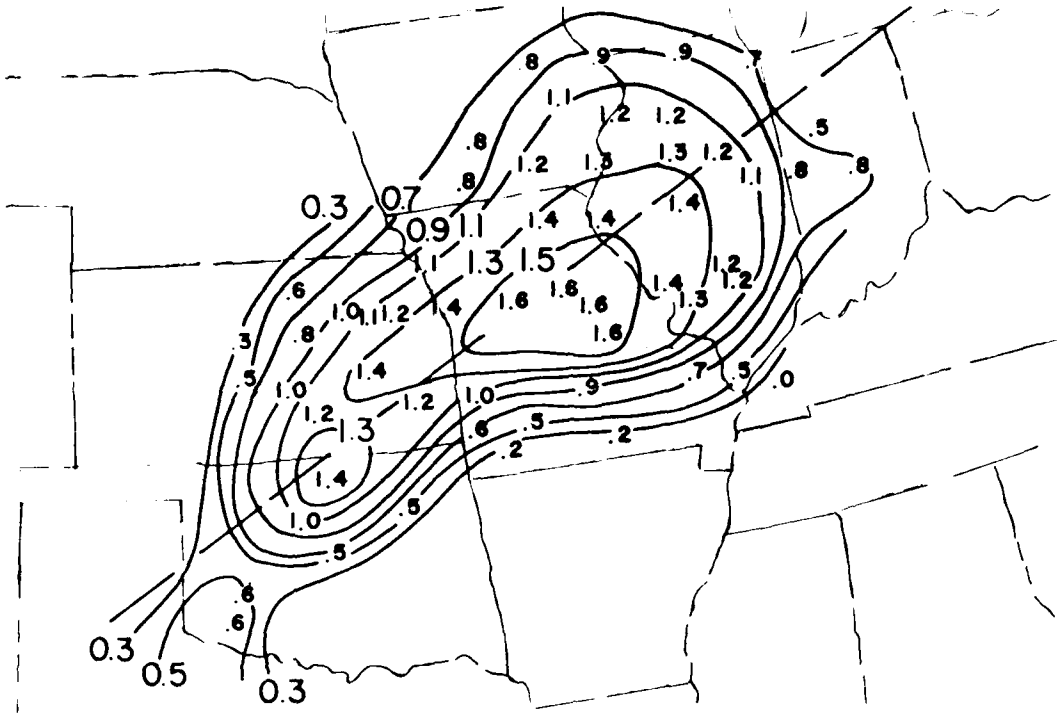

Figure 3. Cumulative six-hour rainfall estimates using the regression equation generated from data in the upwind portion of the convective system for 0000-0600GMT, 26 August 1975. Dashed line separates upwind and downwind portion of convective system.

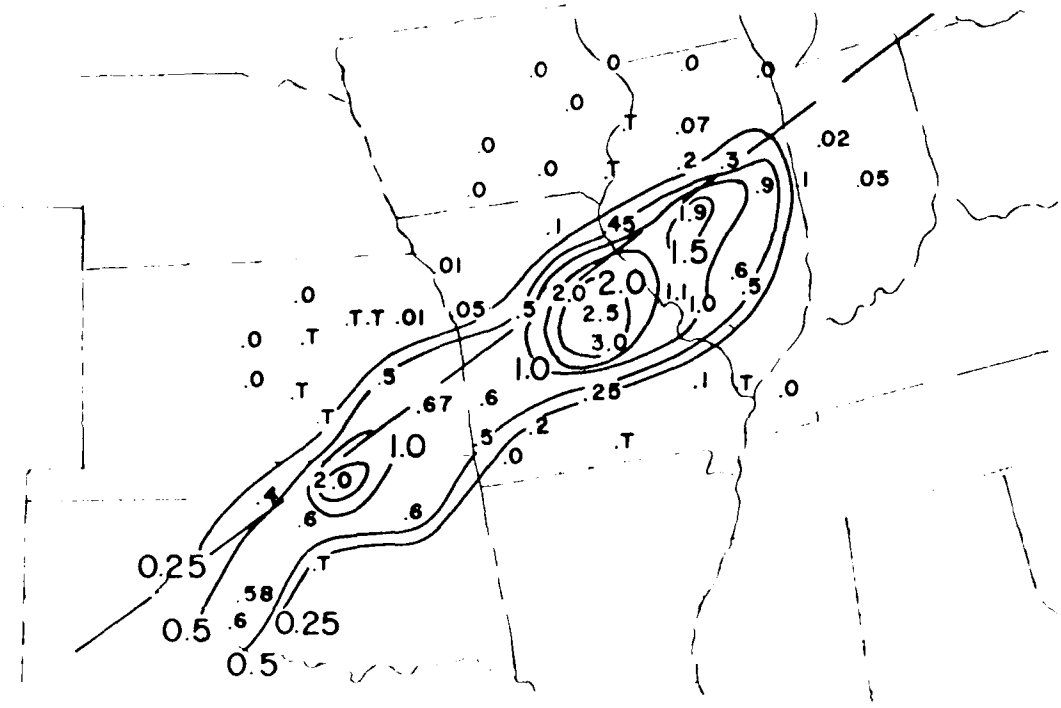

Figure 4. Observed six-hour precipitation amounts (inches) for 0000-0600GMT, 26 August 1975. Dashed line separates upwind and downwind portion of convective system.

112

U.S. DEPARTMENT OF COMMERCE

National Weather Service/National Environmental Satellite Service
SATELLITE APPLICATIONS INFORMATION NOTE 76/18

SATELLITE PICTURES USED FOR LOCATING THE RAINFALL ASSOCIATED WITH A CONVECTIVE SYSTEM OVER TEXAS

Roderick A. Scofield
NESS/Applications Group

One of the ongoing projects in the Applications Group is the fine tuning of a scheme for estimating rainfall amounts from satellite imagery. Enhanced IR and high resolution visible imagery are used to locate rainfall areas in convective systems. A thunderstorm cluster over Texas on May 25, 1976, is used to point out some important factors in using this technique.

Synoptic Situation

The surface analysis for 1500GMT in Figure 1 shows a quasi-stationary front extending from the northern Gulf into north central Texas. Aloft, a north/south ridge extends from Texas into southern Canada at 1200GMT, Figure 2, with a 100 knot jet max located over southern Arizona and New Mexico. Showers and thunderstorms are observed just north of the front under the upper level diffluent flow over Kansas, Oklahoma, and northern Texas. The LFM analysis at 1200GMT in Figure 3 shows ridging throughout the Plains with weak PVA in western Texas and Kansas. A moist area of $\geq$ 70% in the mean relative humidity analysis (Figure 4) is observed over northern Texas and Oklahoma at this time. Presence of a low-level boundary, weak PVA, diffluence aloft, and moisture contributes to the development and maintenance of severe thunderstorms over northern Texas on this day.

Locating Rainfall Areas Using Satellite, Radar and Surface Observations

Surface observations at 1500GMT, Figure 5, continue to show showers and thunderstorms in southwestern Oklahoma and northern Texas. Mineral Wells (MWL), Texas, reports that the thunderstorms north of the station are moving southeastward. Station locations from Figure 5 are shown on the one-mile visible imagery in Figure 6. The visible imagery shows a line of overshooting tops (B) along the leading edge of the thunderstorm area just north to northwest of MWL. By comparing the satellite imagery, Figure 6, with the coincident Stephensville (SEP), Texas, radar observation, Figure 7, the relationship between the bright, textured clouds and overshooting tops and the intense radar echoes becomes apparent. On the other hand, the bright, smooth clouds near Witchita Falls (SPS) and Dallas-Fort Worth Airport (DFW), Texas (Figure 6) represent middle and high cloud debris without precipitation. Also, the radar indicates that the darker clouds (at D in Figure 6), just east and northeast of DFW, do not contain falling precipitation.

One of the characteristics of a convective system is for thunderstorm generation to take place on the upwind side and to propagate to the right of the mean tropospheric wind. The downwind side locates the blown-off anvil material region which contains little or no rainfall. At 1500GMT, the upwind side of the thunderstorm system is just north and northwest of MWL and propagating southeastward. The strong westerly winds aloft with a thunderstorm system propagating southeastward places SPS and DFW in the downwind region (further discussion on upwind and downwind portions of convective systems as related to rainfall is given in Oliver and Scofield,(1976)).

An enhanced IR (Mb curve) picture, taken at 1530GMT (Figure 8), indicates that the upwind portion is composed of a tight gradient of colder temperatures (light gray to white contours). The area from near DFW eastward lies in the downwind portion where the cold temperatures of the blown-off anvil material are still present, but the IR temperature gradient is much weaker. The warmer (darker) areas embedded near the thunderstorm clusters at (A) and (B) may be due to strong compensating subsidence at the periphery of the more vigorous cells. A radar picture at 1530GMT and the surface sectional at 1600GMT, Figures 9 and 10, respectively, show that intense thunderstorms are occurring at MWL. MWL reported hail up to 1 1/4 inch diameter, winds up to 35 MPH, and heavy rain during the 1500-1600GMT period. Over 2 inches of rain was reported at MWL while DFW, which remained in the downwind portion of the convective system, received only 0.08 inches. The radar picture in Figure 9 shows that the intense echoes which encompass MWL are associated with the colder cloud tops and tight IR temperature gradients displayed in Figure 8. The blown-off anvil material from near DFW northward and eastward has cold tops, but is in an area of weak IR temperature gradients. This area is associated with either weak echoes or no echoes.

Summary

In the visible imagery, the heavier rainfall is associated with bright, textured clouds with overshooting tops. Bright, but smooth clouds, and darker cloud areas are associated with little or no rainfall. In the enhanced IR (Mb curve) picture, the heaviest rain is not only associated with cold tops (enhanced light gray to white) but is also in the area of tight IR temperature gradient (upwind portion). The blown-off anvil area contains little or no rainfall, possesses cold tops, and lies in a region of weak IR temperature gradient (downwind portion). There are situations when the upwind portion and active thunderstorm clusters are difficult to find because: (1) the tight IR temperature gradients cannot be discerned, or (2) the colder enhanced IR contours overspread a large area. In such situations during daylight hours, the capability of the high resolution visible imagery to delineate bright, textured clouds and overshooting tops can greatly aid in pinpointing heavy rainfall areas in convective systems.

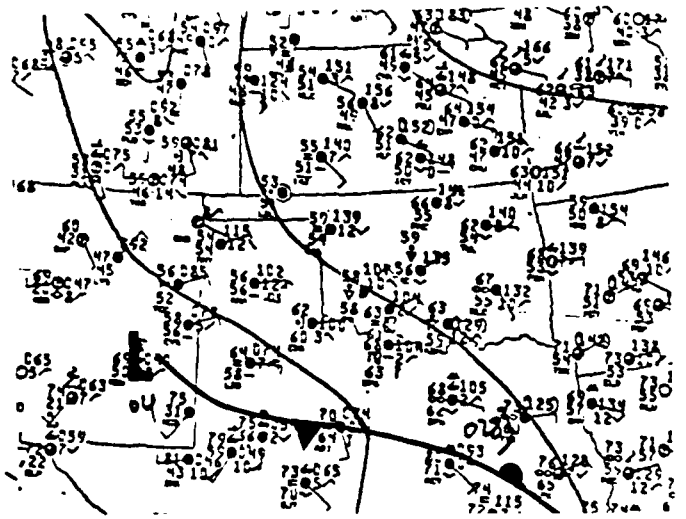

Fig 1. NMC Surface Analysis, 1500GMT, 25 May 76

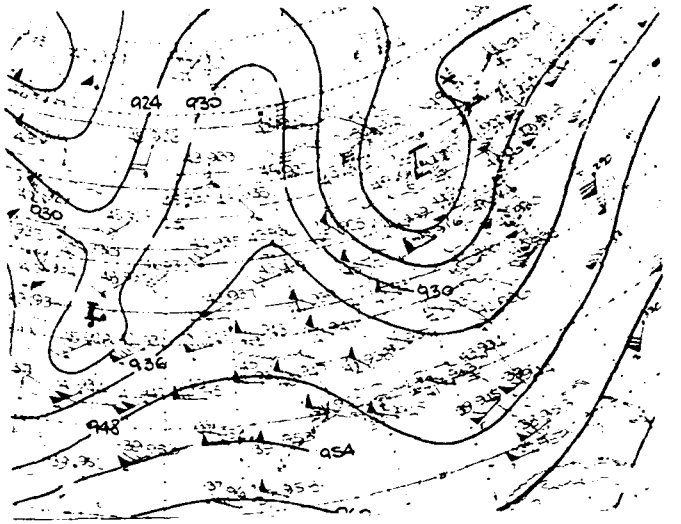

Fig 2. 300mb Analysis, 1200GMT, 25 May 76

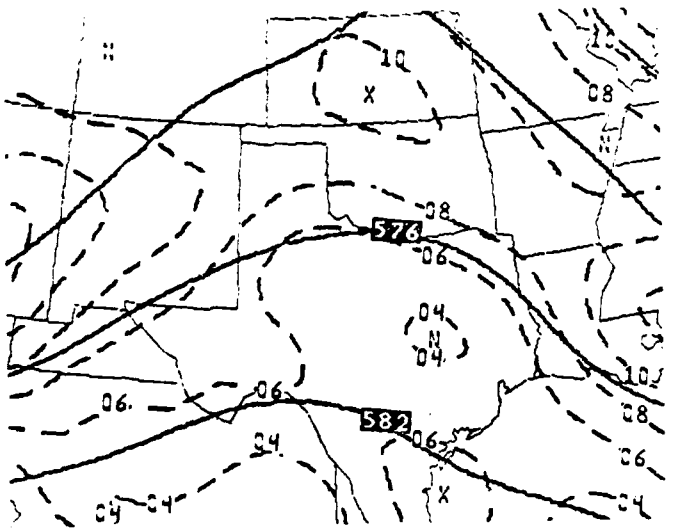

Fig 3. LFM 500mb Heights/Vorticity Analysis, 1200GMT, 25 May 76

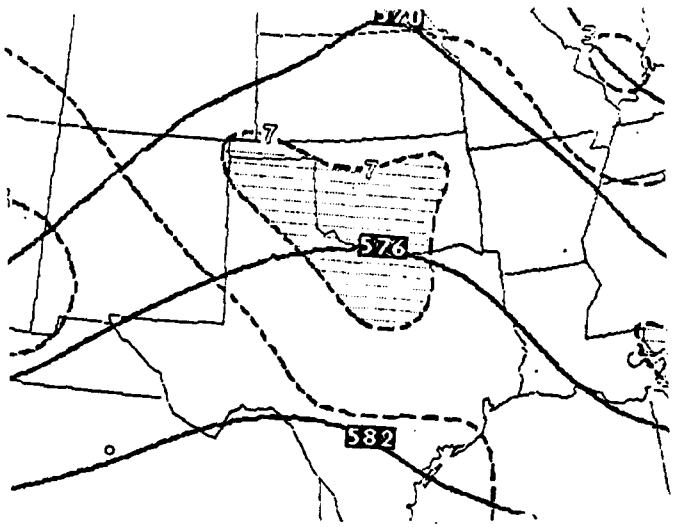

Fig 4. LFM 500mb Heights/Relative Humidity Analysis, 1200GMT, 25 May 76

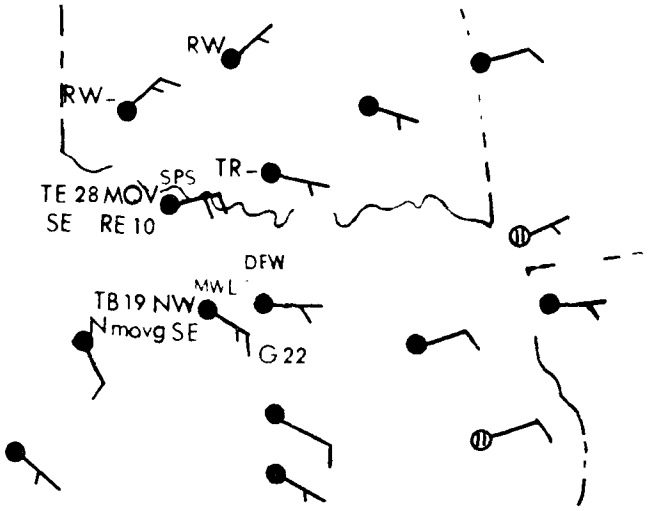

Fig 5. Surface Sectional, 1500GMT, 25 May 76

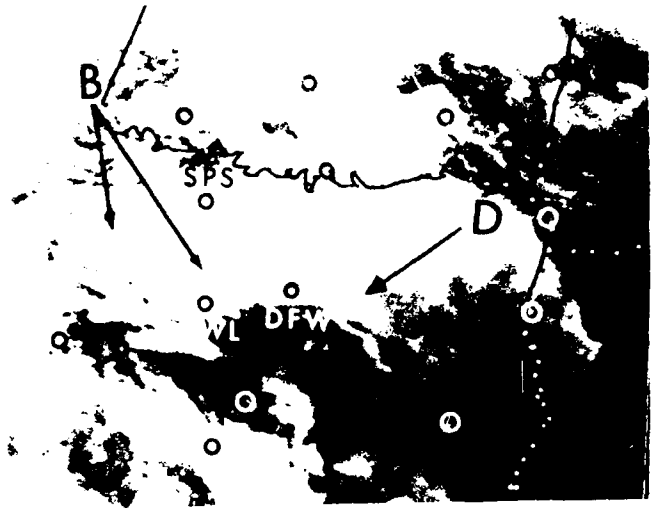

Fig 6. 1-mile Visible Imagery, 1500GMT, 25 May 76

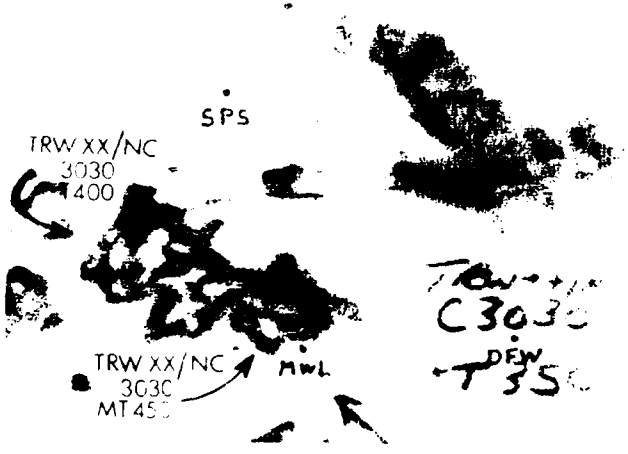

Fig 7. Radar Picture from Stephensville, 1500GMT, 25 May 76

Fig 8. Enhanced IR (Mb curve) Imagery, 1530GMT, 25 May 76

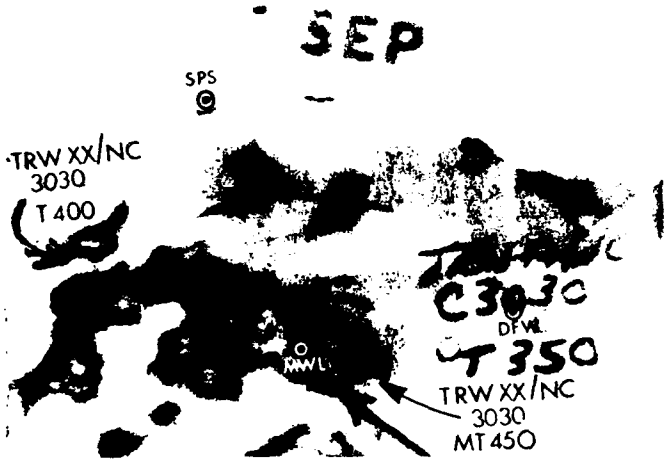

Fig 9. Radar Picture from Stephensville, 1530GMT, 25 May 76

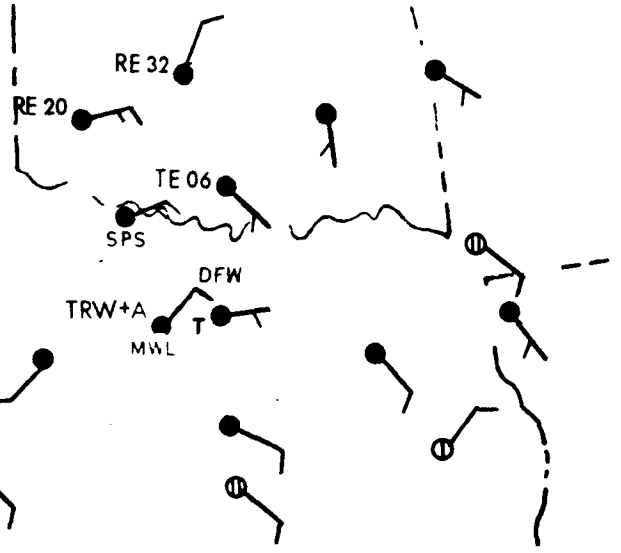

Fig 10. Surface Sectional, 1600GMT, 25 May 76

REFERENCES

Oliver, Vincent J. and R. A. Scofield, 1976: "Estimation of Rainfall from Satellite Imagery," Preprint from the Conference on Hydro-Meteorology, April 20-22, 1976, Ft. Worth, Texas and Preprint from the Sixth Conference on Weather Forecasting and Analysis, May 10-14, 1976, Albany, New York.

U.S. DEPARTMENT OF COMMERCE

National Weather Service/National Environmental Satellite Service
SATELLITE APPLICATIONS INFORMATION NOTE 76/19

FRONTAL WAVE DEVELOPMENT - A MESOSCALE PHENOMENON

Samuel K. Beckman
Satellite Field Services Station, Kansas City, Missouri

A unique characteristic of SMS/GOES satellite imagery is the early detection of mesoscale features which are located between reporting stations. One mile visual pictures from GOES-1 during the afternoon of July 13, 1976, provided an excellent example of the formation of small scale frontal waves along the cold front (Figure 1) over Minnesota and eastern South Dakota.

At 2100 GMT (Figure 2), positive vorticity advection, in advance of a short wave (A-B) over the western Dakotas, created an increase in clouds (C) through the frontal zone (D-E) in eastern South Dakota. The resultant convex bulge toward cold air is characteristic of the wave stage of cyclonic development. A second wave (F) is also evident on the front to the northeast of St. Cloud, Minnesota. Rain was falling out of the post-frontal clouds (P-P') extending from southeast North Dakota to northwest Nebraska. The northern edge of the high cloud band extending from Rapid City, South Dakota (north of B) to central North Dakota (I) was associated with a weak polar jet.

By 2200 GMT (Figure 3) a cluster of convective cells (G) began to form near the crests of the frontal waves where cyclonic circulation associated with the wave augmented surface convergence along the front. At 2230 GMT (Figure 4), a line of cells had developed along the entire cold front (H-I) from northeast Colorado to Minnesota. The 2235 GMT radar summary chart (Figure 5) showed maximum thunderstorm tops of 15km (49,000 feet) near both wave crests.

The storms associated with the wave over southern Minnesota produced 1 3/4 inch hail and wind gusts around 50 knots which caused damage to trees in the vicinity of Redwood Falls, Minnesota. This was the only reported area of severe weather along the front on this day.

This example illustrates how small scale features, such as these frontal waves, can be identified in satellite imagery. Prior to the operational use of satellite imagery, systems of this type were often-times not readily apparent on synoptic scale surface charts. Early detection of these waves was helpful in isolating areas of increased surface covergence along a front which on this day, produced a localized area of severe weather in southern Minnesota.

ERRATA: Note 76/11. Delete "term in the vorticity equation" on page 2, paragraphs 2 and 3, last sentences.

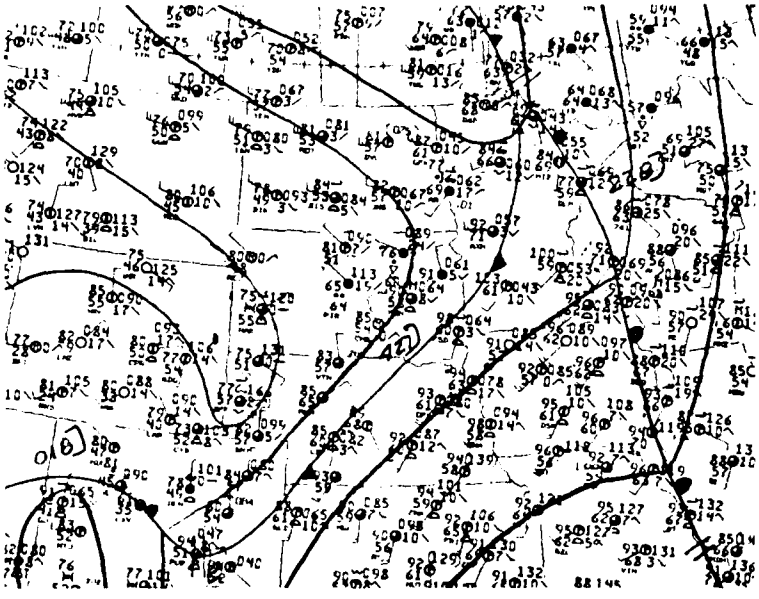

FIG. 1 NMC Surface Analysis, 2100 GMT July 13, 1976

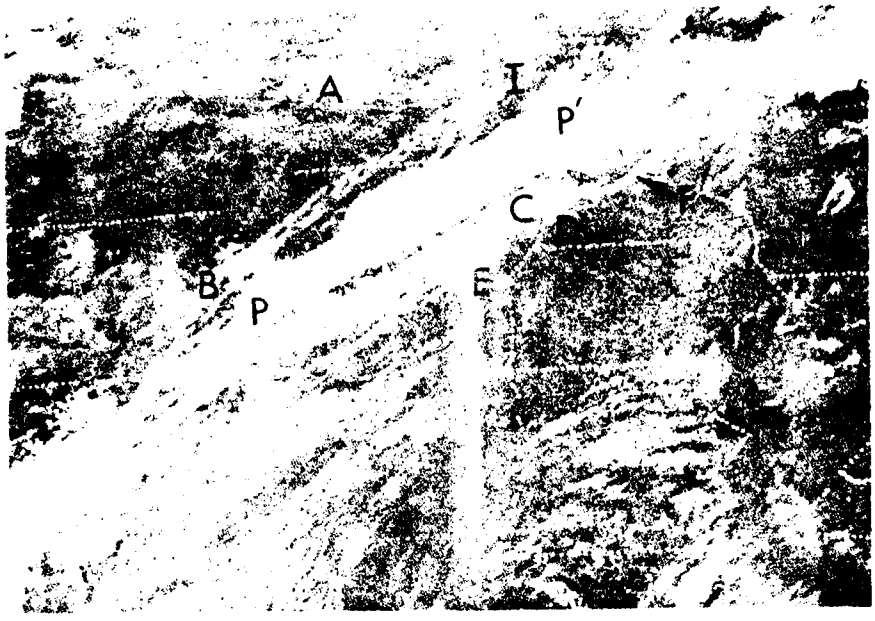

FIG. 2 GOES-1 VIS 2100GMT 13 JULY 1976

FIG.

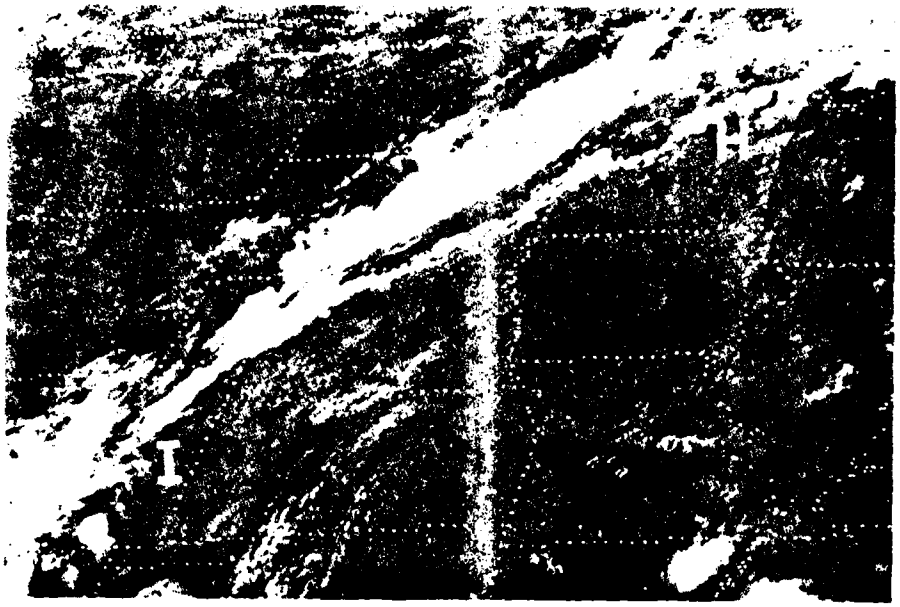

FIG. 4 GOES-1 VIS 2230GMT 13 JULY 1976

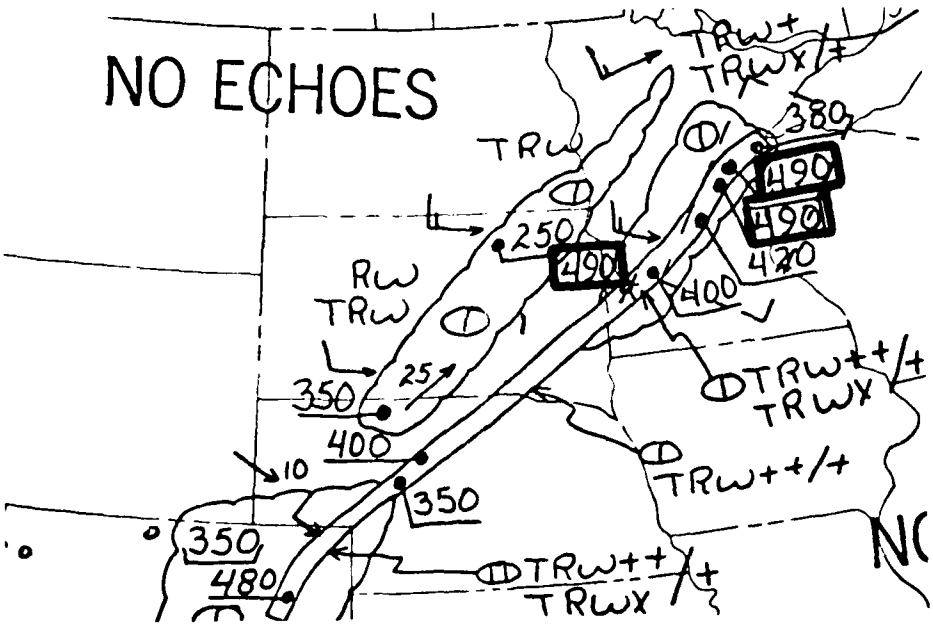

FIG. 5 RADAR SUMMARY CHART 2235GMT 13 JULY 1976

U.S. DEPARTMENT OF COMMERCE

National Weather Service/National Environmental Satellite Service
SATELLITE APPLICATIONS INFORMATION NOTE 76/20

CUMULUS LINE FORMATION IN THE TRADE-WIND EASTERLIES

Robert N. Larson
NESS, Satellite Field Services Station, Honolulu, Hawaii

The ocean area between California and Hawaii, located to the south of the semipermanent Eastern Pacific surface high pressure ridge (35°N), normally is largely covered by an extensive low-level trade-wind cloud field. This cloud field is usually restricted in the vertical by the presence of a strong subsidence temperature inversion. During the summer this inversion height averages from 500 m along the California coast to about 2000 m over Hawaii. Cloud patterns under this inversion vary from thin stratus, predominant near California, to complex mosaics of open-closed cellular stratocumulus (Sc) further offshore, to increasingly more unstable cumulus (Cu) clusters and line formations. Such Cu clusters and lines, when advected over the Hawaiian Islands by the prevailing NE trades, contribute significantly to trade-wind rainfall. Organized Cu patterns such as mesoscale circulation systems and frontal shear lines have recently been considered via geostationary satellite imagery by Weldon (1975) and Larson (1976), respectively. These Cu patterns have frequently been observed to be associated with a disruption of the trade-wind inversion and resultant above-normal rainfall.

Two examples of non-frontal Cu line formation occurred NE of Hawaii during 19-23 April 1976. These lines appeared and behaved very similarly to frontal shear lines which are a frequent source of winter trade wind rainfall in Hawaii. The synoptic pattern during this period was relatively static and not atypical. As seen in Fig. 1 of 0000 GMT, 20 April an E-W surface high pressure ridge was centered near 35°N with prevailing low-level easterlies to the south over the Hawaiian Islands. At the 250 mb level an ENE-WSW trough extended from California to Hawaii. By 23 April the surface ridge shifted southward to near 30°N ahead of an approaching cold front while the 250 mb trough became oriented N-S along 145°W. This latter development was due to the influence of a passing short-wave trough aloft in the westerlies. The presence of upper-level troughing probably contributed to the predominance of open-cellular Cu in the area between Hawaii and 145°W during 19-23 April (Figs. 2-6).

Figures 2-6 reveal sequentially the development and movement of the Cu lines across Kaui (K) and Hawaii (H). The early stage of Cu line formation can be seen in Fig. 2 of 19 April as a zone of open-cellular Cu (A to A') along 25°N from 120°-145°W. In Fig. 3 of 20 April this line, A, has progressed to the edge of the cloud field and begun to separate from it. By 21 April, Fig. 4, line A is approaching the islands as a new line, B, again forms along 25°N. In Fig. 5 of 22 April, Line A has moved through the islands at about 15 knots and has been temporarily weakened in the

process. Line B is now well organized and approaching the islands. Finally Fig. 6 of 23 April shows both lines west of the islands and moving westward at about 20 knots in response to increasing trade wind velocities.

Weather in the islands during the Cu line passages consisted primarily of the light showers at sea level and some heavier showers at higher elevations. Rainfall during the 24-hour period ending 1800 GMT (0800 HST), 22 April, and largely attributable to line A, was in excess of 25 mm at some mountain stations on the islands of Kauai and Oahu. Heavier rainfall, with amounts to 48 mm, were recorded on the island of Hawaii, which was located directly under the 250 mb trough. Rainfall associated with the passage of line B, during the 24-hour period ending 0800 HST, 24 April, was somewhat less overall than from line A, although amounts in excess of 25 mm were again reported on Oahu. This slight reduction in rainfall may have been related to the more rapid movement of line B through the islands and to the dampening influence of a short-wave ridge aloft at the time. Nevertheless both lines produced appreciable and well above-normal periods of trade-wind rainfall. This increased rainfall was evidently attributable to the increased vertical development of the Cu in the lines which were able to penetrate the prevailing 2000 m trade wind inversion. Lihue radiosonde soundings revealed a coincident inversion breakdown during and rapid reformation after the passage of both Cu lines.

The 24-hour SMS-2 satellite coverage now available in Hawaii enables forecasters to more accurately track a variety of transiting mesoscale trade-wind disturbances. Through such observation the impact of these disturbances on island weather is rapidly becoming better understood. Without adequate satellite observation in relatively data-sparse oceanic areas, the forecasting of many mesoscale features would continue to be largely an impossibility.

REFERENCES

Larson, R.N., 1976: Shear Line Weather Regime Over Hawaii, Mon. Wea. Rev. 104, 1081-1083.

Weldon, R., 1975: Low Level Circulation Systems in the Easterlies, NOAA NESS Satellite Applications Information Note 11/75-1, 4 pp.

23

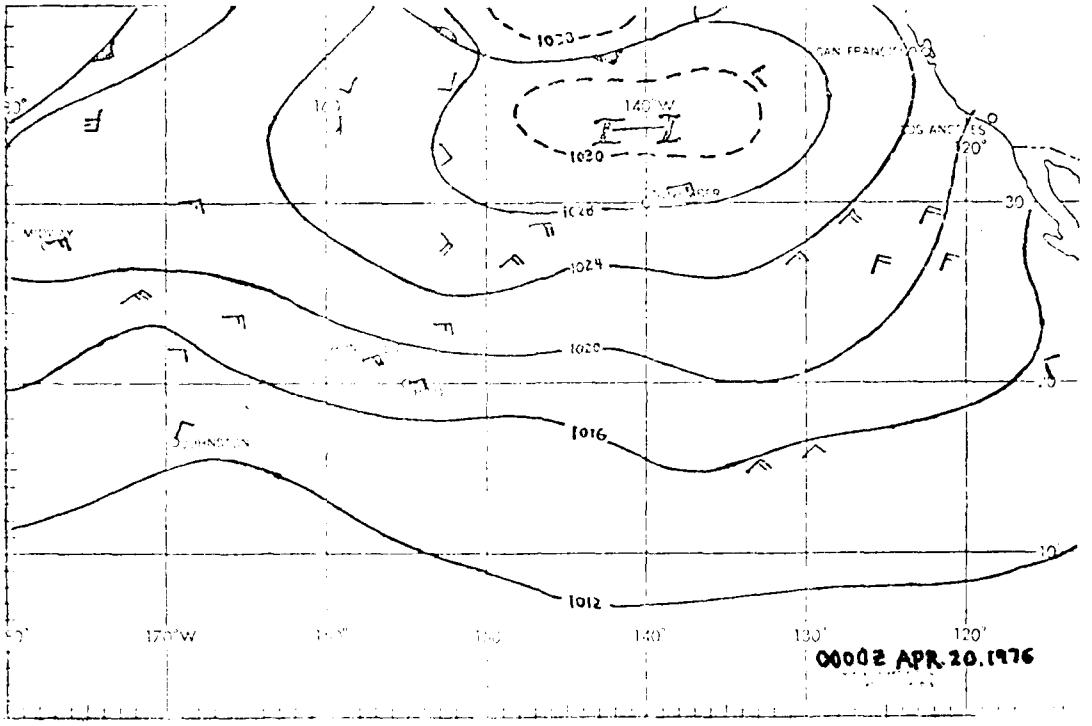

Figure 1. Surface Analysis, 0000GMT 20 April 1976.

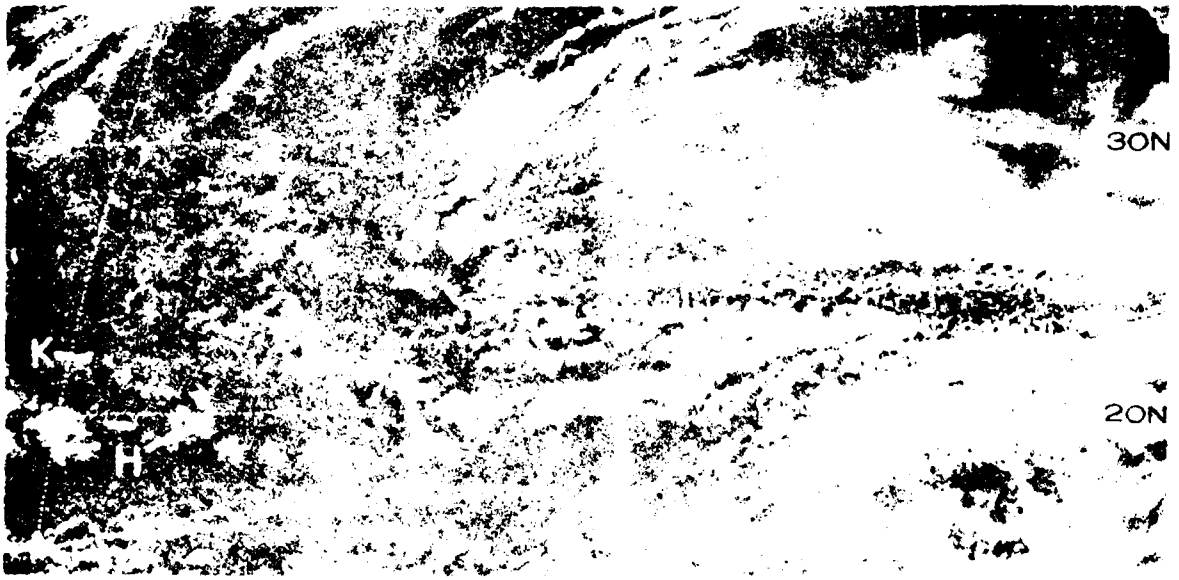

Figure 2. [illegible] Bias Data, 2215GMT, 19 April 1976.

Figure [illegible]. [illegible] Visible Data, [illegible]GMT, [illegible] April 1976.

Figure 8. [illegible] Visible Data, [illegible]GMT, [illegible] April 1976.

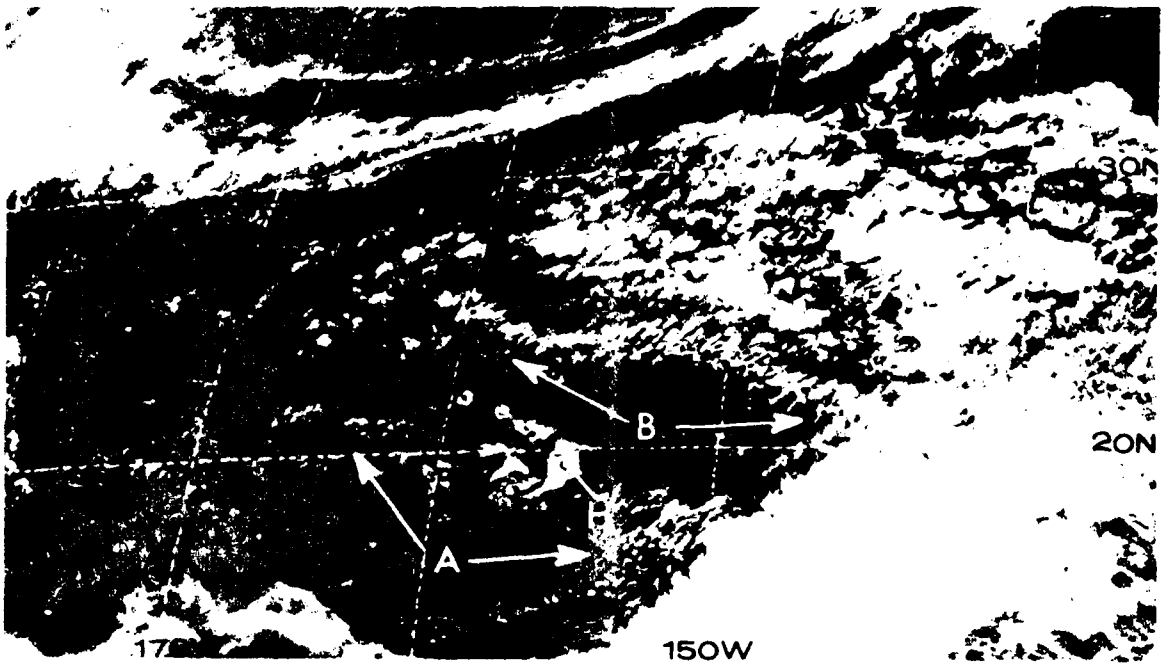

Figure 5. GMS-1 2 km Visible Data, 2315GMT, 22 April 1976.

Figure 6. [illegible] km Visible Data, 2315GMT, 23 April 1976.

U.S. DEPARTMENT OF COMMERCE

National Weather Service/National Environmental Satellite Service
SATELLITE APPLICATIONS INFORMATION NOTE 76/21

MOISTURE EFFECTS AS SHOWN ON GOES-ENHANCED IR IMAGES

Paul M. Duernberger (LCDR. NOAA Corps)
Satellite Field Services Station, Miami, Fla.

The type and amount of cloudiness over an area are certain indicators of atmospheric processes such as air mass movement, convergent areas upper level diffluence, and irregular heating of the earth's surface. The amount and distribution of water vapor is directly connected to these motions and processes.

Under clear sky conditions, atmospheric moisture will absorb outgoing long wave radiation, thus a lower radiance temperature will result and the surface will appear colder in the daytime satellite view than it actually is. (At night the opposite is true; a warmer temperature is observed as water vapor serves to cause a "greenhouse" effect.) In order to delineate "moist" and "dry" areas, a comparison of an enhanced infrared (EIR) picture (GC enhancement curve) with a compatible visible sector is presented to illustrate the effect of moisture on radiance temperatures.

The 1930Z EIR photograph (figure 1) shows many small "dry" zones (white outlines) in the eastern Caribbean Sea (Box 1), a few just east of the Bahamas (Box 2) and three zones in the western Gulf of Mexico (Box 3). Comparing the IR with the 1930Z visible picture (figure 2), note that the general "gray smearing" (G) in figure 1 through the eastern Caribbean Sea east of 75W is an area of very few small clouds (G, figure 2) in the visible. (An easterly wave, located near 82W at this time, had a history of little African dust behind the wave, thus the cooler return is not due to airborne particulate matter.)

Mean mixing ratios for the Caribbean stations showed a moisture decrease of 2.5 grams at Curacao (C) and a 0.8 gram decrease at Trinidad (T) for the period 12Z August 12, 1976, through 00Z August 13, 1976. Based upon these 00Z upper air measurements and the GC enhancement of the IR (figure 1), the area around Trinidad was in a dark or dry zone of 7.0 grams while Curacao, in a gray area, reported an 8.5-gram measurement. Based upon this single comparison, the amount of moisture that will cause this "gray smearing" in this GC curve display is about 8.0 grams. Grand Cayman Island (I) increased 1.1 grams, from 9.9 to 11.0 during this same period, yet was clear in the visible imagery (not shown). The data in figure 1 showed a significant cloud and moisture area poised on the western edge of the island.

Using figures 1 and 2, the "dry" zones (D, D') just east of the Bahamas align very well with the clear zones of the visible picture, yet in between these zones a two-degree-wide "smear band" (G, figure 1) with only widely scattered low clouds (G, figure 2) is present. The surface water temperatures varied very little, and in both areas the thermal gradients were very weak and could not have had any major effect on radiance temperature.

Possible uses of such enhancement curves, besides the present analysis of the Gulf Stream, are the location of areas of large-scale vertical motions preceding a frontal passage and the location of the large moisture pockets for a severe weather outbreak. On the other hand, the dark clear areas provide information about large-scale atmospheric subsidence. The best results using the GC curve, however, have been over water, and an adjustment must be made for any such plotting over land.

A second use would be the estimation of precipitable water for a tropical or semi-tropical area using the available moisture as shown from the picture. Expanding this concept to the trades, the moisture content of an easterly wave could be monitored. However, a significant problem would be the effect of the African dust behind the wave on the radiance temperature. (Visible data could assist in the determination of the cooling process.)

In one recent case, the Miami area forecast was improved as a result of monitoring the movement, expansion,and contraction of a "dry" zone. Figures 1, 3, 4, and 5 show a "dry" zone approaching and crossing the southeast coast of Florida. The Miami sounding confirmed a marked change from a "moist" to "dry" condition between 12Z August 14 to 00Z August 15, 1976, and the stability index increased from a +1 at 12Z August 14 to a +4 at 00Z August 15, 1976.

127

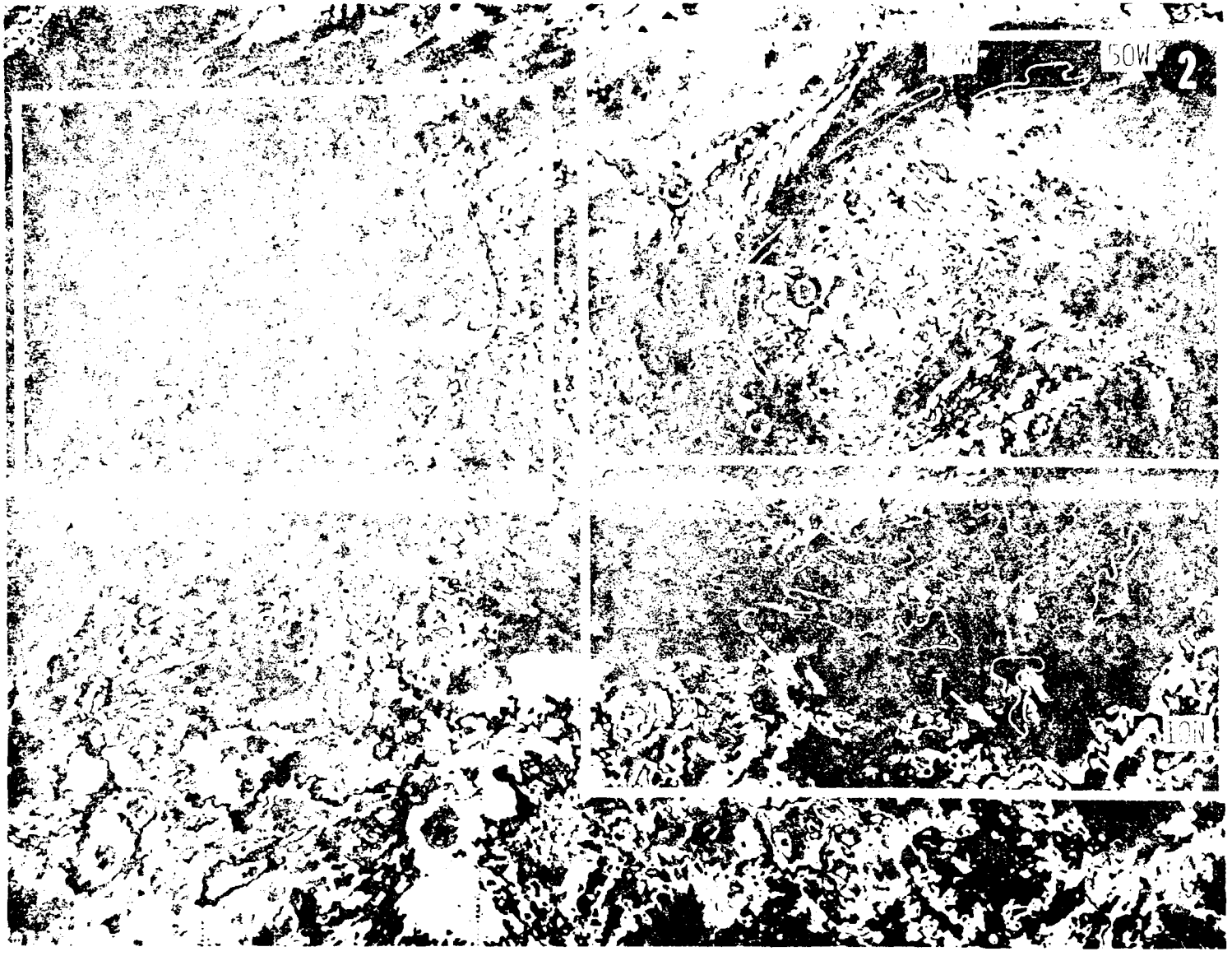

Fig. 1 1930Z August 12, 1976. Infrared photograph with GC enhancement. "Dry" zones outlined in white.

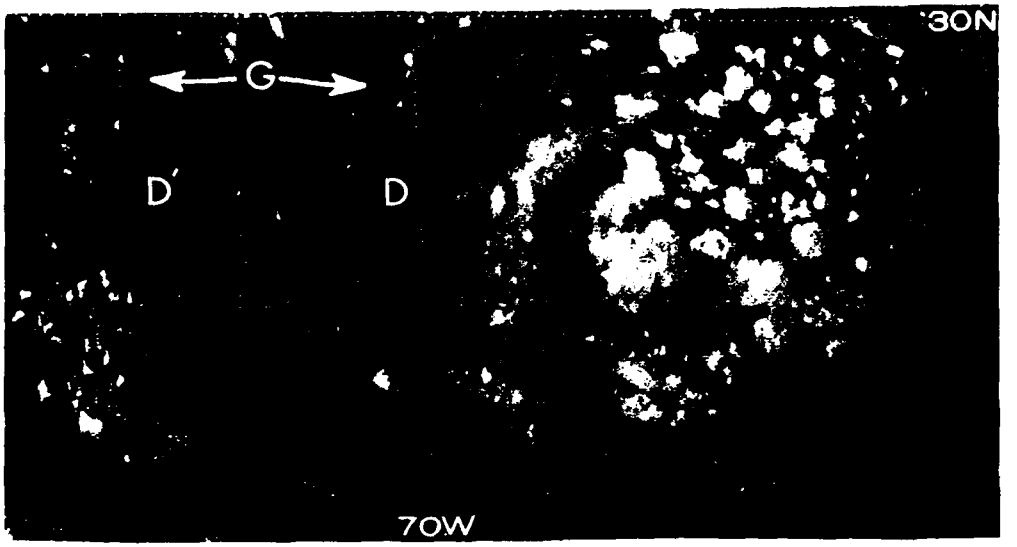

Fig 2. 2030Z August 12, 1976. Visible picture with one-mile resolution.

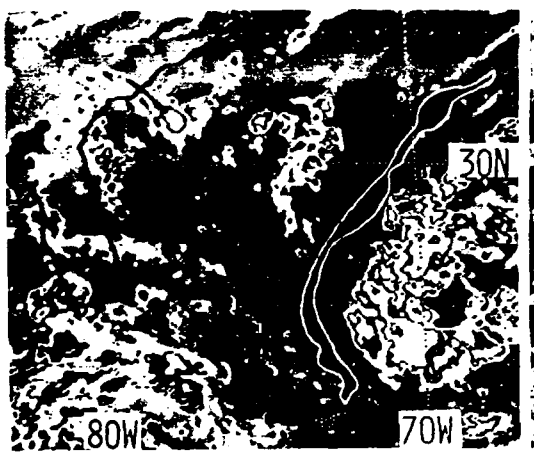

Fig. 3. 0830Z August 13, 1976. Infrared photograph with GC enhancement.

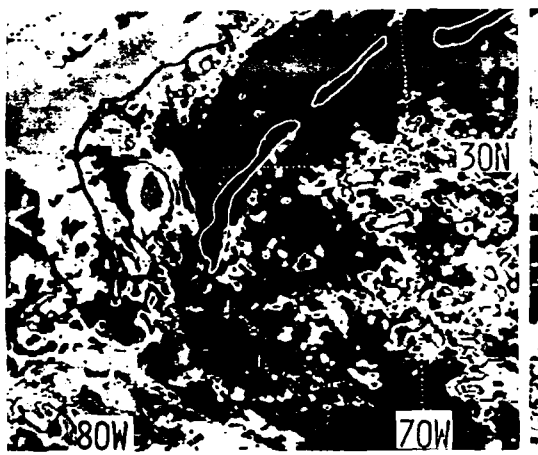

Fig 4. 0830Z August 14, 1976. Infrared photograph using GC enhancement.

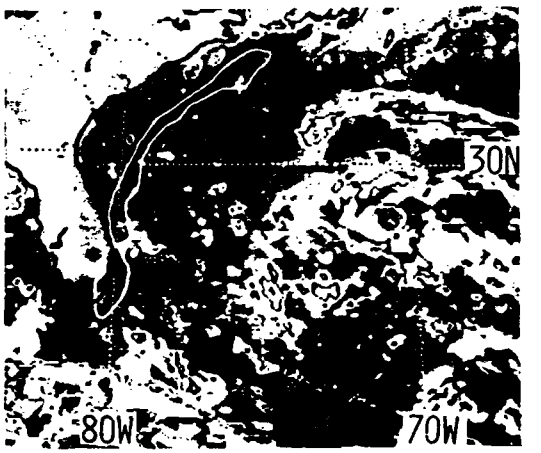

Fig 5. 0830Z August 15, 1976. Infrared photograph using GC enhancement. The "dry" zone has crossed the southeast Florida coast.

U.S. DEPARTMENT OF COMMERCE

National Weather Service/National Environmental Satellite Service
SATELLITE APPLICATIONS INFORMATION NOTE 76/22

AN EXAMPLE OF NIGHTTIME FOG FORMATION IN SOUTH CAROLINA

James J. Gurka
Applications Group/NESS

This information note discusses the use of satellite imagery in the short-range forecasting of fog and stratus formation during the night. Conditions favorable for the formation of advection-radiation fog include clear skies, light winds, and a maximum of low-level moisture. Frequently, areas with a relatively high moisture content in the lower atmosphere can be inferred from the enhanced infrared (EIR) GOES imagery (references 1 and 2). At night, these moist areas will generally appear as warmer regions in the EIR due to the fact that the ground does not cool off as rapidly in a moist air mass as in a dry regime. Therefore, it is not the moist air itself that is seen on the IR imagery, but rather the effect of the moist air on the radiating surface. (It should be noted that the warmer ground temperatures do not necessarily show up at the six-foot instrument shelter height.) Delineation of these warmer, moist areas is important since they will be the most likely areas to watch for fog and stratus formation.

At 0600 GMT on October 14, 1976, skies were clear over South Carolina with a cold front approaching from the northwest (see Figs. 1 and 2). In Fig. 2 and in the visible imagery at 1630 GMT (Fig. 3), there are several lakes and reservoirs (dark areas) that can be seen: H is the Hartwell Reservoir; C is the Clark Hill Reservoir; M is Lake Murray; A is Lake Marion; and O is Lake Moultrie. The front became stationary along the South Carolina coast during the afternoon of the 14th and moved very little throughout most of the following evening. With clear skies and very light winds, there was a good setup for fog formation in the vicinity of the front (Fig. 4). A zone of maximum low-level moisture could be inferred from the 0600 GMT EIR picture (Fig. 5) near the front with boundaries at A and B. The moisture maximum becomes particularly obvious when compared to the ground temperature pattern on the previous evening (Fig. 2). The darkest spots on Fig. 5, however, are the lakes and reservoirs that are shown on Fig. 2. Melding the surface observations with the moisture pattern shown on the EIR picture, isodrosotherms were drawn on Fig. 4. Using both the satellite data and the hourly observations, considerable increases can be made in the presentation of details in the dew point analysis.

By 0800 GMT and 1000 GMT (Figs. 6-8), the darker areas had become more pronounced (A and B, Figs. 6 and 8) with an obscuration due to fog,

first reported at Savannah (SAV) on the 0800 GMT observation (Fig. 7). By 1200 GMT, a very distinct pattern of warm temperatures (C, D, and E on Fig. 9) marked the boundary of the fog, which was verified by (1) the visible picture at 1230 GMT (Fig. 10) and (2) the reports of dense fog at Columbia (CAE) and Charleston (CHS) at 1200 GMT (see Fig. 11). This fog pattern formed within the area of maximum low-level moisture as indicated on the earlier satellite pictures.

Frequently, an enhancement curve with a steeper slope in the warm end than this Mb curve is needed to pick out areas of low-level moisture in the early evening and the fog itself later at night. In this case, however, as can be seen from the Charleston RAOB on Fig. 12, there was at least a 10^{o}C temperature difference between the instrument shelter temperature and the fog top temperature.

The example shown in this information note demonstrates how the EIR satellite pictures could be used to pick out areas of maximum low level moisture which under clear sky conditions represents the location with the greatest potential for fog and stratus formation. Obviously, it should not be assumed that the appearance of a low level moisture maximum will guarantee fog formation, nor should the fog be expected to fit the moisture pattern exactly, but it can give a fairly good estimate. In this particular case, the moisture did not show up well until approximately 0600 GMT; but in other cases, the pattern has been discernible as early as 0100 or 0200 GMT.

REFERENCES

1. Parmenter, Frances C., 1976: Low-level moisture intrusion from infrared imagery, MWR Vol 104, pp 100-104.

2. Gurka, James J., 1976: Using satellite data as an aid to forecasting fog and stratus formation, NWS/NESS Satellite Applications Information Note 3/76-1.

3. Sutton, O. G.: "Micrometeorology" McGraw-Hill, NY 1953, pp 178-179.

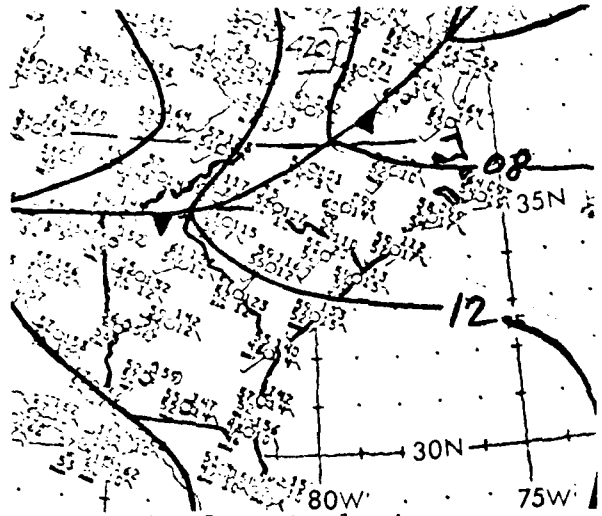

Fig 1. NMC Surface Analysis
0600 GMT, 14 Oct 76

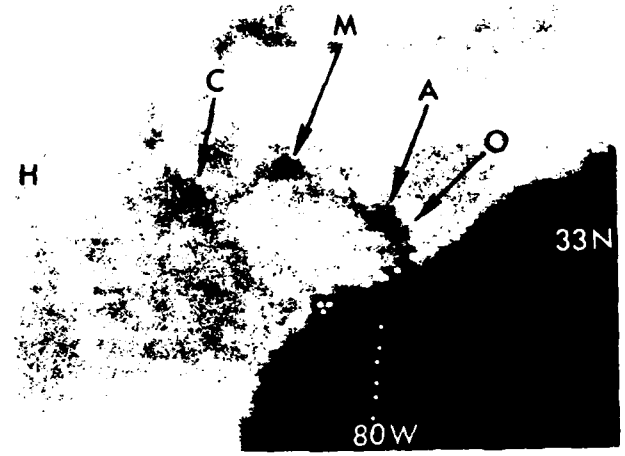

Fig 2. GOES-1 8 km Enhanced IR
(Mb curve) 0600 GMT, 14 Oct 76

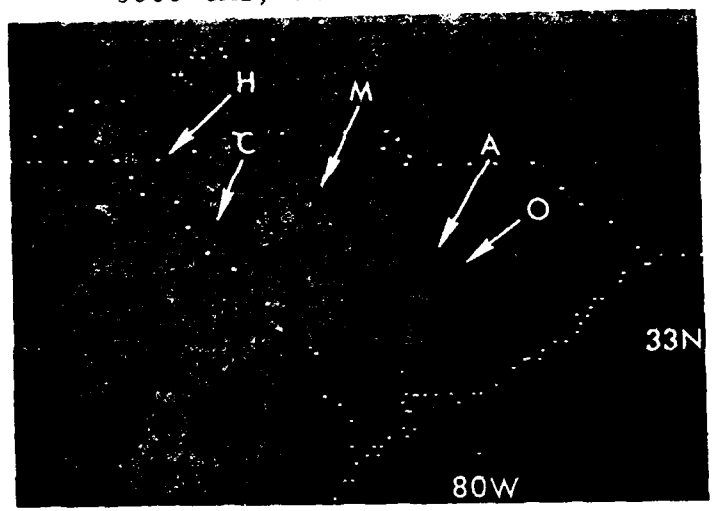

Fig 3. GOES-1 1 km Visible
1630 GMT, 14 Oct 76

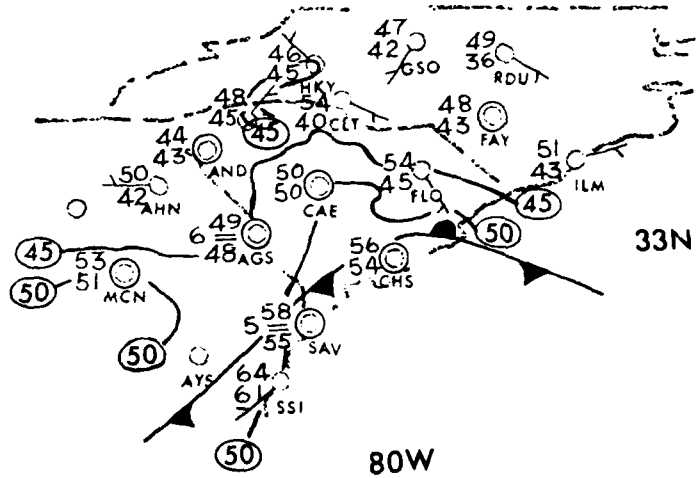

Fig 4. Surface Observations with
Isodrosotherms, 0600 GMT,
15 Oct 76

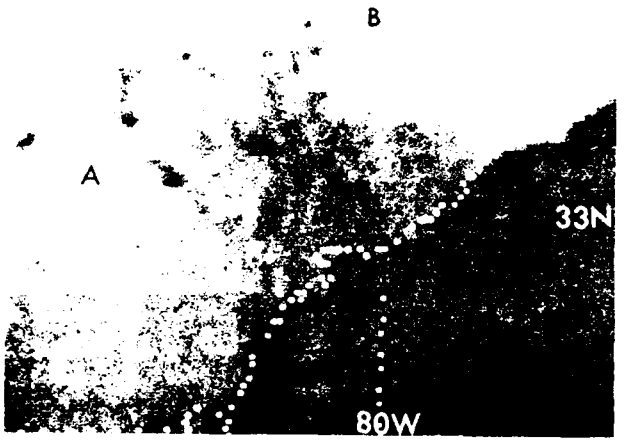

Fig 5. GOES-1 8 km Enhanced IR (Mb curve) 0600 GMT, 15 Oct 76

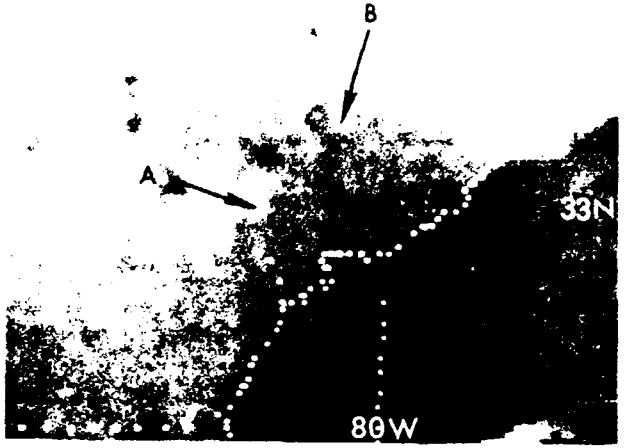

Fig 6. GOES-1 8 km Enhanced IR (Mb curve) 0800 GMT, 15 Oct 76

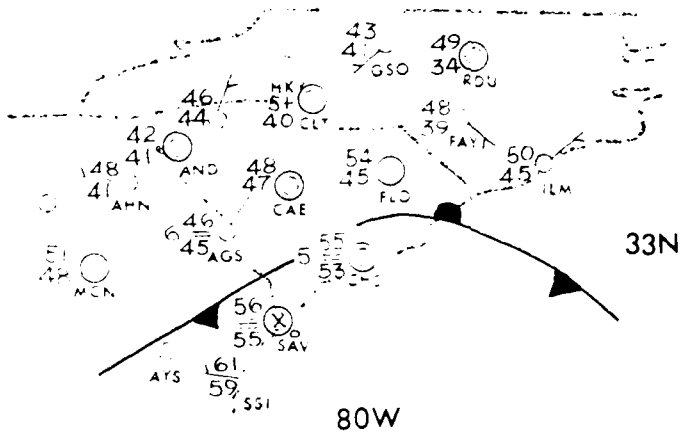

Fig 7. Surface Observations 0800 GMT, 15 Oct 76

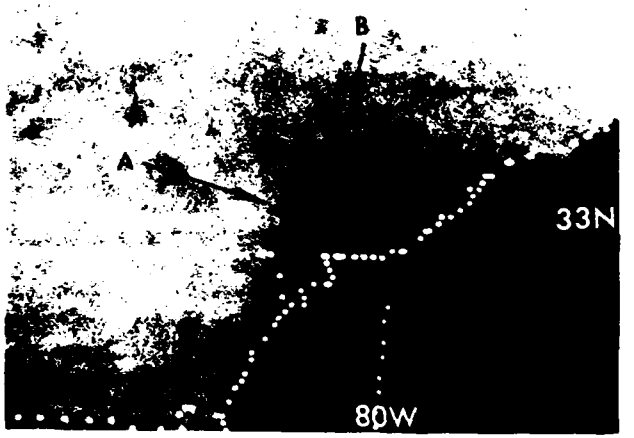

Fig 8. GOES-1 8 km Enhanced IR (Mb curve) 1000 GMT, 15 Oct 76

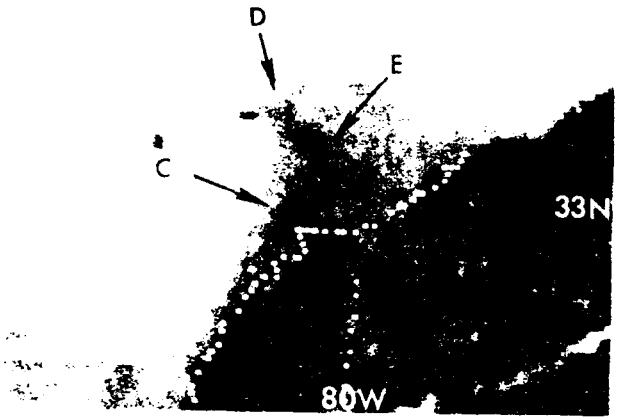

Fig 9. GOES-1 8 km Enhanced IR (Mb curve) 1200 GMT, 15 Oct 76

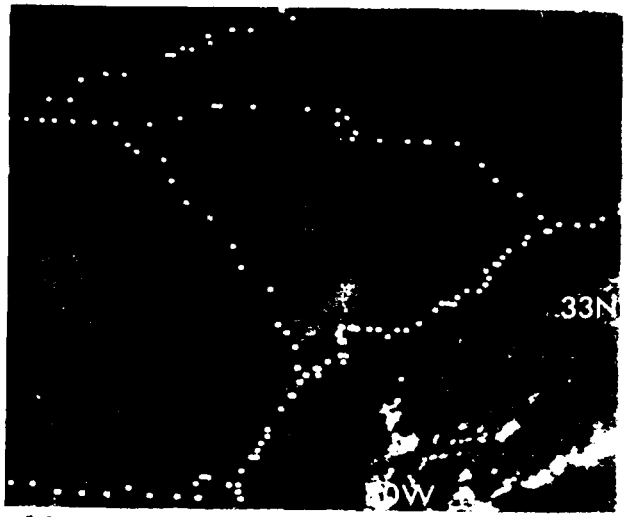

Fig 10. GOES-1 2 km Visible 1230 GMT, 15 Oct 76

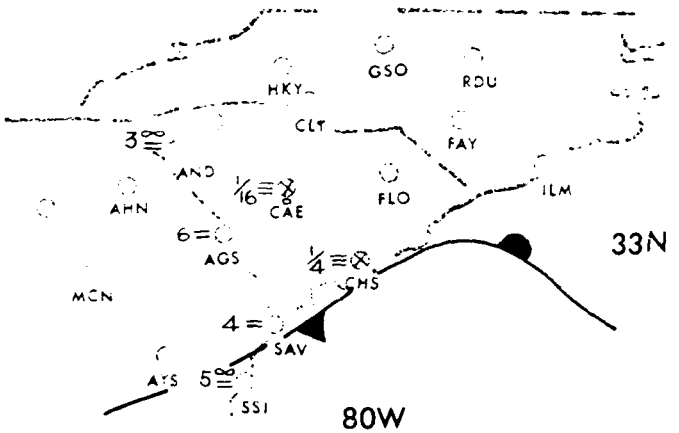

Fig 11. Ceiling and Visibility 1200 GMT, 15 Oct 76

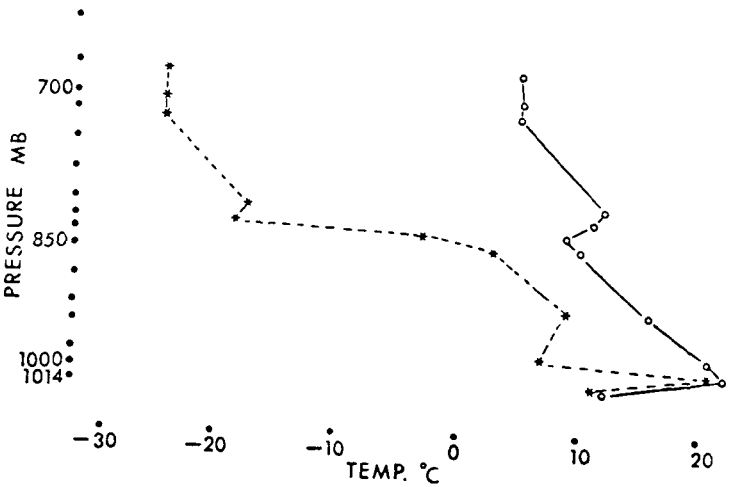

Fig 12. Charleston, SC RAOB 1200 GMT, 15 Oct 76

U.S. DEPARTMENT OF COMMERCE

National Weather Service/National Environmental Satellite Service
SATELLITE APPLICATIONS INFORMATION NOTE 76/23

UTILITY OF SATELLITE DATA OBSERVATIONS DURING FLASH FLOOD WATCHES - FREDRICK, MARYLAND FLOODING, October 9, 1976

Gilbert Jager
Applications Group/NESS

On October 9, 1976, a devastating flood hit the old historical downtown business district of Fredrick, Maryland. Although the area flooded was only a few blocks in extent, more than $4,000,000 of damage was done. Fortunately no lives were lost. Numerical guidance and satellite photographs taken during this event illustrate the potential for heavy rains. A close inspection of the satellite data taken on the day of the flood show, with the benefit of hindsight, that local flooding might have been forecast in this area. A flash flood watch had been issued for the nighttime hours before the event occurred, but it had been cancelled for the period of flood-producing rains.

A deepening surface Low had been moving up from the south along the east flank of the Appalachians during the night and was centered in northwestern Virginia at 1200Z (Fig. 1). Very warm, moist southerly flow and strong vorticity advection occurring between 0000 GMT and 1200 GMT on the 9th (Figs. 2 and 3) combined to produce a very unstable situation. Rain began falling before midnight on October 8 and continued throughout the night. Accumulations in the Fredrick area totaled more than 4 inches (10 cm). This rain was particularly troublesome because the ground was already saturated from heavy rains the previous week.

The enhanced infrared (EIR) picture (Fig. 4) for 9 Oct, 1000 GMT, shows the large convective comma-shaped cloud mass (G-G') associated with the surface system while the cloudiness with the upper level center remained back at (H). By 1300 GMT (Fig. 5), the area of maximum convection (G-G') had moved into eastern Pennsylvania and New York State. The convective tops appeared colder at this time and the pattern more organized and the tail of the comma extended down off the coast. The width of the area of colder cloud temperatures that was over Virginia and North Carolina in Figure 4 had decreased considerably as it moved offshore. Convective activity appeared to be concentrated in the band just off the coast at (C and D).

By this time, the cloud pattern associated with the upper level center had also become better defined (H). The 1300 GMT DAI visible photo (Fig. 6) shows a small Cb cell (A) embedded in the multilayered cloud band near Fredrick. It is also visible as a small point (A) on the 1300 GMT EIR picture (Fig. 5). Examination of the low sun angle

1230 GMT view (Fig. 7) reveals the small Cb cluster (F) that moved up from the southwest across Fredrick. Later, by 1330 GMT (not shown), these build-ups moved northeast to the Pennsylvania border. The thunderstorm appeared to form over the ridges to the southwest of Fredrick, most probably due to low level up-slope motion.

The Patuxent, Maryland, radar pictures showed an intense echo moving over Fredrick around 1300 GMT. The radar supports the idea that the Cb formed to the southwest of Fredrick as the 10-minute interval sequence for the hour previous to 1300Z showed no strong echoes. A line gradually solidified from an amorphous area of precipitation and can be seen in Figure 6 extending from B to B'.

The most intense Cb moved over a heavily built up and paved section to the west and northwest of Fredrick, Maryland. The total rainfall amounted to 6.1 inches (15.5 cm) with about 2 inches (5 cm) falling from the last thunderstorm. This water rapidly drained off into a very constricted portion of Monocacy Creek, thus flooding the Fredrick business district.

The potential for local flash flooding can be assessed from the sequence of EIR photos using the method of Scofield (SAINs 76/17 and 76/18). Close monitoring of the behavior of imbedded Cbs not only along the front, but also in the near quadrant of an extensive storm such as this is a must. The latter type of convective development can be especially dangerous as it may take place after flash flood watches have been cancelled.

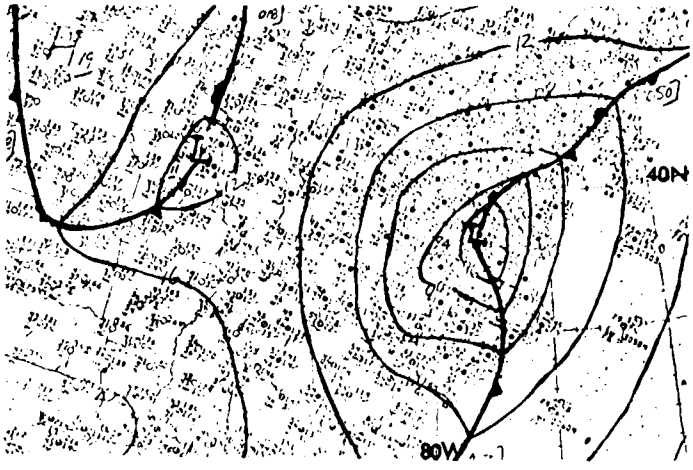

Fig 1. 1200GMT Surface Analysis 9 Oct 76

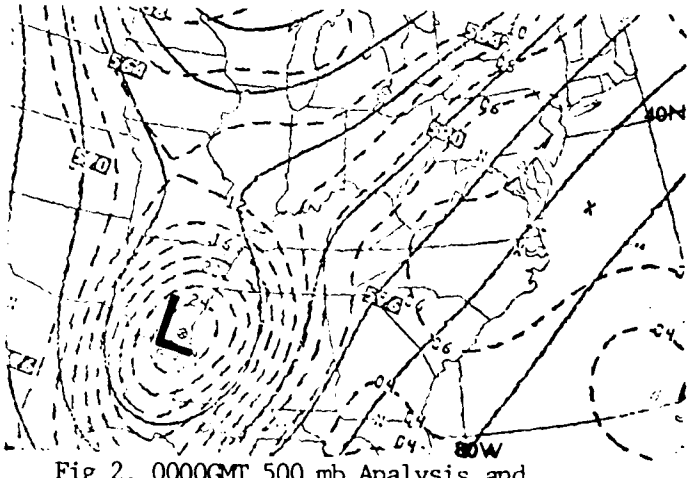

Fig 2. 0000GMT 500 mb Analysis and Vorticity, 9 Oct 76

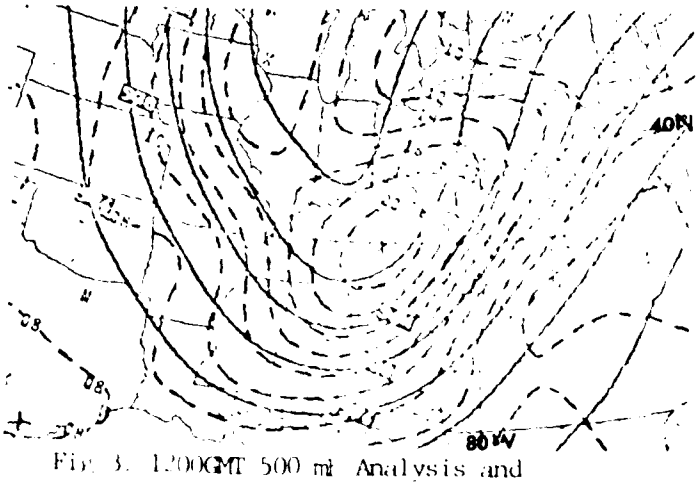

Fig 3. 1200GMT 500 mb Analysis and Vorticity, 9 Oct 76

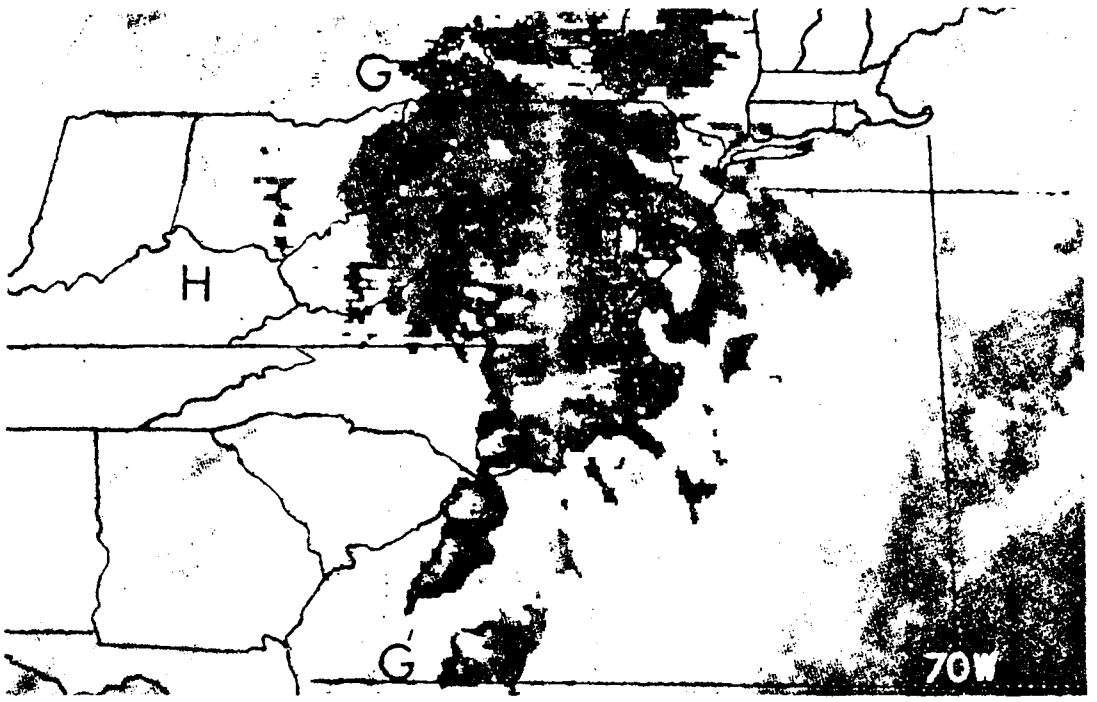

Fig. 4. Enhanced IR MB curve, 1000GMT, 9 Oct 76

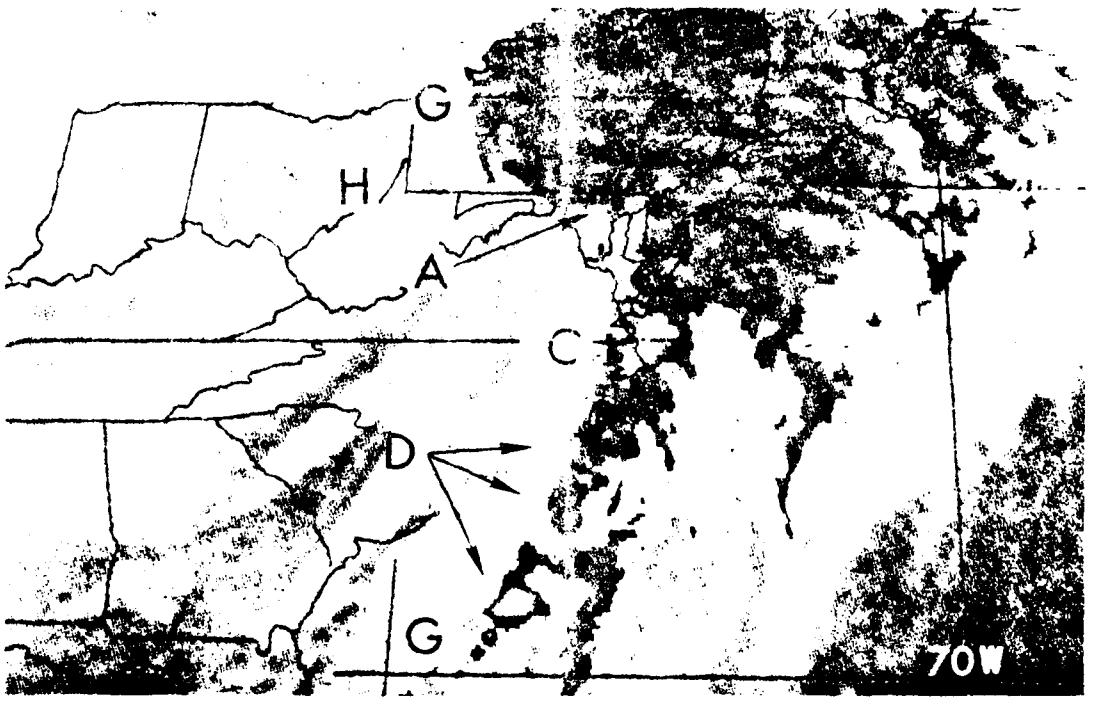

Fig. 5. Enhanced IR MB curve, 1800GMT, 9 Oct 76

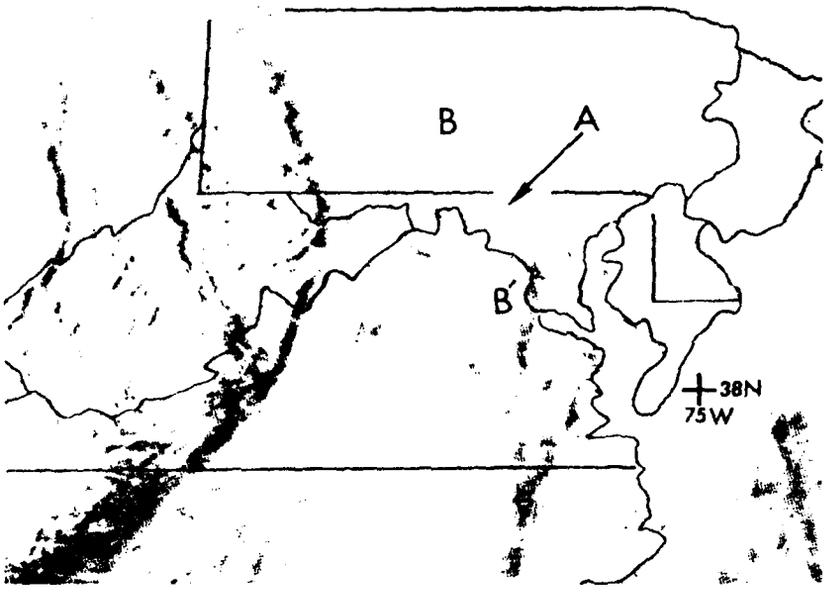

Fig 6. 1300GMT, 9 Oct 76 1 km Visible

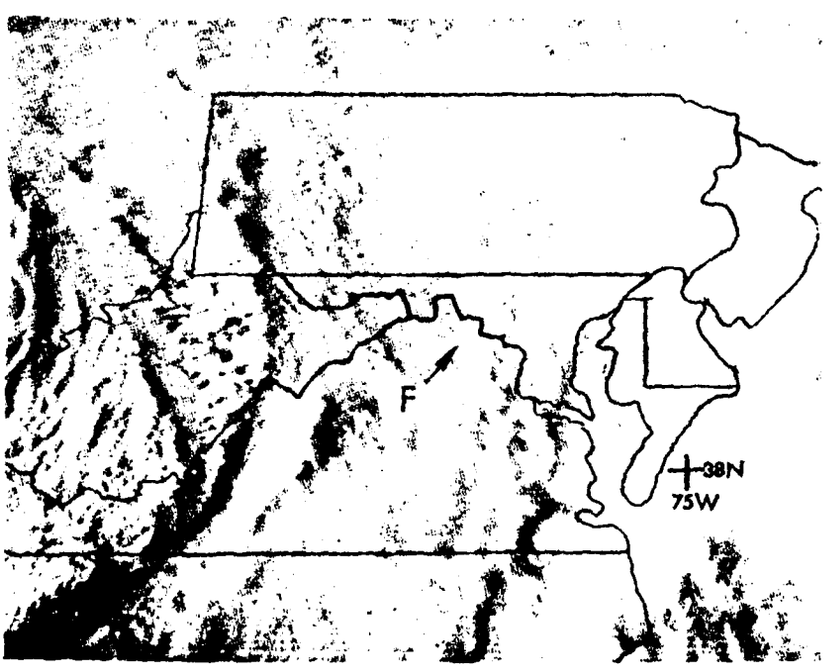

Fig 7. 1230GMT, 9 Oct 76 1 km Visible

U.S. DEPARTMENT OF COMMERCE

National Weather Service/National Environmental Satellite Service
SATELLITE APPLICATIONS INFORMATION NOTE 76/24

PRE-FRONTAL GULF DISTURBANCE

Stanley W. Wright
NESS/Applications Group

During the period beginning in the late fall and extending through the spring, disturbances often form in the Gulf of Mexico and move northward over land. The disturbances serve to enhance precipitation and initiate pre-frontal rain. These features usually appear in IR satellite imagery as low cloud comma configurations. This note describes a pre-frontal disturbance that formed in the central Gulf and moved northward over the Florida Panhandle on October 20, 1976.

The 1500 GMT, 19 October, surface analysis (Fig. 1) showed a cold front approaching the Texas coast. The 1430 GMT, 19 October, IR data (Fig. 2) shows the cloudiness associated with the front. Of particular importance in this situation is the presence of a comma-shaped area of cloudiness (A) that was located in the surface ridge.

Recently, the Winds Section of the Analysis and Evaluation Group (NESS) has started to provide the Kansas City SFSS with a set of low-level wind vectors for the Gulf of Mexico. These derived winds are calculated from low cloud motions. The vectors that were derived for 1530-1700 GMT, 19 October, are superimposed on a 1-km Gulf sector (Fig. 3). On this day, these vectors supported the possibility of a low-level circulation in the central Gulf. The Winds Section informed Kansas City SFSS that a circulation could be seen in the animated version of these data. Subsequent satellite views showed that the disturbance grew both in size and convection as it moved northward at 15 knots. During this period, the strong southerly flow along the Florida Gulf coast was 10 to 20 knots. The low pressure center associated with the disturbance was first indicated in the surface analysis just off the Florida Panhandle at 0600 GMT, 20 October.

The 12-hour LFM precipitation package (Fig. 4) for the period ending at 1200 GMT, 20 October, forecasted no precipitation for the southeast states. The 0900Z, 20 October, observed 6-hour rainfall chart (Fig. 5) indicated that light rainfall had begun. Figure 6 shows the LFM forecast precipitation to be less than one-half inch in the southeast for a 12 hour period ending at 1200 GMT, 20 October. By 0600 GMT, 20 October, the rains had become heavy along the Florida peninsula with more than

one-half inch of rain over western Florida and southeastern Alabama and a maximum of 1.37 inches at Dothan, Alabama (see Fig. 7). The accompanying satellite view (Fig. 8) shows the cloud pattern at this time. By 1200 GMT, the end of the LFM forecast period, more than one-half inch of rain was recorded over a wide area of the southeast (Fig. 9).

This case illustrates the importance of a pre-frontal disturbance in initiating and enhancing pre-frontal precipitation.

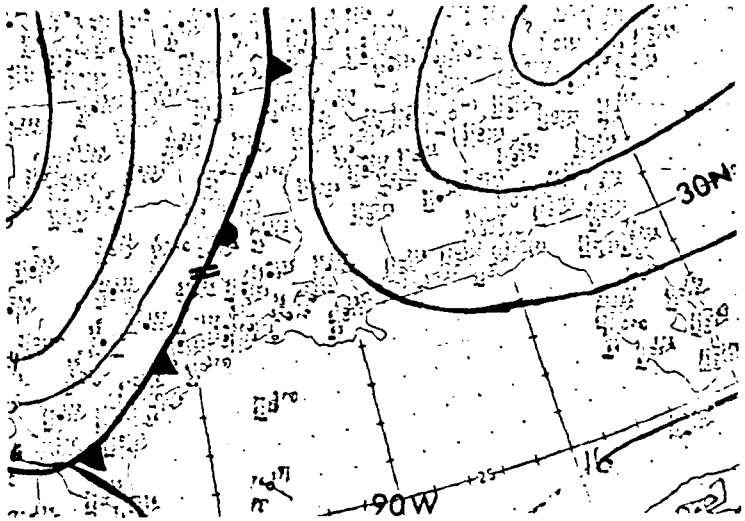

Fig. 1. Surface, 15Z, 19 Oct 1976

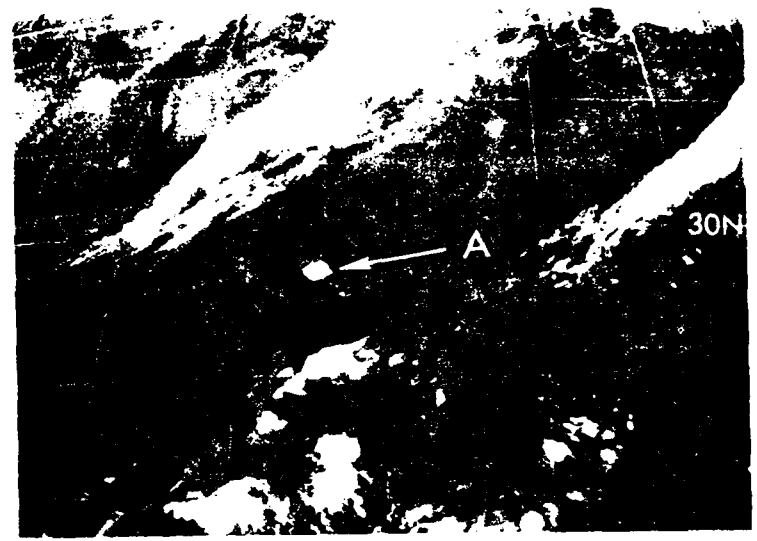

Fig. 2. SMS-1 IR, 1430Z, 19 Oct 1976

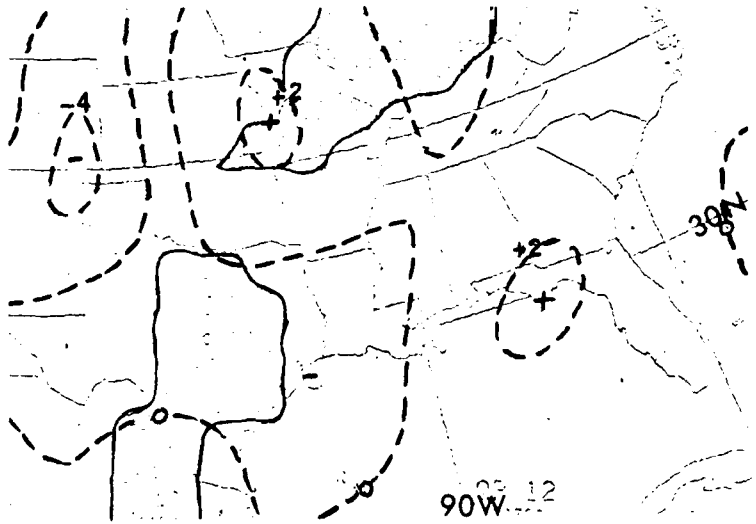

Fig. 4. LFM QP, 00Z, 20 Oct 1976

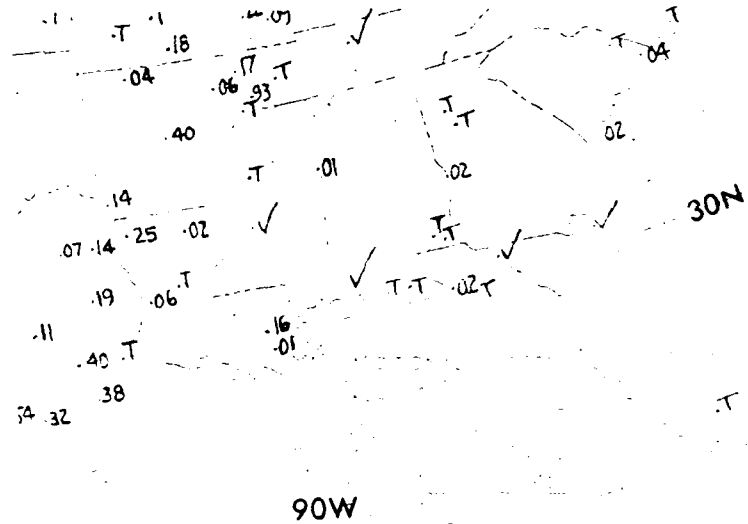

Fig. 5. 6-Hour Precip Chart
00Z, 20 Oct 1976

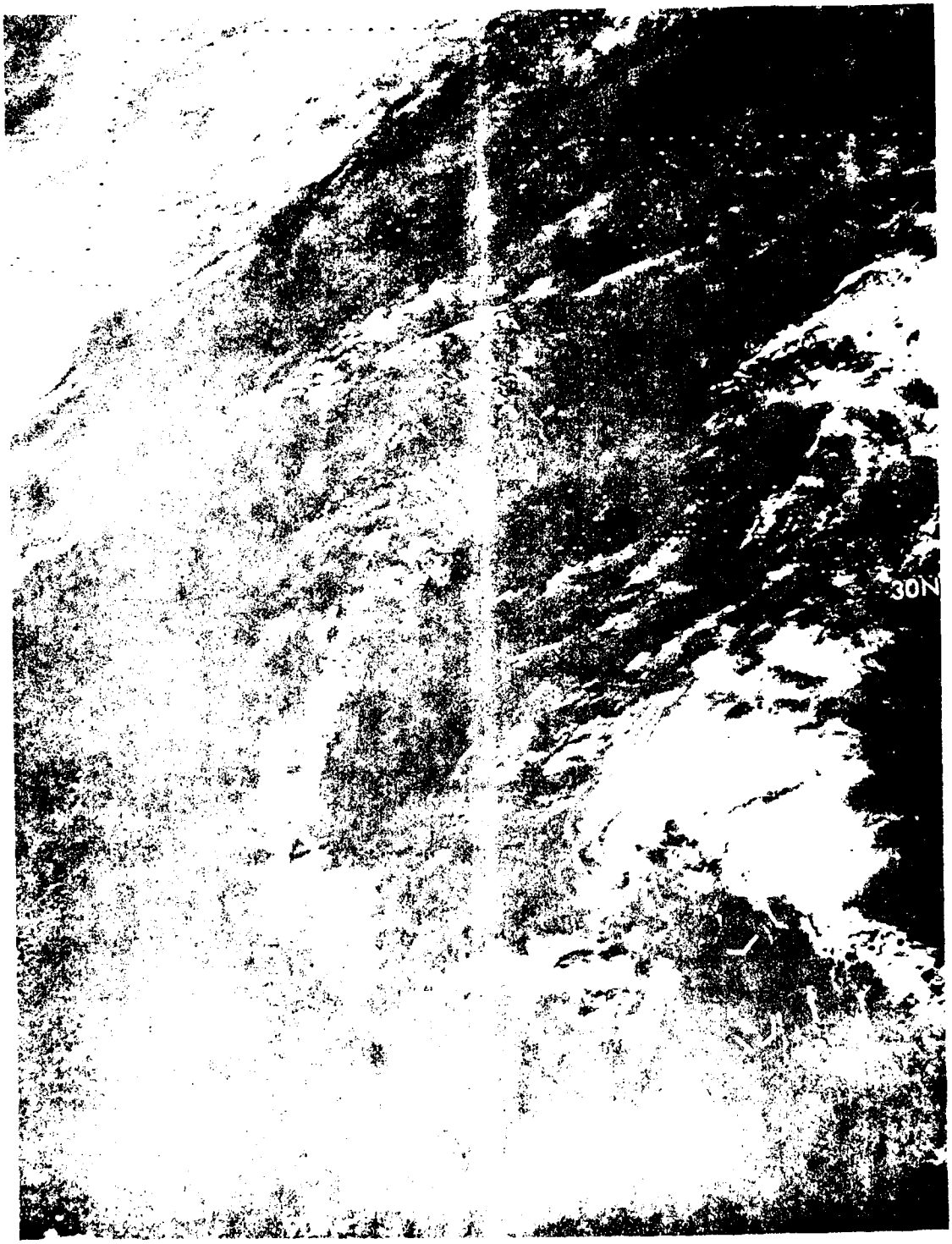
30N

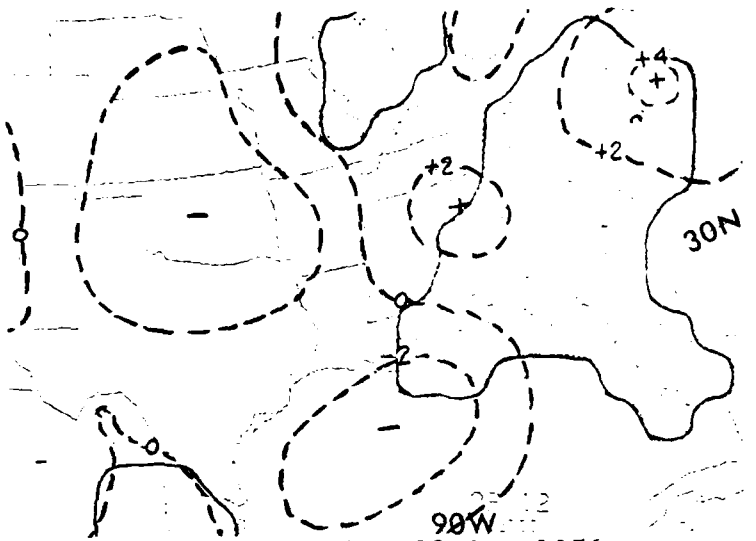

Fig. 6. LFM OP, 12Z, 20 Oct 1976

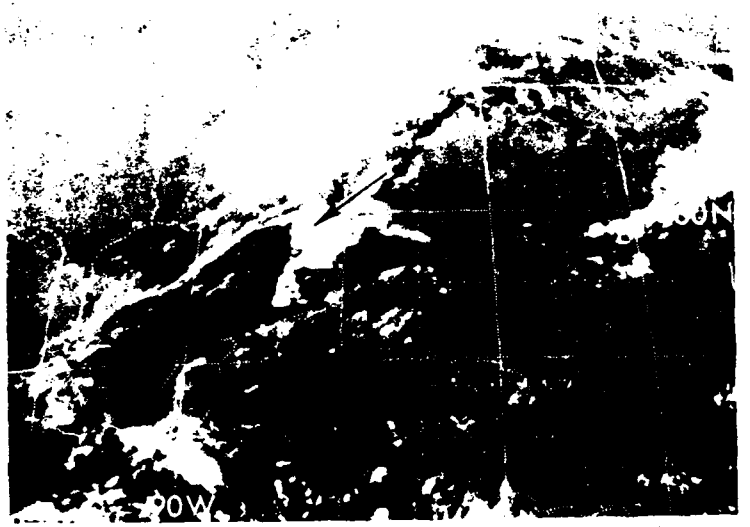

Fig. 8. SMS-1 IR, 0630Z, 20 Oct 1976

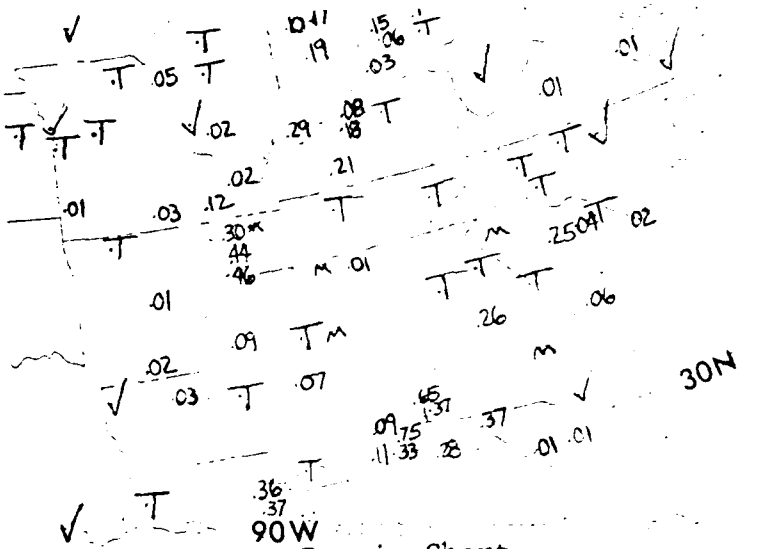

Fig. 7. 6-Hour Precip Chart
06Z, 20 Oct 1976

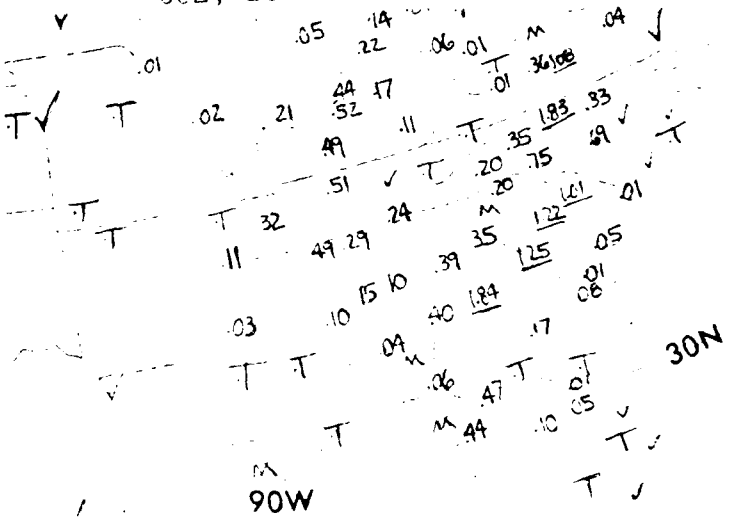

Fig. 9. 6-Hour Precip Chart
12Z, 20 Oct 1976

U.S. DEPARTMENT OF COMMERCE

National Weather Service/National Environmental Satellite Service
SATELLITE APPLICATIONS INFORMATION NOTE 76/25

THE USE OF THE HB IR ENHANCEMENT CURVE TO MONITOR THE ONSET OF FROST CONDITIONS IN THE WESTERN STATES

James J. Gurka and Ralph K. Anderson
NESS, Applications Group

The Hb enhancement curve (Fig. 1), which is used operationally in the Western Region, has a black contour that covers the temperature range from 0°C (32°F) to -3.3°C (26°F). Theoretically, on clear nights, this contour could be used as an indicator of the ground surface reaching freezing and the onset of frost. However, there are no ground temperature data available to check the accuracy of the satellite-observed temperatures on a given evening. The question then arises as to whether the relationship between satellite-observed ground temperatures and the six-foot instrument shelter temperatures is consistent enough to calibrate the temperature values associated with the enhanced infrared (EIR) contouring. Satellite data could then be used to indicate the onset of freezing conditions in remote areas.

In an attempt to answer the above question, a grid with station locations (Fig. 2) was used to estimate the time at which the edges of the freezing contour passed over 30 stations in nine Intermountain states. It is important to determine this time accurately since it is only at the "breakpoint" of a contour that a temperature is defined. For example, if a station is located in the middle of the black contoured area on the Hb curve, the temperature could be any value between 0°C and -3.3°C. However, at the instant that the contour spreads over a station, the ground temperature should be 0°C.

On the evening of October 18-19 of this year, in the Western Region, the colder edge (C on Figs. 1 and 2) of the freezing contour on the Hb curve corresponded fairly closely to an instrument shelter temperature of 1°C (34°F). Thus in this case, the average difference between the satellite-sensed group temperature and the six-foot shelter temperature was 4.4°C (8°F). Figure 3 is a plot of the time that the instrument shelter temperature dropped to 1°C versus the time that the colder edge of the black contour spread over the station.

The best fit straight line on Fig. 3 is $Y = .86X + 1.16$ with a correlation coefficient of .96. The average error from the best fit straight line is 47 minutes with 19 out of the 30 cases having an error less than the average. The larger errors, such as the one case with 2.62 hrs. and another with 2.44 hrs., occurred when the contour remained stationary

near a station location for several pictures, and thus small gridding errors could have made substantial differences. The theoretical best fit straight line should be Y = X. The average error from Y = X on this evening was 52 minutes, with 20 out of the 30 cases having an error less than 45 minutes. Therefore, there appears to be a close and consistent relationship between the satellite-observed temperature and the instrument shelter temperature.

There were several limiting factors in this study: (1) only hourly temperature reports were available; (2) the enhancement IR (EIR) pictures were taken hourly, and thus the arrival of the gray contour and the time at which the termperature dropped to 1°C were interpolated; (3) the resolution of the IR sensor is 8 km, so that the imagery presents a ground temperature that is an integrated radiational field from the ground, tree tops and other vegetation; and (4) slight gridding errors could have made a substantial difference for estimating the temperature at a point. Another possible source of error could be the amount of moisture in the atmosphere. The magnitude of error in satellite-derived temperatures due to water vapor absorption as a function of precipitable water content is shown on Figure 4. The precipitable water chart for 1200 GMT on the 19th (Fig. 5) clearly shows that atmospheric moisture was minimal in this case.

In order to use the EIR satellite pictures to monitor the spread of freezing temperatures, the user should: (1) be familiar with what instrument shelter temperature corresponds to the onset of frost in the area of interest; (2) determine what instrument shelter temperatures are associated with the edges of the black contour in cloudless areas as early in the evening as possible; (3) estimate what portions of the contour will be associated with the onset of frost in the agricultural area of concern.

On the basis of this one case, there appears to be a fairly consistent relationship between satellite-derived temperature and instrument shelter temperature. Therefore, knowing what that relationship is on a given evening and what temperature is associated with the onset of frost in a particular location, the EIR satellite pictures, and in particular the Hb curve, could be used to estimate the spread of frost conditions.

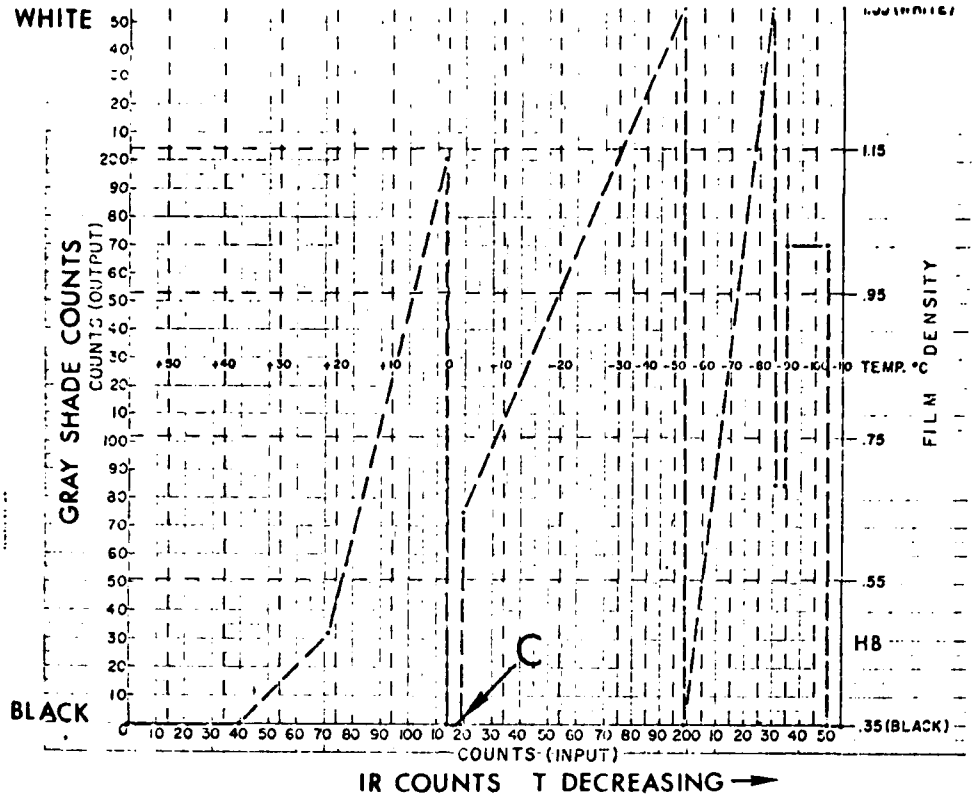

Fig 1. Hb IR enhancement curve: gray shade vs. temperature

Fig 2. SMS-2 8-km IR picture with station locations, 19 Oct 76, 0245 GMT

148

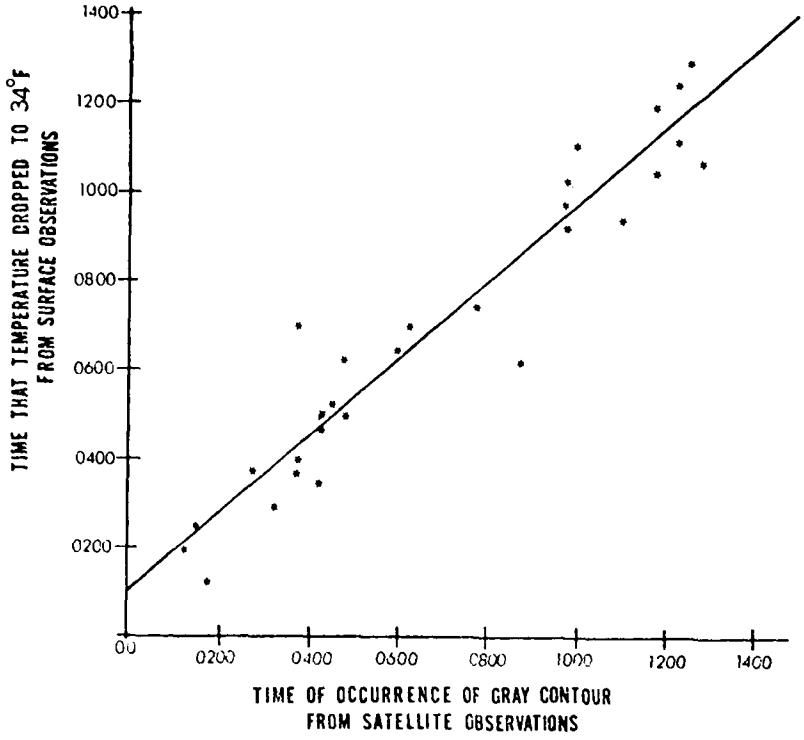

Fig 3. Time that temperature dropped to 1°C as a function of time of occurrence of gray contour.

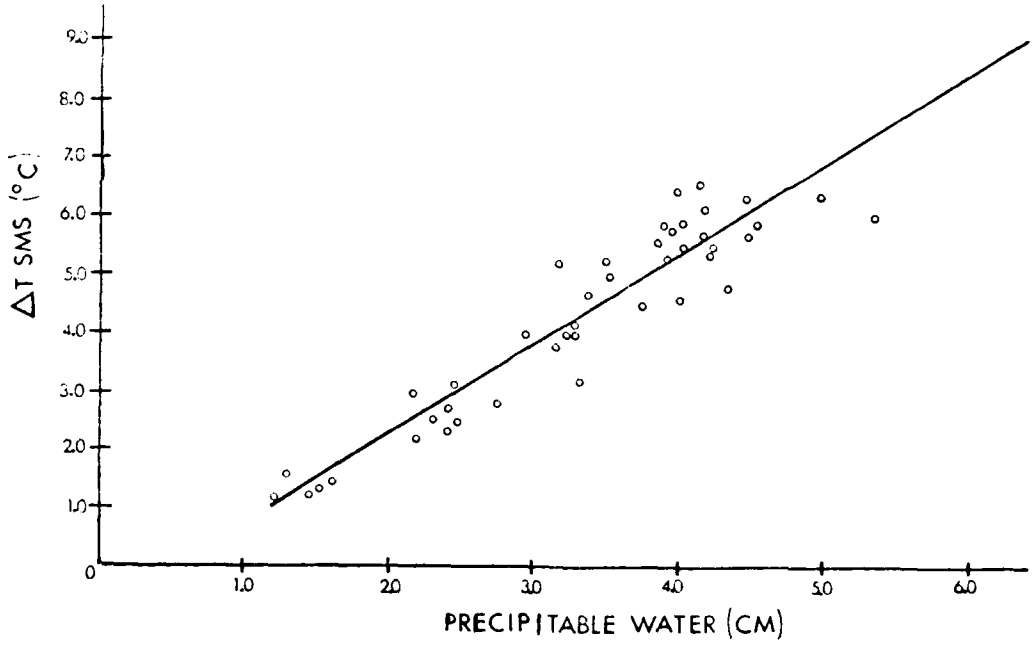

Fig 4. SMS ΔT as a function of precipitable water.

149

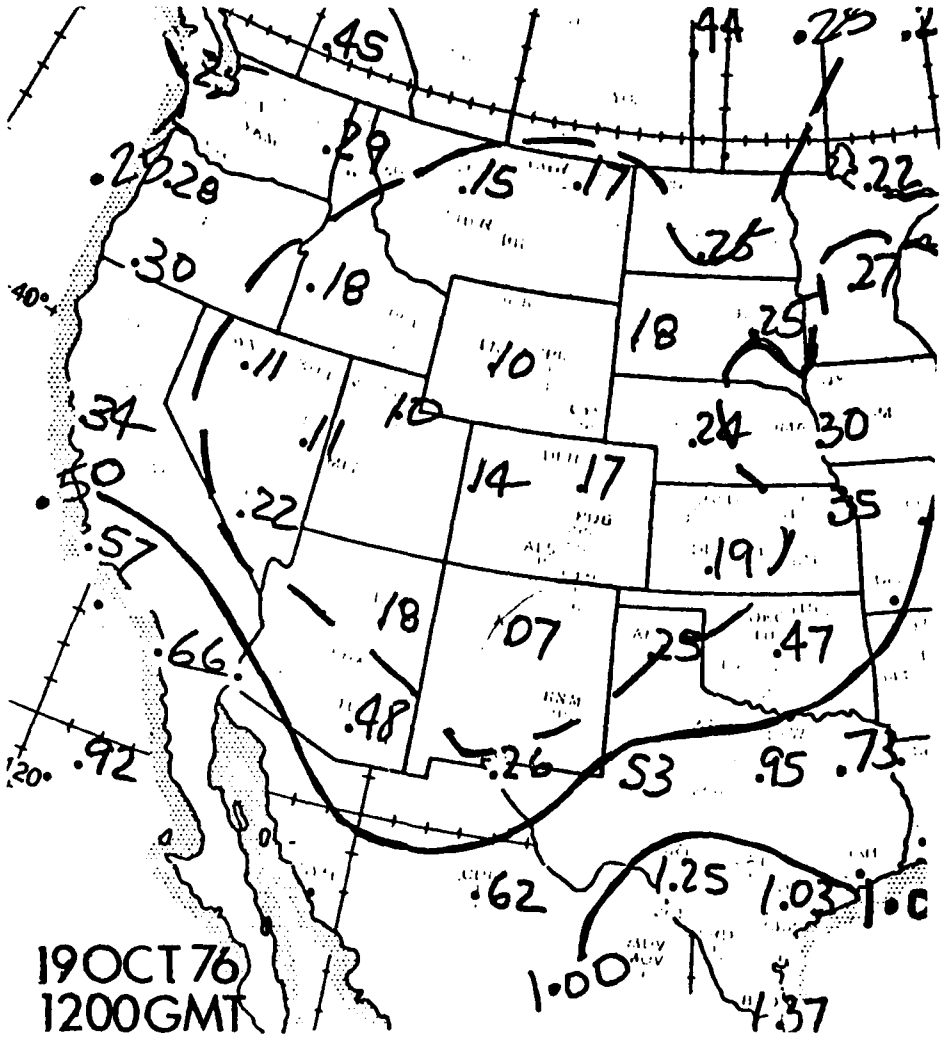

Fig 5. Precipitable water chart - 19 Oct 76, 1200 GMT.

U.S. DEPARTMENT OF COMMERCE

National Weather Service/National Environmental Satellite Service
SATELLITE APPLICATIONS INFORMATION NOTE 2/77

FIRST GLANCES CAN BE MISLEADING IN LOCATING VORTICITY CENTERS

Carl E. Weiss
Applications Group, NESS

A problem in both static and animated IR picture interpretation is that an apparent center of cloud rotation frequently does not coincide with a center of maximum vorticity.[1] This is particularly true with rapidly moving short-wave systems in the westerlies. According to Weldon (1976), a cloud rotation center is defined as "an apparent 'center', 'axis', or 'hub' of rotation within the cloud motions when viewed in time lapse motion." The GOES-1 IR imagery on 3 September 1976 illustrates such an example.

At 0001 GMT on 3 September, cloud rotation about (R), Figure 1, was evident in the IR movies. The LFM vorticity analysis at 0000 GMT overlaid on this view, Figure 2, shows the vorticity center (X) to be farther west than the cloud rotation center (R). This is not an obvious location in view of the cloud pattern. The cloud rotation (R), in this case, lies ahead of the vorticity center and is to the north of mid-level wind maximum (S to S') in the area where the vorticity is strongly cyclonic. The cloud rotation center (R) becomes better defined in the IR imagery at 1200 GMT, Figure 3. Here the curvature (C) of the accompanying cirrus to the north of the center (R) has become more pronounced. At this time, a closed 700 mb low (L) was analyzed to the northwest of the rotation center. Examining the 1200 GMT LFM vorticity analysis with the concurrent IR imagery, Figure 4, one can see that the vorticity center (X) continued to be to the west of the cloud rotation (R) in an area relatively free from any middle or high cloudiness. As before, the cloud rotation is found just north of the leading edge of the wind maximum (S to S') where the vorticity gradient is strong.

This apparent discrepancy between the locations of the vorticity center and the cloud rotation center is common. Several possible explanations for this disagreement come to mind. First, since systems often slope in the vertical, clouds showing rotation in the satellite imagery may not coincide with the analyzed vorticity center at 500 mb. However, studies of systems with cloud tops near 500 mb revealed that a similar spatial difference between the location of maximum vorticity and rotation centers still existed. Secondly, a systematic bias in the vorticity analysis could also lead to this same discrepancy. Typically, only over oceans or at other locations where cumulus congestus or cumulonimbus are found behind the comma cloud, do the vorticity centers and the cloud rotation centers agree. In those cases over the oceans, clouds are sometimes present at the vorticity center and therefore the maximum

1. In this discussion, a maximum vorticity center is defined as a point at a given level where the value of absolute vorticity is at a maximum. At 500 mb, this correspondends to an "X" on an NMC vorticity analysis.

turning is seen there. More commonly, however, the vorticity center is free from any significant cloudiness. It is obvious, but often overlooked, that cloud rotation can only be seen where clouds are present. Therefore, cloud rotation is frequently found at some location other than the vorticity center. Weldon (1976) depicts a typical short-wave comma cloud pattern with the corresponding vorticity and streamline analyses, Figure 5. The vorticity center (X) is just to the rear of the comma head (A). If rotation in the clouds is evident, it will most likely be in the hatched area (B) along the shear axis of vorticity (dot-dash line, D to D'). This relationship between the vorticity field and the cloud pattern is common for most short-wave troughs imbedded in a strong westerly flow. In summary, by recognizing the typical relationship between cloud rotation centers as seen in satellite imagery with analyzed vorticity centers, errors made in locating vorticity centers (which can be more serious than no analysis at all) can be minimized.

REFERENCE

Weldon, R. B., 1976, unpublished satellite training notes. (Available from NESS, Applications Group (S121), World Weather Building, 5200 Auth Rd., Washington, D.C., 20023.)

Errata; SAIN 76/23: Last sentence, first paragraph should read:
A flash flood watch had been issued for the nighttime hours before the event occcurred and had been extended for Western Maryland for the period of flood-producing rains.

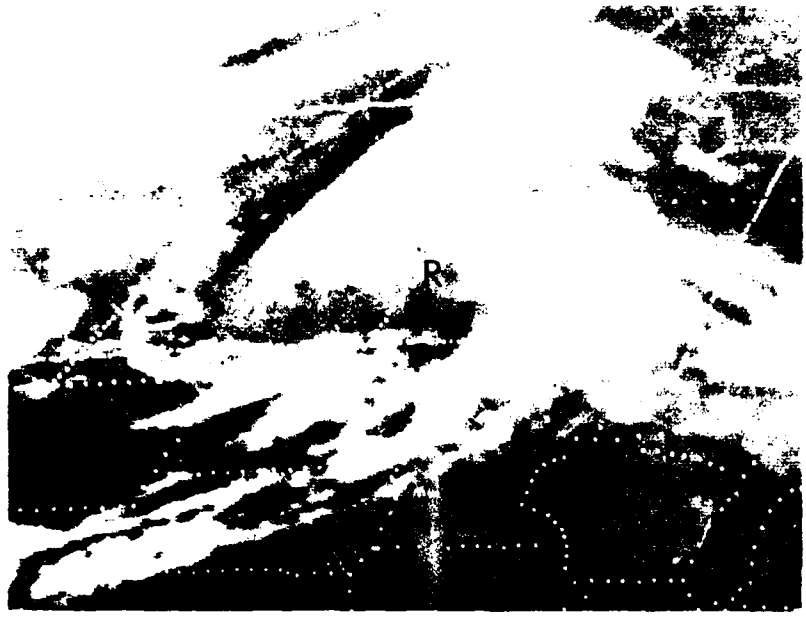

Figure 1: GOES-1 Full-Disk IR Imagery, 0001 GMT, 3 September 1976

Figure 2: GOES-1 Full-Disk IR Imagery, 0001 GMT and NMC LFM Vorticity Analysis 0000 GMT, 3 September 1976.

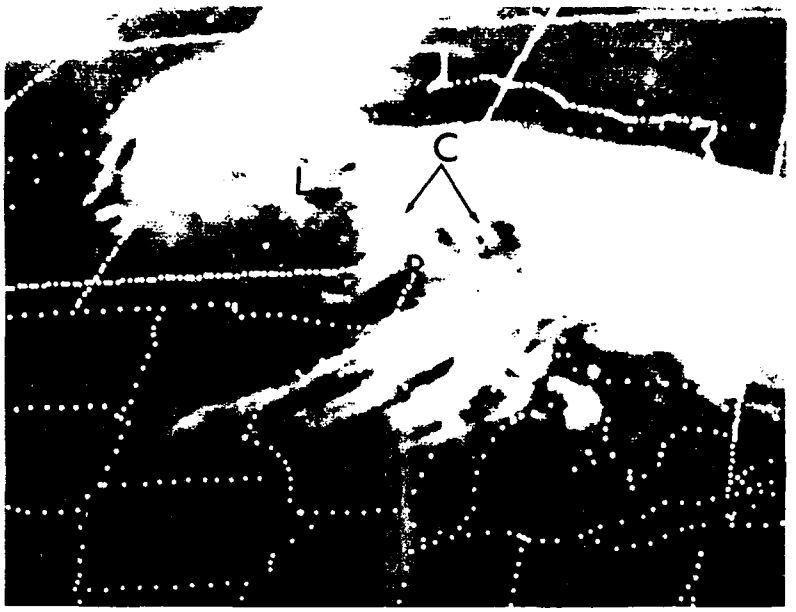

Figure 3: GOES-1 Full-Disk IR Imagery, 1200 GMT, 3 September 1976

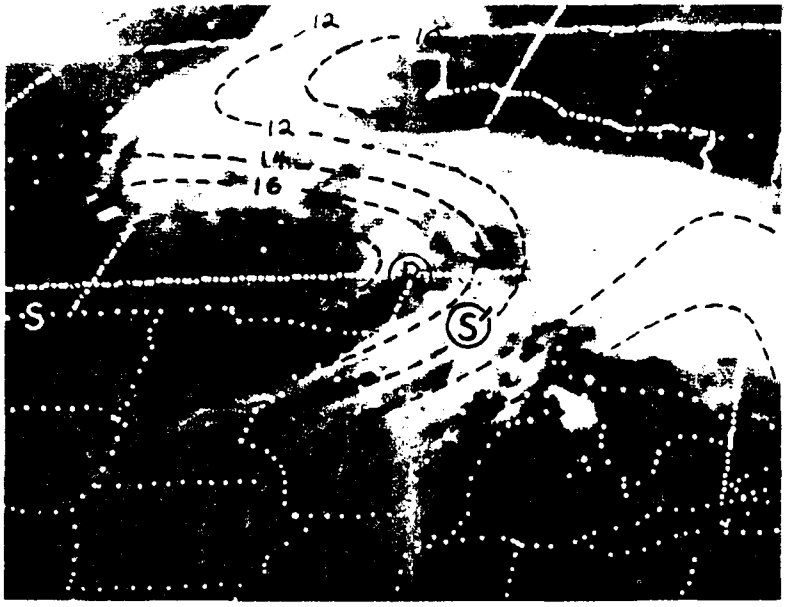

Figure 4: GOES-1 Full-Disk IR Imagery, 1200 GMT and NMC LFM Vorticity Analysis 1200 GMT, 3 September 1976.

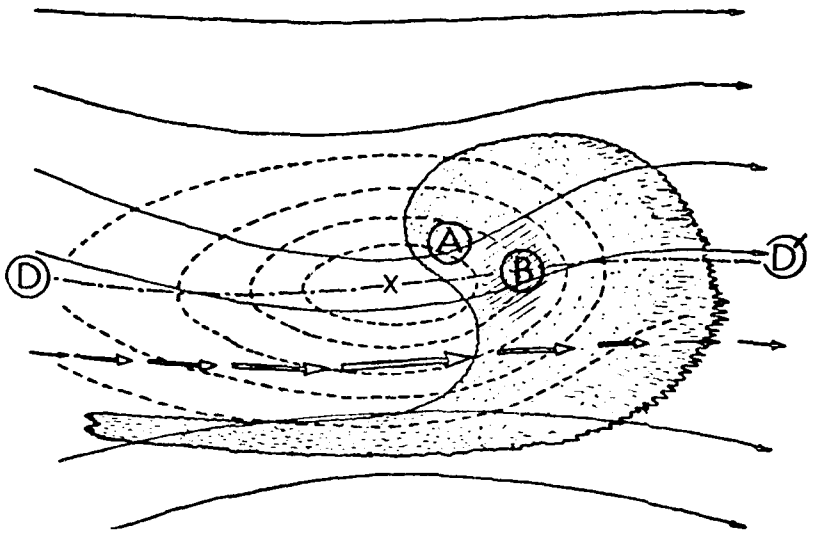

Figure 5: Schematic showing the relationship between the cloud pattern, streamline pattern, vorticity pattern and jet stream in a short-wave system in the westerlies.

U.S. DEPARTMENT OF COMMERCE

National Weather Service/National Environmental Satellite Service
SATELLITE APPLICATIONS INFORMATION NOTE 3/77

A QUICK WAY TO DETERMINE CLOUD FEATURE SPEEDS USING GRIDDED SATELLITE PICTURES

H. M. Johnson
Applications Group/NESS, Washington, D.C. 20233

John D. Thomas, in the Satellite Applications Information Note 76/16, points out the need for care in determining the movement rates of satellite-observed cloud systems or system details when using the usual, operationally available gridded IR or VIS pictures, and presents two simple methods for determining these speeds accurately. This note presents a quick way to apply the second method without doing any numerical calculations (other than the very few required to set up the procedure initially). The procedure is of very general applicability and has been tested by use for several years.

1. What is needed:

   (a) Gridded pictures or an appropriate overlay grid (a full set of latitude and longitude lines is best).

   (b) A two-point divider or equivalent (such as a child's school, circle-making "compass"). A millimeter scale will do in a pinch.

   (c) A small piece of graph paper (one inch paper, 10 squares to the inch, is excellent).

2. How to do it:

   (a) Measure separately, with dividers (or scale), (1) the east-west component of the displacement of interest, and (2) the north-south component of the same displacement, in terms of degrees as shown by the grid.

   (b) Convert these to displacement rates for a time interval of 1 hour (or other standard time interval, if preferred).

   (c) Determine the north-south component rate (in knots from Fig. 1 using the 0° latitude line.

   (d) Determine the east-west component rate (in knots) from Fig. 1 using the latitude (or an approximate "average" latitude) of the feature of interest (interpolating in Fig. 1 as necessary).

(e) Combine the 2 components by simple vector addition, using the graph paper (as shown in Fig. 2). The desired rate "L" can be obtained by a separate piece of graph paper of the same type used as a scale to measure "L" or an arc may be drawn of radius O-B (which is "L") with a compass (or divider) about O as center to the line O-C and the length of "L" read directly from the original graph paper scale (In Fig. 2 a northward rate of 10 knots combined with an eastward rate of 17+ knots gives a vector sum of 20 knots (from 240°).

The two components must be determined separately because the N-S component does not depend on latitude, and the E-W component does depend on latitude, strongly at the higher latitudes, as shown in Fig. 1.

Fig. 1 can be used for loops also. For use with a 10-hour loop, multiply the values on the horizontal scale by 10 (or better, add or substitute a scale renumbered in this way). Similarly for a 12-hour loop, multiply by 12; for a 24-hour loop, multiply by 24, etc.

Note that this procedure is a rapid one largely because once set up, no additional numerical calculations are needed.

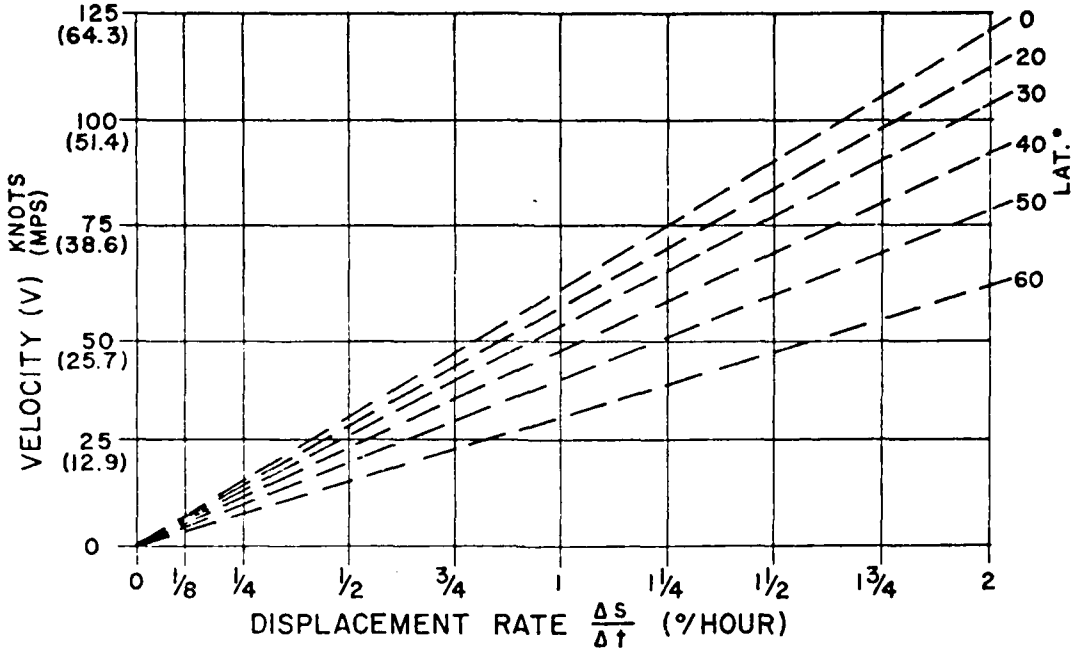

FIGURE 1

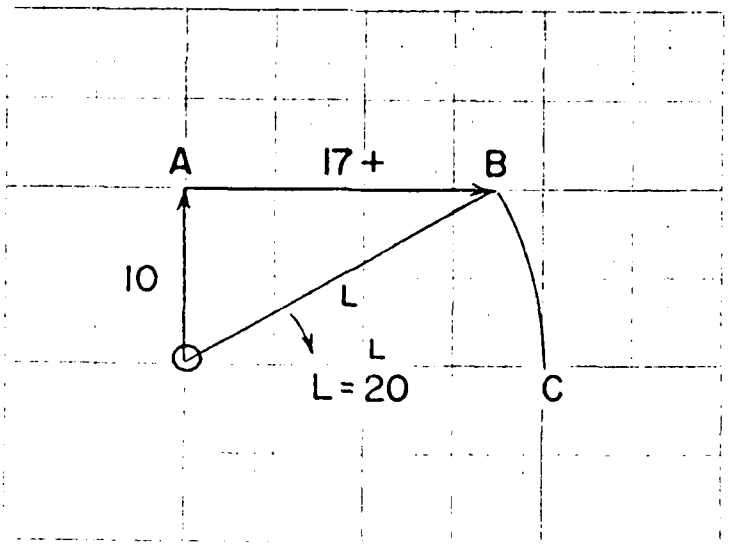

FIGURE 2

U.S. DEPARTMENT OF COMMERCE

National Weather Service/National Environmental Satellite Service
SATELLITE APPLICATIONS INFORMATION NOTE 77/4

EARLY SIGNS OF TROPICAL STORM DEVELOPMENT IN THE WESTERN ATLANTIC

Vernon F. Dvorak
NOAA/NESS, Applications Group, Washington, D.C.

Introduction

During the past three years, a total of 10 tropical cyclones reached tropical storm intensity or more in the western Atlantic after showing early signs of cyclogenesis in the region east of Florida and north of 20° latitude. Satellite pictures of five of these ten storms are shown to illustrate the earliest indications of their development. An analysis of the cloud pattern evolution is made to test the criteria currently used by operational analysts to forecast tropical storm development.

The operational procedure regarding initial development is to monitor all disturbed cloud areas and determine when a cloud system warrants a T1 classification. This number (T1), when used without a minus, forecasts a storm of tropical storm intensity (T2.5) 36 hours from the time of classification (Dvorak 1975). The T1 classification is made when a disturbance meets the following criteria:

(1) A cloud grouping has persisted for more than 12 hours that
(2) includes an area of either dense-appearing convective overcast or cumulonimbus organization of at least three degrees in areal extent with
(3) cloud line curvature defining a cloud system center within an area less than 2-1/2° diameter. The center can be defined either by curved cloud lines associated with cumulonimbus, by low cloud line curvature with the center defined near dense overcast, or by a combination of the two.

Data Description

Figures 1 and 2 show four days early in the lives of tropical cyclones Belle and Gloria, 1976. The pictures, taken 24 hours apart, are arranged in columns with time increasing from the bottom of the picture to the top. In each horizontal row, coincident infrared (IR)[1], enhanced IR (EIR)[2], and "VIS" images are displayed from left to right.

Figure 3a, b, c shows three different tropical cyclones in the IR only, with time also increasing from bottom to top. The disturbances shown are: Figure 3a, Becky 1974; figure 3b, Dolly 1974; and Figure 3c, Candice 1976.

1. Z curve display
2. Applications Group gamma enhancement

In all the storm histories shown in these three figures, the disturbances reached tropical storm (T/S) intensity in National Hurricane Center bulletins from 23 to 33 hours after the time of the picture in the top row.

Data Analysis

Four days before tropical storm (T/S) was named (bottom pictures). In the first views, clusters of convective clouds and cirrus are visible (A) but little, if any, sign of curved convective line structure is apparent. (The right-hand disturbance in Figure 2 does show this but is not discussed in this paper.)

Three days before T/S was named (second picture from bottom). All disturbances now show some convective line curvature (B), but only the patterns in 3b and 3c show good center definition (i.e., within a 2.5° area). The smooth uniform appearance of most of the clouds defining these centers suggests that there may be little convective line structure under them. The "VIS" pictures (not shown) do show the north side of these patterns to be only thin cirrus (C). This leaves the remaining amount of dense clouds too small in area for the T1 criteria. Either T0 or T0.5 is usually used in these marginal cases (depending on the persistence of the features observed in previous pictures). The IR data were shown in preference to the "VIS" to illustrate how well the IR imagery reveals the organization of the cirrus outflow patterns (C). Note the similarity of this pattern for all disturbances at this stage of development.

Two days before T/S was named (second picture from top). Convective line curvature has increased in all cases but the center definition remains marginal in all but those in Figures 2 and 3a. In Figure 2, however, the amount of deep layer convection is too small for T1. In Figure 3a, the pattern showed signs of being in excess of T2, but operational rules constrain the analysis to T1.5 on the first classification. The patterns in Figure 3b and Figure 3c, being still weak, illustrate how the smooth uniform cirrus patterns seen the day before can give the appearance of advanced pattern evolution during the first days of development. With short interval data, these patterns are often seen to be short-lived.

One day (23-33 hours) before T/S was named (top picture). By this time all pictures show convective line curvature defining a cloud system center within a small area. At this stage, one day after T0.5 or more, the cloud pattern is expected to show more organization of dense clouds around the system center. This usually takes on the appearance of a curved "comma" band at the T2 stage similar to the ones seen in Figures 1, 2 (EIR) and 3a (D). The band is more tightly curved than required for T2 in Figures 2 and 3a, but since Figure 2's T-number was only T0.5 the day before, it was held down to T2. The band in Figure 1 has not quite made it to T2 so it is held to the expected change of one number per day.

Summary and Conclusions

1. The earliest indication of cloud pattern organization in the cyclones of the sample was observed about three days before T/S intensity was reached.

2. The first sign of cloud pattern organization was the appearance of a "cold" overcast cirrus pattern over previously existing convective clouds. The cirrus pattern showed anticyclonic cirrus shear across the cloud system. The pattern appeared to be similar in all cases at the same stage in the growth process and usually weakened during the succeeding 24 hours.

3. The developmental criteria tested in the study worked well for all storms except Becky which was forecast 23 hours early. The addition of cirrus cloud pattern criteria for detecting the early stages of cyclogenesis is suggested by the study. Cirrus patterns as well as areas of deep layer convection are easily recognized in enhanced IR imagery.

REFERENCES

Dvorak, V. F., 1975: Tropical cyclone intensity analysis and forecasting from satellite imagery. Mon. Wea. Rev., 103, pp. 420-430

Fig. 1 — Tropical Cyclone [illegible], 1970. — Two ESSA pictures taken 25 hours before [illegible] landfall.

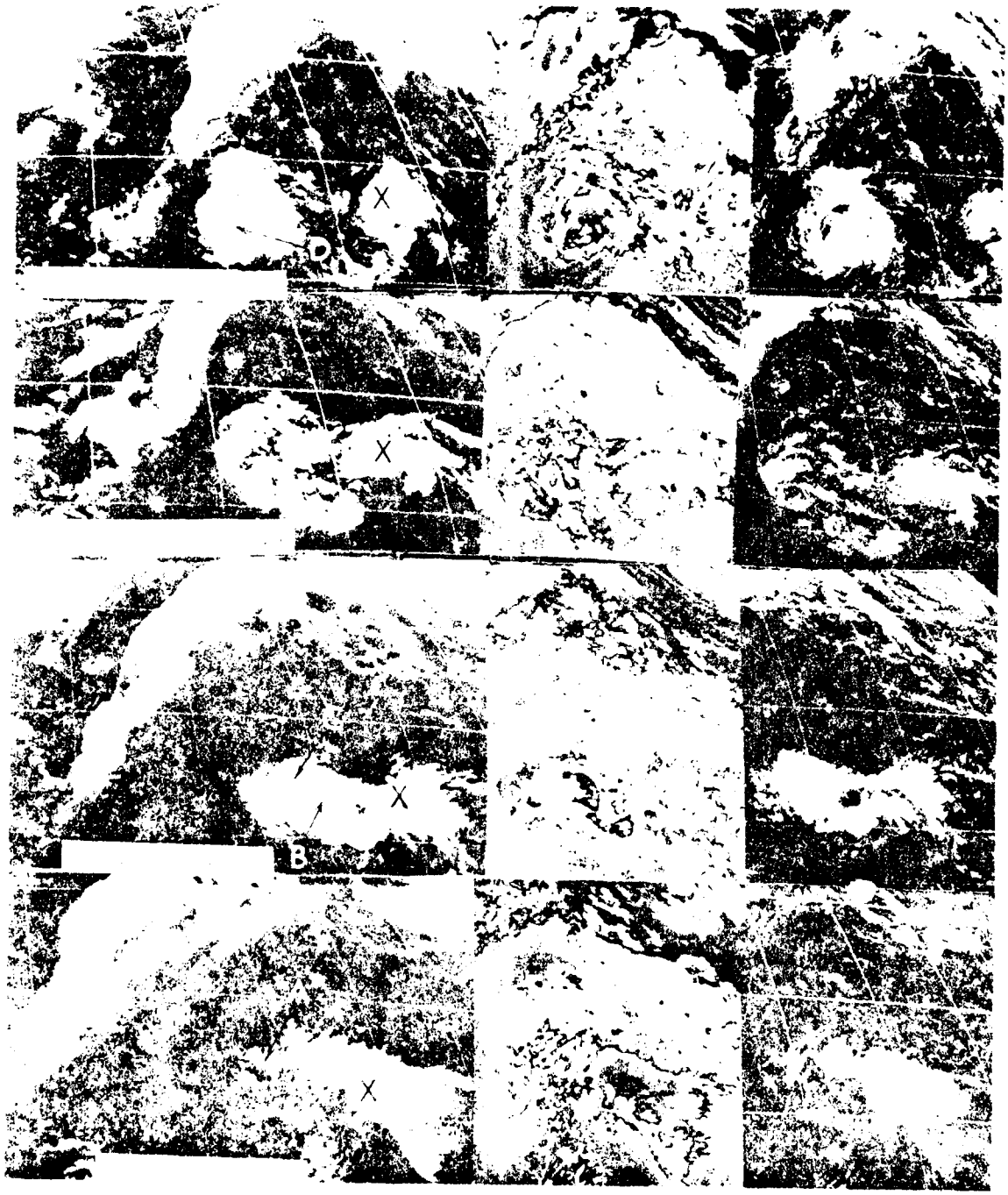

Fig. 2. Tropical Cyclone Gloria, 1976. Top row pictures taken 29 hours before storm was named (hurricane).

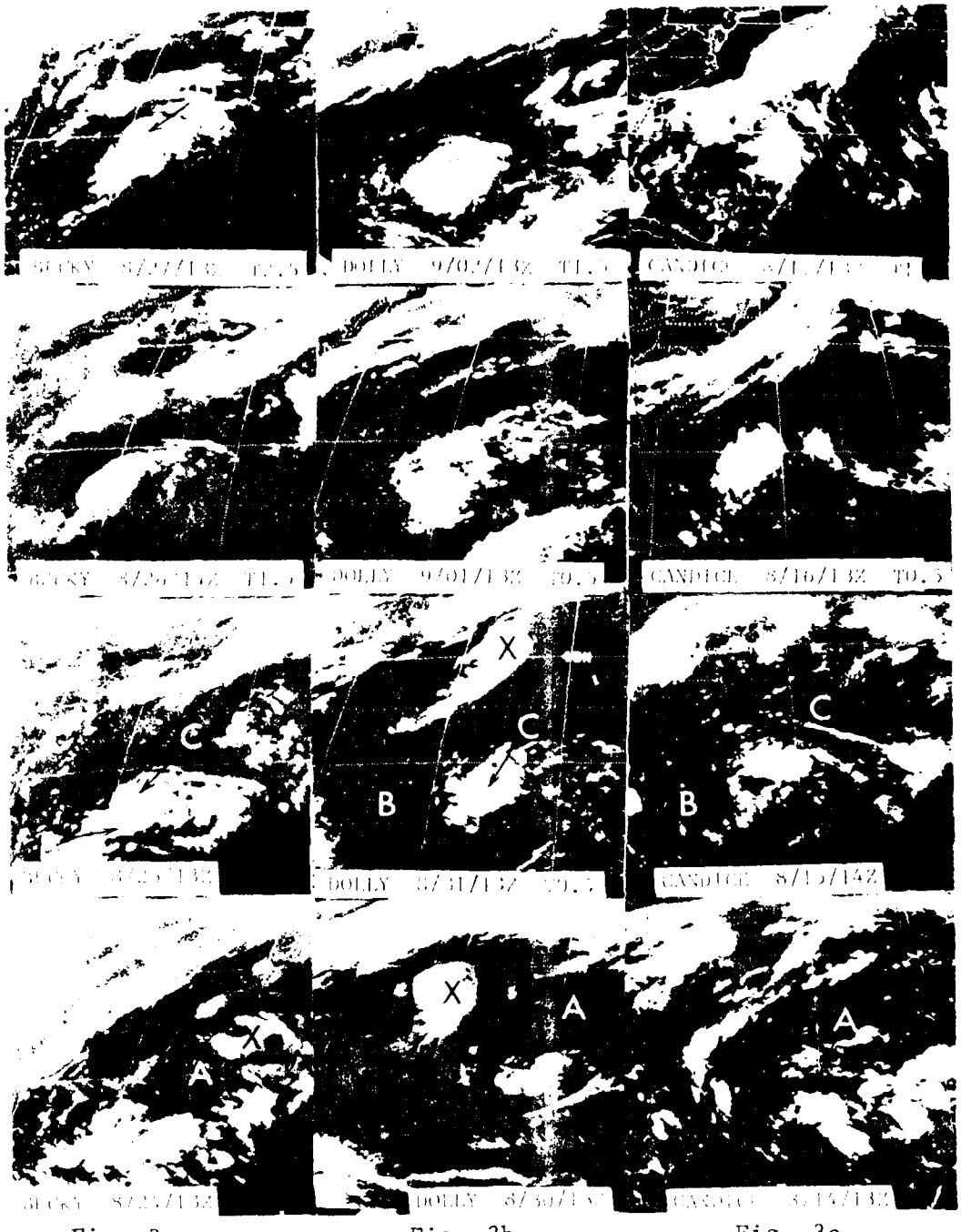

Fig. 3a. Fig. 3b. Fig. 3c

Fig. 3. In columns from left to right, Tropical Cyclones Becky 1974, Dolly 1974, and Candice 1976. Top row picture taken 23 hours, 29 hours, and 33 hours, respectively, before T/S was named.

164

U.S. DEPARTMENT OF COMMERCE

National Weather Service/National Environmental Satellite Service
SATELLITE APPLICATIONS INFORMATION NOTE 77/5

MERGER OF TROPICAL CYCLONE REMNANTS OVER THE NORTHEAST PACIFIC

Arthur C. Pike
NESS, Satellite Field Services Station, Honolulu, Hawaii

An unusual case of two large, distinct tropical cyclonic vorticity maxima of approximately equal strength merging to form a unified system occurred east of Hawaii in August 1976. It was the first such instance to be viewed by the SMS-2 geostationary satellite. The disturbances involved were the late, declining stages of tropical cyclones GWEN and HYACINTH. They are illustrated with SMS-2 daylight sectors of two km resolution, except in figure 4, where the resolution is four km. Since tropical cyclone pairs are commonly observed during the hurricane season over the northeast Pacific (Baum 1976), a future case similar to this one is likely to occur there.

Figure 1 is a view of GWEN and HYACINTH late on August 9 when their centers were 1550 km apart. GWEN, to the southwest near 10°N 125°W, has maximum sustained winds estimated at 45 knots, while HYACINTH appears near peak strength as a 95-knot hurricane near 15°N 111°W. By the afternoon of August 12, figure 2, HYACINTH has moved west-northwest to 22°N 128°W and has weakened to a 55-knot storm over relatively cool, 21°C ocean surface water. GWEN, now only 770 km southeast of HYACINTH and embedded in its convergent counterclockwise flow, is moving north-northwest at 15 knots with 35-knot winds. The Fujiwhara effect (Fujiwhara 1921, Jager 1968), a relative cyclonic rotation about each other of two cyclones as they approach, is now evident.

One day later on August 13, figure 3, both systems are weakening 35-knot storms spaced 480 km apart. GWEN has shifted northeast of HYACINTH and is beginning to move more westward at an accelerated rate of 28 knots. HYACINTH continues west at about 15 knots. Only seven hours later, figure 4, the predominatly stratiform cloud patterns of both cyclones are merging in the general vicinity of 23°N 137°W, although the GWEN vorticity maximum is still well defined about 450 km to the north-northeast of the HYACINTH maximum. Highest winds in the system are estimated at 35 knots just north of the GWEN maximum.

By the morning of August 14, figure 5, the two vorticity maxima have become parts of a single larger-scale cyclonic system near 22°N 141°W. The remnants of GWEN, farther north at this time, and HYACINTH are now only 180 km apart, and are beginning to diffuse vorticity into a common center of circulation between them. In figure 6, taken early in the afternoon of August 15, only one well defined vorticity maximum can be seen, near 22°N 148°W. Highest winds are estimated at 25 knots. The disturbance seen near 24°N 141°W marks the remnants of tropical depression 11, which was not involved in the GWEN-HYACINTH merger although it did execute a Fujiwhara-type motion along the periphery of the merging pair.

Now officially classified as a single tropical depression, T.D. 9, the cyclonic system moved generally west-northwest for the next several days passing 200 km north of Oahu and Kauai in the Hawaiian Islands during August 17. The only associated Hawaiian rainfall occurred in conditions of sea breeze convergence in the col area south of the depression. Although no strong prevailing winds were apparent in the depression, cumulonimbus convection was briefly activated within it on August 17 northeast of Hawaii and on August 20 near 37°N 178°W as it passed through regions of ascending air east of slow-moving upper tropospheric troughs. The system recurved into the westerlies as a minor vorticity maximum on the latter date.

A best track map for GWEN, HYACINTH and tropical depression 9 appears in figure 7. East of longitude 140°W it is based on information supplied by the National Weather Service Forecast Office at Redwood City, CA; farther west it has been constructed by the author.

REFERENCES

Baum, Robert A. (1976): "Eastern North Pacific Tropical Cyclones of 1975". Monthly Weather Review, vol. 104, pp. 475-488.

Fujiwhara, S. (1921): "The Natural Tendency Towards Symmetry of Motion and its Application as a Principle of Meteorology". Quarterly Journal of the Royal Meteorological Society, vol. 47, pp. 287-294.

Jager, Gilbert (1968): "Picture of the Month: An Example of the "Fujiwhara Effect" in the West Pacific Ocean". Monthly Weather Review, vol. 96, pp. 125-126.

A-160

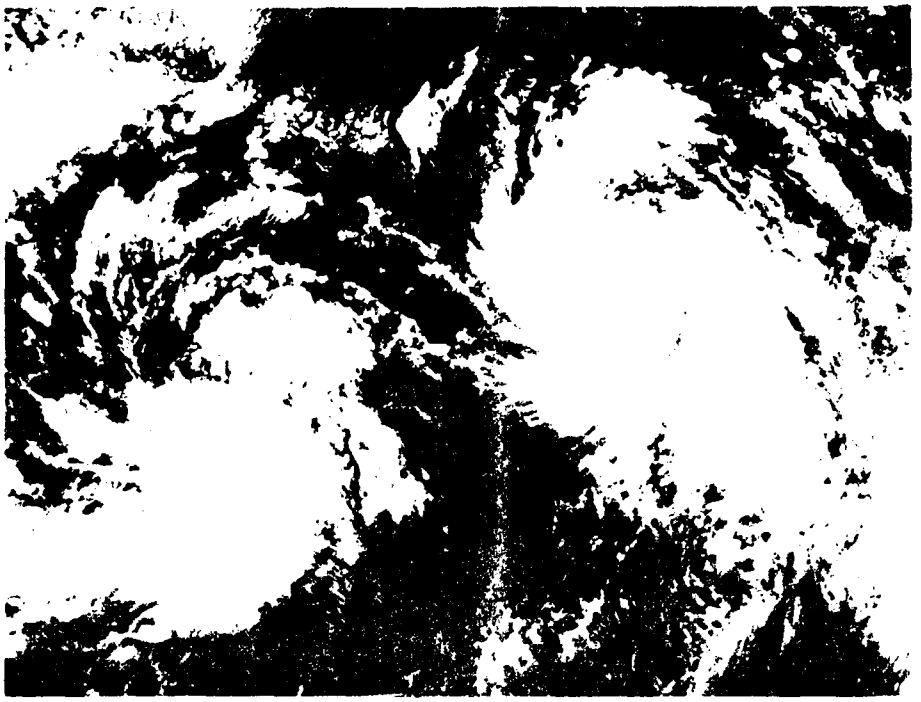

Fig. 1: SMS-2 visible (2 km resolution), 2315Z, 9 August 1976.

G = GWEN, H = HYACINTH.

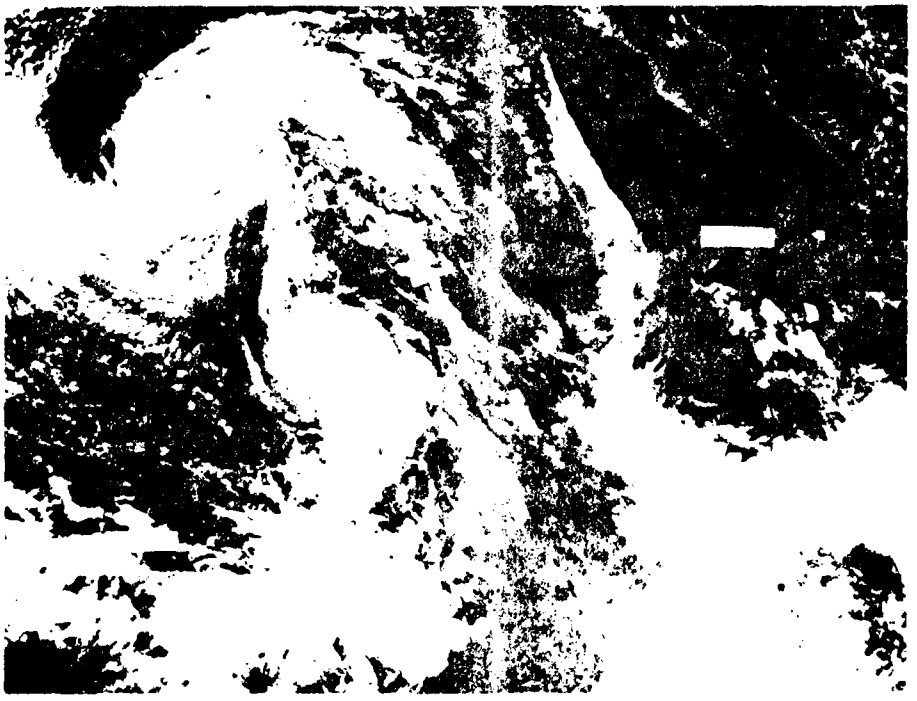

Fig. 2: SMS-2 visible (2 km resolution), 1815Z, 12 August 1976.

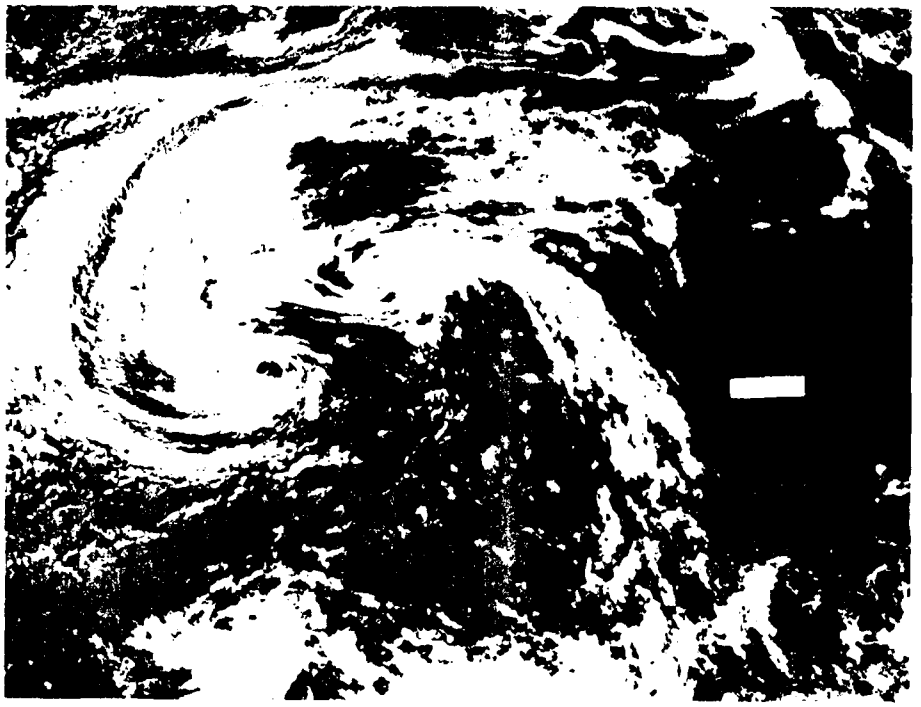

Fig. 3: SMS-2 visible (2 km resolution), 1815Z, 13 August 1976.

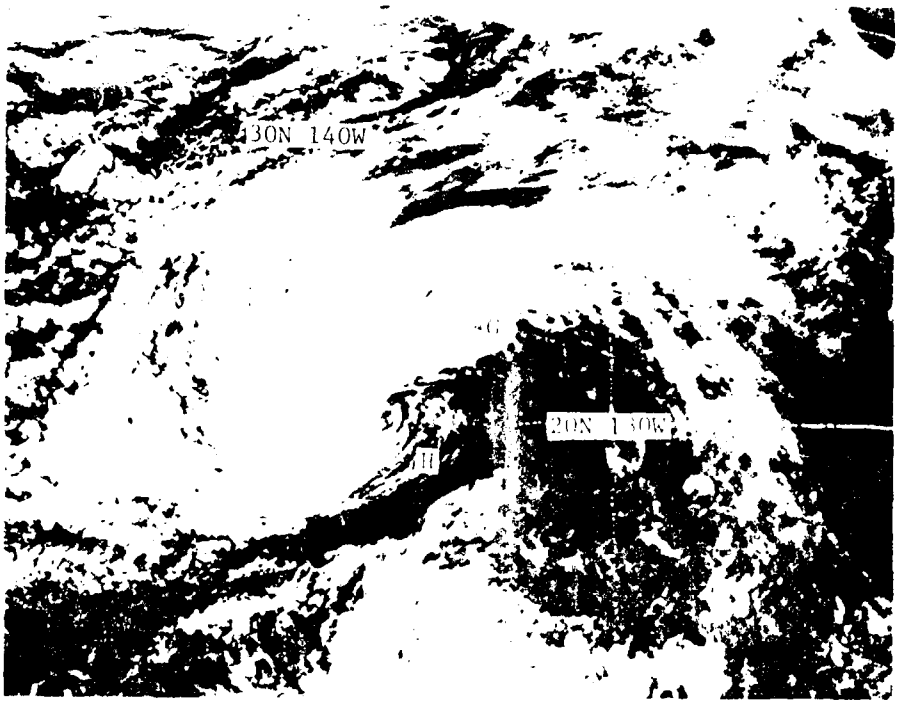

Fig. 4: SMS-2 visible (4 km resolution), 0115Z, 14 August 1976.

Fig. 5: SMS-2 visible (2 km resolution), 1815Z, 14 August 1976.

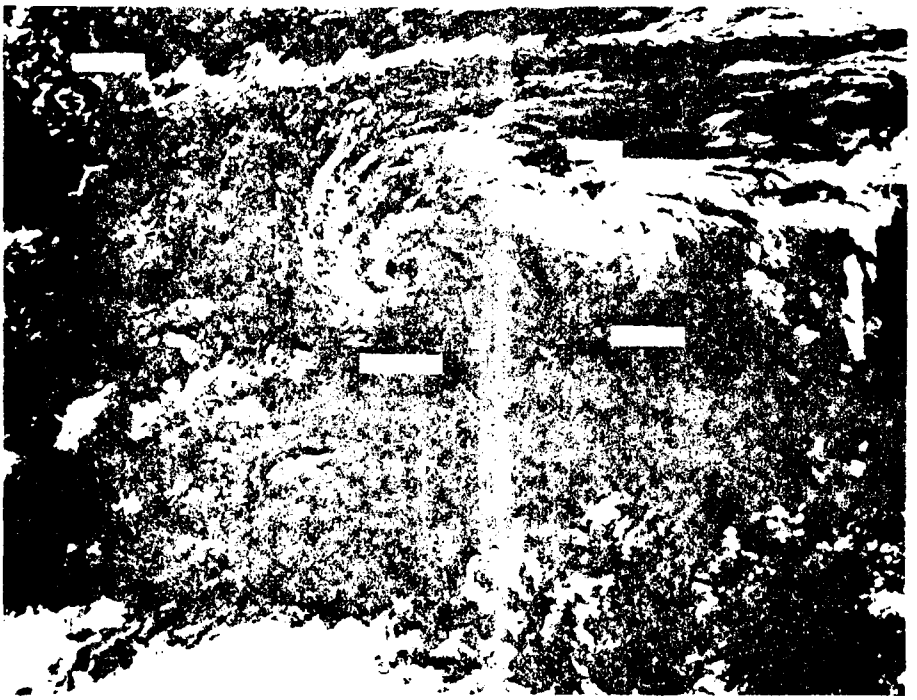

Fig. 6: SMS-2 visible (2 km resolution), 2315Z, 15 August 1976.

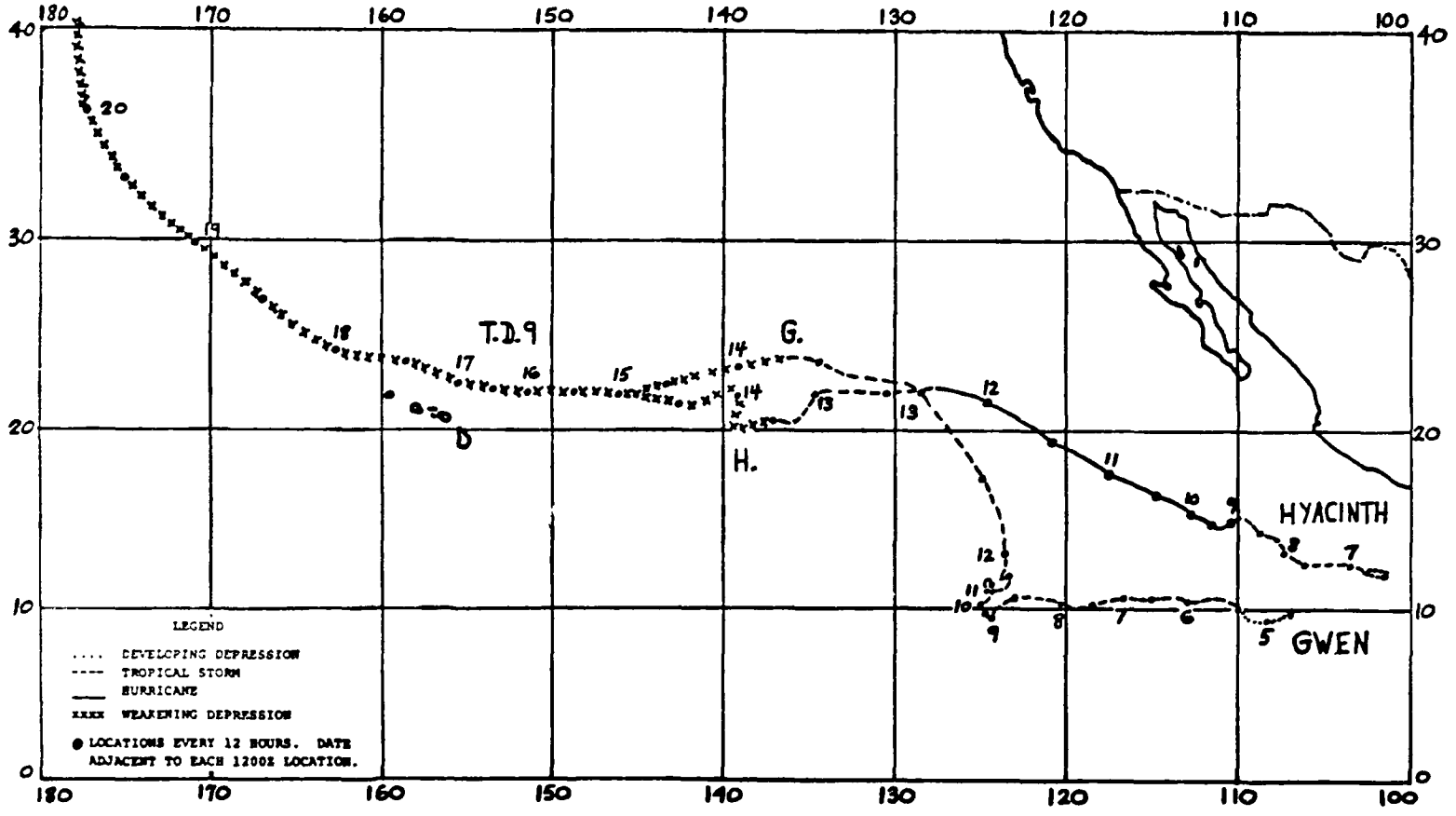

Fig. 7: Best tracks of GWEN, HYACINTH and tropical depression 9 in August 1976.

U.S. DEPARTMENT OF COMMERCE

National Weather Service/National Environmental Satellite Service
SATELLITE APPLICATIONS INFORMATION NOTE 77/6

THE FEBRUARY 23-24 DUST STORM AS VIEWED FROM GOES-1

James J. Gurka
Applications Group
NESS/Washington, D. C.

On February 22, 1977, an intense surface low developed in the lee of the Colorado Rockies (Fig. 1) producing strong winds but very little precipitation in the drought-stricken areas of eastern Colorado, western Kansas, and west Texas (see Fig. 2). As was expected, the storm began producing blowing dust on the 22nd. By February 23 and 24, the storm was responsible for the most spectacular dust storms over North America since geostationary satellite imagery has been available. While the satellite imagery made it possible to monitor the spread of the dust, the 24-hour P.E. trajectory prog. proved to be a useful tool for predicting the spread of the dust on this occasion.

The hourly sequence of visible satellite pictures beginning at 1700 GMT, February 23 (Figs. 3-6) shows the edges of the blowing dust at A, B, C and D. At 1700 GMT (Fig. 3), one area of dust is confined to west central Texas and appears as a hazy, milky-looking area between A and B. Farther north, a more widespread area of dust extends from northeast Colorado, southeastward through parts of Kansas and the Oklahoma and Texas panhandles (D) and then northeastward through central and northern Oklahoma (C). Numerous observations of blowing dust were being reported on the 1800 GMT surface chart (Fig. 7). From 1800 to 2000 GMT (Figs. 4-6), the dust originating near the west Texas border spread southeastward into central Texas, and by 2300 GMT (Fig. 8), into southeast Texas. The edge of the northern dust area at D spread southward during the afternoon, while that at C moved southeastward. The airborne dust can also be seen as a cold radiating surface (A, B and C) in the daytime IR imagery (1900 and 2000 GMT, Figs. 9 and 10).

By 1600 GMT on the next day, February 24 (Fig. 11), the dust extended from southern and western Oklahoma and northeast Texas (D) eastward through portions of Arkansas and Louisiana into Mississippi (E), Alabama and Georgia (A); and then southward into the Gulf of Mexico, with edges at B, C and F. On the 1600 GMT infrared picture (Fig. 12), the dust can be seen over land (A to D); however, in this case, the temperature of the top of the layer approaches that of the sensed water temperature in the Gulf and could mask the actual thermal pattern and lead to errors in determining sea surface temperatures from the satellite imagery.

The dust on both days extended upward through a deep layer in the atmosphere, with several pilot reports taken on February 23 over Texas indicating tops of the layer to be 12,000 to 15,000 feet. On the 24th, reports of dust tops from 7,000 to 9,000 feet were common, with most pilots reporting the thickest dust in the lowest 3,000 to 5,000 feet range.

The 24-hour P.E. trajectory prog. for the 850 mb level (Fig. 13) moved some of the dust-laden air from central Texas into southeastern Georgia between 0000 GMT on the 24th and 0000 GMT on the 25th; another portion was forecast to move into the Gulf of Mexico. For the same time period, the trajectories passing through the dust in Oklahoma extended southeastward to Alabama and then northeastward through northern Georgia and into the Carolinas. From the 2200 GMT satellite picture (Fig. 14), it can be seen that the trajectory forecast was fairly accurate with the dust extending through Georgia and into the Carolinas and southward into the Gulf of Mexico, with edges at A, B, C, D, E, and F. This suggests that the satellite-observed dust patterns, combined with the 24-hour trajectory prog., could be useful tools in the preparation of aviation forecasts during conditions of blowing dust.

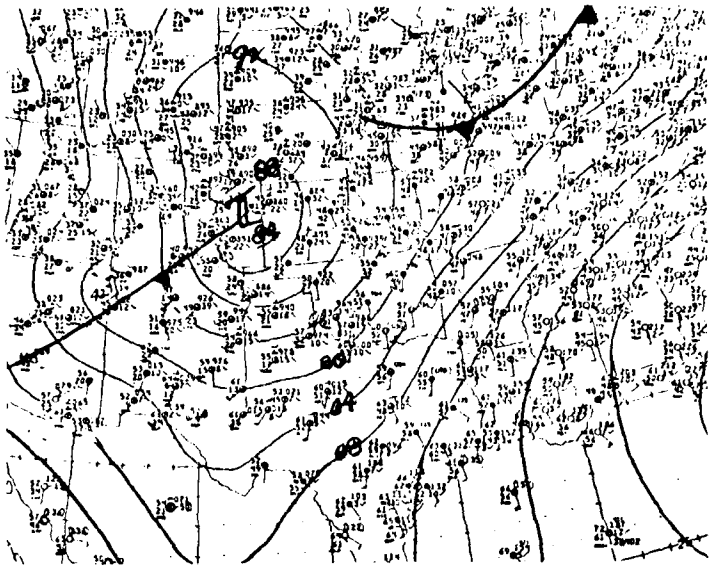

Fig. 1. NMC Surface Analysis, 1500 GMT, 22 Feb 77

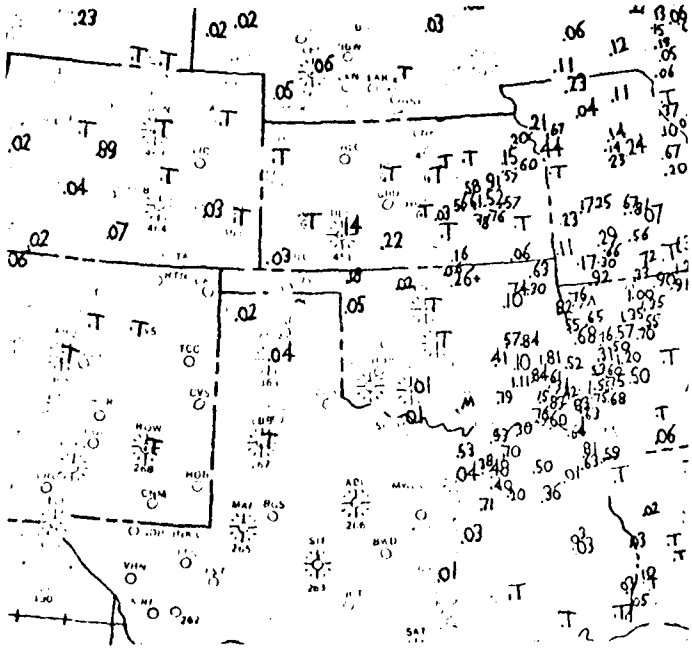

Fig. 2. Observed 24-hour precipitation for the period ending at 1200 GMT, 23 Feb 77.

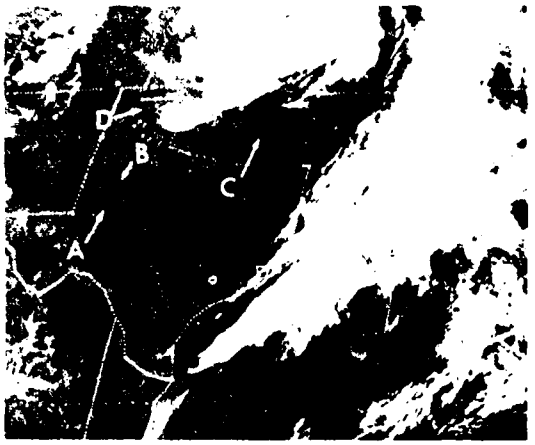

Fig. 5. GOES-I 2-km Visible
1500 GMT, 23 Feb 77.

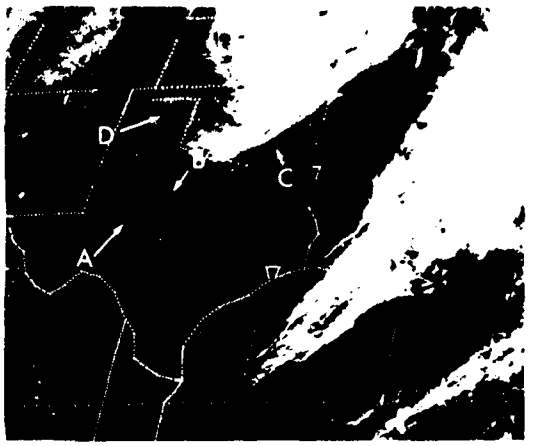

Fig. 6. GOES-I 2-km Visible
2000 GMT, 23 Feb 77.

Fig. 4. GOES-I 2-km Visible
1800 GMT, 23 Feb 77.

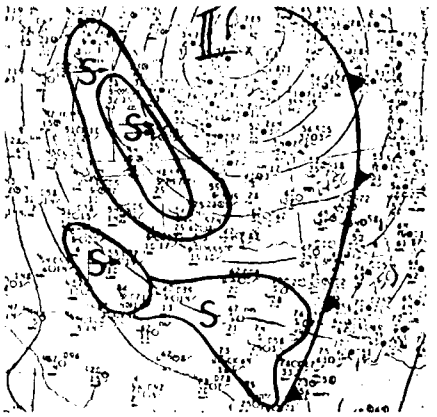

Fig. 7. NMC Surface Analysis, 1800 GMT, 23 Feb 77; area reporting blowing dust as outlined.

Fig. 3. GOES-I 2-km Visible
1900 GMT, 23 Feb 77.

Fig. 8. GOES-I 4 km Visible
2300 GMT, 23 Feb 77

172

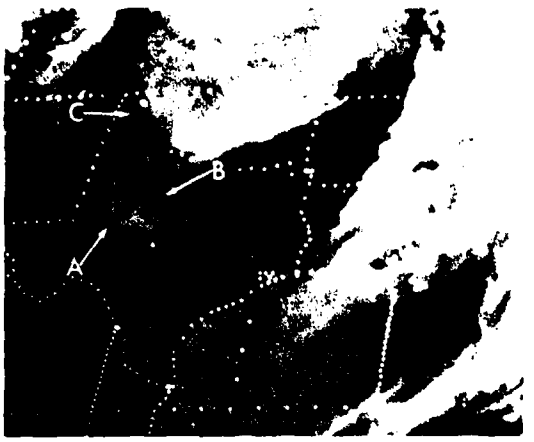

Fig. 9. GOES-1 8-km IR, 1900 GMT, 23 Feb 77.

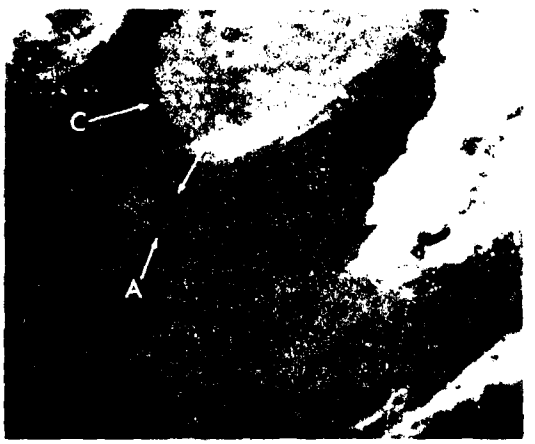

Fig. 10. GOES-1 8-km IR, 2000 GMT, 23 Feb 77.

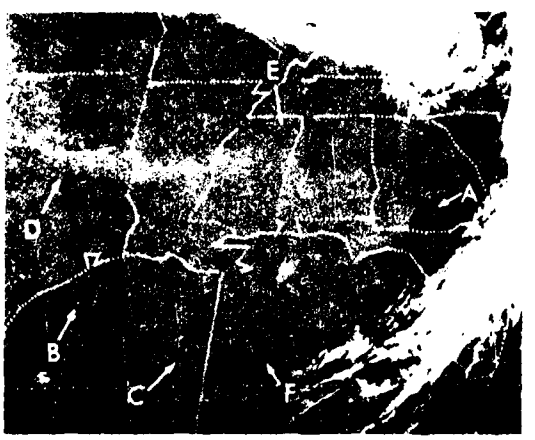

Fig. 11. GOES-1 2-km Visible 1600 GMT, 24 Feb 77.

Fig. 12. GOES-1 8-km IR, 1600 GMT, 24 Feb 77.

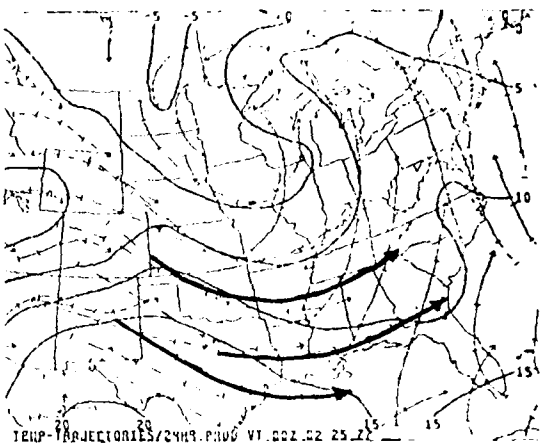

Fig. 13. NMC 850 mb, 24-hour, Temp - Trajectory Prog - VT 0000 GMT 25 Feb 77.

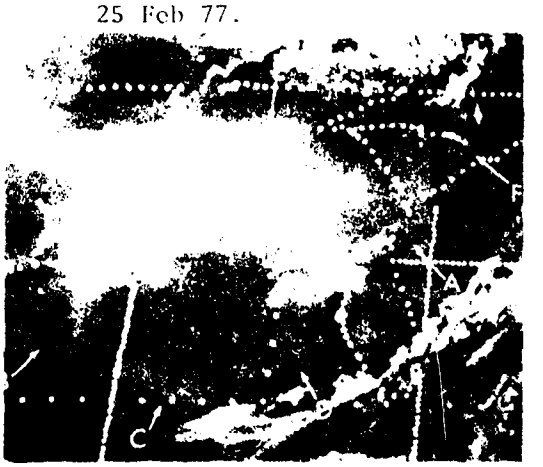

Fig. 14. GOES-1 4-km VIS 2200 GMT, 24 Feb 77

173

U.S. DEPARTMENT OF COMMERCE

National Weather Service/National Environmental Satellite Service
SATELLITE APPLICATIONS INFORMATION NOTE 77/7

AN OCEANIC CYCLOGENESIS - ITS CLOUD PATTERN INTERPRETATION

R. B. Weldon
NESS, Applications Group

Shown is a series of 13 infrared pictures over the Pacific. The pictures are at 3-hour intervals and span a total period of 26 hours. Picture 14 is a visible image which corresponds to the time of picture 6 of the IR series. The cloud pattern evolution shown is a type which is often observed with relatively rapid cyclogenesis over the oceans. Many aspects of the cases are pertinent to weather systems that occur over North America as well.

Note the cloud pattern that is labeled "A" on pictures 1 and 3 and its evolution during the 36 hour period. Some aspects of the cloud pattern and its evolution are unique to the case shown; other aspects are common to many systems of the type. It is those common aspects that are emphasized in the following observations and interpretations.

The cloud pattern evolution:

Most of the cloud pattern change occurred during the 24 hour period which began at 12 GMT, 3 February, and ended at 12GMT, 4 February (pictures 3 thru 11). On picture 3, the cloud pattern - labeled "A" - is well defined with a relatively uniform cold top area and a distinct edge on the poleward side. The "distinctiveness" of the cloud pattern has increased during the previous six hours (compare pictures 1, 2 and 3), although the general "wing" or "leaf" shape has continued. The cloud top area has become more uniformly cold and the poleward edge has sharpened - become better defined. In many cases, this trend is accompanied by a clearing or decrease of cloudiness adjacent to the main cloud pattern, but this is not apparent on the pictures shown here. I have noted that such an increase in "distinctiveness" is an indication that the system is intensifying; the mid-tropospheric vorticity and temperature gradients are increasing with time, and the value of the maximum vorticity associated with the cloud system is probably increasing with time.

Note that tne poleward edge of the cloud pattern on picture 3 has a low amplitude "S" shape. On FIGURE 3 - which contains the same IR image as picture 3 - this edge is identified by the white letters "a", "b" and "c". The shape of the edge reverses from slightly concave to slightly convex at point "b", an inflection point. On picture 4, that portion of the edge which was concave west of the inflection point (section "a-b" on Figure 3), now appears as a separate cloud band. The clouds which were south of the edge in that portion of the system have begun to dissipate - or have stopped forming. This trend continues. On picture 6, the edge band itself is no longer detectable; and the cloud pattern has begun to form a comma-like shape.

That part of the edge which was convex east of the inflection point (section "b-c" on Figure 3) has been maintained. This has evolved to become the border of the "head" portion of the emerging cloud comma pattern. On picture 6, a protruding cloud point or "tip" (labeled "D") appears at the rear of the comma "head". When viewed by 30 minute interval time-lapse motion - film loops - the tip appears to have evolved from the inflection point of the original edge. A small clear "slot" appears to the south of the "tip". It is the presence of the "slot" that differentiates between having a "tip" rather than an inflection point at the location where the edge reverses its shape from concave to convex. During the ensuing pictures of the series (pictures 7 thru 13) the slot becomes larger, the portion of the edge which is concavely shaped (south and west of the slot on picture 6) rotates cyclonically with time, and the tip "hooks" cyclonically around the center of maximum vorticity.

Picture 14 is a visible image which corresponds in time to the IR image of picture 6. This was the first high sun angle visible picture available to me for that date. Note the bright distinct pattern and the smooth top appearance of the main cloud system on the visible picture. Such distinctiveness on both the visible and IR images is an indication that the cyclogenesis is occurring through a vertically deep layer. With such a case over an oceanic environment, it is likely that significant surface cyclogenesis is accompanying the upper level cloud system development. Had there been visible data available for the time of picture 3 (about midnight local time), cloud pattern "A" would likely have displayed a similar bright well defined pattern as on picture 14. This opinion is based upon observations of other similarly developing systems at the same phase of their evolution.

The cloud system "movement" and relationships to the wind field:

Which way will it move? If, at the time of one of the first 3 pictures, cloud system "A" had been recognized as an incipient pattern of a developing storm system, this would have been one of the basic questions asked. Another related question is: "which way did it move?" The first requirement for answering either of those questions is to define "it". Figure 4 is a drawing which depicts the movement of the edge "a-b-c" which was indicated on Figure 3. The edge position is shown at six hour intervals. The numbers correspond to picture numbers. Point "a" was defined as the location where the cirrus which was coming over the upstream high level ridge crossed the "tail" end of cloud system "A". Point "b" was defined as the inflection point of the original edge, which became the "tip" as the system evolved. Point "c" was defined as the point on the "outflow" end of the edge where the clouds either ended or became ragged. Keeping in mind that picture 9 was a 0615 GMT picture 30 minutes later than it should have been to maintain the 3 hourly intervals, the following observations are made:

Note that prior to picture 5 the cloud system had changed little in shape and moved rapidly toward the east-southeast. It was during the period between pictures 4 and 6 that the "a-b" section of the radar edge became banded and disappeared - shifting that part of the edge southeastward and forming the comma-like shape. It was during the same time period that the inflection point/tip part of the cloud system changed from moving eastward or slightly south of eastward to northeastward. Both the change of direction and the transition of the cloud pattern are coincident with the development of southwesterly winds in advance of the vorticity center at mid tropospheric levels. A "waving" or increase of amplitude of the streamlines at middle levels occurred, and the system began to "turn the corner".

Studies of such cloud systems over the U.S. data network have shown that the "vorticity center" - or the point of maximum absolute vorticity value of the 500 mb winds - is located just to the rear of the inflection point on the clear side of the distinct edge - as seen on pictures 1,2, or 3. On picture 6 it would be located southwest of the "tip" feature. As the pattern evolves and the amplitude of the "trough" in the wind field and height contours increases, the vorticity center moves faster than the "tip". I have placed dots on Figure 4 indicating where I believe the vorticity center would most likely be located with respect to the cloud pattern at each of the 6 hour intervals. Note that a line drawn between the vorticity center and the "tip" (or the inflection point of the edge) at each picture time would rotate cyclonically as the pattern evolved. This changing relationship is directly related to the fact that the system was developing an increasing amplitude trough (and eventually a closed low and streamline center) and to the fact that the vorticity center (and the tip feature and comma head) were moving in a path that curved increasingly to the left with time.

In regard to the part of the system that moved northeastward, another point to consider is: can we determine from the satellite pictures when the upper level center "closed" in the contours and streamlines - if it did? Consider picture 7. If we examine the cloud motions on movie loops at the time of that picture, or those of other comma shaped cloud systems in a similar phase of development; the following is observed. The small cloud elements on the north or northwest side of the slot are moving backwards - or losing ground - with respect to the overall cloud system movement. Clouds are dissipating at the edges of the tip. On the other side of the slot, clouds seem to be forming. In other words, the air northwest of the slot is losing ground to the moving cloud system, and the air southeast of the slot - and along the edge southward of that area - is gaining ground with respect to the system. At this phase of development, this differential motion is due mostly to wind shear and only slightly to curvature. The air northwest of the vorticity center - at cloud levels - is still moving from the west or southwest with respect to the map, but not with respect to the system which is moving faster. A "Closed" circulation is present in the relative motion of the air, but not in the winds. As the system evolves and the circulation "closes" in the wind field, the following behavior is observed on movie loops. Cloud elements move back along the tip area and dissipate; those that move furthest before dissipating define the end of the tip. There is considerable variation in this process at half hourly intervals, and a corresponding variation in the

shape and extension of the tip. As the system evolves, these elements tend to move more to the left and further along the path than their predecessors before they dissipate. The result to the pattern is, that the tip begins to hook cyclonically around some point moving with the system. In the case shown, this pattern appears on picture 9 and is better defined by picture 10. Experience has shown that this process of the tip hooking around into a curved pattern occurs at about the same time that the elements begin moving back with respect to the ground (as well as with respect to the system). Thus, the hooked tip pattern is a good indication that the system is "closed" in the wind field - and contour field - at cloud levels. Careful study of the film loops for the case shown indicates that the system was "closed" in the cloud level flow: probably by picture 9 and definitely by picture 10. Note that the tip can be hooked completely into a circle; and, if the system is still moving, the vorticity center will not be in the center of the circle formed by the hooked tip. It will be offset to the right of the center of the hooked circle looking downstream in the direction of system movement.

Whereas the comma "head" portion of the cloud system turned northeastward, the part of the cloud edge indicated by "a" continued to move eastsoutheastward until picture 8, then eastward until picture 10. Section "a-b" of the edge rotated cyclonically, such that point "a" which was about 500 miles westsouthwest of "b" on picture 1 is nearly the same distance to the southsoutheast of "b" by picture 13. Edge section "a-b" forms the rear edge of the "tail" cloud feature of the evolving storm cloud "comma". The tail cloud band, in this case, indicates a vertically deep frontal zone extending thru the middle and lower troposphere. Significant convection occurs along that frontal zone from the comma head southward (or southwestward on the earlier pictures) to point "a" where the cirrus crosses over the frontal zone. The northern edge of the cirrus which crosses the tail/frontal zone is near to and parallel to the axis of maximum winds at high tropospheric levels. Thus, point "b" represents the point where the axis of the jet stream crosses the lower level frontal zone. At low levels the frontal zone extends under the jet stream cirrus. The cloud band labeled "f" on picture 14 and on IR picture 6 is likely very close to the location of the surface cold front associated with the developing cloud system.

At the time of picture 9, the southern end of the tail/frontal zone where the jet stream cirrus crosses has been moving eastward, and active convection has been occurring. In the interest of forecasting the weather to the east of the tail at those latitudes, the significant question is: is it safe to extrapolate the past movement of the southern end of the active frontal zone. From experience I have noted that, as long as the cirrus coming over the upstream ridge extends downstream to - or across - the frontal zone tail band as a well defined band or edge nearly parallel to the high level winds, the frontal zone - where the cirrus crosses - will continue to move, and convection will occur along the tail to the left of where the cirrus crosses. When the cirrus edge or band coming over the upstream ridge is well defined, the axis of maximum winds tend to be parallel to the edge and parallel to the isopleth-of vorticity. If such an edge is present and nearly straight upstream to the

177

ridge or back upstream 10 or 15 degrees longitude, then the frontal band at the crossing point will remain active and move in the direction of the cirrus that crosses it. I can reliably extrapolate the frontal band movement for 12 hours or more. If the definition and straightness of the edge is maintained, but the upstream ridge is building northward with time the jet and cirrus band will rotate anticyclonically and the crossing point will move increasingly to the right of its previous track. In this case, none of the above are occurring. Examination of the clouds of the upstream ridge indicates two changes occurring during pictures 9, 10, and 11. The flow between the upstream ridge and the frontal band is increasing its amplitude. The cloud edge near the ridge is more and more anticyclonically curved and that near the frontal band is more cyclonically curved. The cirrus edge near the frontal band is rotating cyclonically in concert with this increase of amplitude; and the point "a" of the system begins to turn toward the northeast. Also, as the increase in amplitude occurs, the cirrus no longer extends from the ridge to the frontal band. The second change occurring is that the edge near the ridge is becoming ragged indicating that the flow is across the vorticity isopleths in an "negative vorticity advection" sense. This also indicates that the strong winds in that area will be spread over a wide area; the axis of maximum winds will be difficult to define. The first change indicates that the point of cirrus crossing the frontal band will turn toward the northeast (or more to the left of its previous track); and the second change indicates that the system will begin to shear out and weaken. Note on Figure 5 that the 300 mb contours spread in a different pattern between the upstream ridge and the evolving storm cloud system. During the period from picture 11 until picture 13, the cloud system elongated into a northwest - southeast orientation, and the cloud bands became thinner. Studies of such cloud system behavior over data rich areas indicate the following: An elongated region or "lobe" or higher vorticity values extends from the vorticity center to the point where the cirrus crosses the frontal band. As the cloud system stretches or elongates in the manner shown here, the vorticity lobe also elongates, the vorticity gradients decrease, and the value of the vorticity center decreases.

Because of the change of structure of the upstream ridge, the demise of the system can be guessed at the time of picture 11. By picture 12, the guess is reinforced, and by picture 13, the trend is well established. After that the system continues to "shear out" as it moves against the blocking ridge-trough pattern over the North American continent.

The early cloud pattern identity - a "baroclinic leaf"

How soon was the development identifiable on the satellite pictures? The answer is - in my opinion - at the time of picture 1. Although the cloud pattern was identifiable prior to that time, it was less distinct. By picture 1, the pattern had a distinct "wing" or "leaf" shape which is characteristic of the incipient cloud patterns in many cases of cyclogenesis. I refer to such an incipient cloud system as a "baroclinic leaf". I could not be sure at the time of picture 1 - based merely on the shape alone - that the cloud pattern "A" was of the "baroclinic leaf" category. However, there are some additional clues which reinforced the identity.

178

(1) If the "leaf" shaped pattern is a "baroclinic leaf", it should be located within the jet stream zone, or in the exit region of an advancing jet stream with weaker flow ahead of it. The differences of the low clouds in picture 1 indicate that pattern "A" is within the jet stream zone.

(2) The logitudinal cloud axis of a "baroclinic leaf" pattern will most likely be oriented in a direction which is rotated counter-clockwise by some acute angle with respect to the direction of the upstream jet axis. This is difficult to check on picture 1, since the upstream jet stream is on the horizon of the picture. A related characteristic which can be checked is that the axis of the "leaf" will usually be in a direction oriented counterclockwise from the direction of propagation of the cloud system. This is true at the time of picture 1. The axis of the "leaf" is WSW-ENE, and the direction of propagation a little south of eastward.

(3) On an IR picture, the cloud top area of a "baroclinic leaf" system is usually colder and smoother on the wider portion, with the cloud tops becoming progressively warmer and more irregular toward the narrow "tail-like" end.

From the above combination of characteristics, the "baroclinic leaf" identity of cloud pattern "A" was firmly established; and the interpretation that significant development was underway was a highly reliable one. The primary remaining question is: What is the vertical depth involved in the development? The coldness of the pattern on the IR image indicates that system is affecting the high troposphere, but some "leaf" cloud patterns and their associated development are confined to the higher levels.

In this case, I concluded that the development was vertically deep and probably included the surface. The conclusions were based on the following:

(1) Such coldness on the IR image with respect to other cloud systems on the same picture, implied a vertically thick cloud system.

(2) The jet stream associated with the system appeared to be vertically deep because of the effects on the convective clouds on opposing sides.

(3) The development was not in the southern branch of a split in the westerlies, but appeared to be within the main branch of the jet stream. High level development often occur in the southern branch of splitting westerly jet streams.

(4) The development was over the ocean where a large availability of low level moisture existed.

Another point to check in this regard is:

(5) Does a low level tail-like band of clouds - such as those associated with a surface front - extend to the rear of the narrow end of the "leaf"? If it does the development involves the lower atmosphere. In this case the area where the low band would be is obscured by higher clouds. So, this clue cannot be checked.

Figure 3 shows the 300mb contours from the NMC analysis superimposed on the IR image of picture 3. The purpose of the figure is to illustrate the relationships of this particular "baroclinic leaf" pattern to the long wave environment. Figures 1 and 2 depict "baroclinic leaf" patterns within two other types of environments.

The following conditions are common to "baroclinic leaf" patterns in all 3 types of environments:

(1) The region of the atmosphere under the leaf is frontogenetic. In early stages of most cases, the frontogenesis was strongest in the middle troposphere, and was occurring in the deformation zone in advance of a speed maximum in the jet stream upstream from the leaf. The overall frontal zone is parallel to the longitudianal axis of the "cloud leaf". As the system progresses, lower level frontogenesis begins or increases under that part of the leaf with the concave rear edge. This appears to be enhanced by sinking air to the rear of that part of the cloud system. At high tropospheric levels the frontogenesis is greatest near the convex portion of the edge.

(2) The presence of the "leaf" is an indication that cyclogenesis is likely. If the development is not halted by some change in the environmental conditions, the "leaf" will evolve into the storm cloud comma pattern.

(3) Although the "rear" edge of a "leaf" is often well defined, the winds and height contours at cloud top levels are oriented across the edge at angles ranging from very large at the narrow (usually equator-ward) end to very small or paralled at the wide (usually poleward) end.

(4) The leaf pattern is located within a tight gradient of 500mb vorticity isopleths. The 500mb winds cross the isopleths in a positive advection direction. The vorticity gradient is usually increasing with time. For those systems that are developing rapidly, the vorticity isopleths are parallel to the contours and winds along the jet axis upstream from the narrow end of the "leaf".

(5) The jet stream axis is NOT along the well defined edge of the leaf. The jet stream axis normally crosses the leaf pattern in a manner depicted by the arrows on Figures 1 and 2. The jet stream is usually well defined and strong at middle levels upstream from the leaf where the cross-hatched arrows are shown on Figures 1 and 2. There is more variability in the jet structure on the other side of the leaf.

The following differences which depend upon the 3 types of environments shown:

Figure 1:

Here the "baroclinic leaf" is located over a pre-existing or established low level or surface frontal zone. The clouds associated with the low level

front are indicated by the hatched band. As the deep layer frontogenesis occurs, the low level increasing gradient will be merged with the existing gradient of the established surface front along the tail portion of the leaf. In such cases, when the surface cyclogenesis occurs north of the established front, that portion of the newly forming cold front which is north of the established front, will be "an instant occlusion". If the surface cyclogenesis occurs in the surface frontal zone of the pre-existing front, a "frontal wave development" will occur. My observations indicate that the place where the surface cyclogenesis occurs in most dependent upon where the middle and upper level strong wind zones are. The lower level environment - especially the availability of warm moist air - appears to influence the rapidity at which the surface cyclogenesis proceeds. This may be related to the fact that when a "leaf" cloud pattern does occur over or near to an already established surface frontal zone, the convex curved portion of the edge and the clouds in that portion of the "leaf" dominate in coldness and brightness. In fact the cloud system quickly takes on more or an "arch" shape rather than a "leaf" or "wing" shape on the IR images.

Figure 2:

Here the "leaf" occurs on the forward side of a relatively high amplitude trough. Frequently in such cases considerable high cloudiness is present on the warm side of the jet stream axis. Note that the edge of that cloud pattern coincides closely with the axis of the jet stream indicated by the arrows. The edge of the "leaf" does not. In regard to the low level frontal locations, similar variations occur as in the case of Figure 1, since often there is a pre-existing low level frontal zone under the jet stream related cirrus. Frequently a new surface front will form along the tail of the "leaf" before it accelerates eastward and overtakes the colde pre-existing front.

Figure 3:

Here, as in Figure 1, the "leaf" is forming within a relatively low amplitude branch of strong westerlies. However, in this case there is no pre-existing surface frontal zone near the "leaf". Note the southwest to norteast oriented warm cloud bands well to the southeast of the "leaf". These are the remnant frontal cloud bands of previous systems which have moved east and dissipated against the blocking ridge. One of these still had active convection along it in picture 1. In such a case as this - during the early stages of the "leaf" - a surface front may exist, trailing back upstream under the middle and upper level jet/baroclinic zones, or it may form under the tail end of the "leaf" as the system intensifies.

AD-A167 989 SATELLITE APPLICATIONS INFORMATION NOTES OCTOBER 1975 - DECEMBER 1978(U) AIR WEATHER SERVICE SCOTT AFB IL AUG 79 AWS/TN-79/003 3/4

UNCLASSIFIED F/G 4/2 NL

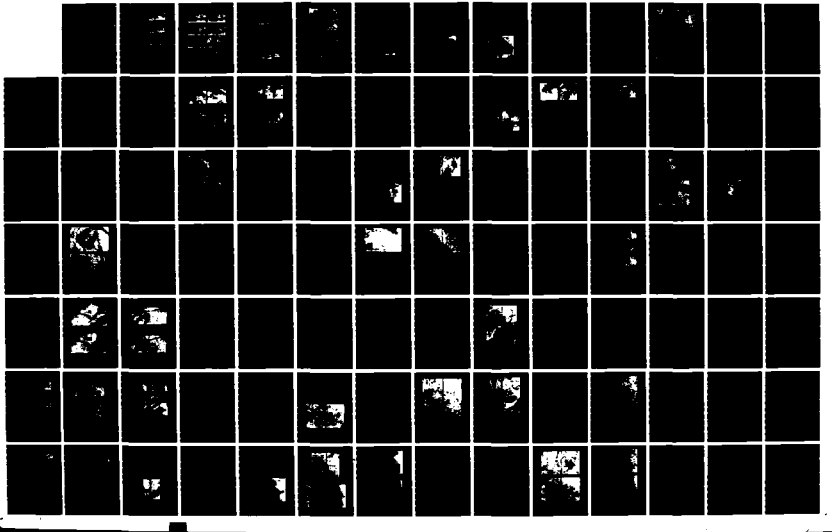

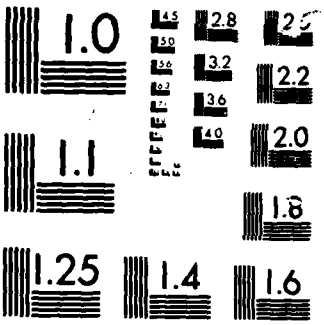

MICROCOP CHART

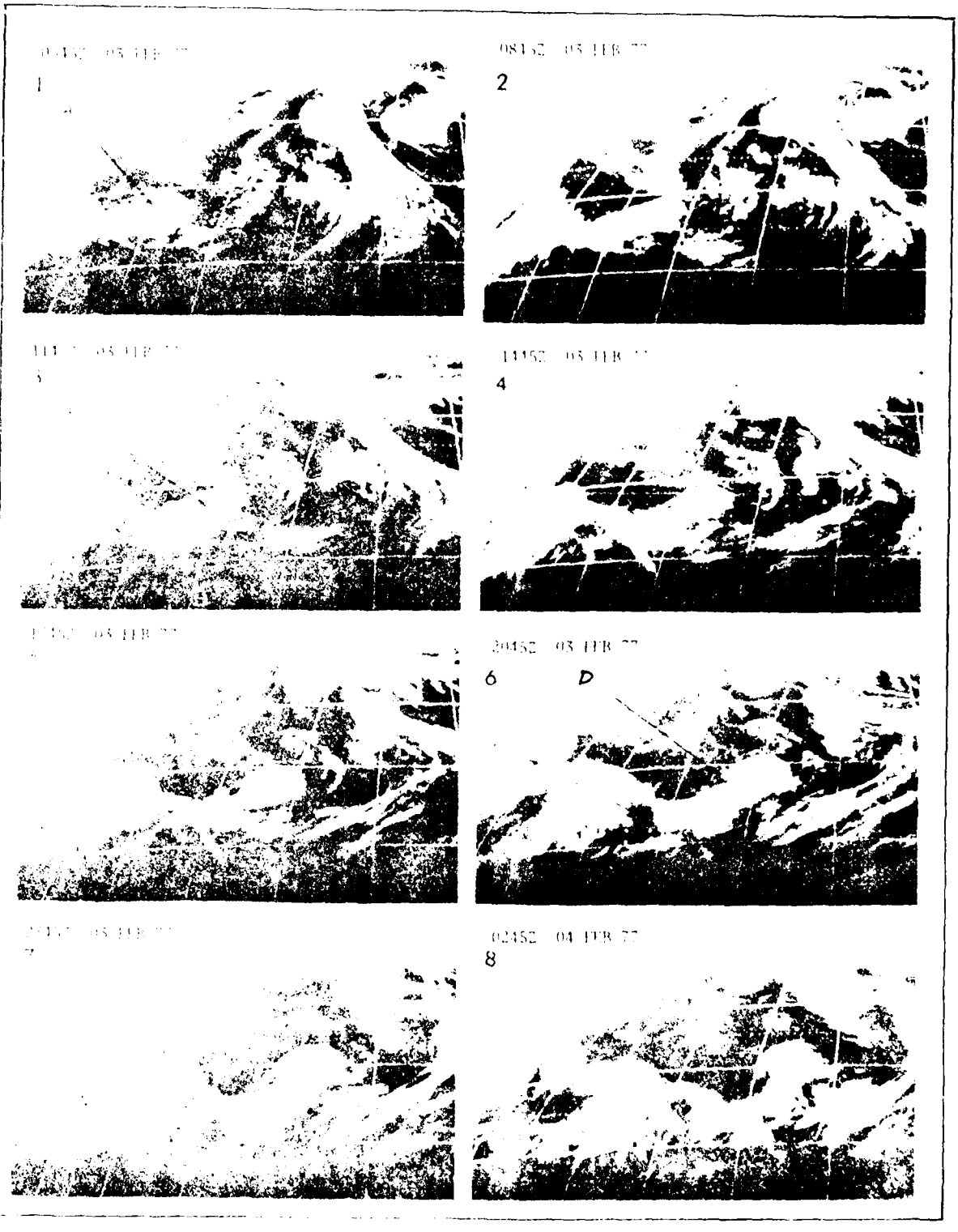
1
2
3
4
6
D
8

0615Z 04 FEB 77

9

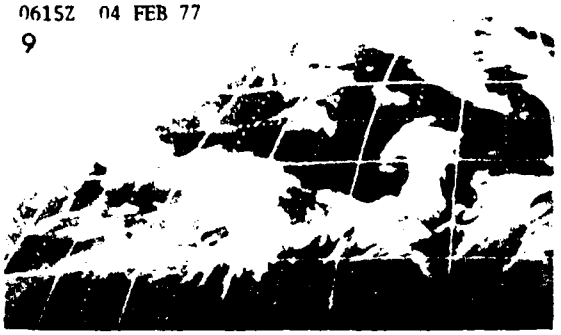

0845Z 04 FEB 77

10

1145Z 04 FEB 77

11

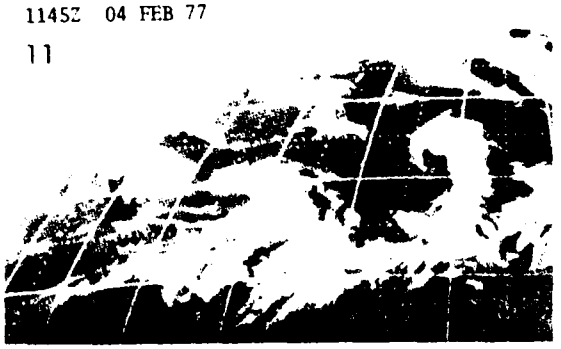

1445Z 04 FEB 77

12

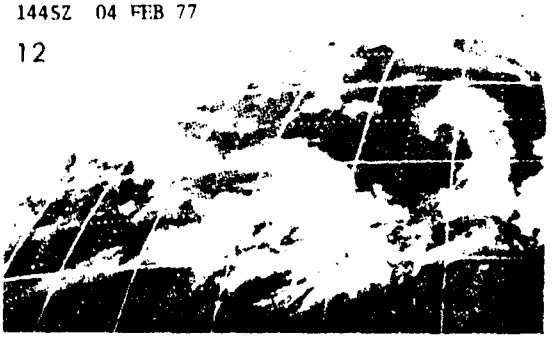

1745Z 04 FEB 77

13

2045Z 03 FEB 77 visible

14

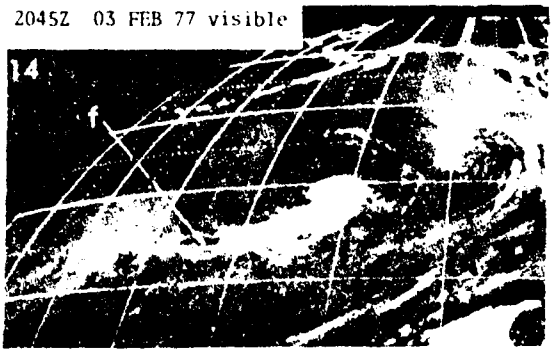

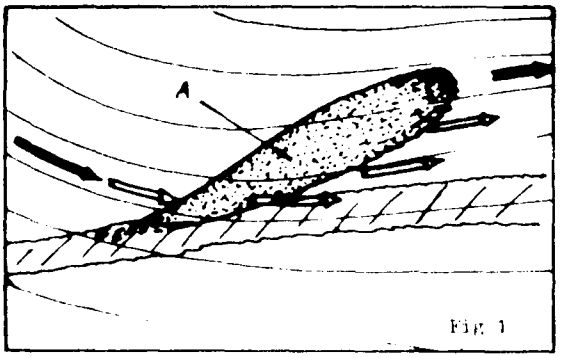

Fig. 1

Fig. 2

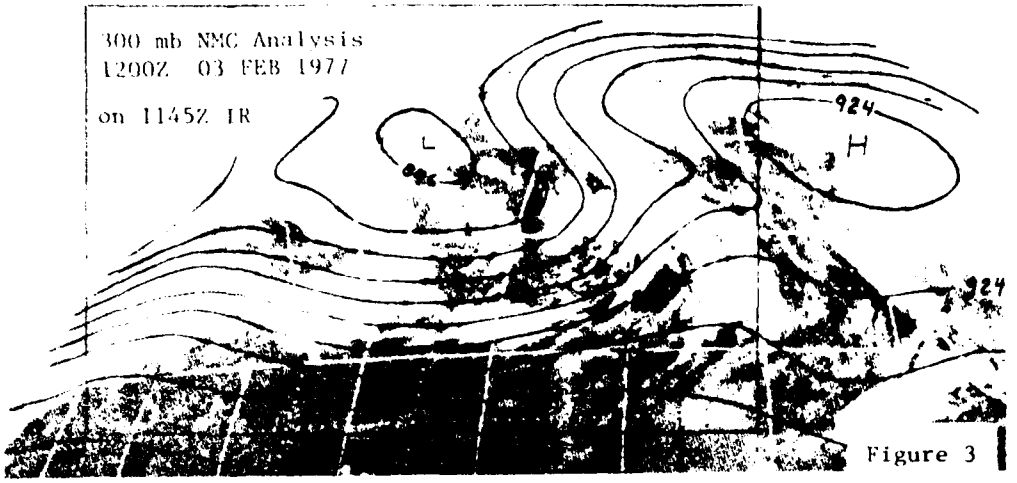

Figure 3

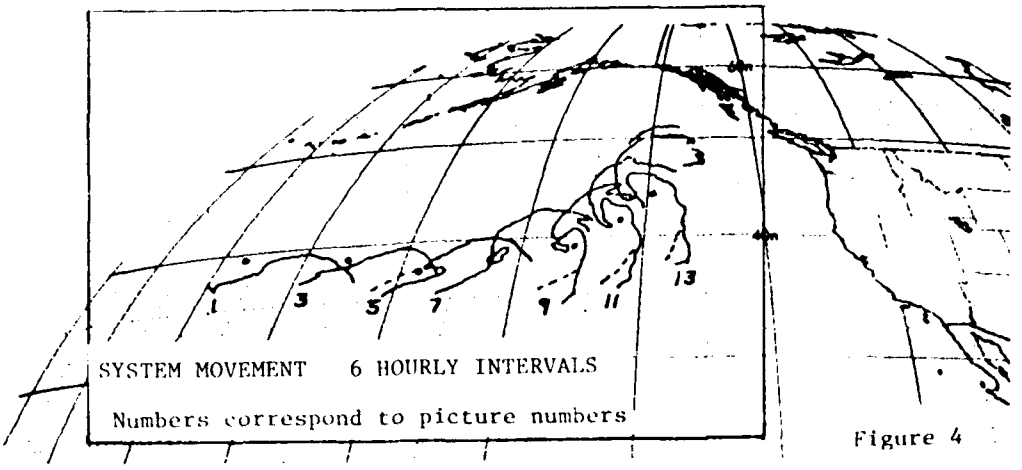

Figure 4

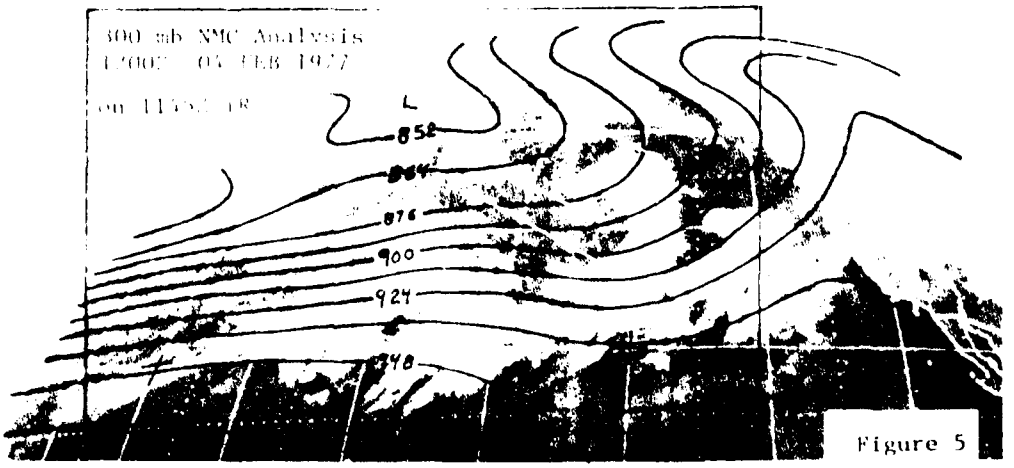

Figure 5

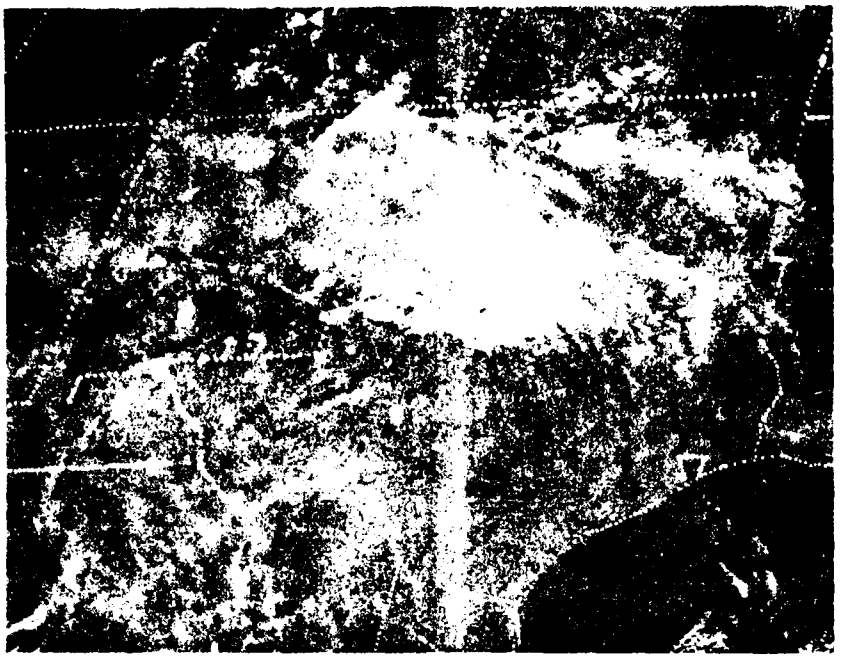

Figure 1. GOES-1 Visible (2 km) 1430 GMT, 8 March 1977.

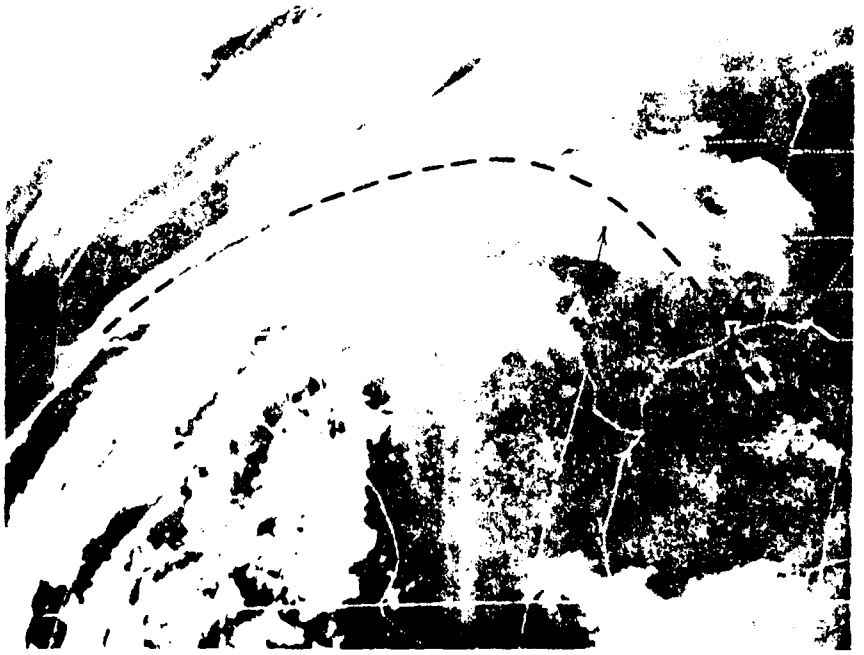

Figure 2. GOES-1 Enhanced IR (6 km) Cb Curve 1530 GMT, 8 March 1977.

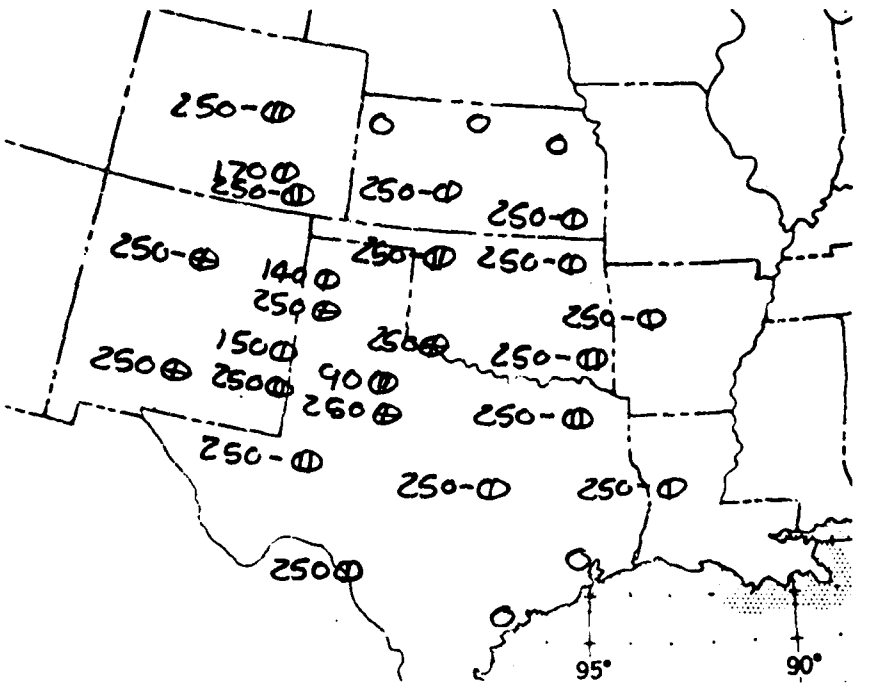

Figure 3. Cloud Depiction at 1500 GMT, 8 March 1977.

Figure 4. GOES-1 Visible (2 km) 1700 GMT, 8 March 1977.

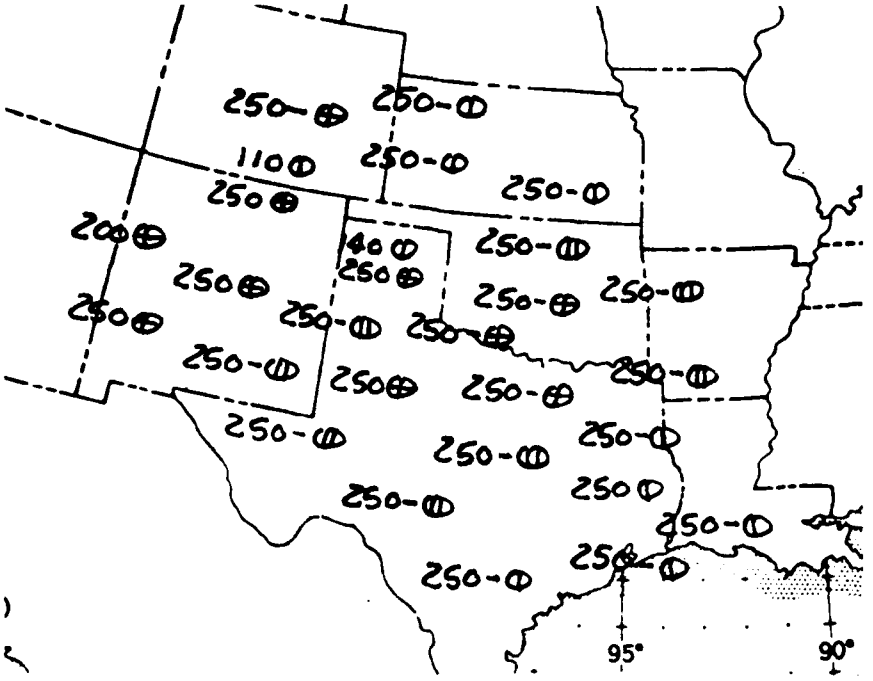

Figure 5. Cloud Depiction at 1700 GMT, 8 March 1977.

Figure 6. GOES-1 Enhanced IR (4 km) Cb Curve 1700 GMT, 8 March 1977.

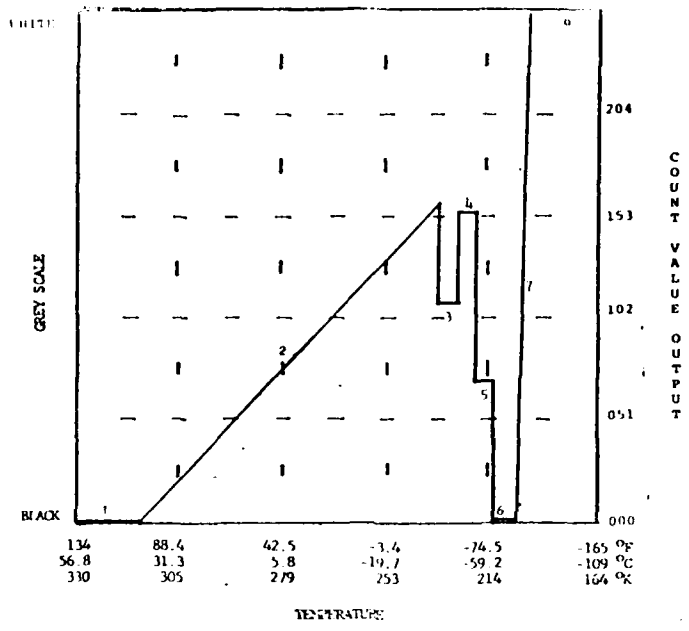

SEGMENT NUMBER	°C Temperature To	COMMENTS REASON FOR SEGMENT ENHANCEMENT
1		
2		
3		
4		
5		
6		
7		
8		

Figure 7. Enhancement Cb Curve.

Figure 8. GOES-1 Visible (2 km) 2200 GMT, 8 March 1977.

U.S. DEPARTMENT OF COMMERCE

National Weather Service/National Environmental Satellite Service
SATELLITE APPLICATIONS INFORMATION NOTE 77/10

LIFE CYCLE OF AN ATLANTIC SUBTROPICAL LOW

James B. Lushine
Satellite Field Services Station, Miami, Fla.

The subtropical cyclone has drawn increased attention by Atlantic tropical meteorologists due to its greater frequency in recent years and its potential for transformation into a tropical cyclone (Frank, 1976). Hebert and Poteat (1975) have described three principal types of genesis of subtropical lows that predominate in the Atlantic. One of these is the type which forms east of an upper tropospheric trough but not in a frontolyzing zone. The evolution of this type of subtropical cyclone near Bermuda during the period 11-15 March 1977 will be examined and probable reasons why it did not become a tropical cyclone will be offered.

A mid-tropospheric short wave moved eastward off of the southeastern U.S. coast on 10 March 1977. By 1501 GMT, 11 March 1977, this short wave was centered along 68°W between 25°N and 35°N and was reflected on the surface as an inverted trough (Fig. 1). Twenty-four hours later the middle level short wave had moved eastward and surface pressures had fallen about 3mb. Fig. 2 shows the 1800 GMT surface analysis superimposed on the 2 mile resolution visible picture taken at 1501 GMT on 12 March 1977. During the next 24 hours, the system moved southward at 5-10 knots and convection increased dramatically. Bands of thunderstorms began to align themselves in the familiar comma-shaped configuration seen in the formation of some tropical cyclones. Visible movie loops at this time indicated a low cloud circulation center had developed. Fig. 3 is a 1/2 mile resolution visible picture taken at 1501 GMT on 13 March 1977 with an 1800 GMT surface analysis superimposed. Surface pressures had now dropped approximately 6mb in the past 24 hours. Wind speeds up to 30 knots were observed well away from the low center, a distinguishing feature of subtropical cyclones as opposed to purely tropical cyclones. Although exhibiting some tropical characteristics, the still cold air environment around the low is indicated by the stratified low clouds seen northwest of the center. The surface low center had now moved southward at 10 knots. By 1801 GMT on 14 March 1977 (Fig. 4), weakening of the system was inferred from the satellite pictures as the convection had diminished and become displaced well to the east of the low-level circulation. This circulation was then indicated by rather poor alignment of the low-level cumulus elements. Although surface pressures in the low remained nearly unchanged from 24 hours earlier, falling pressure ahead of an approaching cold front weakened the pressure gradient and winds around the low subsided. By 1331 GMT, 15 March 1977, the convection had moved further eastward and decreased rapidly (Fig. 5). The surface low center had moved slowly southward and was barely discernable as a weak 1014 mb low pressure center. Six hours later there was no evidence of the low center on the surface, either from conventional data or from cloud motions.

The reasons that this subtropical cyclone failed to become tropical were twofold. First, sea surface temperatures were 3°C-8°C below the commonly recognized threshold value of 27°C needed for tropical storm formation (Palmén, 1948). These sea surface temperatures were obtained operationally from satellite observations, a weekly summary of which is shown in Fig. 6. The other factor which inhibited the transformation to a warm core tropical cyclone was the strong vertical shear of the horizontal winds. Mean wind shear charts (not shown) derived by subtracting the 1000-600mb mean wind from the 600-200mb mean wind indicated shears of 15-30 knots in the area of the subtropical low. This shear is 5-20 knots greater than is normally associated with tropical storm formation in the Atlantic (Hope, 1975).

Satellite depiction of cloud cover, sea surface temperature, and wind flow has given the tropical meteorologist an opportunity to observe and evaluate the potential of disturbances over data sparse areas.

Thanks go to James Eskdale for his drafting and photographic expertise and to Suzanne Melisano for the typing.

REFERENCES

Frank, Neil L., 1976: Atlantic Tropical Systems of 1975, Mon. Wea. Rev., 104, 466-474.

Hebert, P. J., and K. O. Poteat, 1975: A Satellite Classification Technique for Subtropical Cyclones, NOAA Tech. Memo. NWS SR-83 National Weather Service, 25 pp.

Hope, John R., 1975: Atlantic Hurricane Season of 1974, Mon. Wea. Rev., 103, 285-293

Palmén, E. H., 1948: On the Formation and Structure of Tropical Hurricanes, Geophysical, 3, 26-38.

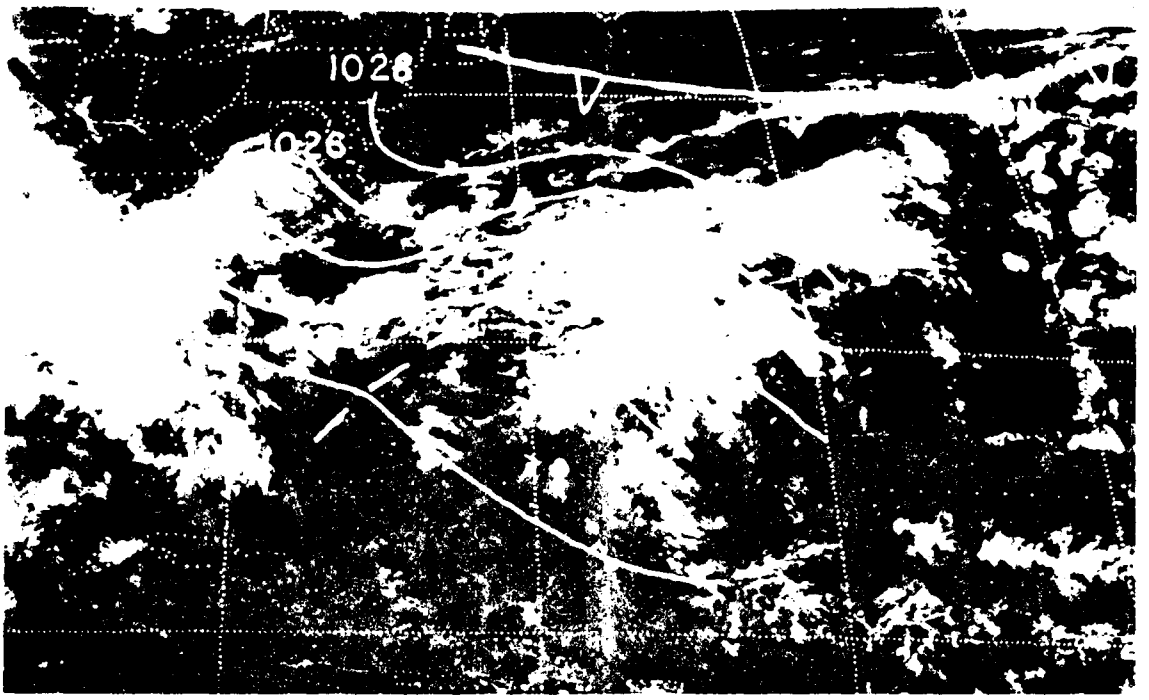

Figure 1. GOES-1 4 km VIS picture 11 Mar 77, 1501 GMT with 1500 GMT surface analysis.

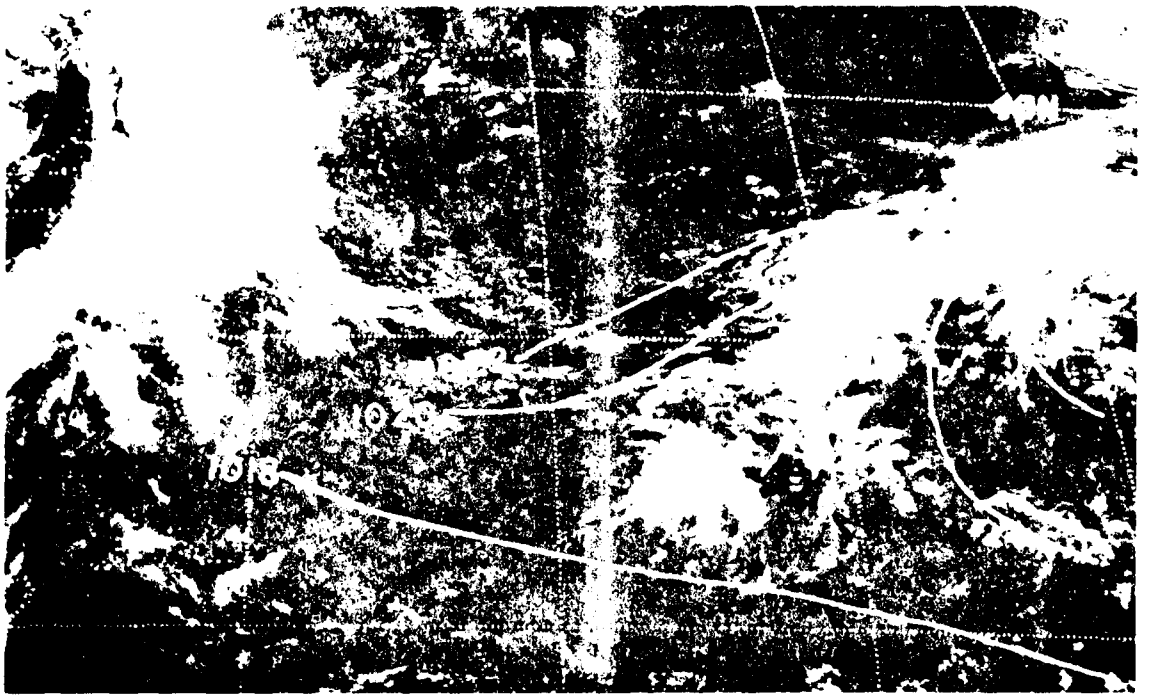

Figure 2. GOES-1 4 km VIS picture 12 Mar 77, 1501 GMT with 1800 GMT surface analysis

30°N
25°N

Figure 7. GOES-1 1 km VIS picture 15 Mar 77, 1331 GMT with 1200 GMT surface analysis.

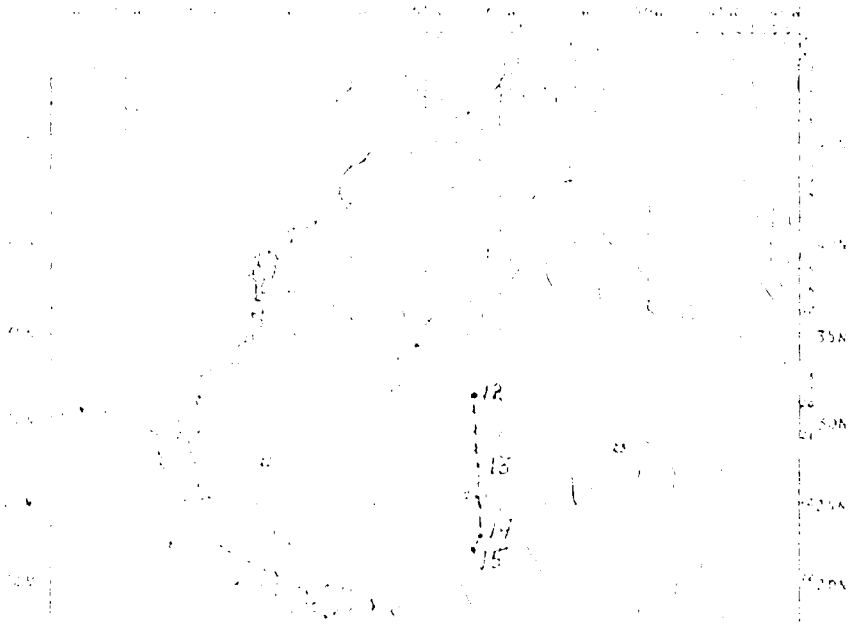

Figure 8. [illegible] derived sea surface temperatures for the week ending 16 Mar 77 with approximate 1500 GMT position of the cloud system for the period [illegible] Mar 77.

U. S. DEPARTMENT OF COMMERCE

National Weather Service/National Environmental Satellite Service
SATELLITE APPLICATIONS INFORMATION NOTE 77/11

AN EXAMPLE OF THE IMPORTANCE OF SUBSYNOPTIC FEATURES IN FORECASTING

Warren M. Wisner
Satellite Field Services Station, Anchorage, Alaska

The use of GOES/SMS-2 imagery in forecasting for the Alaska area got a big boost when the Synchronous Meteorological Satellite (SMS-2) was moved to 135W some 35,795 kilometers above the ocean. This satellite is orbiting eastward at the same rate as the earth's rotation giving it the appearance of being stationary over the same location on the ocean. Since the opening of the National Environmental Satellite Service's (NESS) field station in Anchorage in December, 1975, the use of the SMS-2 Infared (IR) data, which is received hourly, has become a major input for the locating and tracking of weather systems as they move towards the Alaska mainland. However, weak looking but potentially important short-wave or subsynoptic features are often overlooked by the forecasters as important weather producers. An example of this occurred on April 26 and 27, 1977.

The 0000 GMT Monday, April 26, 1977, 500mb analysis, Figure 1, shows a trough through western Alaska. The corresponding surface analysis, Figure 3, shows a weakening occluded front from a low in northeastern Alaska through Anchorage and Kodiak. The SMS-2 picture for about the same time shows the cloud pattern associated with this front, ABC on Figure 7. Note also at this time that a poorly organized system was located about 800 kilometers west of Washington state with clouds spreading northward to southern southeast Alaska.

Figures 8 and 9 show that the frontal clouds over the Gulf of Alaska dissipated as the front moved eastward. Also one can see on Figure 8 at 'D' what appears to be the start of a speed maximum coming into southwest Alaska. This speed maximum, DE on Figure 9, reaches the bottom of the trough aloft over Kodiak Island and from the conservation of vorticity laws, develops a weak vorticity comma 'D' on Figure 10. This vorticity comma moved eastward across the Gulf of Alaska with the 500mb trough, see Figures 2 and 12.

Meanwhile, the cloud system south of southeast Alaska first weakened and then with the approach of the vorticity comma, began to reintensify and move northward. This development reached its maximum when the vorticity comma reached the southeastern Alaska coast, Figure 13. The intensification of this system was missed by both the LFM and PE prog series and also by the guidience forecasters at WSFO Anchorage. The forecasts for southeast Alaska underplayed the precipitation and ended it too soon. The precipitation ended with the passage of the 500mb trough which could have been timed by using the speed of the vorticity comma which apparently was tied to the bottom of the trough.

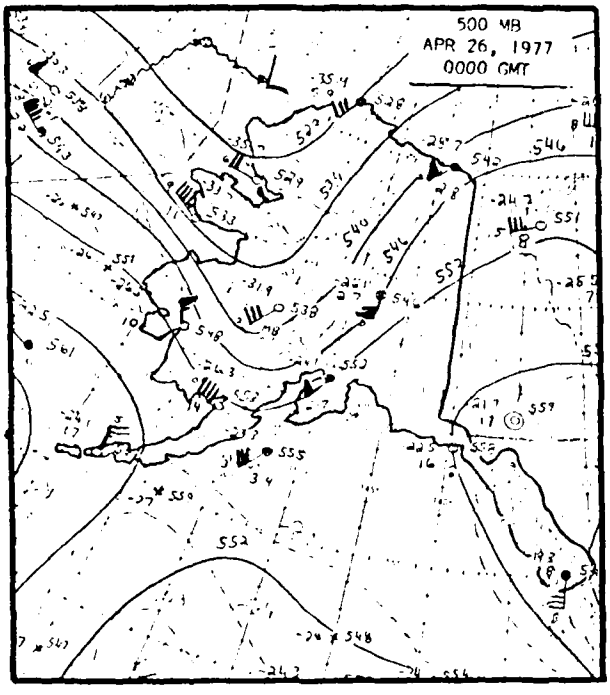

FIG. 1: 500mb ANALYSIS 0000 GMT

APRIL 26, 1977

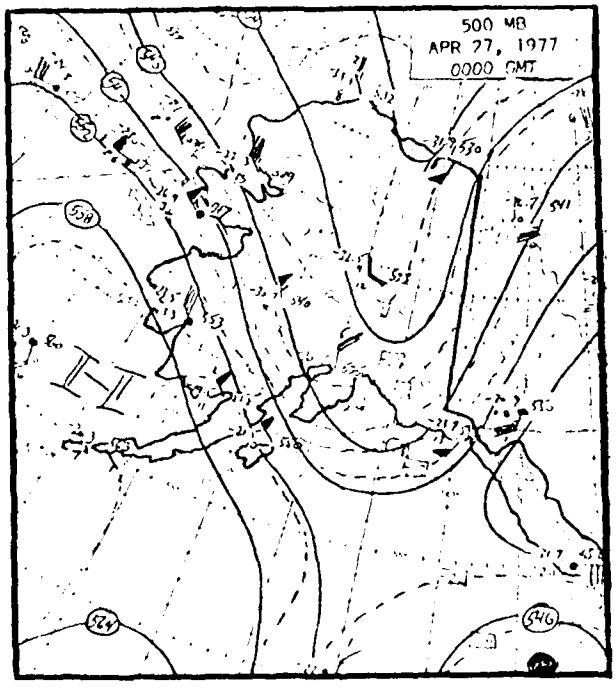

FIG. 2: 500mb ANALYSIS 0000 GMT

APRIL 27, 1977

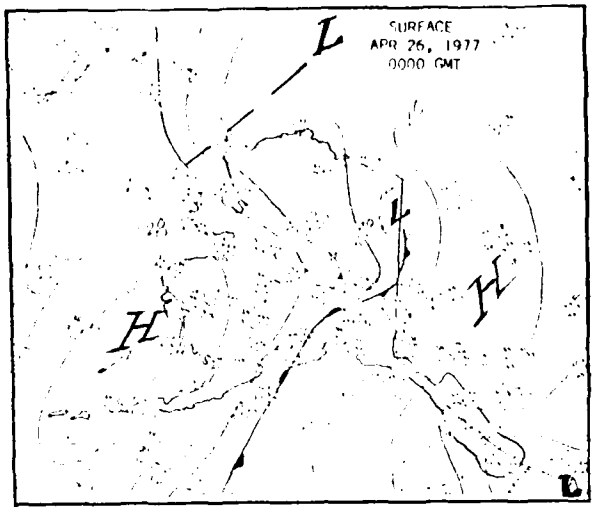

FIG. 3: SURFACE ANALYSIS 0000 GMT

APRIL 26, 1977

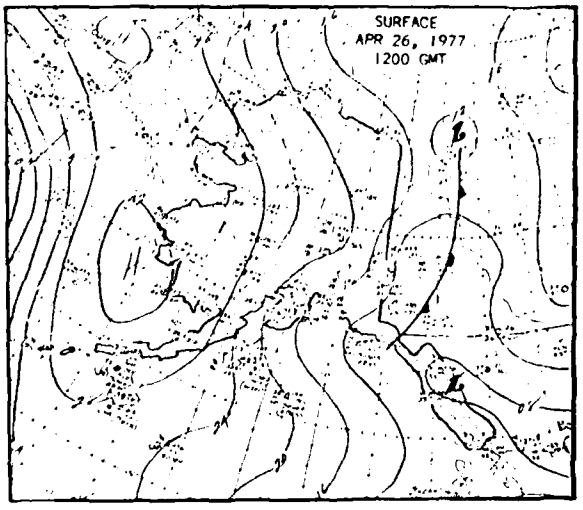

FIG. 4: SURFACE ANALYSIS 1200 GMT

APRIL 26, 1977

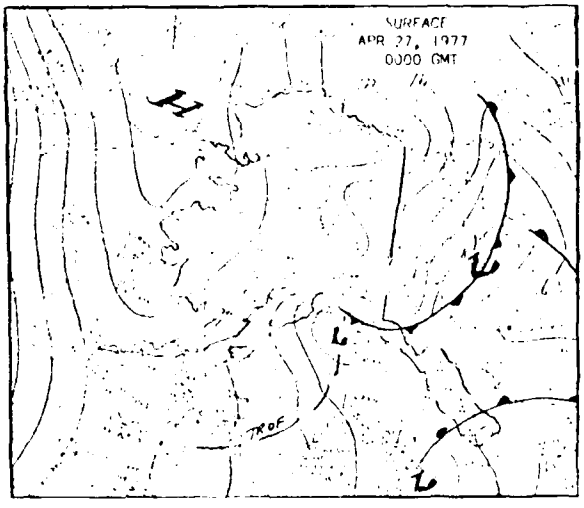

FIG. 5: SURFACE ANALYSIS 0000 GMT

APRIL 27, 1977

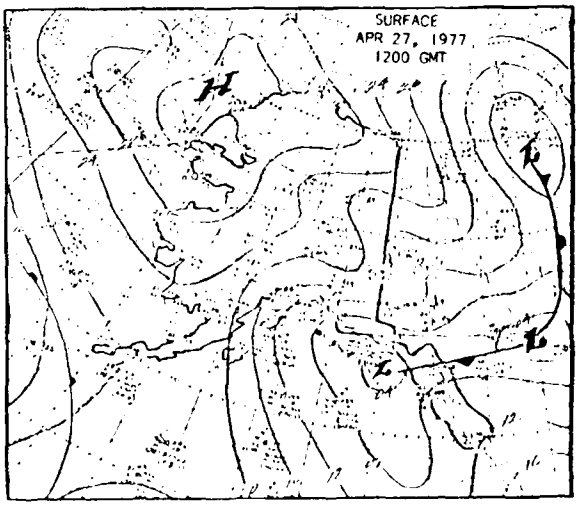

FIG. 6: SURFACE ANALYSIS 1200 GMT

APRIL 27, 1977

196

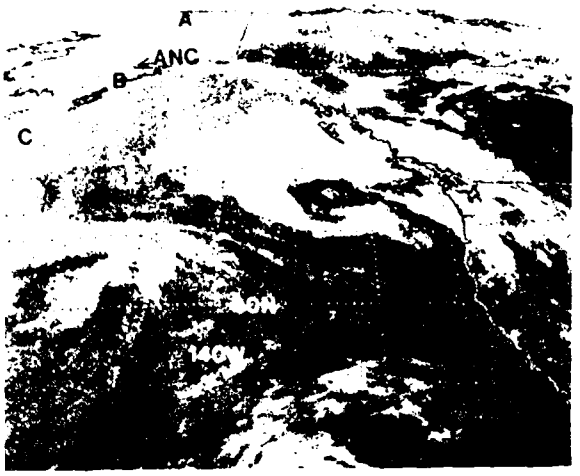

FIG. 7: SMS-2 IR (Z Curve) 0045 GMT

APR 26, 1977

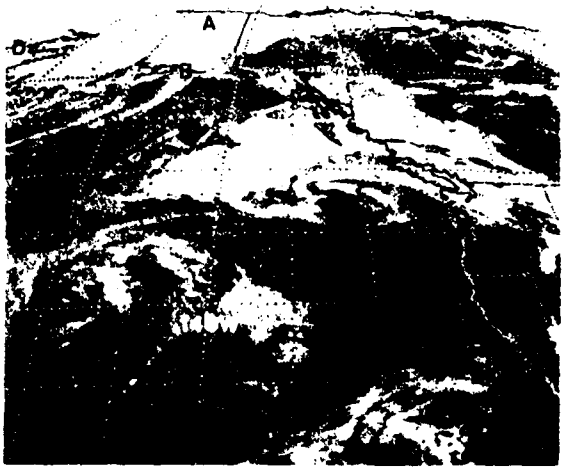

FIG. 8: SMS-2 IR (Z Curve) 0745 GMT

APR 26, 1977

FIG. 9: SMS-2 IR (Z Curve) 1145 GMT

APR 26, 1977

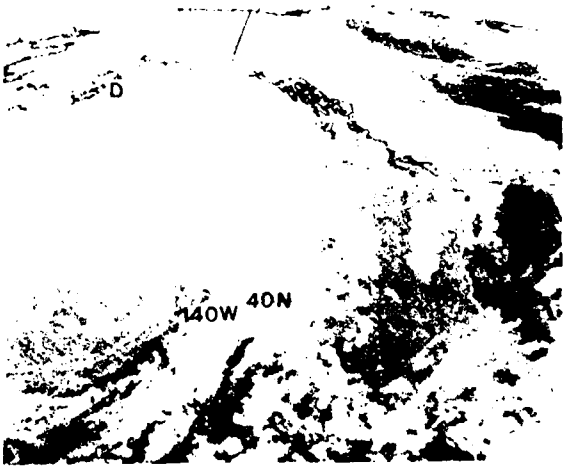

FIG. 10: SMS-2 IR (Z Curve) 1745 GMT

APR 26, 1977

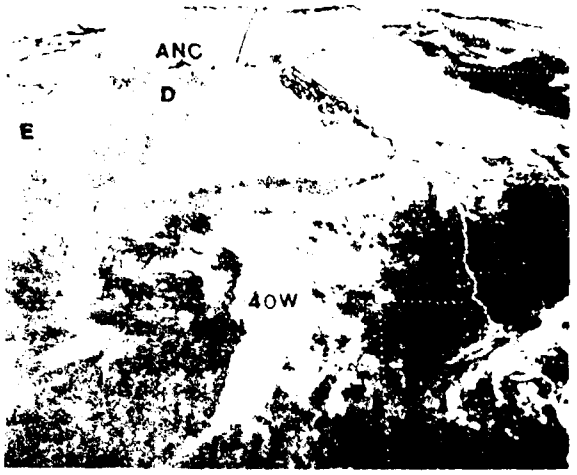

FIG. 11: SMS-2 IR (Z Curve) 2045 GMT

APR 27, 1977

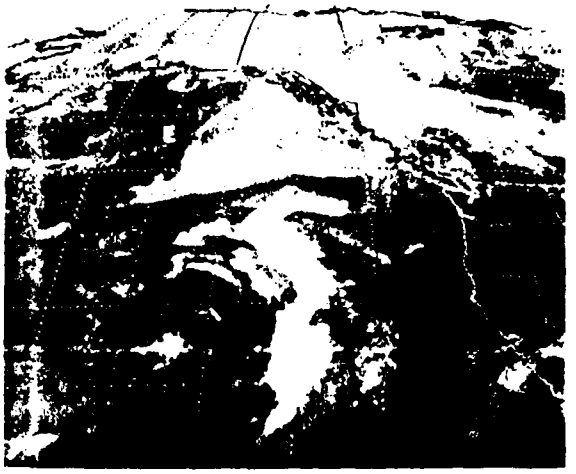

FIG 12: SMS-2 IR (Z Curve) 0045 GMT

APR 27, 1977

FIG. 13: SMS-2 IR (Z Curve) 1145 GMT

APR 27, 1977

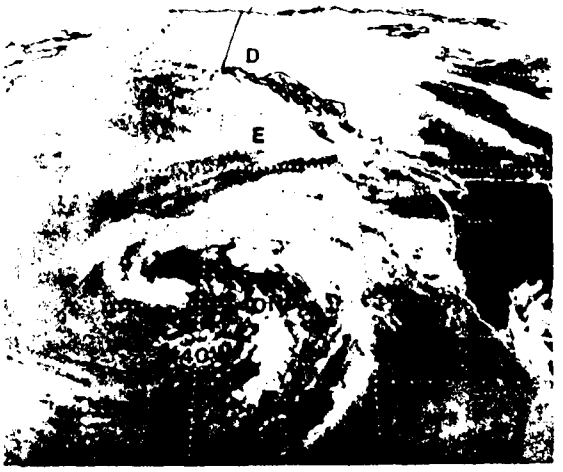

FIG. 14: SMS-2 IR (Z Curve) 1745 GMT

APR 27, 1977

U.S. DEPARTMENT OF COMMERCE

National Weather Service/National Environmental Satellite Service
SATELLITE APPLICATIONS INFORMATION NOTE 77/12

AN EARLY MORNING FOG BOUNDARY AND ITS EFFECTS ON AFTERNOON CONVECTION

Charles F. Burger
NESS/Applications Group
Washington, D.C.

The formation areas of afternoon convection are, in many cases, influenced by a variety of mesoscale features, such as differential heating, the sea breeze, and terrain. One such case occurred on 11 July 1977. The MOS thunderstorm forecast available that morning (Fig. 1) showed a broad region of 60 to 70 percent thunderstorm probabilities over Virginia, the Carolinas, and Georgia for the period from 1200 GMT 11 July to 1200 GMT 12 July 1977. An important task for the forecaster is the refinement of synoptic scale forecasts such as this through the specification of areas where convection is most likely to form and the direction that it is likely to move. This task can be aided by using satellite imagery for analysis and for delineating regions and boundaries that might contribute to convection.

The NMC surface analysis for 1200 GMT (Fig 2) shows a broad area of low stratus and fog in the region of 60 to 70 percent thunderstorm probabilities. Differential heating due to the fog can affect the formation of afternoon convection (Purdom and Gurka, 1974). The most likely formation area is on the clear side of tne fog boundary, and the least likely area is near the center of the fog region. It is therefore important to be able to analyze the fog boundary correctly. The 1230 GMT GOES-1, 2 km, visible imagery (Fig 3) reveals that the fog and stratus is separated into two distinct areas, which were not obvious on the surface chart (Fig 2). One area is located over central North Carolina (A), and the other area is located in the mountain valleys to the west (B). The 1200 GMT GOES-1, 2 km, IR (MB enhancement) imagery (Fig 4) shows low, warm cloud tops at A and B, indicating that high clouds are not covering the fog and stratus in these regions.

Fog and stratus on a scale the size of A (Fig 3) have been shown to correlate with the formation areas of afternoon convection. The patches of valley fog at B (Fig 3) cover much smaller areas, and their effect on convection is complex and localized.

A more detailed view of the fog and stratus at A can be seen in the 1300 GMT GOES-1, 1 km, visible imagery (Fig 5). The fog and stratus boundary is marked with arrows. By 1800 GMT, the GOES-1, 1 km, visible imagery (Fig 6) indicates that all of the convection is occurring on or outside this 1300 GMT boundary, which is shown as a dashed line. The first thunderstorms are developing at this time at C and D.

The thunderstorms at C are forming in a warm tongue and surface convergence region, as shown by the 1700 GMT surface temperature and surface streamline analysis (Figs 7 and 8). The dotted triangle is the region of storm development. The cooler air to the north of the triangle is a result of the morning fog. The cooler air to the east is probably caused by the sea breeze, which was easily detected on the GOES-1, 1 km, visible film loop and confirmed by the surface wind reports (Fig 8). The thunderstorms forming along the northwestern fog boundary (Fig 6, D) are located on the slopes of the Appalachian Mountains, thereby indicating terrain and differential heating effects.

The 1930 GMT GOES-1, 1 km, visible imagery (Fig 9) shows that the initial thunderstorms have moved northeastward from their original 1800 GMT positions at C and D, following closely the 1200 GMT, 700 mb flow. The thunderstorms are just starting to enter the region of morning fog. A new line of thunderstorms is beginning to form at E. This line is probably the result of a moisture maximum being advected onshore from near F and of peninsular convergence of the sea breeze at Cape Fear, which is just west of F.

The 2100 GMT GOES-1, 1 km, visible imagery (Fig 10) shows that the thunderstorms are continuing their northeastward movement. Clear, stable air still remains at this time near the center of the early morning fog and stratus region. (The 1300 GMT fog boundary is indicated by the white dashed line, and the 1630 GMT fog boundary by the black dashed line (Fig. 10). In this case, there is a definite relation between the duration of fog in a certain area and the probability of convection occurring in that same area later in the day.

Differential heating due to an area of morning fog had an effect on the formation areas of afternoon convection in this case. The sea breeze, terrain, and moisture maximum also influenced thunderstorm formation. Satellite imagery was used in this example as an aid for analysis and for pointing out regions and boundaries that might contribute to convection.

It is important to note that solar heating was the main driving force behind convection in this case, with the synoptic scale situation being of less importance. Our observations have shown that differential heating effects also contribute to the weather patterns and evolution in cases where the synoptic scale wind field is stronger. However, in those cases, the interactions between the large and small scales are complex and difficult to forecast correctly. Therefore, differential heating as a tool in forecasting thunderstorms is used most reliably when the sun's heating is the major factor in convective development.

REFERENCE

The Effect of Early Morning Cloud Cover on Afternoon Thunderstorm Development, James F. W. Purdom and James J. Gurka. Reprint Volume, Fifth Conference on Weather Forecasting and Analysis. March 4-7, 1974. Am. Meteo. Soc., Boston, Mass.

ACKNOWLEDGEMENTS

I would like to thank Roger Weldon of the NESS Applications Group for his help in writing this report.

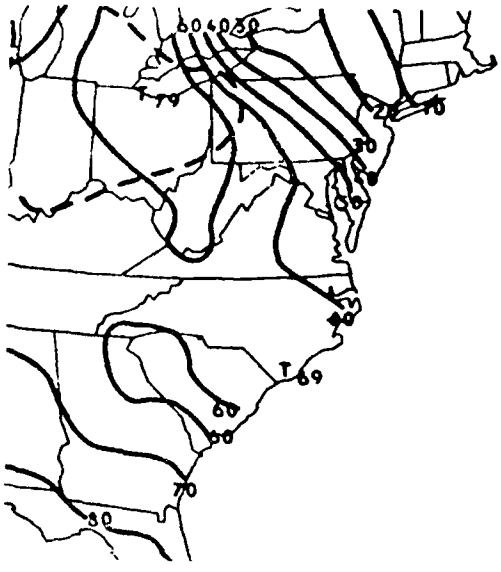

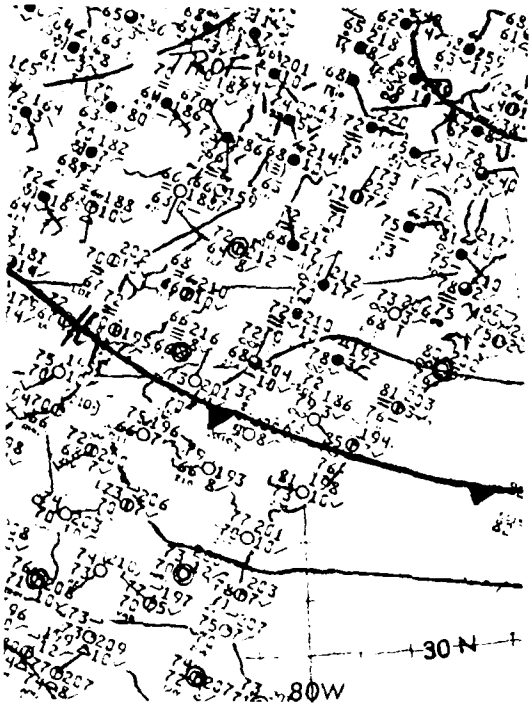
TROF
30 N
80W


35N
B
A

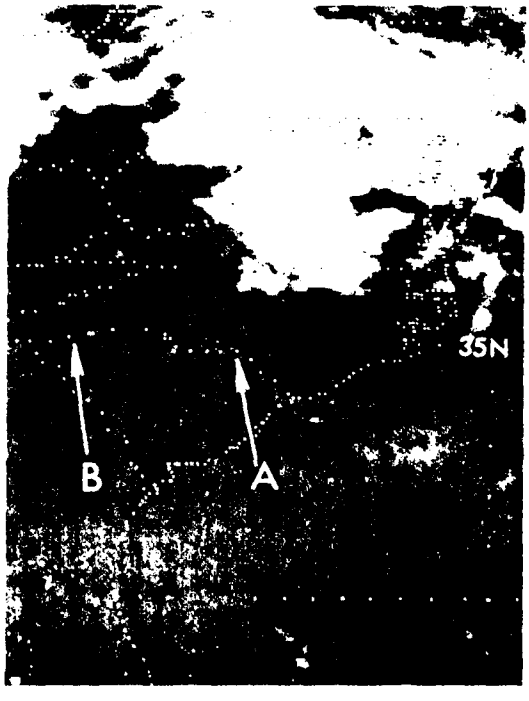
35N
B
A

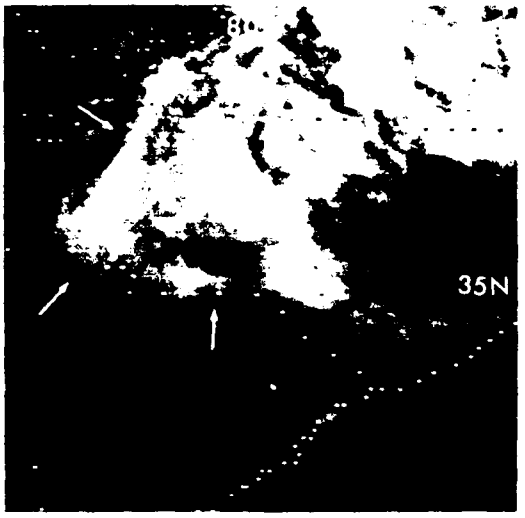

Fig 5. GOES-1 1 km Visible Imagery 1601 GMT 11 July 1977.

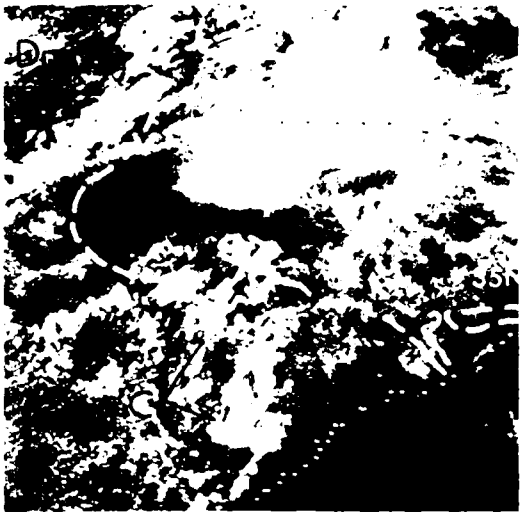

Fig 6. GOES-1 1 km Visible Imagery 1800 GMT 11 July 1977.

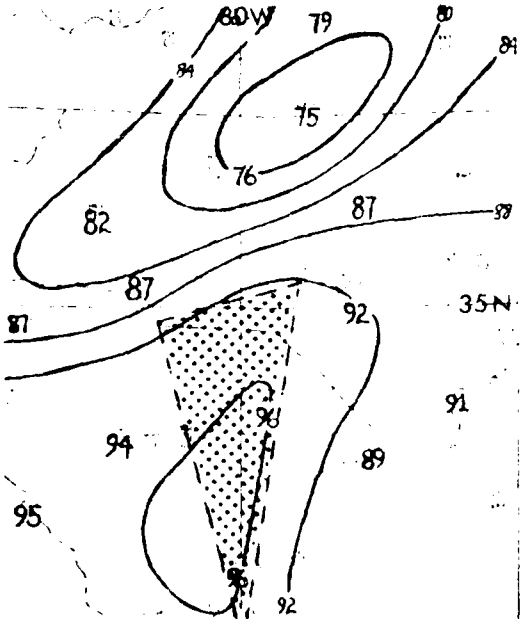

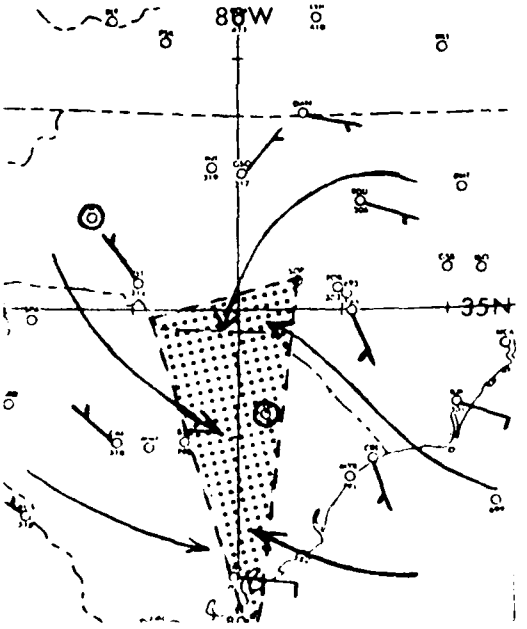

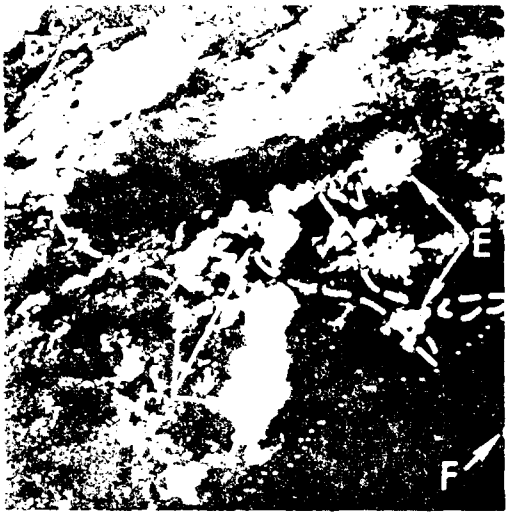
E
F

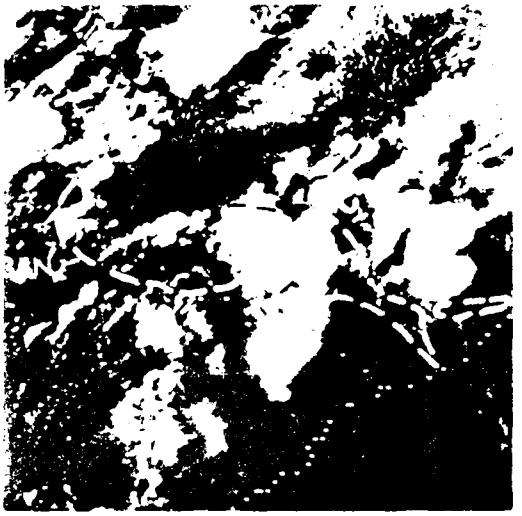

U.S. DEPARTMENT OF COMMERCE

National Weather Service/National Environmental Satellite Service
SATELLITE APPLICATIONS INFORMATION NOTE 77/13

USE OF THE TEMPERATURE GRAY SCALE IN ENHANCED INFRARED SATELLITE PICTURES

John P. Kearns
NESS, Satellite Field Services Station, Honolulu, Hawaii

All enhanced infrared (EIR) GOES pictures now display the "gray scale with temperature values." Thin vertical lines interrupt the gray scale at 10°C intervals and can be used in estimating the temperatures of cloud tops or surface features.

Since the enhancement "curves" (actually series of straight lines) are already provided in the GOES/SMS User's Guide, why the reduntant gray scale on each picture? Here are some reasons:

(1) Having the enhancement on the picture itself is a great convenience. Reference to an auxiliary chart should rarely be required once the user becomes accustomed to the gray scale.

(2) The mental gymnastics of attempting to visualize how dark or light a shade should be from its graphical value, and vice versa, are largely eliminated. One can see the gray shades on the gray scale and compare them directly with those on the picture.

(3) Because the gray scale is so narrow, several can be taped into an array on the same chart. Different enhancement schemes can be compared at a glance, facilitating the selection of an enhancement for a special sector.

(4) If, for any reason, an entire enhanced IR picture is produced darker or lighter than normal, the gray scale will be correspondingly darker or lighter also. Such variations in overall tone complicate the comparison of imagery with enhancement graphs, but with the gray scale these are automatically compensated for.

In short, the gray scale is analogous to the color code insert for topography found on many geographical maps. Unfortunately, however, the temperature marks on the scale are not labeled, and one must learn how to use them.

The temperature marking scale is fixed on all sectorized pictures regardless of the specific enhancement curve being used. The gray scales which are superimposed on the temperature scale vary according to the particular enhancement curve being used. Although figure 1 may be used as a reference, the following remarks apply to all sectorized pictures.

(1) The thin vertical lines are at intervals of ten degrees Celsius; warm on the left, cold on the right.

(2) The leftmost line is for +50°C. This line is usually found just

below and to the left of the time indicator group in the picture legend.

(3) In the picture legend, the fourth group is a five-digit numeral which (except for sectors entirely below 11°S) begins with a zero. The line for 0°C is below and just to the left of the first digit. Hence, zero for zero.

(4) Although the lines are all at 10°C temperature intervals, those on the left two-thirds of the scale are spaced twice as far apart as those on the right. The line for -30°C marks the change from wide to narrower spacing and may be used as a starting point for quick labeling of the colder temperature line.

(5) The far right line is for -100°C.

Enhancement functions portray a range of temperatures as either a constant or a linearly changing value. A constant value is depicted as a horizontal line in the graphs of the User's Guide and as a uniform tone in the gray scale. For example, with the CA enhancement (Figure 2), temperatures between -32.2°C and -41.2°C (Segment 4) are represented graphically as a line with constant count value of about 130 and as a block of medium gray in the scale. The next colder interval, from -42.2°C to -52.2°C (Segment 5), is another constant with a line on the graph at about 155 and a block of a lighter gray. Temperatures from +40.8°C to -0.8°, Segment 2, are rendered as a linearly changing variable, represented by a straight line with a fairly steep slope in the graph and on the gray scale by an apparent continuum from black to a nearly white going from left to right.

The conversions between graph and gray scale seem at first to be quite straightforward but this is not always the case. Our ability to depict and perceive temperature gradients by gray shade differences on a picture is dependent upon the following limitations:

(1) The number of gray shades that can be displayed on the picture.

(2) The ability of the human eye to perceive gray shade differences.

(3) The ability of the system to resolve temperature differences.

(4) The ability of the system to resolve horizontal distances.

In the examples shown here, there are 64 gray shades available to display the range from black to white. For most of us, our eyes can detect such differences quite well in the middle gray tones, but cannot detect the same amount of shade differences in the light or dark ends of the range. In the third CA segment (-0.8°C to -31.2°C), for example, the graph shows a more gradual change in brightness as temperatures decrease. The change in slope is not nearly as obvious from the gray scale alone. Further, for temperatures from around -20°C to the end of the segment, the gray scale appears to be nearly constantly bright. Our eyes (mine, at least) don't perceive small changes in bright tones.

Dark tones are also troublesome. The CA gray scale is apparently black until the temperature increases to about +30°C; however, the graph shows that the gray tones in this range are being lightened according to the fairly steep slope of Segment 2.

In practice, this means that features of about -25°C cannot be readily distinguished from those of about -30°C when CA is used. One would probably overestimate cloud top heights when they are at the warmer temperature since they are "just as white" as the higher clouds. Also, surfaces of +35°C would appear hotter than they are.

Effects of the first two limitations have been illustrated; now consider the third limitation. In Segment 8 of the CA graph, gray shades range from black to white over a temperature range of only 7.5 degrees C (from -63.2 degrees to -70.7 degrees). Note that this temperature change is displayed by a stepped pattern using only 8 of the 64 available gray shades. The reason is that, in this cold portion of the temperature range, the temperature resolution capability of the system is limited to about one degree C. Therefore, the number of gray shades used is limited by the number of temperature differences that the system can resolve, and a gradual change from black to white cannot be displayed.

For the CA Segment 8, the displayed gray tone changes from deepest black to brightest white as temperatures decrease from -63.2°C to -70.7°C. The almost vertical line of the graph appears as a series of narrow black, gray, and white stripes in the gray scale, where no artistic license is permitted. Very cold CB tops then have their bright white centers surrounded not by a ring smoothly from black to white, but a series of narrow gray bands.

When designing an enhancement, the use of line graphs is highly practical. The graph describes the numerical substitution process; but to see how the enhancement will be perceived in the imagery, one should also look at its gray scale presentation. To illustrate the differences between the enhancement as it is designed, and how it is seen in the picture, the dashed lines of figure 2 show how the CA graph would look if it were to be drawn from the appearance of its gray scale.

(1) Segments 4, 5, 6, 7, and 9 are constants and stay the same.

(2) Segment 1 is extended to +31.3°C (Segment 3A), reflecting the difficulty of discriminating the dark blacks and the brilliant whites.

(3) Since the change of gradient between Segments 2 and 3 is not noticed in the gray scale, a single sloping line from +31.3°C to -20°C is shown instead (Segment 2A).

(4) The discontinuous nature of Segment 8 is seen after it is drawn as 8A.

Note that a uniform temperature scale is used for the graph in figure 2. This is much more convenient for the user than having the temperature scale change abruptly at -30°C, as it does in the graphs in the User's Guide.

Before attempting to show how the gray scale can be applied in an example, a few cautionary statements for the use of complex enhancement curves should be mentioned.

(1) The ZA curve used for the full disk infrared (FDIR) is a simple enhancement where the rule "the brighter, the colder" holds. More complex enhancements, however, may have more than one temperature represented by a single gray shade. The sequence of tone from outside a cloud to the coldest part should be compared to the left-to-right sequence in the gray scale; otherwise, large errors can result.

(2) However, if the temperature changes rapidly in the horizontal, some intermediate shades from warm to cold may be skipped. Often these intermediate shades are seen in some directions but not others; e.g., frequently more are seen downwind from the coldest feature than in other directions. Before assigning a temperature to a feature the analyst should check the sequence of shades in several directions.

(3) A complex enhancement of an area should be compared with a simpler one, such as that for the FDIR.

In figure 3, an Eastern Pacific tropical disturbance which became Tropical Storm Ava, is seen with the CA enhancement. The coldest clouds here appear as mottled islands within a broad white river -- the cirriform outflow.

There is little difficulty assigning temperatures colder than -70°C (CA Segment 9) to the bright area (A) near the center of the picture and to another to the right (B). Neither is brighter than the white "river's edge" depicted by the cold end of Segment 3, but both are ringed by dark gray (Segment 6) and black (Segment 7). The narrow gray rings of the very steep Segment 8 may be seen just inside the black.

The cold area, C, has tops colder than -70°C also. But here, especially to the north, several of the shades between Segments 3 and 9 are skipped. This is an effect of the fourth limitation listed previously; the temperature change in the atmosphere occurs over a distance which is too small to be resolved by the system. We can see the proper sequence of shades somewhat better to the south and southeast of the center than in other directions.

In examples marked D, no trace of the dark gray of Segment 6 nor the black of Segment 7 is evident, so we can assign temperatures warmer than -31.2°C to the white centers.

We continue to compare the picture with the gray scale and label figure 3 according to the segments of the CA enhancement, or if we wished, by the approximate temperatures of the cloud tops themselves. With practice, the process of comparing picture tones and gray scale tones becomes both easy and fast. The user should find it a much more comfortable task than using the enhancement graphs, although reference to the graph may occasionally be quite helpful.

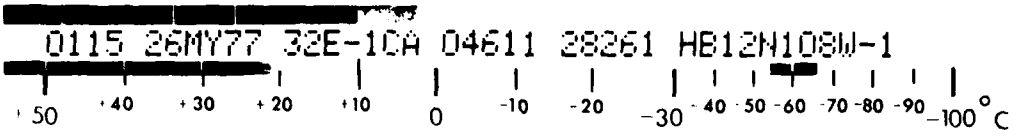

Figure 1. Gray scale for CA enhancement, with temperature marks labeled.

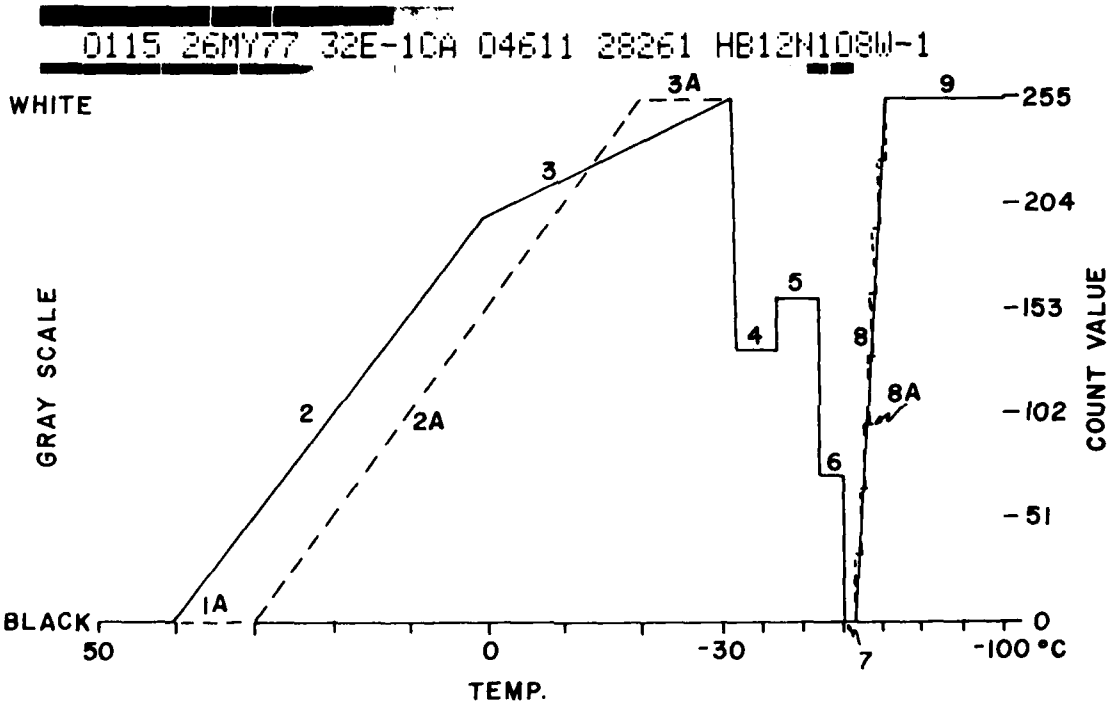

Figure 2. Gray scale and corresponding graph for CA enhancement. Solid lines are the graph as originally designed and shown in the User's Guide. Dashed lines are the changes if the graph were derived from appearance of the gray scale.

2/c

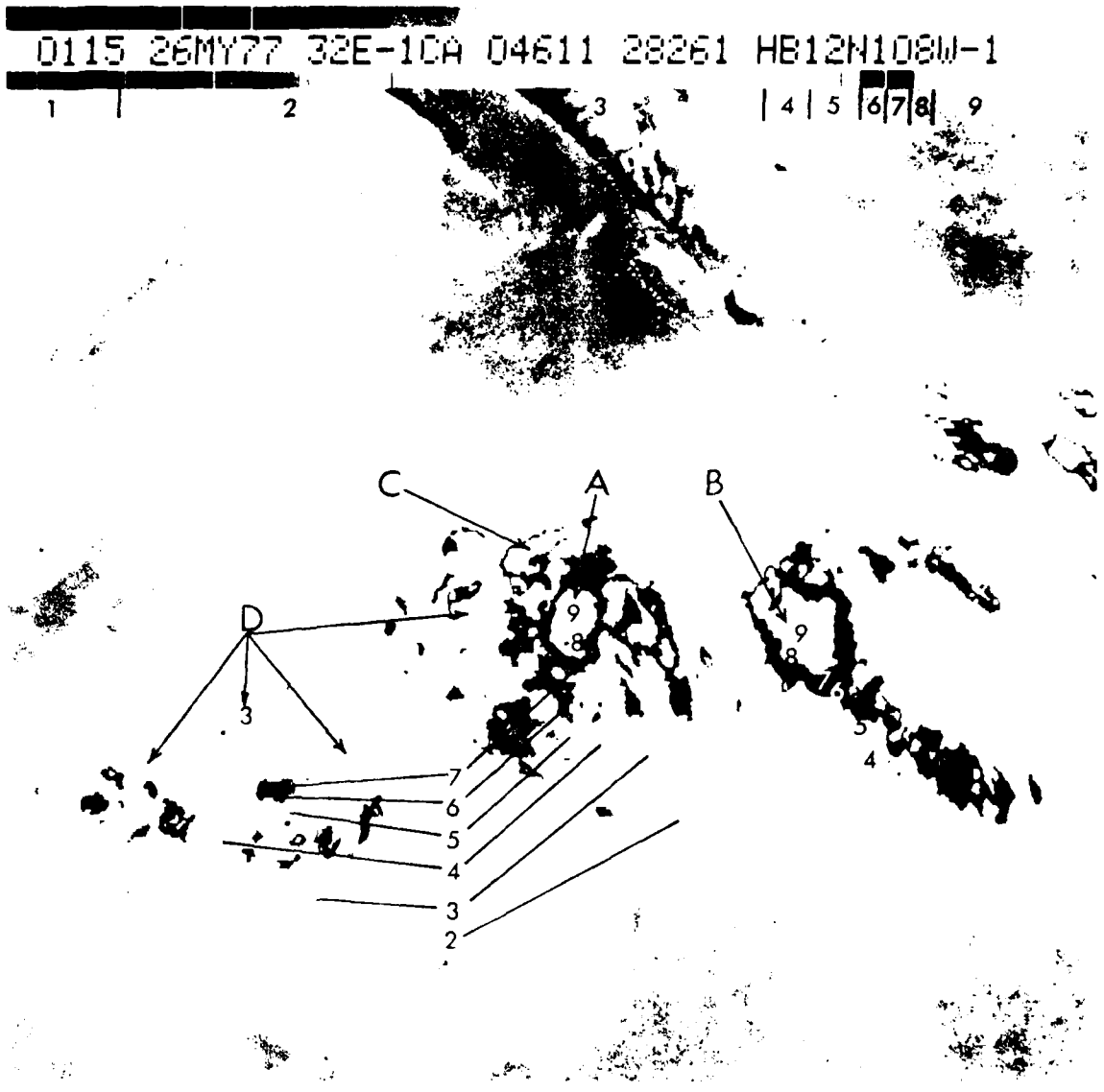

Figure 5. B-scale picture with CA enhancement showing tropical systems southwest of Mexico, 26, May 19[illegible].

U.S. DEPARTMENT OF COMMERCE

National Weather Service/National Environmental Satellite Service
SATELLITE APPLICATIONS INFORMATION NOTE 77/14

LOW-LEVEL WIND INFORMATION DERIVED FROM HIGH RESOLUTION SATELLITE IMAGERY

Carl E. Weiss
Applications Group
NESS/Washington, D. C.

Many mesoscale surface weather systems go virtually undetected in the operational surface observation network. Detailed analysis of the low-level wind field associated with the sea breeze, for example, is difficult unless the surface data coverage can be somehow augmented. By observing the distribution of cumulus clouds over an area with SMS high resolution (1 km) visible imagery, much low-level wind information can be inferred. The weather situation over the Chesapeake Bay area on 22 May 1977 shows how satellite imagery can be used to help bridge surface data gaps.

At 1500 GMT, the surface ridge line was analyzed to extend from the Atlantic Ocean southwestward over the Delmarva Peninsula into Virginia and North Carolina (Figure 1). 1400 GMT surface reports around the Chesapeake Bay area (Figure 2) show the anticyclonic wind flow associated with the ridge. Winds over the extreme southern Bay were generally east-northeasterly between five and ten knots. Near the Potomac River and Washington, D.C. the winds turned more southerly averaging about five knots. From Baltimore northward and eastward, winds were mostly south-westerly at five knots. Notice the gaps in the data along both shores of the Bay, the Atlantic coast of the Delmarva Peninsula and eastern Virginia from the Potomac River southward to near Norfolk.

The 1400 GMT 1 km visible picture (Figure 3) shows the effect of land and water surfaces on the distribution of cumulus. The cool Bay and rivers inhibited the formation of cumulus, thus the skies over these areas remained generally cloud-free. Cumulus developed over the adjacent land areas in response to the strong solar heating.

A closer examination of the cumulus pattern in Figure 3 reveals the details of the local low-level wind flow. For example, the edge of the clear skies (A to A'), along the western shore of the Bay, is located inland. This clearing edge marked the boundary of the cooler, more stable onshore flow of Bay air. What little cumulus (B) can be seen near the eastern Bay shore was located over the shoreline. Thus, this cumulus distribution indicated that there was little or no onshore flow along the eastern Bay shore.

Clear skies (C to C') can also be seen along the Atlantic coast of the Delmarva Peninsula. Here, the prevailing southeasterly flow coupled with the sea breeze has spread ocean air over the adjacent shore and prevented cumulus formation. To the north, near the shore of Delaware Bay, the clearing edge at (C'') was located closer to the water than farther south over the Atlantic coast at (C) or (C'). This pattern arose because southeast winds were more closely parallel to the shoreline of Delaware Bay than along the Atlantic coast and thus, they were not as efficient in advecting the clear, cooler, and more stable Atlantic air inland.

The influence of the cool river waters on cumulus formation is evident by the bands of clear skies (D) located along the rivers in eastern Virginia. The clearing extended over the southern and western banks of the rivers while the cumulus over land persisted to the water's edge along the northern and eastern river banks. The alternating pattern of clear and cloudy skies near these rivers suggested that the onshore flow associated with each river was displaced downwind (to the west) by the easterly and southeasterly prevailing winds. The cumulus field near the Potomac River, south of Washington, D. C., also appeared affected by the southeasterly wind flow. Here, clear skies (E) from over the river had spread northwestward over the western bank in response to the low-level southeasterlies. Farther north, the cumulus (F) was aligned in north-south cloud streets indicating a more southerly low-level wind flow.

The 1600 GMT Chesapeake Bay surface map (Figure 4) shows little change over the Middle Atlantic States. Winds over most of Maryland, Delaware, and eastern Virginia were generally southeasterly at five to ten knots. Over New Jersey, the winds continued south and southwesterly at five to ten knots.

The effects of subsidence on the dissipation of cumulus is apparent from the 1600 GMT 1 km visible picture (Figure 5). Skies had cleared over most of central Maryland and east-central Virginia (G to G'). The edge of the Chesapeake Bay breeze had all but disappeared from view along the western Bay shore. A small enhanced band of cumulus (A) was the only trace of the Bay breeze boundary left at this time.

Over the Atlantic coast of the Delmarva Peninsula, skies remained cloud-free (C) as the southeasterly flow of cool, stable ocean air continued to prevent cumulus growth. The clear skies associated with the rivers in eastern Virginia (D) continued along the western banks.

Many details concerning the low-level wind field can be identified by the cumulus distribution as seen in high resolution SMS visible imagery. Various wind directions produce these distinct and repetitive cloud patterns that forecasters might find particularly useful for short-range forecasting. This information can also supplement existing surface observations to aid in analyzing many mesoscale weather systems.

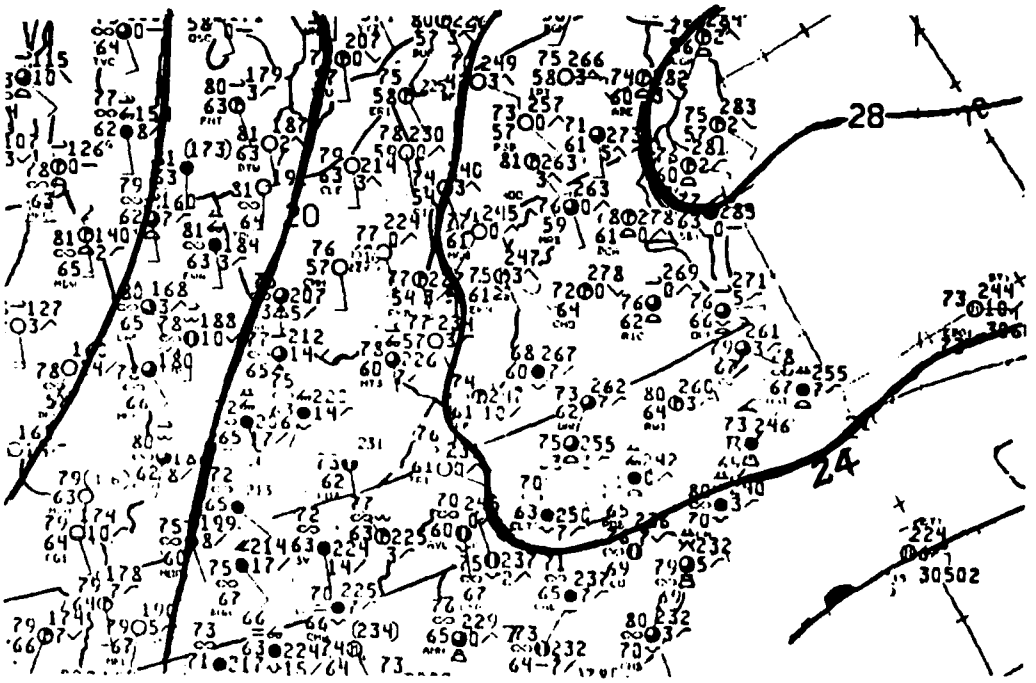

Fig 1. NMC Surface Analysis, 1500 GMT, 22 May 1977.

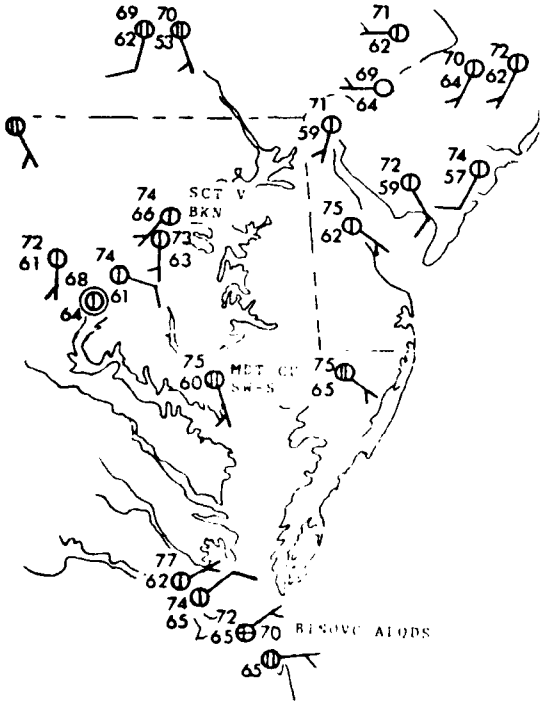

Fig 2. Chesapeake Bay Surface Map, 1400 GMT, 22 May 1977.

Fig 3. GOES-1 1-km Visible Imagery, 1400 GMT, 22 May 1977.

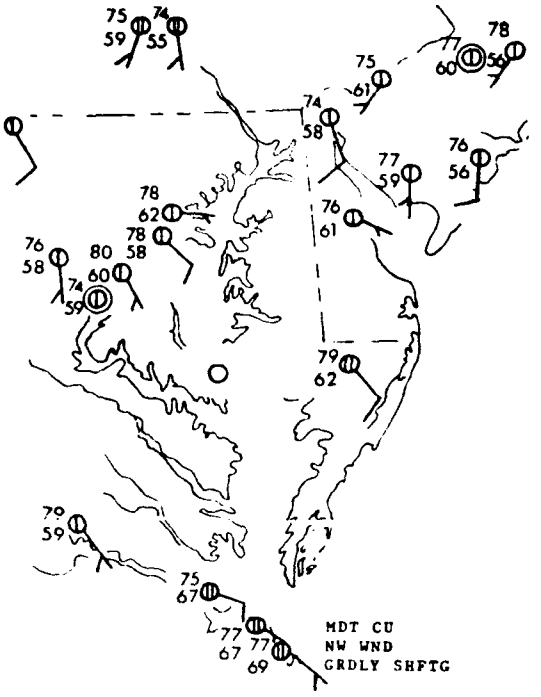

Fig 4. Chesapeake Bay Surface Map, 1600 GMT, 22 May 1977.

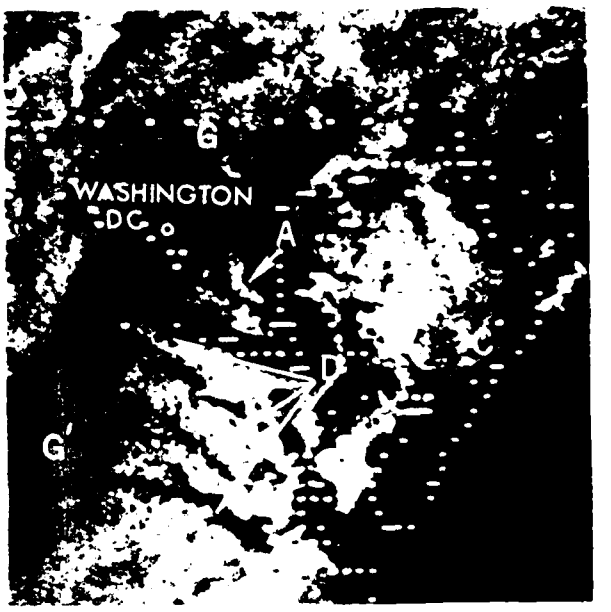

Fig 5. GOES-1 1-km Visible Imagery, 1600 GMT, 22 May 1977.

U.S. DEPARTMENT OF COMMERCE

National Weather Service/National Environmental Satellite Service
SATELLITE APPLICATIONS INFORMATION NOTE 77/15

DELINEATING HAZE AND POLLUTION BOUNDARIES FROM SATELLITE DATA

Frances C. Parmenter
NESS, Applications Group, Washington, D.C.

During the spring, summer, and fall of the year, the large-scale circulation establishes synoptic conditions resulting in prolonged air stagnation in the eastern United States. This usually occurs when the westerlies reside in Canada, a west coast upper-level trough extends to low latitudes (over Baja), and a large and deep anticyclone covers the eastern two-thirds of the country. At the surface, the winds are usually light and variable except in the areas affected by local circulations such as the sea and lake breezes. Strong subsidence traps particulates in the lower atmosphere resulting in reduced horizontal and vertical visibilities that are a concern to aviation and marine activities. Likewise, photochemical activity, under poor ventilation, can create hazardous air quality conditions requiring the issuance of air pollution advisories and alerts for the public agriculture interests.

Recent articles (Ernst 1975, Parmenter 1976, 1977) have addressed the subject of haze and pollution. Generally, haze or suspended particulate matter appears as a milky gray area, or band, in the visible satellite data. It is most apparent in the early morning and late afternoon imagery when the sun is low on the horizon and scattering is at a maximum. As the air mass over an area becomes more moist, the hazy areas appear increasingly lighter (whiter) in tone in the satellite data. This is due to the growth of particulates due to the presence of water droplets. This process in turn increases the albedo of the air mass being considered. From the ground, an observer would note a more turbid or increasingly whiter appearance to the sky.

Not all the haze seen in satellite data is surfaced-based. Thus, one may not find evidence of restricted horizontal surface visibilities in conventional synoptic reports. The haze layer can be sandwiched between a surface-based inversion and the upper-level subsidence inversion. This, for instance, is the mechanism by which Saharan dust is transported across the vast distance of the Atlantic to the Antilles (Prospero and Nees 1977). Presence of the haze layer aloft does, however, reduce the incoming solar radiation during the day and affect the outgoing long wave radiation at night. Usually, as the haze over an area becomes thicker, daytime maximum temperatures will peak and then level out or decrease and nighttime minimums will be subsequently warmer as this condition continues. When the haze is ground-based, it also serves as a vehicle for the formation of shallow ground fogs that look like haze in the imagery.

Narrow haze bands often are the remnants of fronts that no longer carry recognizable weather, temperature, or wind discontinuities at the surface, and thus, do not appear on analyzed maps. Residual atmospheric moisture and particulate matter, however, are conservative and continue to be recognizable features in the satellite data. These bands can also mark the ridgeline where the greatest subsidence and calmest winds are observed.

Figure 1a, an early morning visible picture, taken 15 June 1977, shows such a band of haze extending from the cloudiness at (E), across Florida to (F), then becoming broader as it swings northwestward towards Louisiana (G). This picture is repeated with a new, experimental visible enhancement curve* in Figure 1b. The haze is now more detectable, especially in the Gulf of Mexico. This air mass appears brightest near (E) where abundant moisture is present along the edge of the frontal cloud band. Note the increased brightness of this moist and hazy band as it crosses over the brighter land of the Florida peninsula between Cape Canaveral (H) and Ft. Meyer (H'). Surface reports (Figure 2) indicated haze and light fog in this area. Continuing westward, this enhanced visible display brings out the details in the terminator zone of the image. Although clouds obscure some of the view, one can see that the hazy air mass (G), Figure 1b, was being advected onshore around the back side of the ridge.

Differential heating resulting from early morning cloud cover or sea and lake breeze circulations is a well established principle. Haze and moisture bands, such as Figures 1a and 1b, are also important for the formation and distribution of general afternoon convection. This can be seen over Florida, Figure 1c. Dashed lines outline the early morning haze area from Figures 1a and 1b. Note that convection has developed north and south of this zone.

Data taken on 31 July 1977 shows a large, amorphous haze area off the northeastern and mid-Atlantic coast (Figure 3a). Variations within this air mass are best viewed in the enhanced display, Figure 3b. Note that the heaviest concentrations over the water curl from off the Massachusetts coast (A) westward to the Delmarva Peninsula (B), then southeastward toward (C) about a dissipating cloud system at (D). Relatively clear areas (darkest spots) can be noted off the New Hampshire coast (E), the tip of Long Island (F), and in the subsidence zone (G) around the system (D). Note the very bright appearance to the land areas of New Jersey, Delmarva Peninsula, and portions of Maryland, Virginia and North Carolina (H), Figure 3b. (Clouds in this enhanced display are dark gray.) Light winds and light fog or haze were reported throughout this near coastal area (Figure 4). Later on this day (not shown), thunderstorms formed south and west of the dashed line extending inland from (C), Figure 3b; thick fog and stratus formed in the hazy air about (A), Figure 3a, by 2030 GMT.

*The operational gray scale and experimental enhanced visible gray appear alongside of Figure 1. Normal display is black (0 counts) to white (256 counts). The experimental display alternates gray shades for land and cloud brightness.

Recapping the points discussed above, the analyst should keep in mind the following:

1. Areas of haze, smog, pollution, clear-sky moisture maximums, and light fog are best seen in early morning and late afternoon visible satellite pictures.

2. Narrow bands of haze may mark frontal zones and/or surface ridges.

3. Large areas of particulate matter usually portray the general haziness associated with stagnant conditions under a ridge; localized clearings may occur with mesoscale systems.

4. Forecasters should be aware that:

a. Satellite data can provide information about improving or deteriorating air quality, moisture influxes, and reduced visibilities.

b. The obscurations and reduced visibilities suggested by the satellite data may reside entirely aloft and not be reported at the surface.

c. Light fog frequently forms during the night, over land, under hazy skies.

d. Thick fog and stratus frequently forms, at any time, over large cool water bodies (e.g., Atlantic, Great Lakes) in such an air mass.

e. This hazy air mass affects maximum and minimum temperatures.

f. Afternoon thunderstorm activity may form along the edge and outside of the haze areas.

REFERENCES

Ernst, J. A., 1975: A Different Prospective Reveals Air Pollution. Weatherwise, V 28, pp 215-216.

Parmenter, F. C., 1976: Effect of the Great Lakes on Weather in the Surrounding States. Preprint: Sixth Conference on Weather Forecasting and Analysis, American Meteorological Society, Boston, Mass., pp 246-251.

Parmenter, F. C., 1977: Monitoring Air Quality from Satellites. Monthly Weather Review, V 105, pp 789-792.

Prospero, Joseph M. and Ruby T. Nees, 1977: Dust Concentration in the Atmosphere of the Equatorial North Atlantic: Possible Relationship to Sahelian Drought. Science, V 196, pp 1196-1198.

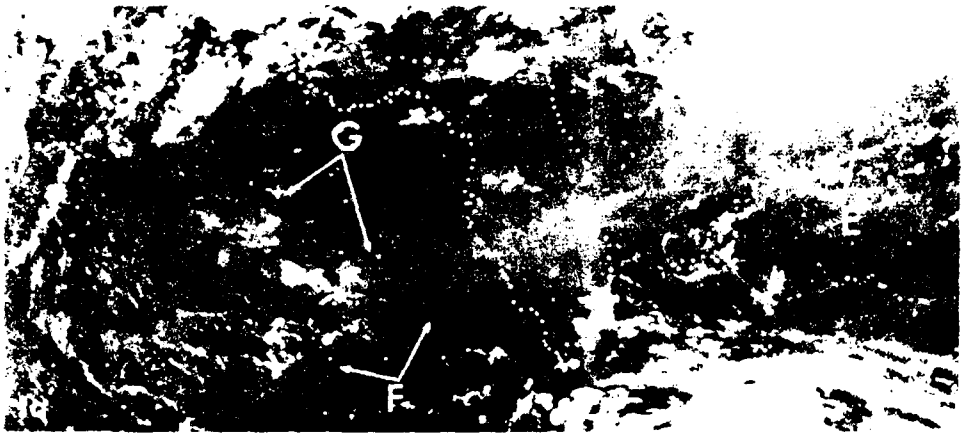

Fig 1a. GOES-1 visible data (2 km) 1230 GMT, 15 Jun 77.

Fig 1b. Same as Fig 1a with an experimental enhancement display.

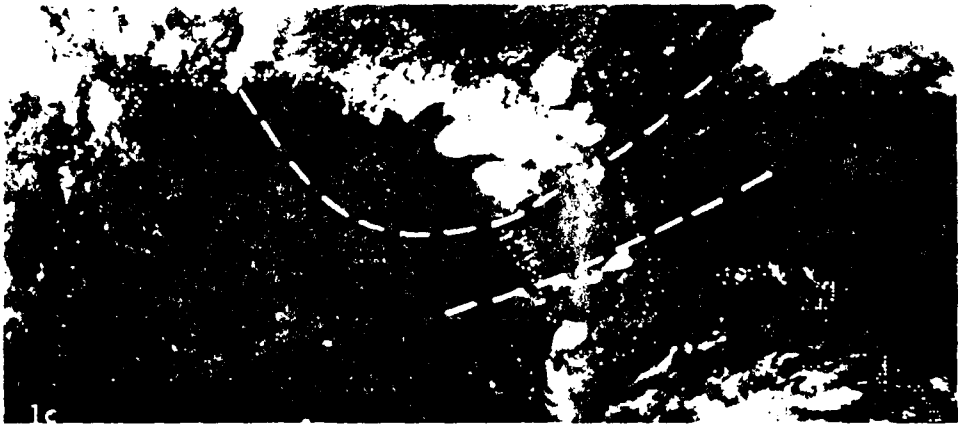

Fig 1c. GOES-1 visible data (2 km) 2030 GMT, 15 Jun 77; dashed line = morning haze boundary.

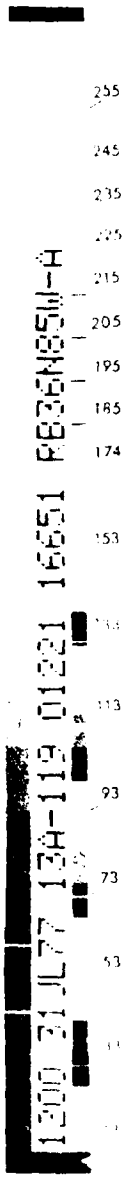

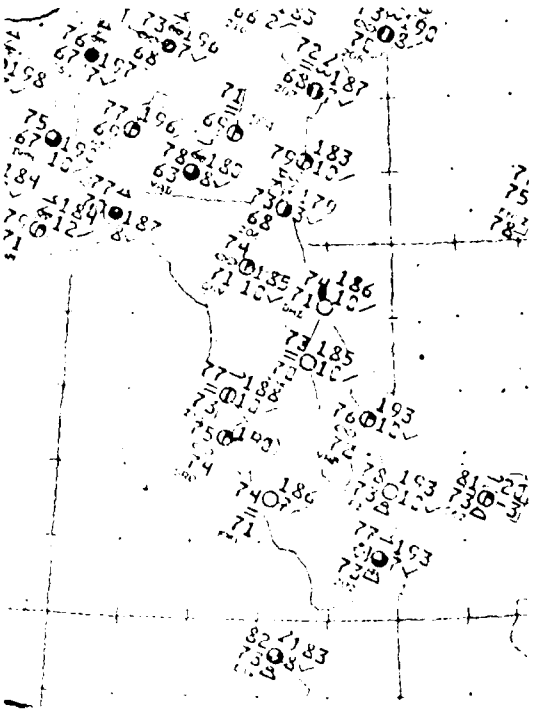

Fig 2. Surface analysis for 1200 GMT, 15 Jun 77.

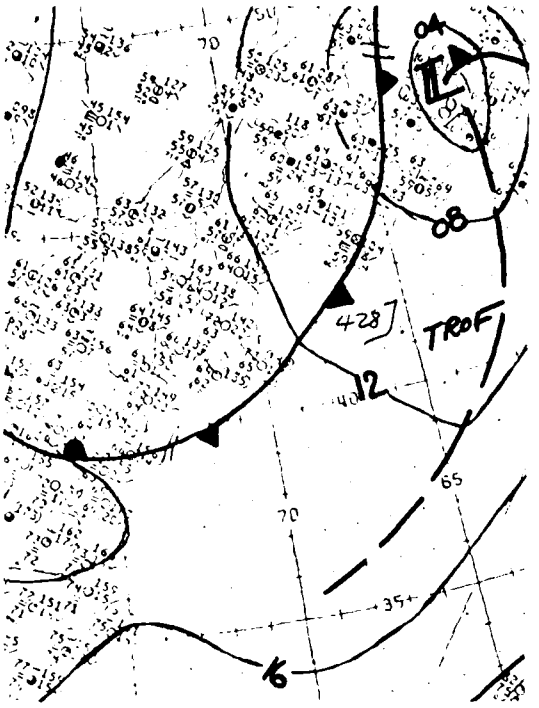

Fig 4. Surface analysis 1200 GMT, 31 Jul 77.

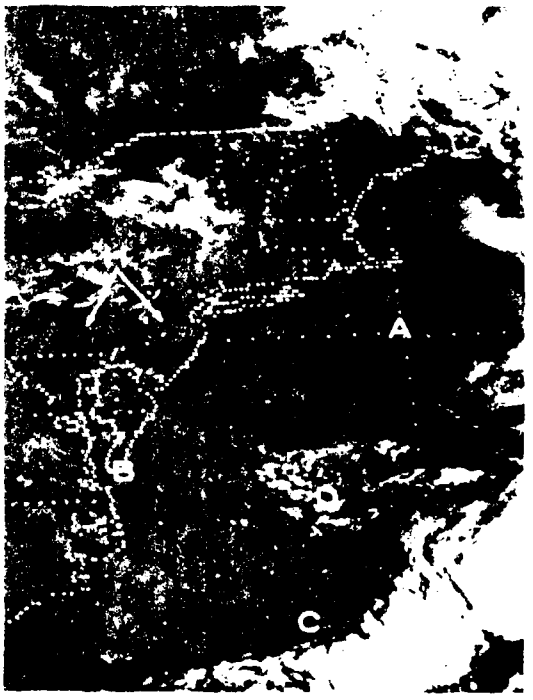

Fig 3a. GOES I visible data (2 km) 1730 GMT, 31 Jul 77.

Fig 3b. Same as Fig 3a with experimental enhancement.

U.S. DEPARTMENT OF COMMERCE

National Weather Service/National Environmental Satellite Service
SATELLITE APPLICATIONS INFORMATION NOTE 77/16

A MIDDLE TROPOSPHERIC TROPICAL CIRCULATION DEFINED BY SATELLITE OBSERVATIONS

Donald C. Gaby and Gregory C. McLaughlin
Satellite Field Services Station, Miami, Fla.

Meteorologists working in tropical latitudes commonly recognize two distinct and essentially independent flow fields in the lower and upper troposphere with a transition zone between. At the National Hurricane Center (NHC) the lower tropospheric flow is usually depicted by the Analysis Tropical Oceanic Lower Layer (ATOLL) which includes rawins, ship winds, and satellite-derived low-level winds. The upper tropospheric flow is depicted by the NHC's 200-mb analysis which includes rawins, aircraft winds, and satellite-derived cirrus-level winds. Both of these analyses have been automated to provide objective, computer-drawn streamlines and isotachs. Since the advent of jet aircraft, pilot reports at middle levels such as the 700-mb level have become rare and the 700-mb chart is not commonly analyzed over the open ocean. However, closed circulations frequently occur in the basic easterly flow at these levels and are generally only well depicted by satellite observations. Since such circulations may develop into hurricanes, they are closely monitored by the Miami SFSS and the NHC. This paper will present an example of such a circulation as seen on 3 August 1977. It was the 25th tropical system (easterly wave) of the season and passed off the African coast south of Dakar three days before at the end of July.

Figure 1 shows a 1-km resolution VIS sector of the system at 1300 GMT 3 August 1977 with the small cross at 11.3N 33.8W marking the center of the middle-level circulation. We see mostly low cumulus clouds in the north quadrants with some convection in the central mass and in the ITCZ along the south edge. The central convection probably does not extend to very high altitudes. Figure 2 shows a portion of the 8-km resolution FDIR image at the same time depicting the area from Africa to the Lesser Antilles. The irregular box includes the area shown in the 1-km VIS sector. The general cloud structure suggests a circulation, but the meteorologist is hard pressed to locate it precisely or establish the level of circulation. A short movie loop was produced from the high-resolution visible sectors covering the period 1300 to 1529 GMT to aid in the analysis.

Figure 3 shows a portion of the NHC's 200-mb analysis to match the area shown in Figure 2. For clarity, some arrowheads have been added to the streamlines. Again the irregular box includes the area shown in the 1-km VIS sector. Although there were no wind observations in the area of interest, the analysis is generally well defined by surrounding observations and is consistent with earlier analyses. The 13 bold wind vectors plotted without heads were extracted from the movie loop and are believed to represent winds near the 700-mb level defining a center of circulation marked by the letter C. Note the unbroken

high-level east or northeasterly flow across this middle-level circulation. (The absence of cirrus-level satellite-derived winds is doubtless due to the fact that no clouds extended to the necessary height.)

Figure 4 shows a portion of the NHC's ATOLL analysis to match the area shown in Figure 2, and the irregular box includes the area shown in the 1-km VIS sector. The numerous wind vectors shown with triangular heads pointing down are as derived by satellite using the "picture pair" technique. They are objectively extracted by computer using the measurement of cloud-top temperature to determine the level desired, which in this case is near 900 mb. The computer-drawn streamlines fit all of the observations well and are very close to what a human analyst might have drawn. The six bold wind vectors plotted without heads are part of those extracted from the movie loop and believed to represent winds near the 700-mb level defining a center of circulation marked by the letter C. Note especially that, whereas the lower level flow is unbroken northeasterly, the middle level circulation is clearly defined by the movie loop winds to lie above it.

Figure 5 shows a composite of the flows at the lower, middle (actually the upper part of the lower troposphere), and upper tropospheric levels. Unfortunately, this circulation near 700 mb is not depicted on any of the standard analysis charts, even though it holds the greatest interest for the forecaster. There are at least two solutions to this deficiency. One might be to reinstate the 700-mb analysis as a standard chart depending heavily upon satellite input over the ocean. Another might be to invent a symbol for showing such middle-level circulations on the surface chart. Since the surface chart is drawn at almost all weather stations, this alternative would appear to be preferred. The availability of enhanced IR data would often permit determining the level of the circulation with confidence.

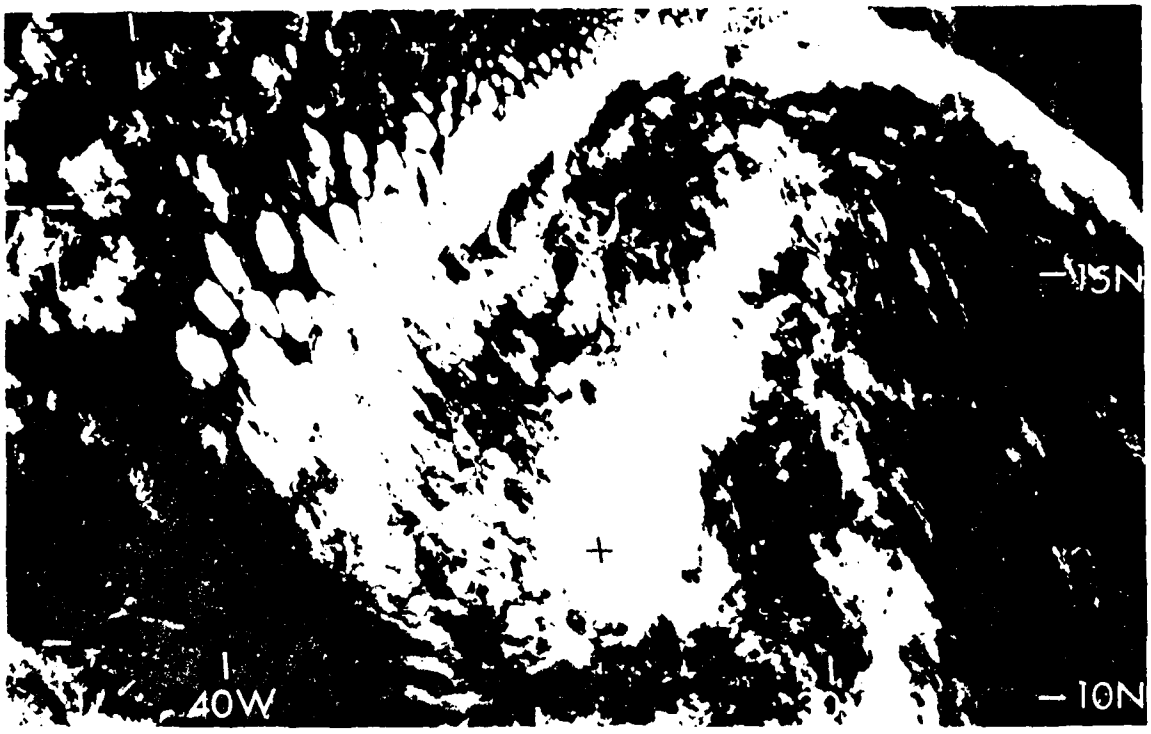

Figure 1. GOES 1-km resolution visible sector at 1300 GMT, 3 August 1977.

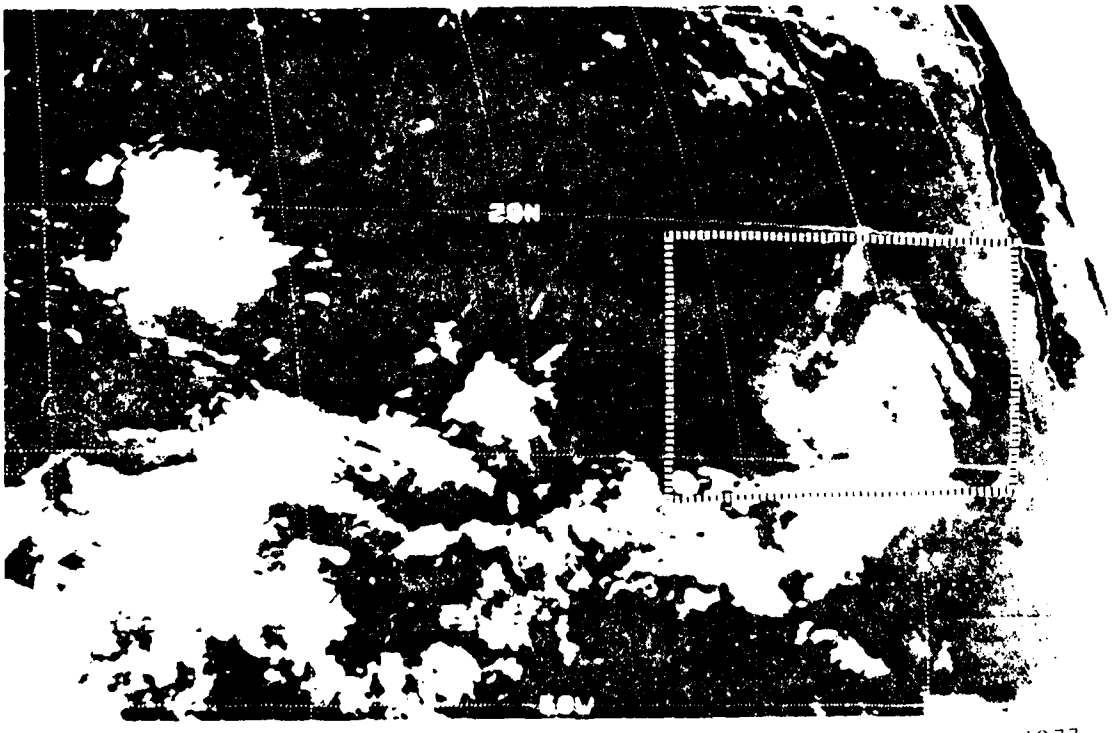

Figure 2. GOES 8-km resolution infrared image at 1300 GMT, 3 August 1977.

223

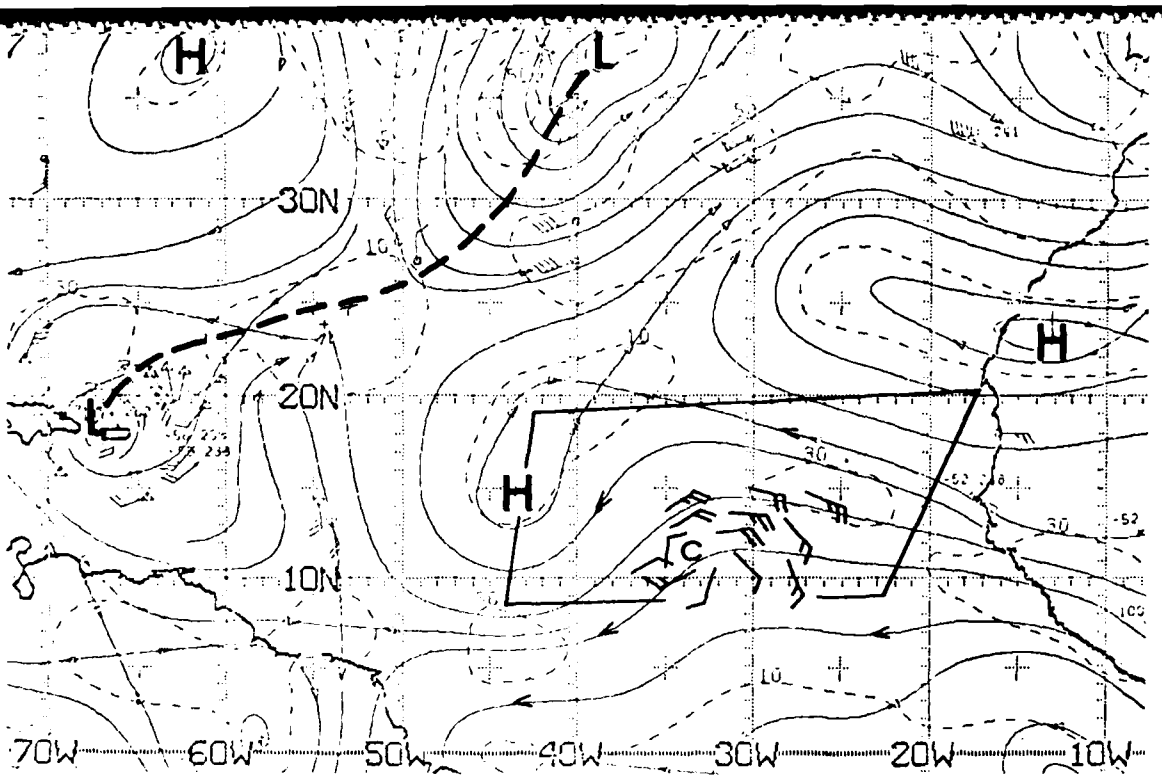

Figure 3. A portion of the NHC's 200 mb analysis at 1200 GMT, 3 August 1977.

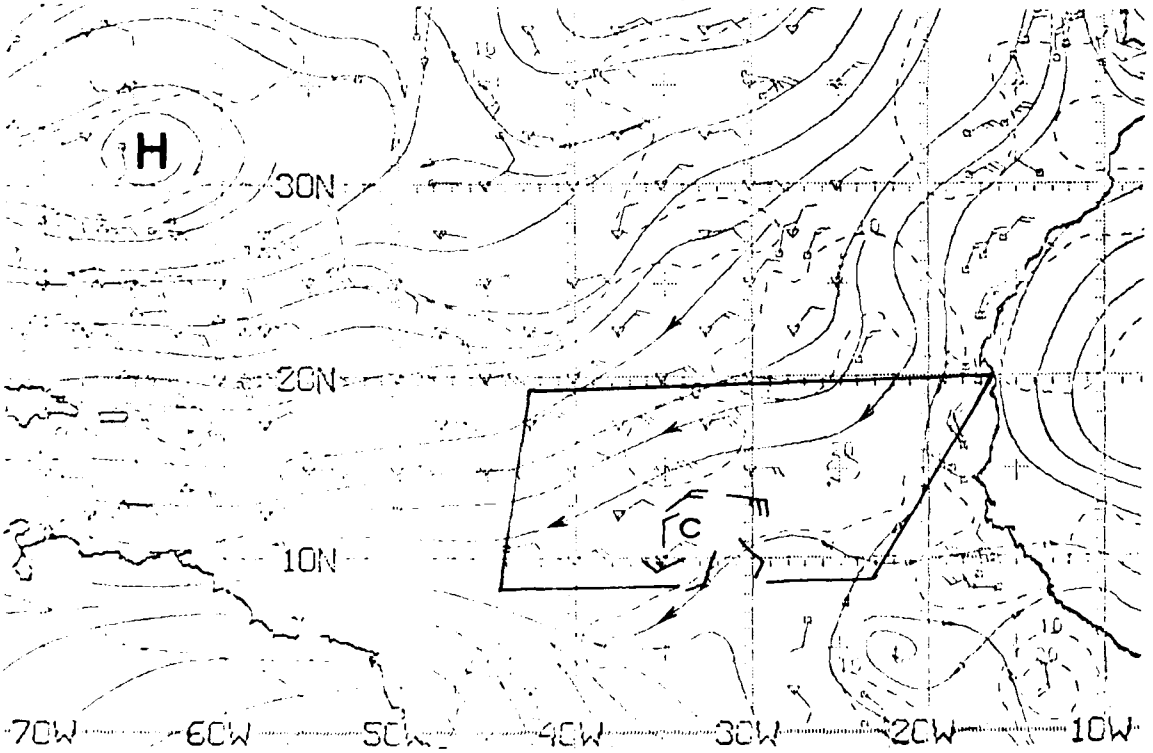

Figure 4. A portion of the NHC's ATOLL analysis at 1200 GMT, 3 August 1977.

220

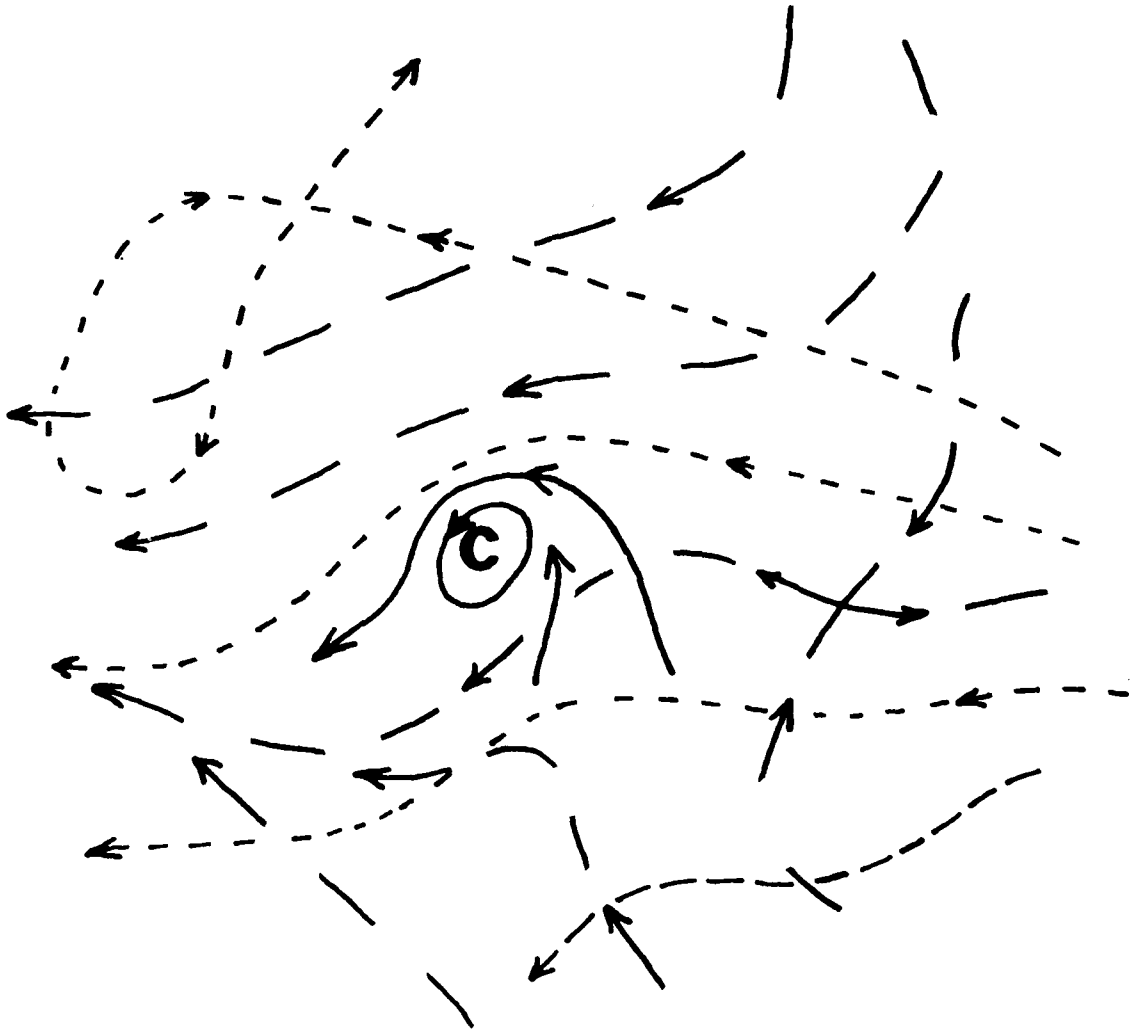

Figure 5. A composite chart derived from Figures 3 and 4. The solid lines show the middle level flow defining the closed circulation. The long dashed lines depict the lower level (ATOLL) flow, and the short dashed lines depict the upper level (200 mb) flow.

U.S. DEPARTMENT OF COMMERCE

National Weather Service/National Environmental Satellite Service
SATELLITE APPLICATIONS INFORMATION NOTE 77/17

DETECTION OF LOW-LEVEL MOISTURE IN THE SOUTHWEST U.S. ON GOES IMAGERY

Carl E. Weiss and Vincent J. Oliver
Applications Group, NESS, Washington, D.C.

Low-level moisture can be detected on satellite IR pictures. Although not explicitly observed, the presence of the moisture can be inferred by its effects on the outgoing surface radiation. We find that during the daytime the sun heats the ground rapidly with little or no observable difference in the dry area from the moist area. However, at night the moisture in the atmosphere is quite effective in slowing down the cooling of the ground since it absorbs the outgoing long wave radiation much better than it absorbs the incoming short wave radiation. The result of this is that during the night, where the air is dry, large differences in ground temperatures are observed, which in satellite pictures show up every hill and dale, mountain and valley, and coastline very distinctly. On a moist night, the cooling is much slower and results in a much more uniform surface temperature. It is often so uniform that frequently even the coastline of the Gulf of California is undetectable.

Figure 1 is an SMS-2 HB enhanced IR image for 1245 GMT 16 June 1977. Details of the terrain in interior southern California, southern Arizona, and extreme northwestern Mexico are clearly visible, including the old lava bed, Cerro Pinacate (A). The northeastern and eastern coastline of the Gulf of California (B) is also distinct. These details in the temperature pattern are what we would expect with dry air over the region. Farther south, along the east coast of the Gulf of California (C), the land features are not distinct; in fact, the coastline is barely discernible in the temperature field. The general dark tone over the area is indicative of moist air. The 1200 GMT surface chart (Figure 2) shows that the air over the desert southwest was very dry with dew points along the lower Colorado valley and in interior southern California ranging from the mid 20's to the mid 40's. The presence of the moist air to the south along the east coast of the Gulf was evidenced by dew points of 68°F and 70°F in this region.

The HB enhanced IR picture for 1145 GMT 13 July 1976 (Figure 3) illustrates a different atmospheric moisture regime. None of the detail in the terrain in the desert southwest that was apparent in the previous example can be seen at this time. The coastline of the Gulf of California has vanished. Water surfaces are indistinguishable from land surfaces. The entire area A to A' has a similar gray tone. This temperature pattern suggests that moist air covered most of the lowland area surrounding the northern Gulf of California. Dew points varied from 53°F to 70°F over southern California and from 68°F to 75°F along the east coast of the Gulf.

It follows from this that an operational procedure would be to save and post a picture taken on a dry night showing all the terrain details visible under such conditions. Then each night compare the incoming picture with this sample. Where the contrast is missing, the reason is likely to be the presence of moisture. It is of course necessary that an IR enhancement curve be used that will show great detail in the temperature range covered by the Gulf of California waters and the adjacent land areas at night. The HB enhancement curve depicts these surface temperature details the best of the operational enhancement curves at the present time (Fall 1977).

227

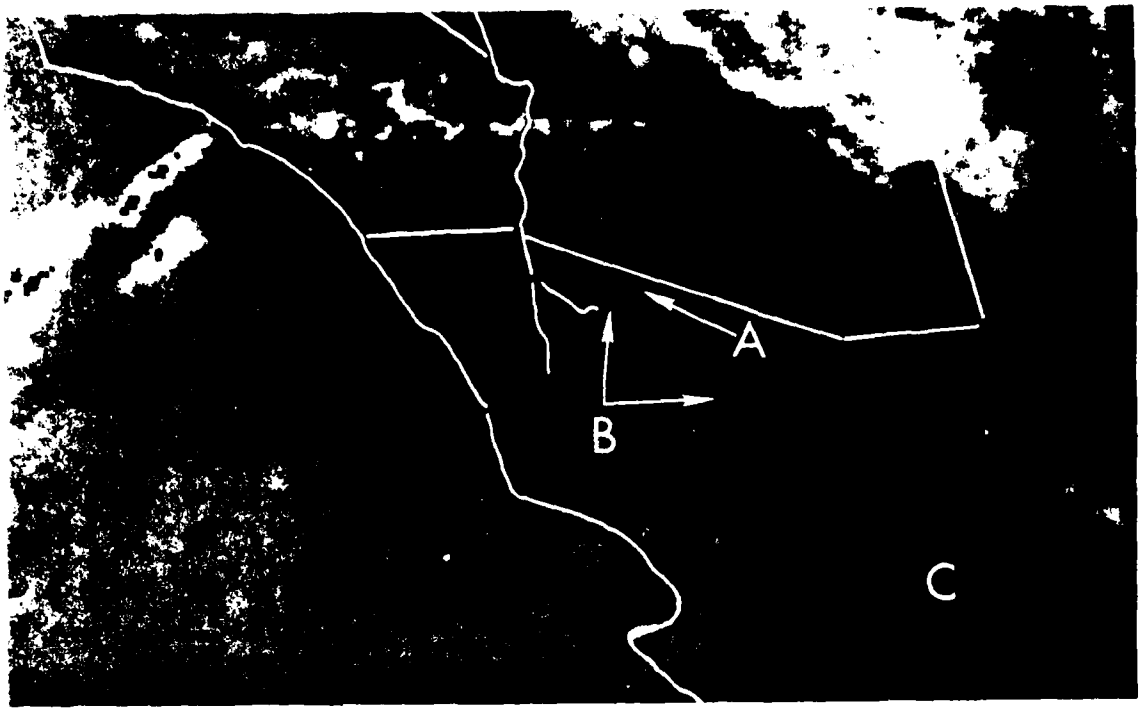

Fig 1. SMS-2 HB Enhanced IR Imagery, 1245 GMT, 16 June 1977.

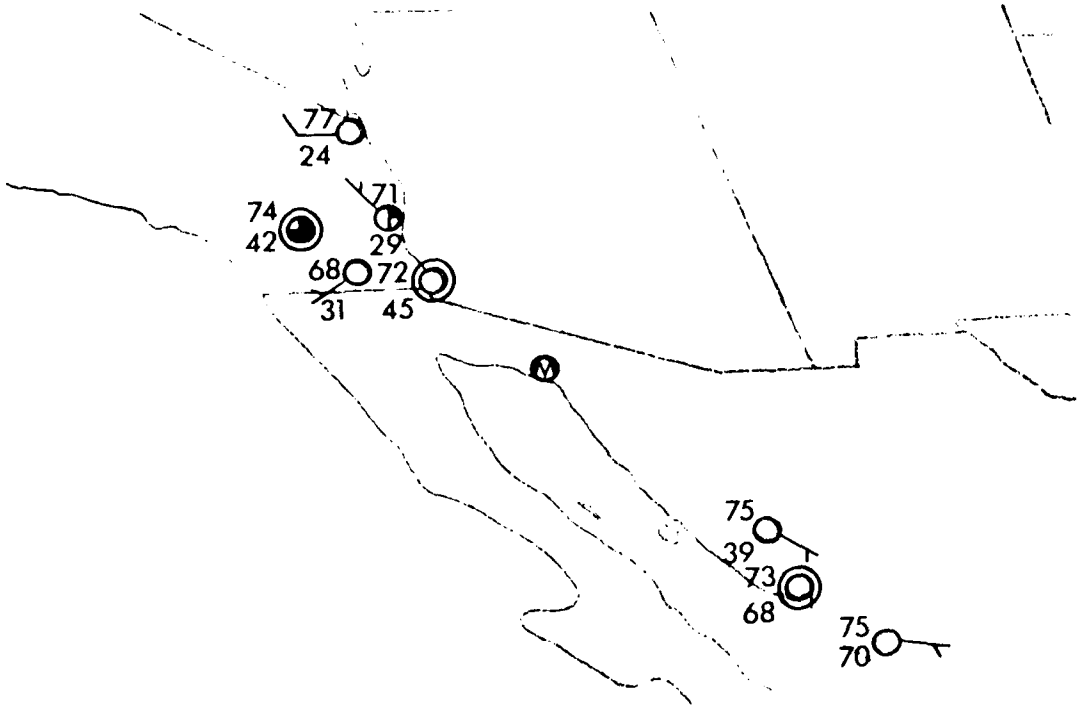

Fig 2. Surface Map, 1200 GMT, 16 June 1977.

228

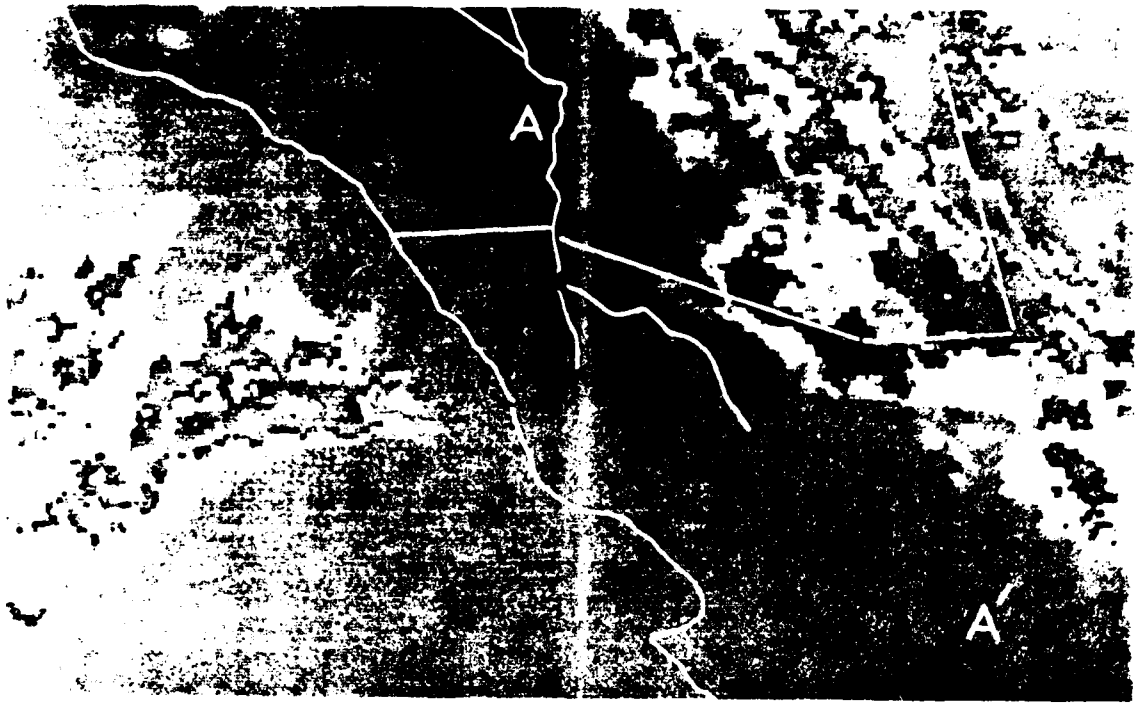

Fig. 3. SMS-2 HB Enhanced IR Imagery, 1145 GMT, 13 July 1976.

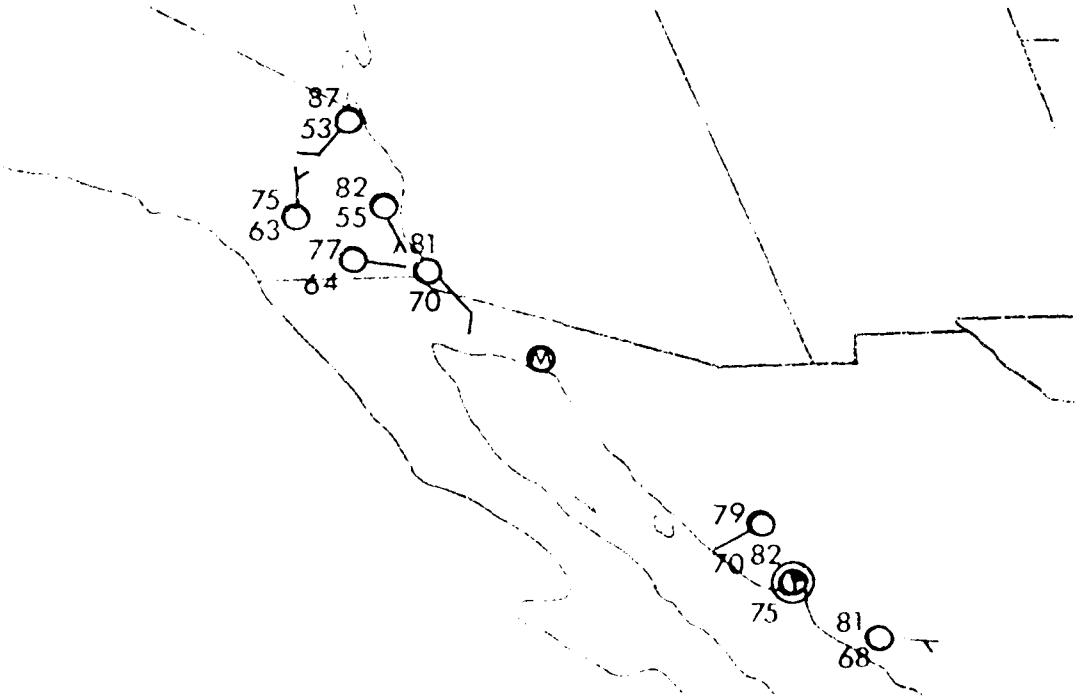

Fig. 4. Surface Map, 1200 GMT, 13 July 1976.

U.S. DEPARTMENT OF COMMERCE

National Weather Service/National Environmental Satellite Service
SATELLITE APPLICATIONS INFORMATION NOTE 77/18

AN UNUSUAL GRAVITY WAVE

Deborah Hasselberg and Vincent J. Oliver
Applications Group, NESS, Washington, D. C.

During the past few years, satellite pictures have revealed long, well-defined lines of abrupt clearing which propagated for long distances through existing cloud fields. Studies by Jager, Williams (1953), Gossard and Monk (1954), and Stilke (1973) have attributed these cloud phenomena to gravity waves. The cloud pattern discussed in those studies appeared as a group of parallel lines in stable air masses or as a sudden clearing zone behind those lines. However, the wave impulse described here is different in that it consisted of a swiftly propagating line along which clouds either abruptly formed or were enhanced, rather than dissipated.

The gravity wave (A-B) seen in Figures 1 and 2 appears as a band of clouds with a well-defined eastern edge. When observed on a movie loop in time-lapse motion, the feature can be traced from 10°S (Fig. 3), and it appears to have originated in the Southern Hemispheric jet stream zone near 20°S. The wave speed was not entirely constant, averaging from 17 to 20 knots, moving more swiftly in its northern end.

The feature was well-defined (Fig. 1a and 1b) as it passed through the low and middle cloud field south of the ITCZ on September 21, as can be seen in the GOES-2, 1-mile visible imagery. Note the enhanced clouds (A-B) associated with the wave in the morning picture (Fig. 1a) and the highlights and shadows (C-D) evident in the late afternoon image (Fig. 1b), indicating a higher elevation behind the wave than ahead of it. The multiple line structure (E) of the wave can be seen in both the 1800 GMT and 2300 GMT pictures.

The SMS-2 infrared pictures (Figs. 2a and 2b) bring out the most outstanding characteristic of this wave. As the impulse (Fig. 2a) passed through the altostratus layer (F), it not only lifted that stable deck leaving an area of elevated stratus to its rear, but also served to lift the high level moisture from earlier cumulonimbus anvil dissipation to produce a stable cirrus deck above (G). The convection that was evident ahead of the wave (H and I, Fig. 2a) was further enhanced (Fig. 2b) after the wave frontal passage. Thus, the impulse had deep vertical extent and synoptic scale influence.

REFERENCE

Gossard, Earl E. and William H. Hooke, 1975: Waves in the Atmosphere, Elsevier Scientific Publishing Co., New York, N.Y., p 5.

Figure 1a. GOES-2, 1-mile visible imagery, 1803 GMT 1 September 1977.

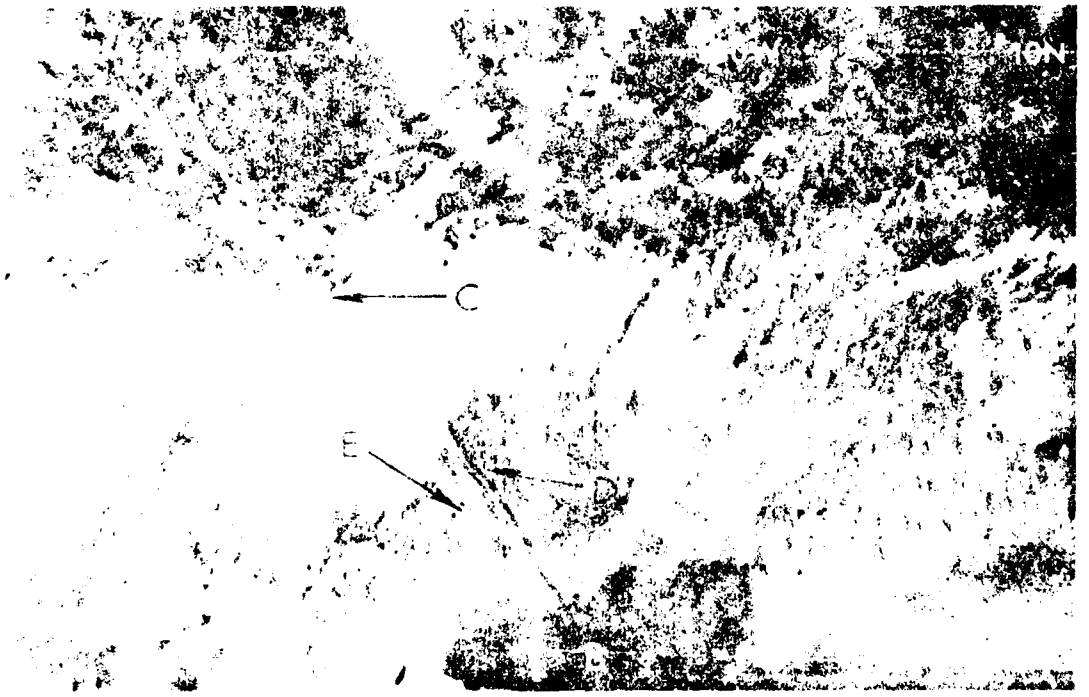

Figure 1b. [illegible] 1-mile visible imagery, [illegible] September 1977.

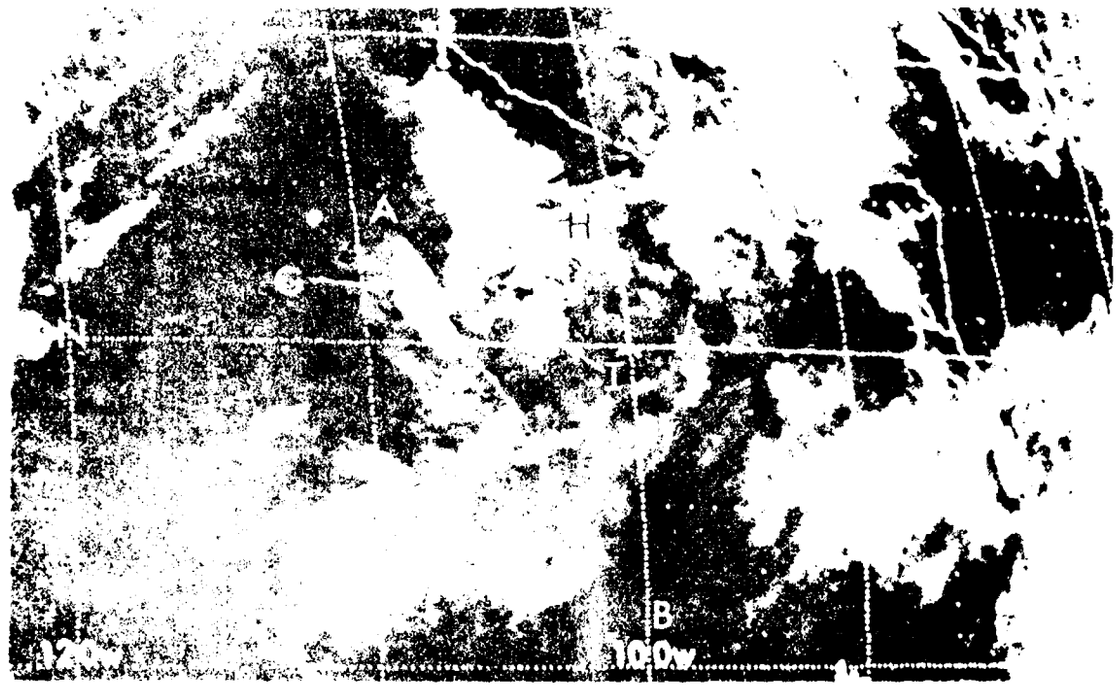

Figure [illegible] SMS-1 Geostationary Satellite IR Imagery, 0645 GMT
[illegible] October 1977.

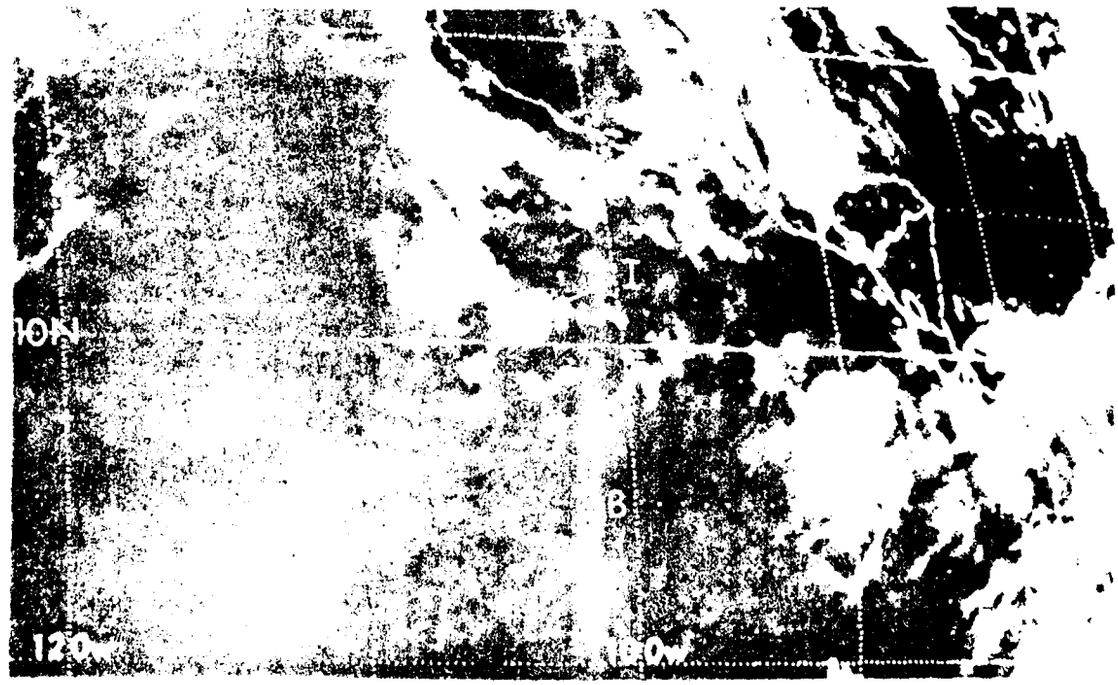

Figure [illegible] SMS-1 Geostationary Satellite IR Imagery, 1015 GMT
[illegible] October 1977

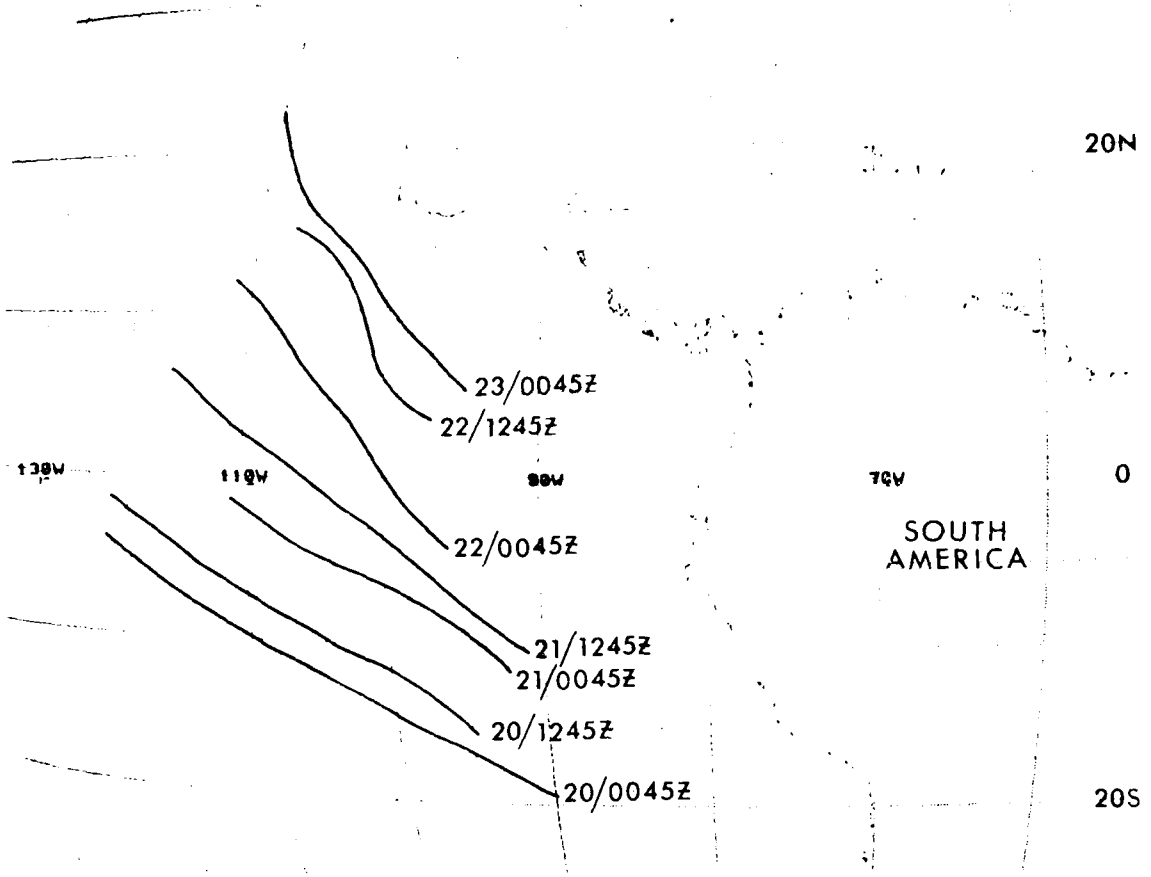

Figure 3. Twelve hourly position of wave front from 0045 GMT 20 September 1977 to 0045 GMT 23 September 1977.

233

U.S. DEPARTMENT OF COMMERCE

National Weather Service/National Environmental Satellite Service
SATELLITE APPLICATIONS INFORMATION NOTE 77/19

ESTIMATING RAINFALL FROM SATELLITE IMAGERY -- A TEST OF THE DECISION TREE

Robert N. Craig
NESS, Satellite Field Services Station,
Kansas City, Missouri

For the past two years, the Kansas City SFSS has been testing various techniques for estimating precipitation from satellite pictures. One experiment used infrared pictures that were electronically enhanced according to the Mb curve. Results showed very little correlation with observed precipitation.

A variation of our method, that takes a number of additional factors into account, is described in NOAA Technical Memorandum NESS 86, "A Scheme for Estimating Convective Rainfall from Satellite Imagery" by Scofield and Oliver. Computations with the Scofield/Oliver scheme have been made for a number of heavy precipitation events with promising results. One test of this technique at the Kansas City SFSS involved computing precipitation estimates for six stations for a continuous period of two months. Verification of this effort has yet to be completed.

This "Decision Tree" estimation process outlined in TM NESS 86 assumes there is a primary relationship between rainfall intensity, cloud top temperature (implied height), and storm growth as determined from GOES imagery. Tropopause penetration, cell mergers, and line intersections are also taken into account. The scheme attempts to eliminate computation of rainfall amounts from inactive areas of convective clouds.

Inaccuracies in picture gridding and the gross resolution (approximately 8 km) of the infrared sensor imposed limitations on the estimation (and verification) of point values. However, reasonable real-time estimates for general areas can be made which should prove quite helpful for early "flagging" of possible flash flood situations.

The rainfall estimation technique requires computations for each 30-minute period. At the Kansas City SFSS, these computations are made from 4-km "equivalent" resolution (electronically enlarged) Mb enhanced IR pictures.*

During the early morning hours of September 12, rains of up to 8 inches fell in the Kansas City metropolitan area with a "repeat performance" that night, which brought 24-hour rainfall totals to as much as 16 inches. Figure 1 is a map of the area showing storm total rainfall. Precipitation estimates for the storms that occurred during the day were made from the IR data. This was supplemented with 2-km resolution visual pictures that were most helpful in defining overshooting tops and provided a more positive identification of active convection areas.

*See GOES/SMS USERS GUIDE for details.

Table 1 shows the estimated and observed precipitation at the Kansas City International Airport (MCI) and at Independence, Missouri. Only the storm total was available for Independence, but hourly values are shown for MCI. It was not possible in this case to differentiate appreciably between total rainfall amounts at the two locations which are approximately 25 miles apart although separate thunderstorm cells were indicated much of the time. Both periods of heavy rain occurred almost entirely during hours of darkness so overshooting tops could not be identified except at Independence at 2330Z, September 12 (the last visible picture of the day). Had visible data been available, estimates could have been made with greater accuracy.

Figures 2 and 3 are photographic enlargements of the 4-km equivalent infrared (EIR) used in the computation of the very heavy rainfall. Figure 2a, 0700Z September 12, was used to assess cell growth and changes during the 30-minute period ending 0730Z September 12 (Figure 2b). Similarly, Figures 3a and 3b were used to estimate the rainfall ending at 0100Z September 13. Figure 4 shows the portion (step 4) of the "Decesion Tree" that applies to the computations.

In Figure 2b, the white area near point C is new and its coverage is about 0.5 degrees latitude. From Figure 4, a convective cell with a white enhancement level increase of more than 1/3 degree but less than 2/3 degree, produces an estimated 30-minute rainfall amount of 1.00 inch at Independence (B), Figure 2b. Repeat IR gray levels at the same expansion rate at MCI (A) resulted in a 0.75 inch estimate.

The storm center (C) in Figure 3b appears brighter and has increased approximately 3/4 degree of latitude during the half-hour period. Repeat gray levels with an expansion rate greater than 2/3 of a degree (Figure 4) results in an estimate of 1.50 inches of rain in 30 minutes at both stations (A and B). The hourly rainfall estimates do not closely agree with the observed rainfall (Table 1), but amounts estimated do show excessive precipitation was occurring.

Though additional verification and testing of this technique is needed, results to date suggest satellite imagery can be effectively used to identify convective systems which have potential for producing flash floods.

235

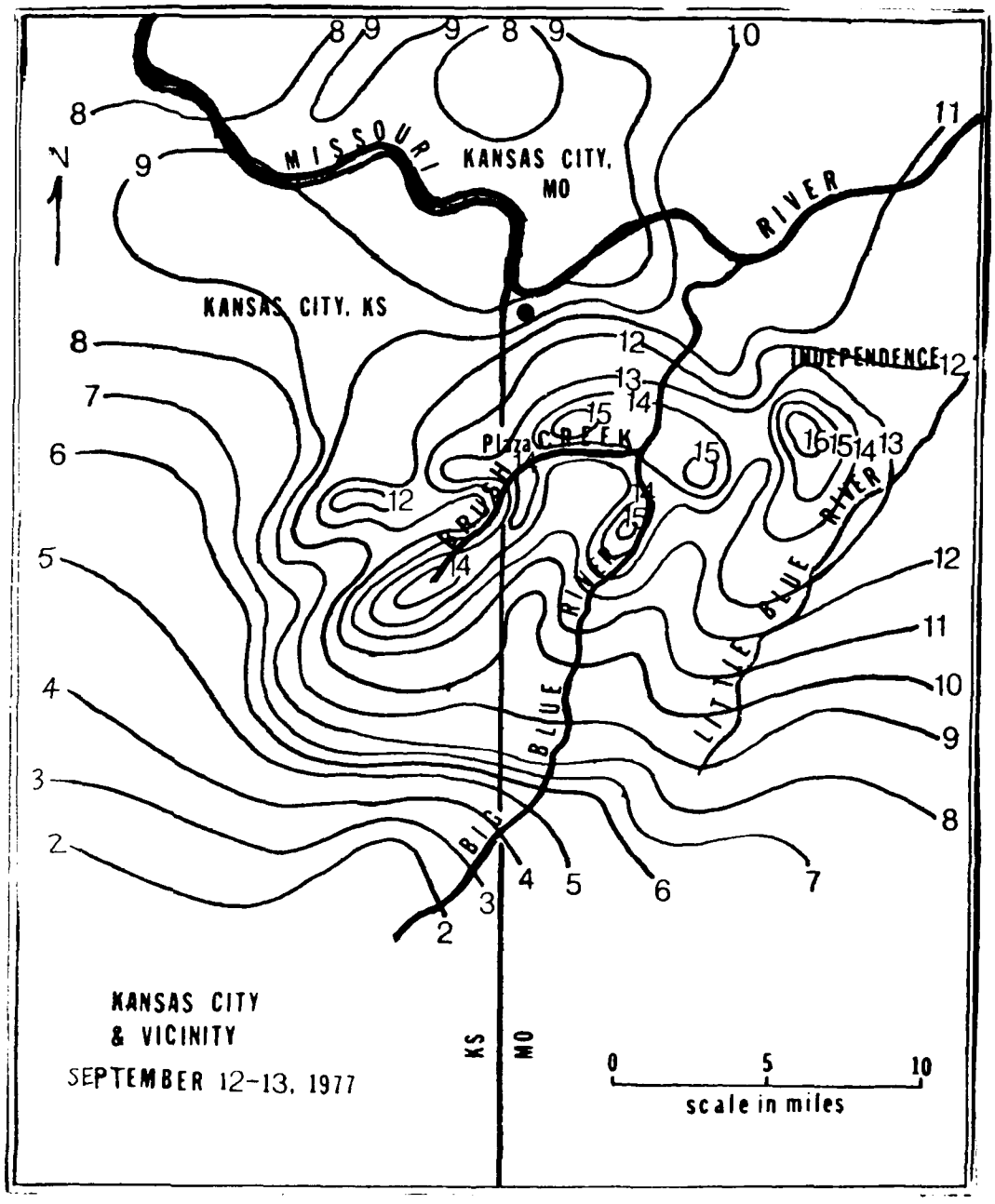

Fig. 1. Storm Rainfall, September 12-13, 1977

234

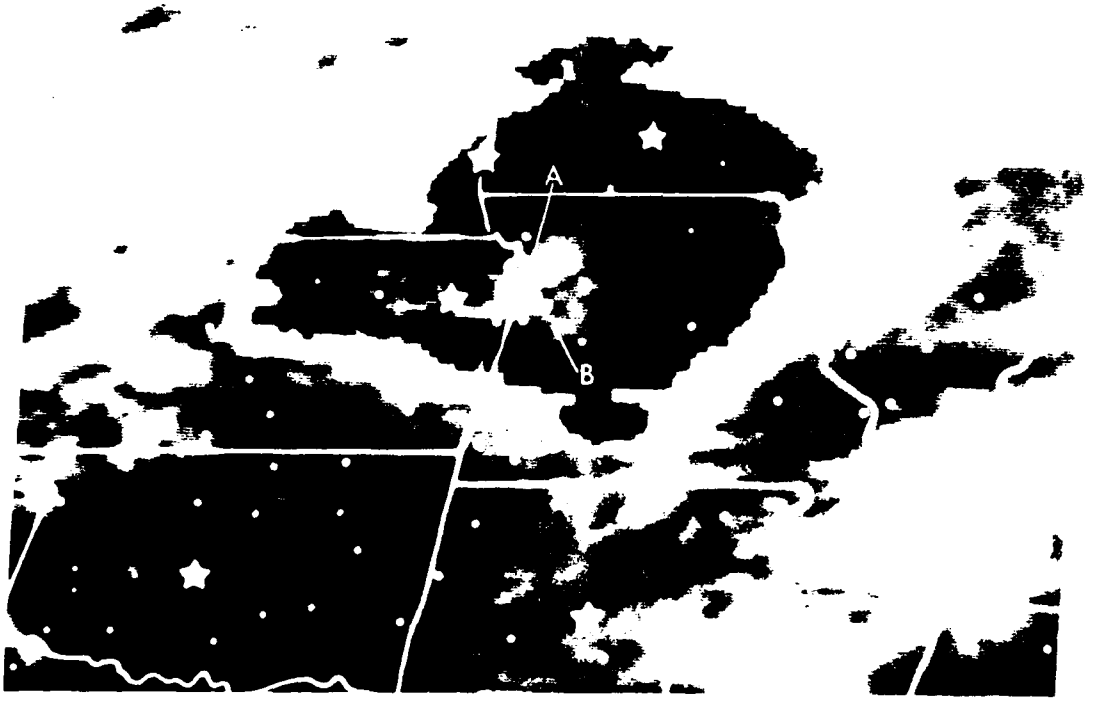

Fig. 2a. 4km Res. Enhanced IR, M_B curve, 0700Z September 12, 1977

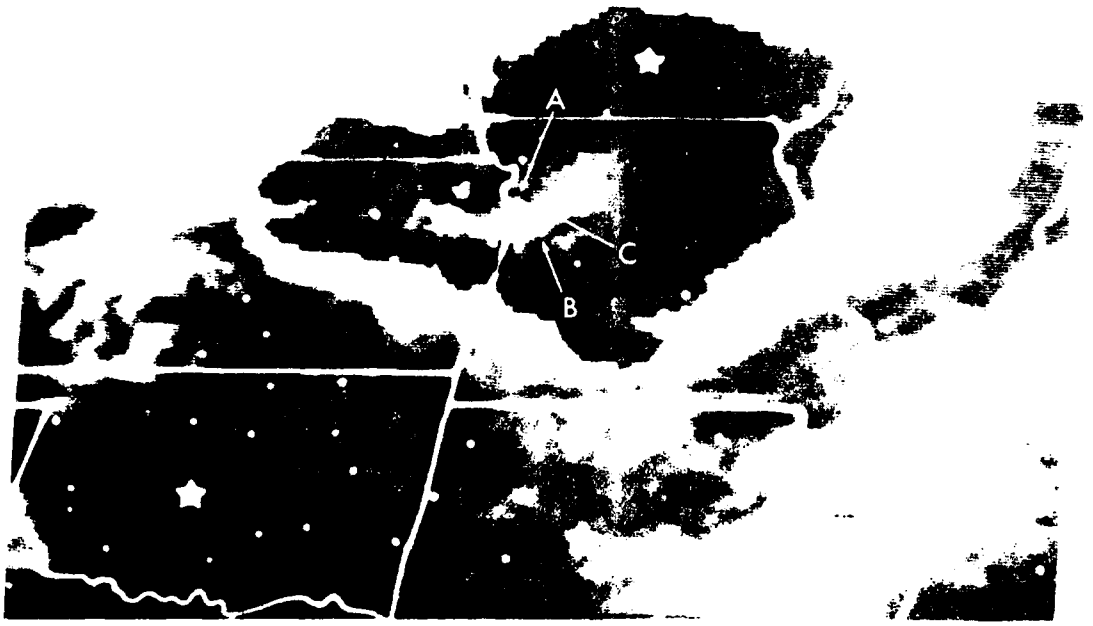

Fig. 2b. 4km Res. Enhanced IR, M_R curve, 0730Z September 12, 1977

237

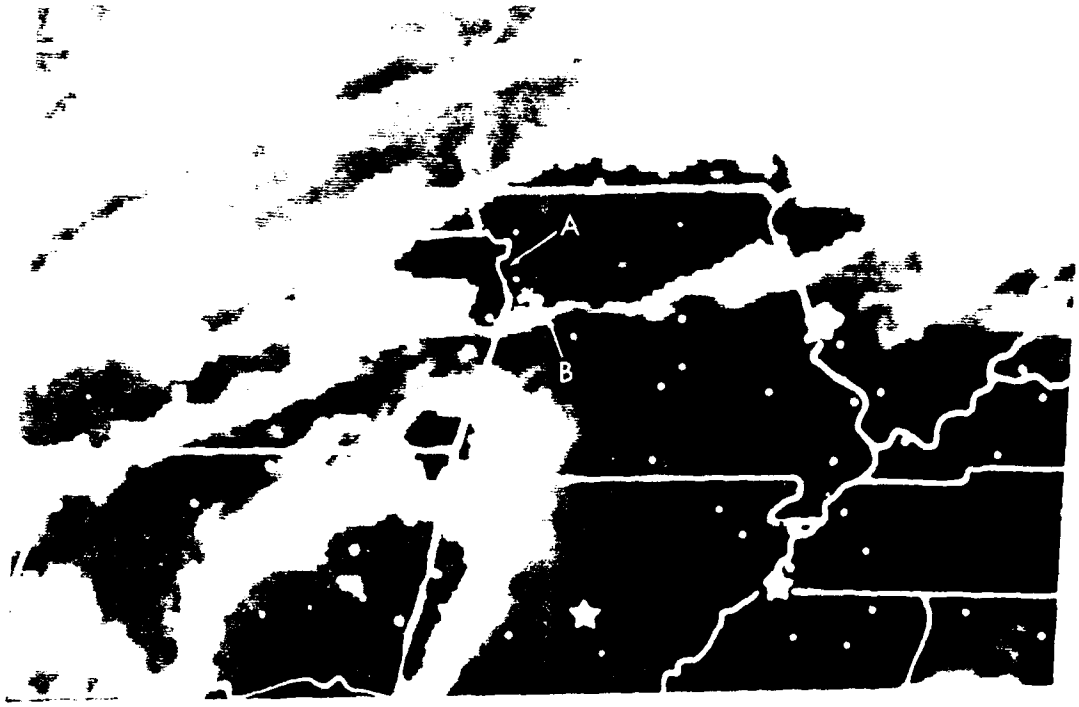

Fig 3a. 4km Res. Enhanced IR, M_B curve, 0030Z September 13, 1977

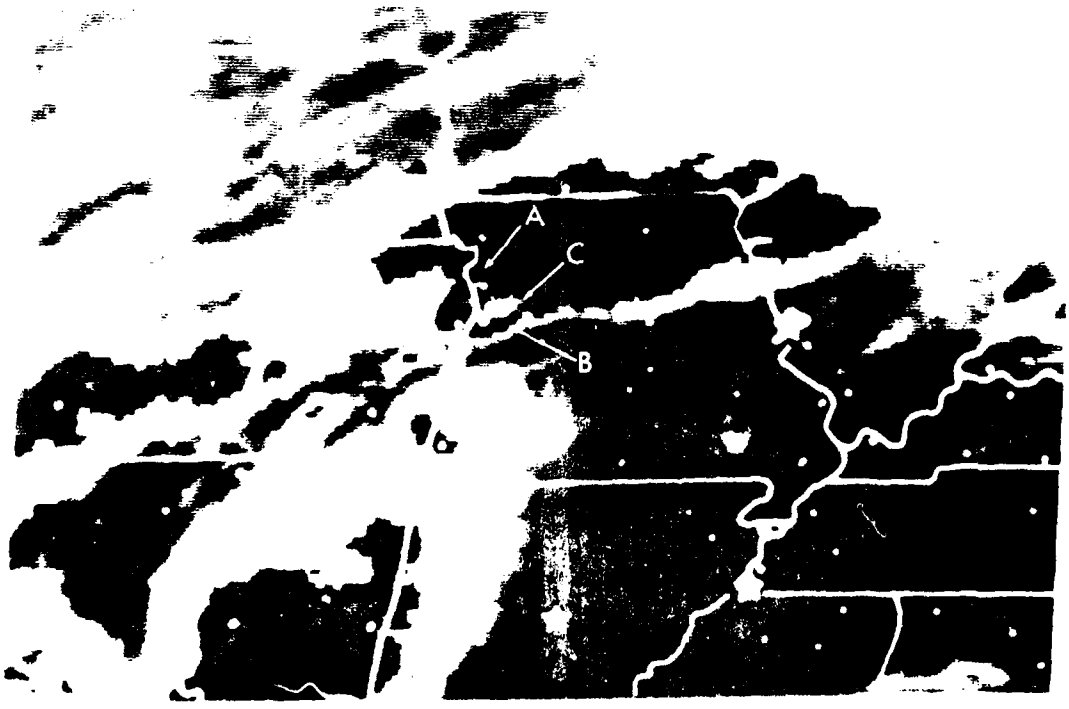

Fig 3b. 4km Res. Enhanced IR, M_C curve, 0030Z September 13, 1977

238

STEP 4.
Estimate half-hourly precip rates as a function of cloud top temperature and temperature change.
USE ENHANCED IR.

- Rainfall is heaviest when and where clouds are still getting colder and coldest area is growing.

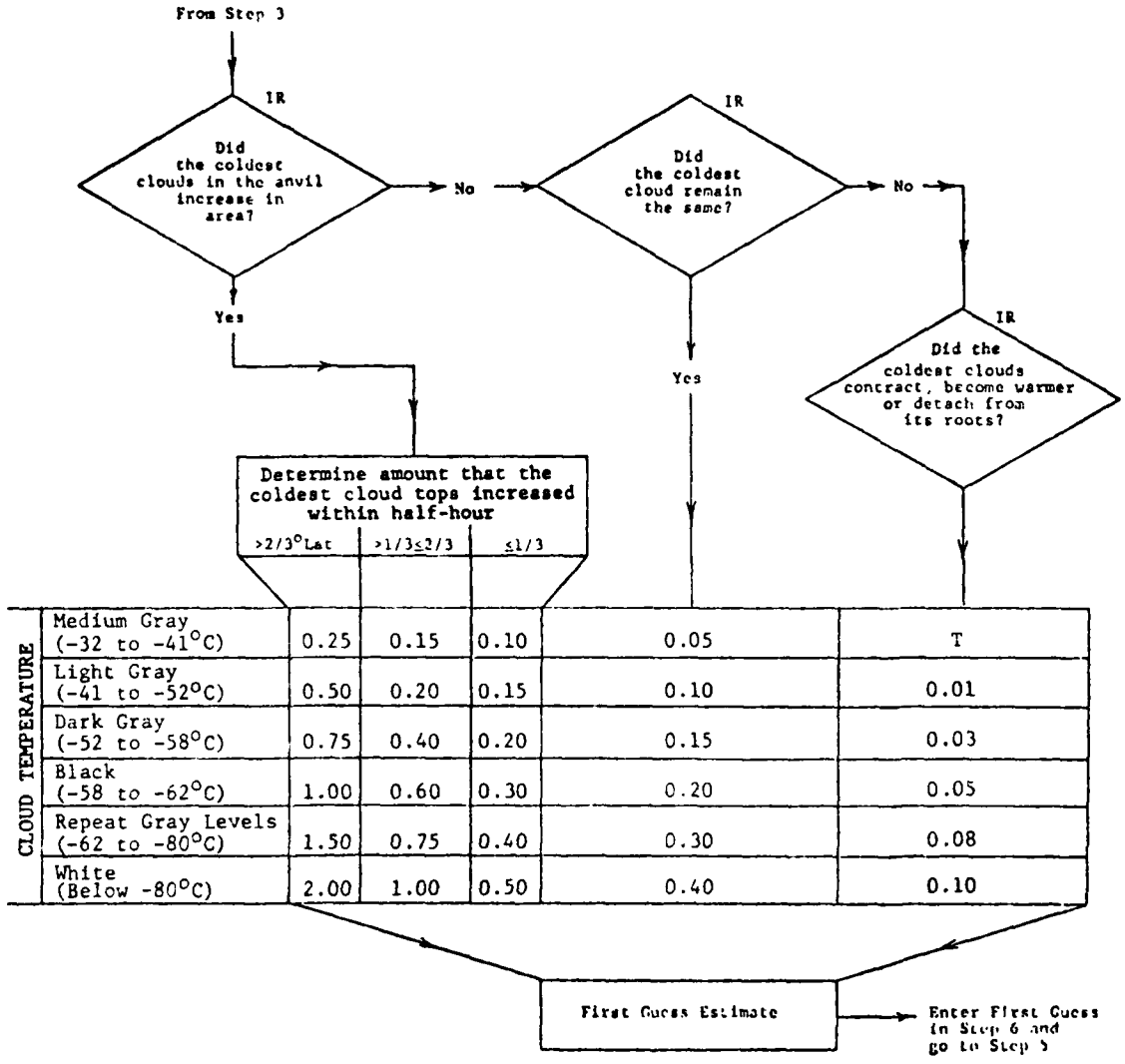

Figure 4. Step 4 from "decision tree". (Scofield/Oliver 1977)

TABLE 1

PRECIPITATION ESTIMATES - SEPTEMBER 12-13, 1977

Time (GMT)	9-12 0630	0700	0730	0800	0830	0900	0930	1000	1030	1100	1130	1200	SUM	
Computed Rainfall														
Independence	.30	.30	1.00	.40	.50	.08	.01	.01	E.01*	.01	.01	.20	2.83	
MCI	.30	.30	.75	.30	.40	.01	.08	.08	E.01	.01	.08	.30	2.62	
Observed Rainfall														
MCI		1.58		.78		.24		.55		.22		.18	3.55	

Time (GMT)	1230	1300	1330	1400	1430	1500	1530	1600	1630	1700	1730	1800	SUM	
Computed Rainfall														
Independence	.08	.03	E.01										.09	
MCI	.08	.05	E.03	.01									.17	
Observed Rainfall														
MCI		.69		.64		.06		.08					1.47	

Time (GMT)	1830	1900	1930	2000	2030	2100	2130	2200	2230	2300	2330	9/13 0000	SUM	
Computed Rainfall														
Independence									EO	E.30	1.20	.20	1.70	
MCI						.20	E.60	E.60	EO	0	.30	.40	2.10	
Observed Rainfall														
MCI												.73	.73	

Time (GMT)	9-13 0130	0100	0130	0200	0230	0300	0330	0400	0430	0500	0530	0600	SUM	24-hr. total
Computed Rainfall														
Independence	.61	1.50	.75	E.40	E.40	E.40	.30	.08					4.43	9.05
MCI	.75	1.50	.75	E.40	E.30	E.30	.01	.01					4.02	8.91
Observed Rainfall														
MCI		.15		.71		1.12		.78					2.76	8.51
Independence														#16.15

* "E" DENOTES ESTIMATES BASED ON PARTIALLY MISSING DATA.

\# TIME BASE MAY VARY SLIGHTLY FROM COMPUTED VALUES. MCI REPORTED 0.19 AT 0600Z 9/12 WHICH IS NOT INCLUDED. THERE WAS NO SATELLITE DATA AVAILABLE 0430Z TO 0530Z BOTH DAYS DUE TO SATELLITE ECLIPSE.

U.S. DEPARTMENT OF COMMERCE

National Weather Service/National Environmental Satellite Service
SATELLITE APPLICATIONS INFORMATION NOTE 78/1

TWO SNOW PLUMES IN UNCOMMON PLACES

Brian G. Smith
NESS Satellite Field Services Station
Washington, D.C.

The ability of the Great Lakes to generate clouds and snow showers under certain wind regimes is well known; just ask anyone in Buffalo or Cleveland. What may not be as well known is that any body of water can do the same thing if the wind is parallel to it. This SAIN shows two such cases.

The cloud plumes mentioned here were formed in the wake of a very intense cyclone that had raced up the east coast on 9 January 1978. By 1630 GMT on the 10th, the low was centered between Labrador and James Bay. Strong, cold cyclonic flow in its southeast quadrant provided a long over-water fetch down the lengths of Long Island Sound and the Gulf of Maine. The water temperature for both bodies of water, shown in Fig. 1, was some 25°F warmer than the air over the land masses surrounding them. Fig. 2 depicts the synoptic weather pattern at 1500 GMT, with the station plots clearly showing the wind blowing the length of the two bodies of water.

The low-level convergence needed to form the plumes came from two sources. One of these was converging wind flow, which can be inferred from Fig. 2. The other was differential warming of the dry, cold air mass, from beneath, by a narrow body of water between two land masses.

Fig. 3 shows the resulting plumes at 1630 GMT on 10 January. A-A' shows the snow plume originating over Long Island Sound. At about the time of the picture, snow showers were being reported at Otis AFB, MA (FMH) and Hyannis, MA (HYA). (Fig. 3 gives the station locations.)

B-B' marks the plume set up by the Bay of Fundy. Since this bay is wider than Long Island Sound, this plume is also wider. Surface reports at 1700 GMT showed light snow showers at Summerside, PEI (YSU) and Moncton, NB (YQM), a moderate shower at St. Johns, NB (YSJ), and a heavy snow shower at Greenwood, NS (YZX).

As the day went on, the strong low-pressure system continued northward, the cyclonic flow relaxed, and the plumes weakened. They both had lasted for some time though. Backtracking through the satellite data showed that the plume over the Bay of Fundy first appeared about 0700 GMT, and the Long Island Sound plume showed up around 0200 GMT. Both plumes produced substantial snow. As the surface reports indicated, heavy snow showers did occur; in fact, WSFO Boston had to issue travelers' advisories over Cape Cod because of the snow.

The point of this SAIN has been to alert forecasters to the possibility of unexpected clouds or precipitation due to "pluming". When the wind blows parallel to a relatively long body of water, and if there is enough land/water temperature differential, cloud plumes may result. This is something to look for, even in areas - such as the two noted here - where "pluming" is not frequent.

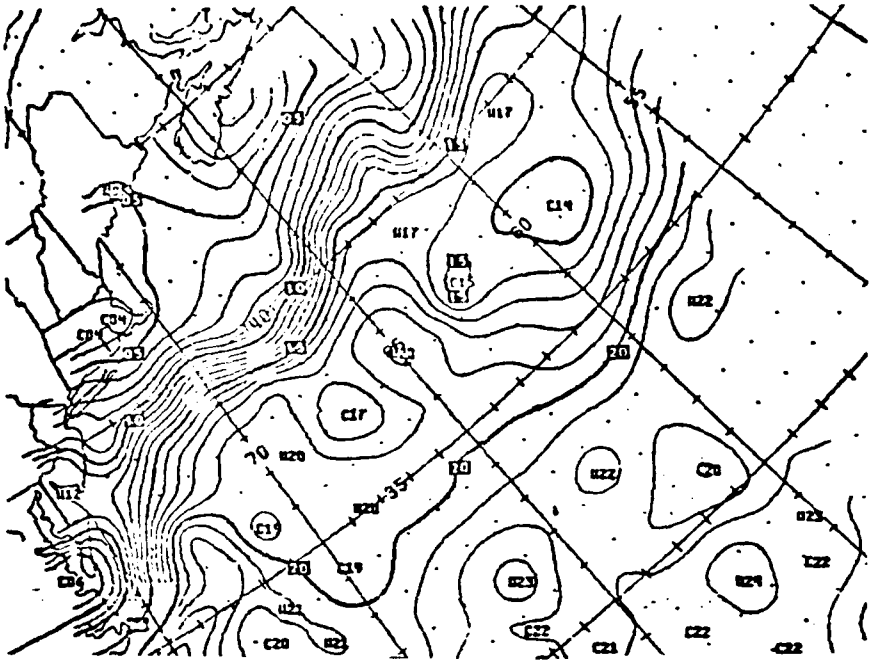

Fig. 1. National Weather Service sea-surface temperature analysis, 5-9 January 1978. Isotherms are at intervals of 1°C.

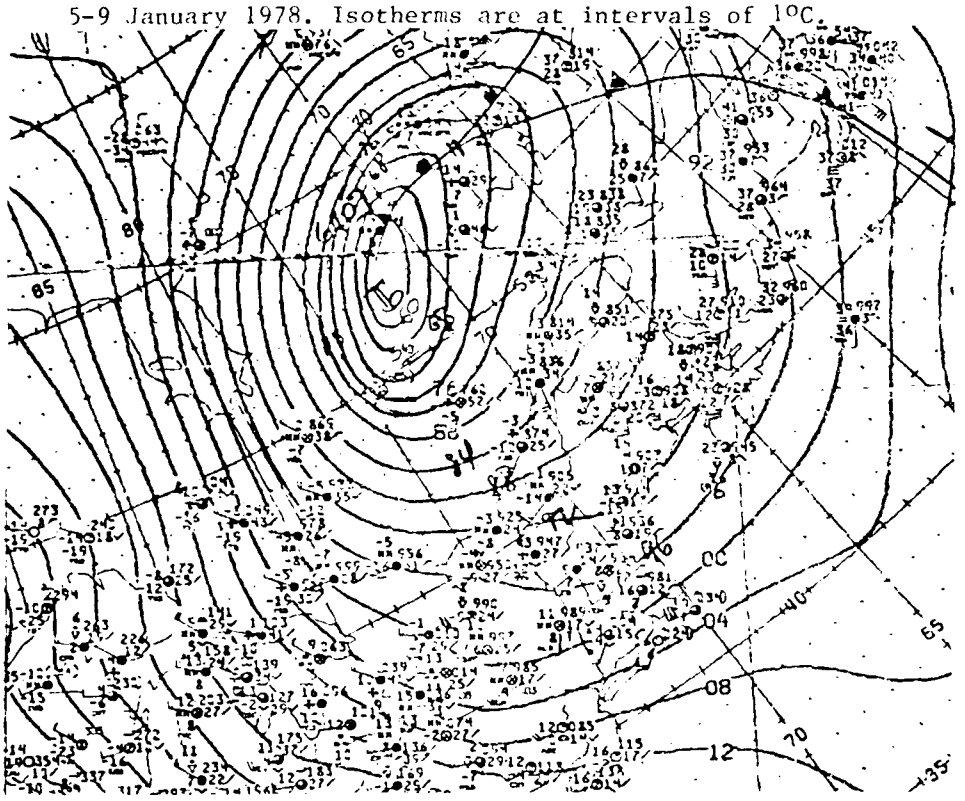

Fig. 2. Portion of NMC North American surface analysis, 1500 GMT, 10 January 1978.

243

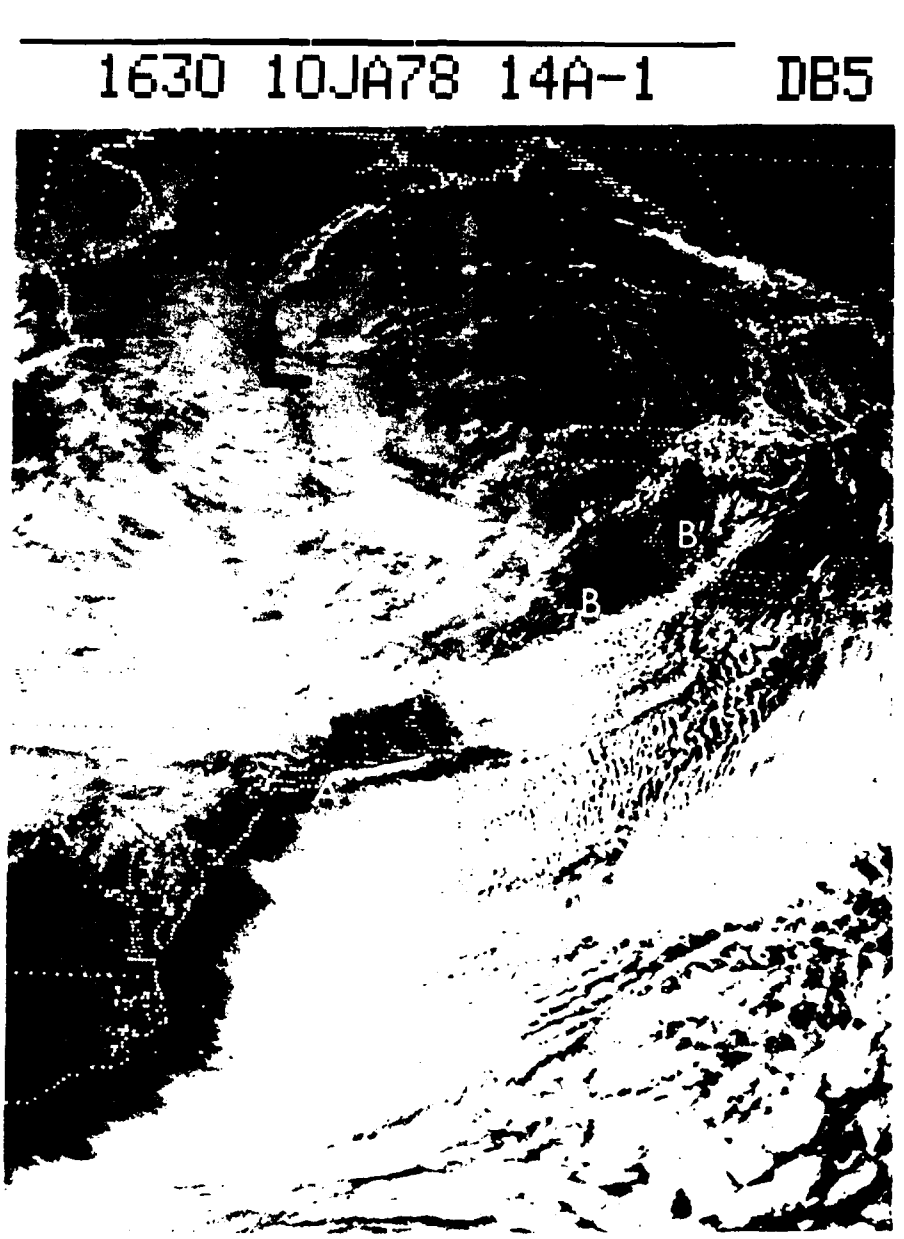

Fig. 3. Part of a GOES-2 DB-5 1-nm visible sector, 1630Z, 10 January 1978. The large "L" marks the center of the storm causing the cyclonic flow.

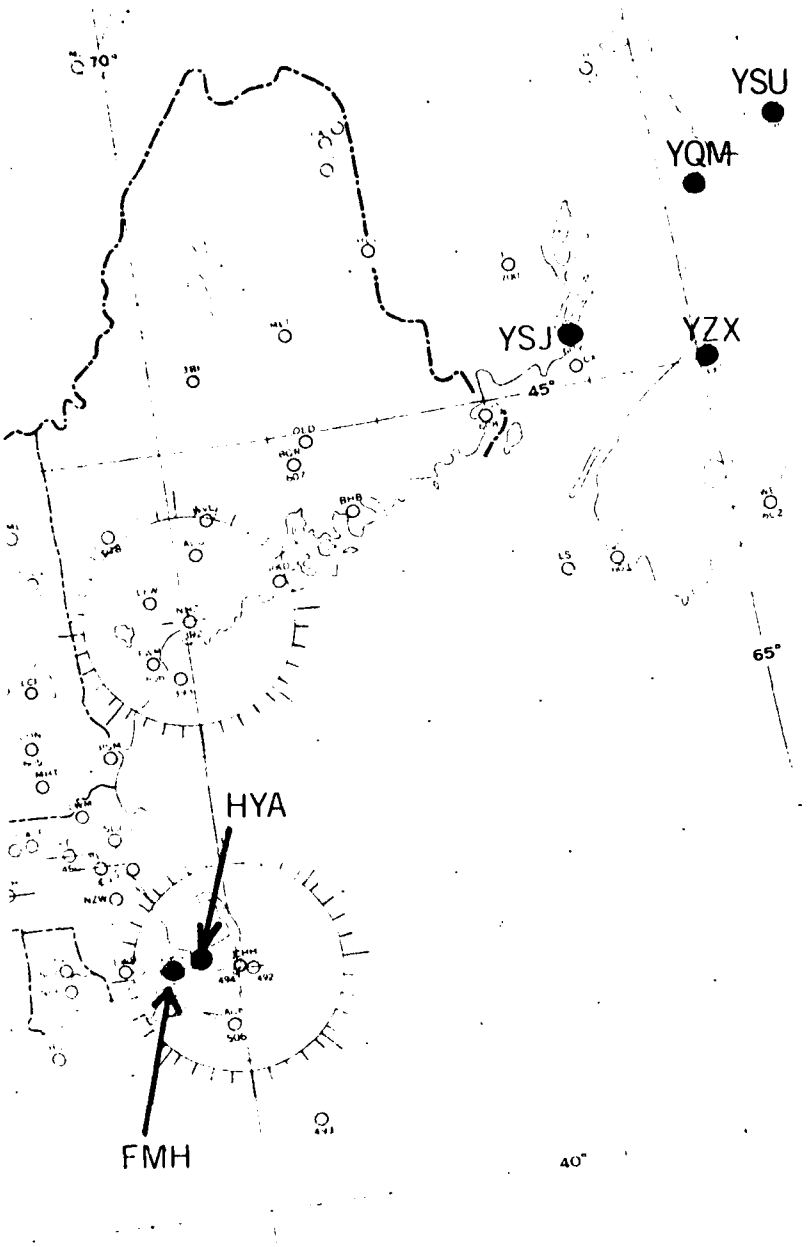

Fig. 4. Location of stations reporting snow showers at 1700 GMT, 10 January 1978, from the two snow plumes.

U.S. DEPARTMENT OF COMMERCE

National Weather Service/National Environmental Satellite Service
SATELLITE APPLICATIONS INFORMATION NOTE 78/2

CLOUD SYSTEMS MOVING WITHIN A SOUTHERN BRANCH OF THE WESTERLIES

Some Clues for Determining the Presence of Precipitation Using Satellite IR Imagery

Stanley Wright
NESS, Applications Group, Washington D.C.

Most significant rain systems in the westerlies exhibit cloud patterns that are vertically deep in the atmosphere. Cloud tops of these systems are generally at cirrus level, and the cloud pattern signatures of the systems are distinctly cold when observed by IR satellite images. However, other systems in the westerlies have cloud patterns which are quite similar in shape and evolution, but the clouds are limited to the upper levels. The cirrus level tops of these cloud patterns also appear cold on IR images, but no precipitation occurs or reaches the ground. Such high-level cloud systems frequently occur within the subtropical westerlies, or within the southern branch of a higher latitude split in the westerlies.

Although the IR satellite pictures are an excellent tool for locating and following the high-level systems, it is often difficult to determine which ones extend downward into the lower troposphere and have precipitation reaching the ground. The following cases illustrate some of the problems and offer some clues to use to determine whether or not precipitation is occurring with the cloud system.

The six IR pictures in Figure 1 are in time sequence at 4-hour intervals. The total period between pictures 1a and 1f is 20 hours. Note the specific cloud systems labeled "A", "B", & "C" on picture "1b". System "C" has decreased in area as it moved over the Oregon coast, whereas system "B" has increased in size during the same time period. System "A" has also increased markedly in size and has become better defined.

Now consider the question of whether or not significant precipitation is occurring under the cloud systems shown. At 1500 GMT - shortly after the time of picture 1b - precipitation was reported over southwestern Washington, western Oregon, and at Crescent City in the northwest corner of California. Thus, there is precipitation under system "C".

Figure 2 is an IR view at 1245 GMT; midpoint in time between pictures 1a & 1b. Superimposed on the picture are height contours from the NMC 250-mb analysis for 1200 GMT; arrows indicate the locations of maximum wind speeds. Note that cloud systems "B" & "C" are located on the east side of a major

trough. The arrows around the trough, indicating maximum wind speeds at & near 250 mb, would closely represent the location of the jet stream axis with the trough. This stream of the westerlies can be considered the polar jet stream location in the longitudes involved. Cloud systems "B" & "C" are located within this "main branch" of the westerlies. Cloud system "A" is located within a southern branch of the westerlies, which can be considered the "subtropical jet stream" location. Wind speeds along the northern jet stream at the 31 to 37 thousand foot levels ranged from 105 knots on the west side of the trough to 80 knots at 250 mb over both Oregon sounding stations. Along the northern California coast, speeds were in the 60-knot range, then increased to 130 knots at Vandenberg which was nearly under the maximum wind axis of the "subtropical" jet stream branch.

The shapes of cloud systems "A" & "B" on picture 1b are of the type referred to by Weldon (1) as a "baroclinic leaf". He stated that such cloud systems, when showing cold tops on IR imagery, were usually accompanied by mid-tropospheric frontogenesis; and that many such systems evolved to comma-shaped systems associated with cyclogenesis. Weldon cautioned, however, that in many cases these processes may be limited to the upper troposphere, especially when the system was located within the subtropical westerlies or in the southern branch of a split in the westerlies. He listed several clues that could be used in the interpretation of IR pictures to determine whether or not a cloud system was confined to high levels or extended downward into the lower troposphere. These clues can be applied to the systems of Figure 1 in order to estimate whether or not precipitation is reaching the surface under systems "A" & "B".

System "B" is located within the "polar jet" branch of westerlies; and it, along with system "C" which preceded it, can be considered as "waves" along the primary frontal zone associated with the trough shown on Fig 2. This is an indication that the systems are vertically deep in extent, and that the circulation involved probably reaches the surface. Thus, precipitation is mostly likely occurring under system "B" as well as the system "C". Clues on the IR pictures that strengthen this conclusion are: (1) warmer - and probably lower - cloud "tails", labeled T1 & T2, extend southwestward from systems "B" & "C", and (2) the tails merge into a band of low clouds which form a boundary between stable appearing stratiform clouds to the south and more unstable appearing stratocumulus cells on the north side. The band/boundary zone feature has the appearance of a oceanic surface frontal zone of moderate or less strength. All indications from satellite data interpretation are that precipitation will occur with system "B" as it swings into the west coast.

Extrapolation of the movement of system "A" indicates that it will move over California in advance of or south of system "B". Will precipitation occur when it does? System "A" has increased in size and become better defined by 1445 GMT; and it has taken on the "baroclinic leaf" shape of a developing system - similar to that of system "B". The top area of system

"A" is very cold on the IR pictures indicating relatively thick clouds with high tops. There is still doubt in regard to the relative thickness of the clouds with "A" with respect to those of "B". The visible picture of Figure 3 shows that by 1945 GMT the clouds of system "A" are nearly as bright as those of "B", although the area coverage of the bright clouds is not as great. In addition, the clouds of system "A" have a "convective appearance". The forementioned aspects indicate that precipitation would occur when system "A" reaches the coast. The following clues indicate that precipitation is NOT likely. (1). System "A" formed in a southern or subtropical branch of the westerlies. This can be seen by observing the track of the system as it evolved during the first few pictures of Figure 1. (2). No low or warm cloud "tail" extends southwestward from the system. Such a "tail" feature is usually observed when a system extends downward into the lower troposphere. (3). No well-defined boundary in low cloud types is observed across the system. This should be expected, especially to the rear of the system, if a low-level frontal surface was formed by the system. Although there is a low cloud boundary near system "A" - between stable clouds to the south and clearing to the north - this interface existed ahead of the system as well as behind it; and, there is not good continuity between the interface and the system with time (Note all pictures of the Figure 1 IR series.).

As system "A" swung into California ahead of the tail end of system "B", some precipitation was reported in the central valley and along the coast, north of San Francisco; but it was not wide spread or of large amounts. The largest amount reported was 0.78 inches at Sacramento prior to 00 GMT with a shower ahead of system "A" (note the convective clouds in that area on picture 1d). Heavy precipitation did occur generally under the cloud band of system "B" which entered the coast after 0600 GMT on the 19th.

Another case is illustrated by Figures 4 and 5. Consider cloud systems "A" & "B" on Figure 4. System "B" consists of an area of towering cumulus and CB cells - sometimes referred to as "enhanced cumulus" - at 1145 GMT, 27 February 1977 (Figure 4a). This system system evolves into a comma shape by 1845 GMT (Figure 4b) and swings northeastward. A well-defined warmer cloud "tail" feature and low cloud frontal boundary are observed at the rear of the system on IR pictures 4b, 4c, and 4d. All clues indicate that system "B" would have significant precipitation occurring under it. As in the first case illustrated, system "A" forms to the south of system "B" and swings northeastward ahead of it. In this case, by the time of figure 4b, system "A" has a well-defined low cloud tail trailing from its southwest end. This feature is well illustrated on the visible picture at 2045 GMT (Figure 5). The tail feature also serves as - or is located with - a well-defined interface between ragged appearing stratocumulus clouds to its south and a clear band on the north. In this case the southern cloud system (system "A") which roughly resembled the "baroclinic leaf" shape, consisted of a wave perturbation along an older frontal zone already in existence to the south & east of the new front formed with the comma cloud system "B". The satellite interpretation clues indicate that precipitation will be occurring with system "A" as it enters the west coast. During the period between 21 GMT on the 27th until 06 GMT on the 28th precipitation was reported at all Oregon stations plotted on the NMC Surface Analyses and at some stations in northwestern California. The precipitation became light

and widespread after 06 GMT, but increased in amount over a wide area the following day as the frontal zone of system "B" entered the coast.

In both cases illustrated the formation & evolution of systems "A" were directly related to the development of their northern counterparts - systems "B". In the second case system "A" formed along an older frontal zone, but was "induced" by the polar jet stream associated with the formation of cloud comma "B". Again system "A" moved northeastward in advance of "B". In other cases, the "A" system may form in the southern branch of a split in the polar westerlies, instead of in a truly subtropical branch. In all cases, such systems may form unexpectedly and move into the west coast - or into the southwest U.S. thru Mexico - south and east of another system in the main branch of the westerlies. With such systems, high cold clouds are nearly always present, and frequently the clouds are relatively thick and appear convective, even in cases where precipitation is not occurring. This paper illustrated some clues that may be used to estimate whether or not precipitation is occurring.

Reference: Weldon, Satellite Applications Information Note 77/7
Title " An Oceanic Cyclogenesis - Its Cloud Pattern Interpretation

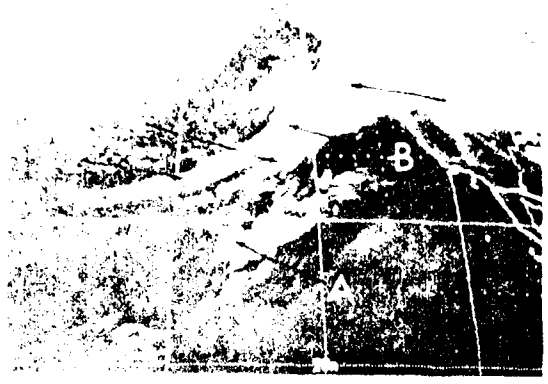

Sep 77.

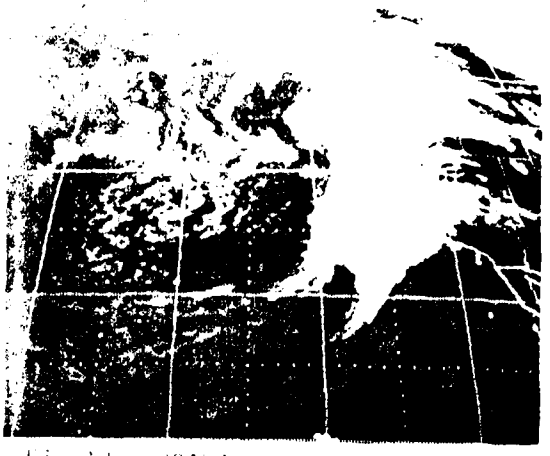

Fig 1d. 02457, 18 Sep 77.

Sep 77.

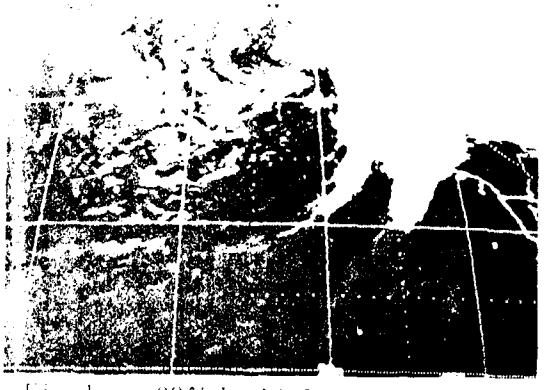

Fig 1e. 02457, 19 Sep 77.

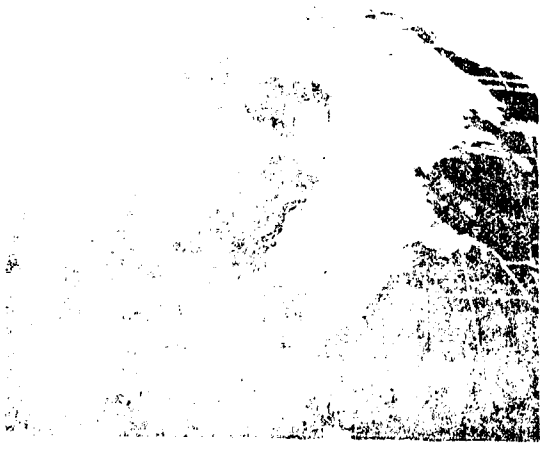

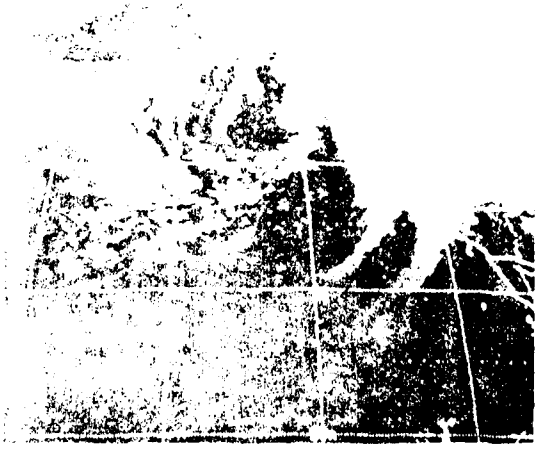

Sep 77.

Fig 2. 250 mb NMC Analysis for 1200Z, 18 Sep 77, on 1245Z IR image.

Fig 3. SMS-2, 2-mile Visible imagery , 1945 GMT, 18 Sep 77.

Fig 4a. 1145Z, 27 Feb 77.

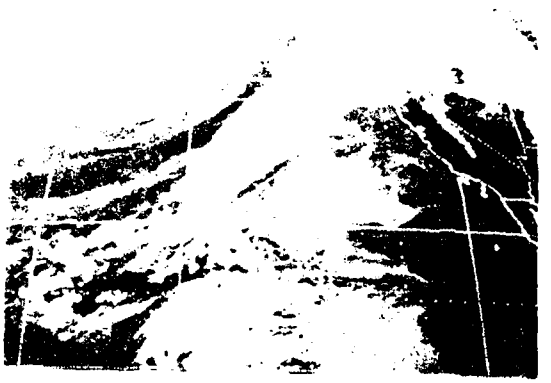

Fig 4b. 1845Z, 27 Feb 77.

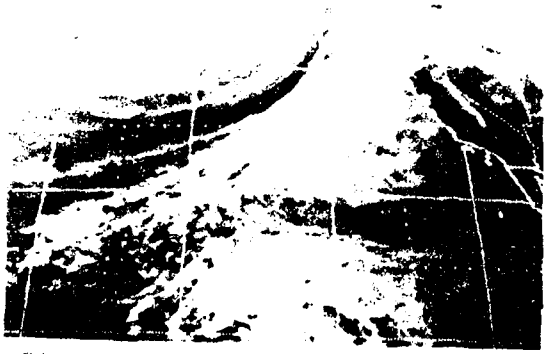

Fig 4c. 2345Z, 27 Feb 77.

Fig 4d. 0545Z, 28 Feb 77.

Fig 5. SMS-2, 2-mile Visible imagery, 2045 GMT, 27 Feb 77.

U.S. DEPARTMENT OF COMMERCE

National Weather Service/National Environmental Satellite Service
SATELLITE APPLICATIONS INFORMATION NOTE 78/3

WHENCE COMETH THE VOG?*

Donald R. Cochran & Robert L. Pyle
NESS, Satellite Field Services Station
Honolulu, Hawaii

At 1930 Hawaiian Standard Time on Tuesday evening 13 September 1977 (0530 GMT 14 September 1977), Kilauea Volcano erupted. Figure 1 shows the location of the eruption (E) on the "Big Island" of Hawaii, one of the six major islands in the State of Hawaii. The Big Island was formed from several ancient volcanic cones. Two of these, Mauna Kea (MK) and Mauna Loa (ML), tower some 4000 m above sea level after rising nearly 6000 m from the ocean floor. At about 1200 m elevation on the eastern slopes of Mauna Loa sits Kilauea (KV), cited by volcanologists as one of the worlds's most active volcanoes. The September 1977 event was the first at Kilauea since the shallow earthquake of November 1975, which set off a brief eruption and triggered a local tsunami.

The infrared sensor aboard the SMS-2 geostationary satellite, with nominal resolution of 8 km, was unable to resolve the initial hot spot. The next day, however, a volcanic cloud began to appear in the high-resolution (1 km) SMS-2 daylight pictures. By late afternoon (Figure 2) this hazy cloud -- a mixture of ejected volcanic ash, smoke from burning vegetation, condensed water vapor and dust, locally termed "vog", for volcanic smog -- was clearly visible. The vog had spread not only around Mauna Loa's base and out to sea, but also downwind to the west and back around into the usually crystal clear Kona resort area on the west shore of the island. An observation from Kona Airport (K in Figure 1) Wednesday afternoon noted visibilities to the east and south restricted to 6 and 7 miles, respectively, due to "smoke".

This vog cloud, maintaining its identity over a period of days, revealed in a unique way the patterns of lower atmospheric circulation downstream from the eruption site. As a marker of the air and its movement, it was more effective and revealing than the usual water cloud tracers which appear and disappear on much shorter time scales in response to unmeasurable variations in moisture distribution. Eruptions come only rarely, but when they do, they can provide a unique view of the atmosphere in motion.

*"VOG" is a locally derived term for volcanic smog. It is composed of volcanic ash, smoke, condensed water vapor, dust, etc.

The radiosonde at Hilo (H in Figure 1) for 0000 GMT 15 September showed a 4° Celsius trade inversion based at 2000 m, which probably confined the vog to the upper part of the marine layer below that level. Synoptically, during the period, the usually strong mid-Pacific high had been weakened by a stationary deep low well to the northwest of the Hawaiian Islands. The normally brisk northeast trade winds had veered and diminished to easterlies of 10 knots or less extending vertically to near 3300 m elevation.

On the west (leeward) side of Hawaii Island, the onshore flow from the usual afternoon sea breeze and the dynamic effect of winds channeling around the mountainous island itself, often combine to produce a well-defined anti-cyclonic eddy to the west of the island. Cloud patterns in satellite pictures sometimes show this leeside eddy, and the circulation is likely to be there at other times when cloud amount is insufficient to reveal it. During the first 24 hours of the eruption, the vog was transported around in this eddy and back to the normally protected areas near Kona. The Honolulu Satellite Field Services Station's time-lapse movie made from successive high resolution daylight images on 14 September confirmed this trajectory.

After sunrise Thursday, 15 September the plume cloud (arrow) immediately above the eruption was clearly visible in the 1 km visual SMS-2 photo (Figure 3), but the vog cloud was less clearly evident because of the unfavorable sun angle at that time. Later that afternoon, the vog could be easily seen (Figure 4) extending downwind 1000 km to the southwest.

Some restriction to surface visibility accompanied the vog across the Pacific. By 0500 GMT, 17 September, Johnston Island at 16.7N 169.5W (1500 km southwest of Hawaii) reported visibility lowered to 4 miles in smoke and haze.

Variations in strength and height of the trade inversion also allowed vertical diffusion of the vog. On 18 September at 0030 GMT an FAA aircraft flying at 5400 m altitude near 15N 180W estimated the top of the vog layer at 5100 m. Apparently this lobe of the vog was too thin to be seen by the satellite, since in the picture at 0219 GMT 18 September (Figure 5) less than 2 hours after the aircraft report, the main western edge appears to be near 176W.

Calculations indicated the mean lower tropospheric flow along the vog trajectory averaged about 15 knots toward the west. Forecasters discussed the likelihood of a significant reduction in visibility in the Marshall Islands west of 170E, such as occurred after an eruption of Kilauea in early 1969 when Kwajalein's visibility lowered to 2 miles. However, successive images each day at 0219 GMT indicated slower westward progress to 178E on 19 September and to 174E on 20 September.

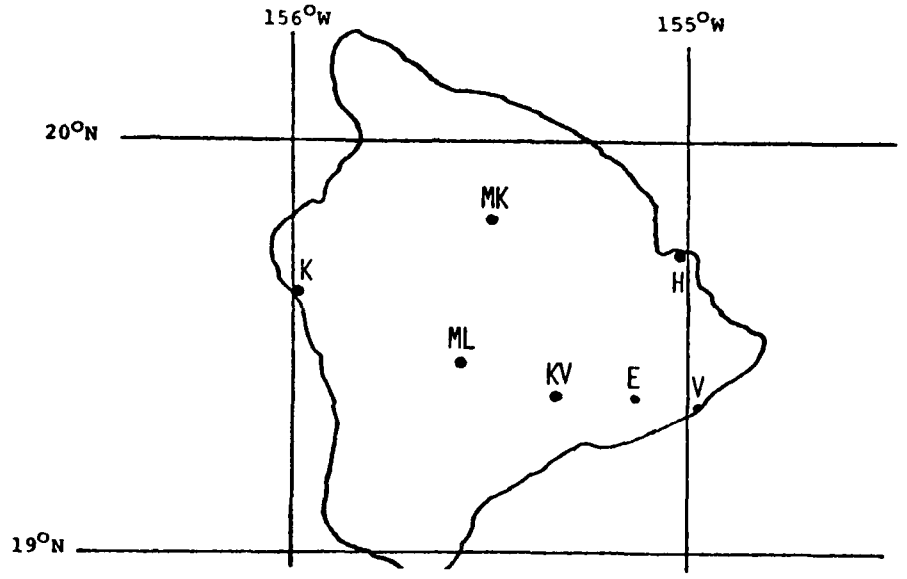

FIGURE 1. HAWAII ISLAND SHOWING ERUPTION SITE (E), HILO (H), KONA AIRPORT (K), KILAUEA VOLCANO CRATER (KV), MAUNA KEA (MK), MAUNA LOA (ML), AND KALAPANA AND KAIMU VILLAGES (V).

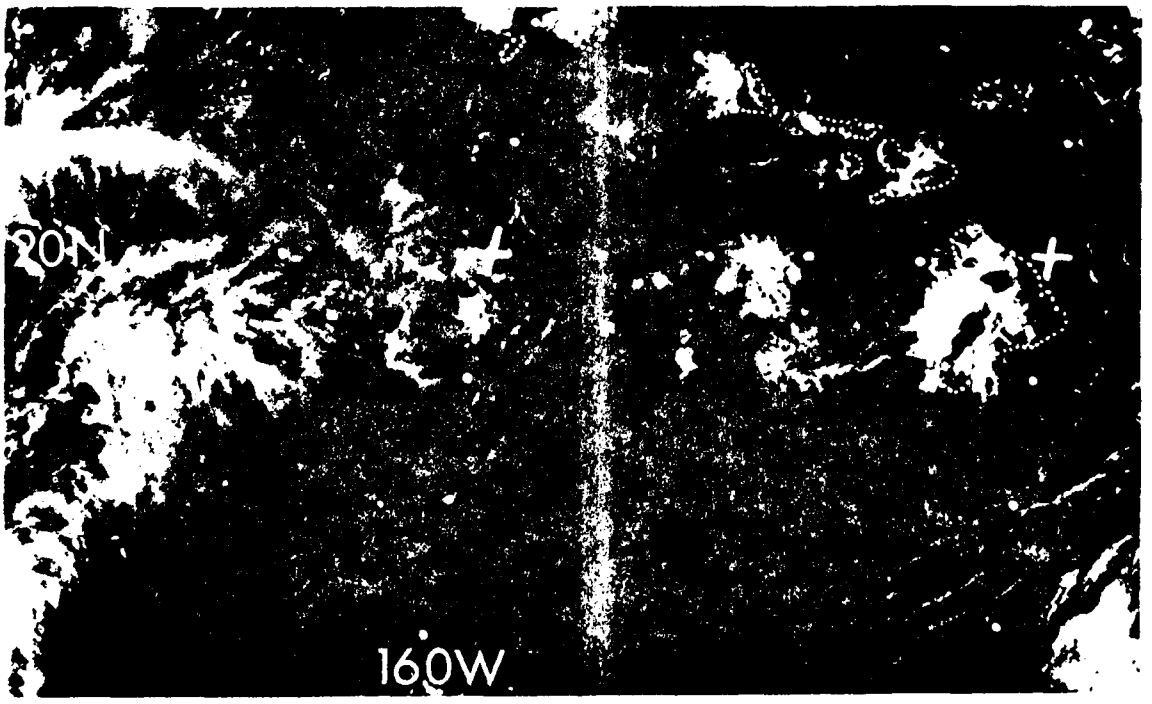

FIGURE 2. 0219 GMT 15 SEPTEMBER 1977, 1-KM RESOLUTION.

Eruptive activity at Kilauea came to a temporary halt on 21 September. A deepening vortex to the northwest of Hawaii drew most of the vog near the islands northwestward into the vortex (Figure 6). The far western edge could now be seen near 171E at 12-15N. The portion of vog crossing the dateline evidently dispersed before reaching the Marshall Islands, as no visibility restriction was noted at Kwajalein or Majuro.

Madame Pele, the ancient Hawaiian volcano goddess, continued her sporadic act, culminating in a massive eruption beginning 25 September. To determine the likely future path of the vog, analysts used radiosondes at Johnston Island and Kwajalein, and tracked movie loop cloud tracers. At this time, a deep trough to the west of Hawaii had eroded the surface ridge, and the normal trade wind regime had given way temporarily to light and generally southerly winds. The vog, emanating from this new burst of activity was watched closely in the WSFO.

On 28 September an air stagnation alert, which is very rarely issued here, was put out for parts of Hawaii Island. The satellite pictures were instrumental in delineating the area to be covered in the alert. They showed the extent of the volcanic plume and its drift toward the ENE where it would not affect the more densely populated areas of that island.

Winds remained light and variable. Two days later the stagnation alert was extended to the entire State for 30 September and 1 October. Accumulating contaminants reinforced by the vog restricted the visibility at Honolulu Airport to less than 7 miles during most of 1 October, lowering to 5 miles for 2 hours at midday. Visibility finally began to improve after sunset, and by the next day increasing winds allowed lifting the alert.

Again, satellite photographs (Figure 7) were used operationally to determine the intensity and areal coverage of the volcanic cloud. They proved essential to the National Weather Service in quantifying for the public both when and where to expect events during this unique "coming of the vog".

256

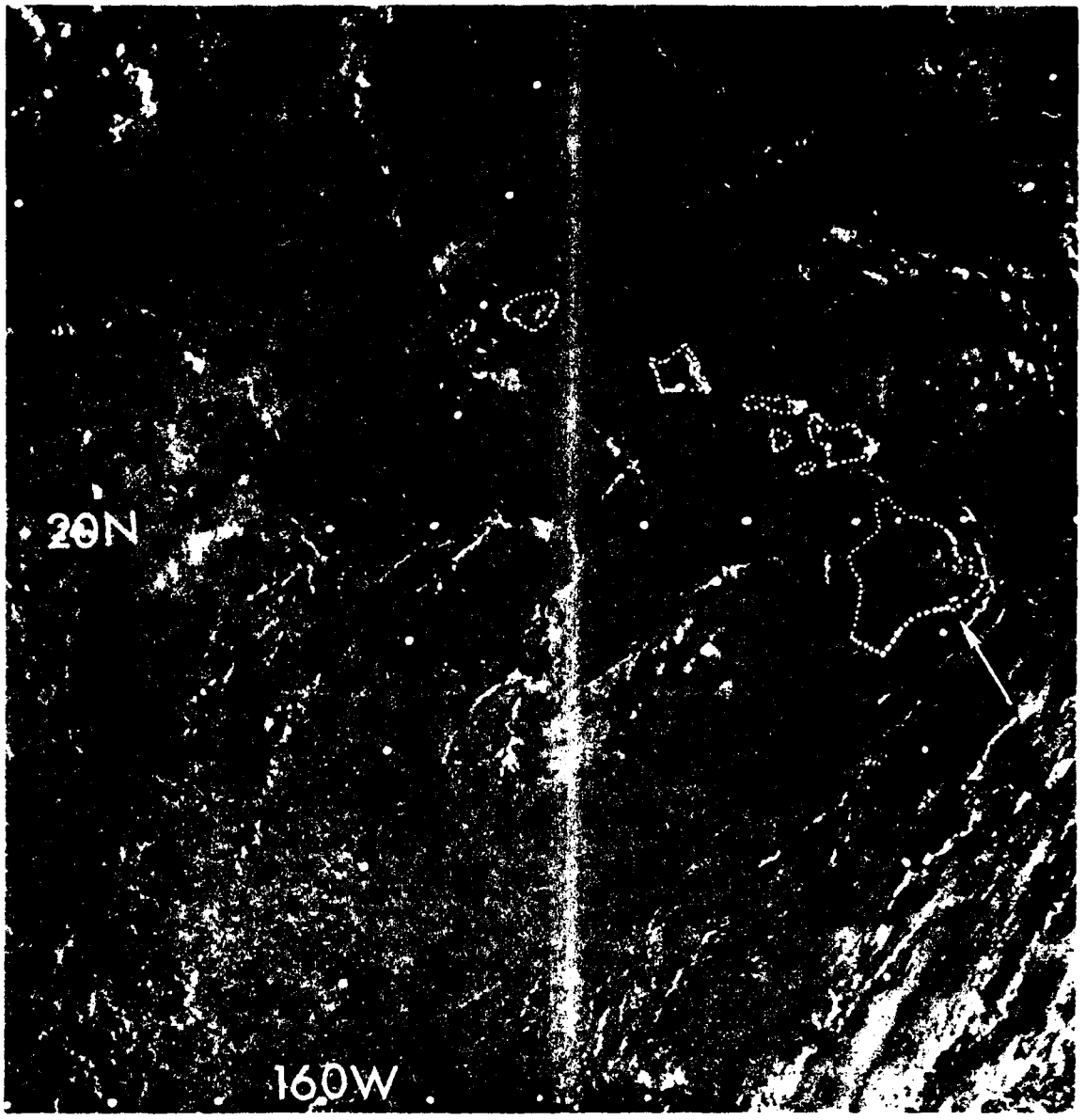

FIGURE 3. 1715 GMT 15 SEPTEMBER 1977, 1-KM RESOLUTION.

257

FIGURE 4. 0249 GMT 16 SEPTEMBER 1977, 1-KM RESOLUTION.

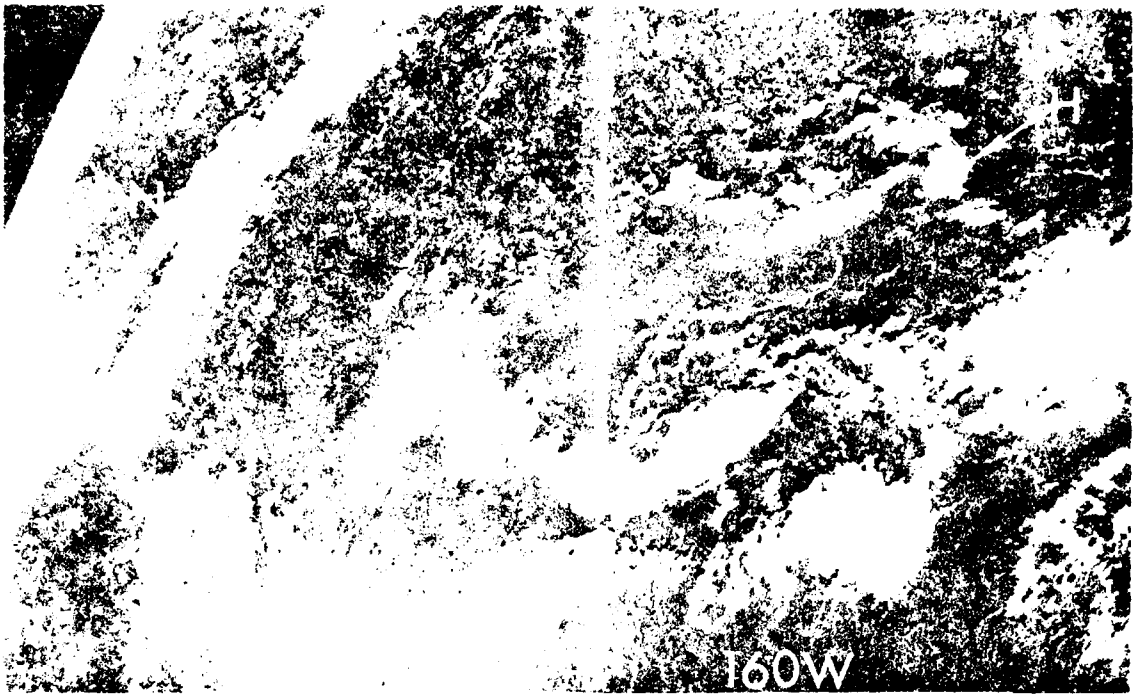

FIGURE [illegible] SEPTEMBER 1977. 4-KM RESOLUTION.

[illegible] SEPTEMBER 1977. [illegible]

[illegible] 0259 GMT 1 OCTOBER 1977, 1 KM RESOLUTION.

U.S. DEPARTMENT OF COMMERCE

National Weather Service/National Environmental Satellite Service
SATELLITE APPLICATIONS INFORMATION NOTE 78/4

THE USE OF ENHANCED VIS IMAGERY FOR FOG DETECTION AND PREDICTION

James J. Gurka
Applications Group, NESS, Washington, D.C.

The purpose of this information note is to illustrate the advantages of digitally enhanced visible imagery for the detection of fog at sunrise and the prediction of its time of dissipation. (In this paper, the term fog refers to fog and/or stratus.)

First of all, fog can be seen earlier on enhanced visible pictures than on conventional imagery. A comparison between an enhanced and an unenhanced visible picture is shown in Figures 1 and 2. Valley fog is shown at points A, B, E, F, G and H, while the western edge of a more extensive area of fog is shown at C and D. The fog is more obvious in the enhanced image even though its resolution is 1-mile, while the resolution of the unenhanced image is half-mile. Terrain features, such as the coastline at M on Figures 1 and 2, are also more obvious on the enhanced visible.

Figures 3 shows the enhancement curve used in Figure 1. The abcissa shows the input from the satellite in terms of brightness values which range from 0 to 255, with 255 being the brightest. The ordinate represents gray shades on a scale of 0 to 255 with 255 being white. The curve is designed so that the fog is contoured in increments of 8 brightness counts with gray shade separation chosen so that each brightness contour can be identified. This allows the analyst to objectively determine the relative brightness of cloud tops within a fog or stratus formation. For example on Figure 4, the dark gray at J is segment number 7 on the enhancement curve; the white at N is segment #6, the light gray at O is segment #5, and the gray shade at P is segment #4.

The contouring, seen at J on Figure 4, makes it possible to identify the brightest spots within a fog area (Figure 5 shows the corresponding unenhanced visible picture). The brightest spots are either the thickest or the densest portions of the fog and are usually the most persistent. As can be seen from the sequence of pictures in Figures 6-8, the brightest spots at J on Figure 4 persisted the longest. (The clouds at Q on Figure 8 are cumulus, which form and grow with time.)

Furthermore, since the fog is contoured, it is possible to objectively determine the relationship between brightness and dissipation time. Figure 9 shows the results from four days' worth of data in western Oregon and Washington state; it is a plot of brightness difference (ΔB) vs dissipation time interval (Δt) for 36 locations in Washington and Oregon on August 30, 31, and September 1, 1976, and August 15, 1977. The brightness difference is defined as the brightness of a point in the fog minus the brightness of the land surrounding the fog (reference brightness). The plot shows a strong positive correlation between "brightness difference" and the fog dissipation time interval. Brightness difference between cloud and land is used since this is more conservative than absolute brightness of the cloud. The absolute brightness can change due to day-to-day variations in the visible sensor and in atmospheric turbidity. On a hazy day, for example, the absolute brightness value of fog is greater than the same condition on a clear day, but the land also appears brighter. The brightness difference would not vary as much as the absolute brightness. The brightness will also change as a function of time of day and season. The brightness differences shown on Figure 9 were computed from visible satellite data taken at 1545 GMT on each day (2 1/4 to 2 1/2 hours after sunrise). Therefore, if the fog dissipated at 1845Z in a particular location, its Δt would be three hours.

For operational use of the relationship between fog brightness and persistence, there are several factors that must be considered:

(1) In order to be meaningful, the fog brightness must be determined at the same time (relative to sunrise) every day. The optimum time is approximately 1.5 hours after sunrise.

(2) The relationship between the brightness and dissipation time will have to be adjusted seasonally because of the difference in solar heating. Perhaps even a monthly adjustment might be necessary.

(3) The amount of solar heating also varies with latitude so that a prediction scheme developed for Washington State will not be valid for southern California. Adjustment of the brightness values as a function of incoming solar radiation should be adequate to compensate for differences in latitude. This type of adjustment was used in reference 1.

(4) Terrain differences must be accounted for. The relationships shown in this paper were established for the relatively flat portions of western Washington and Oregon and might not be valid for valleys bounded with steep slopes. It is probably impossible to develop a simple graphical forecasting technique that would be applicable to the entire western region; however, given the premise that there is a positive correlation between fog brightness and persistence, it should be a simple matter to develop a series of local forecasting schemes using the enhanced visible imagery.

Therefore, enhanced visible imagery offers the user several advantages including:

(1) Fog and other clouds can be seen earlier than on conventional pictures.

(2) The brightest spots within an area of fog, which are generally the most persistent, can be easily identified.

(3) Terrain features and haze boundaries can be seen earlier.

(4) A contoured display, such as the one described in this paper, makes possible a numerical evaluation of brightness difference.

Therefore, objective fog forecasting schemes relating fog brightness differences to dissipation times can be developed.

REFERENCES

Gurka, James J., 1974: "Using Satellite Data for Forecasting Fog and Stratus Dissipation" Preprint Volume, Fifth Conference on Weather Forecasting and Analysis, Amer. Meteor. Soc.

Fig. 2. GOES-1 1-km visible 1230 GMT, 20 Oct 77.

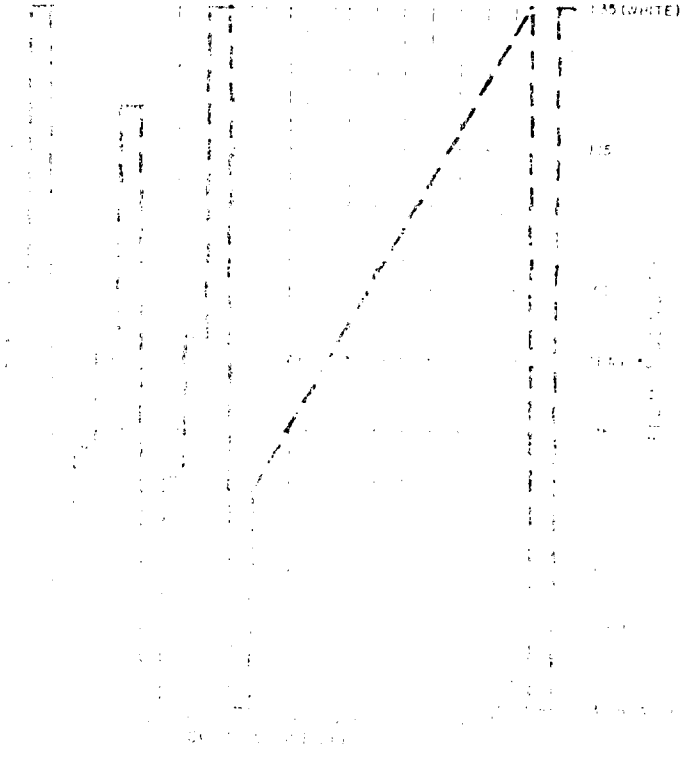

Fig. 4. GOES-1 enhanced 2-km visible 1300 GMT, 20 Oct 77.

Fig. 5. GOES-1 1-km visible 1300 GMT, 20 Oct 77.

Fig. 6. [illegible]

Fig. 7. [illegible]

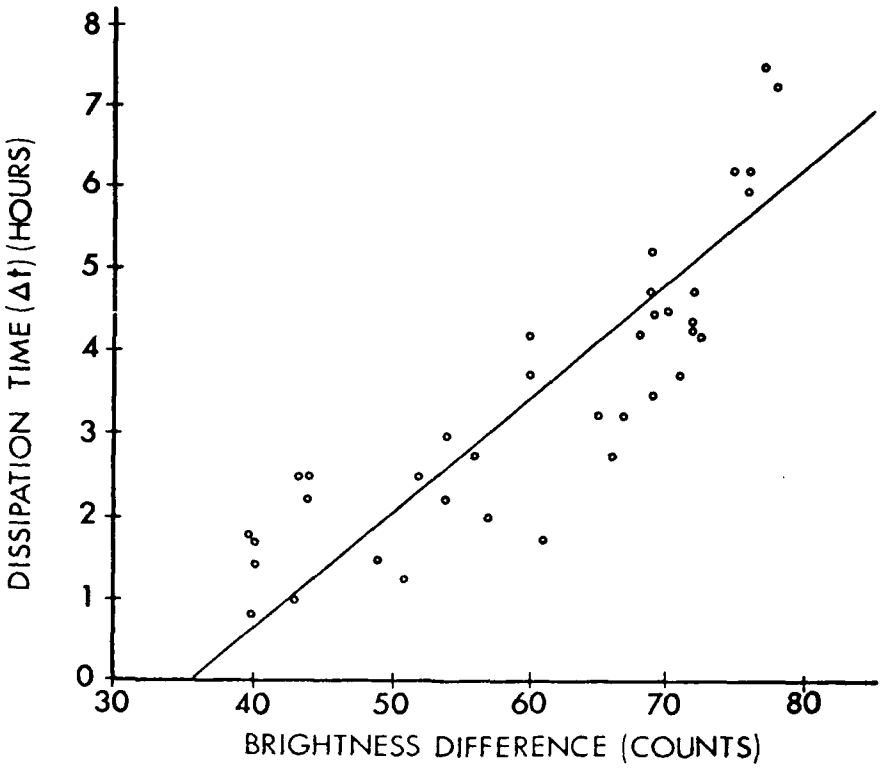

Fig. 9. Brightness difference (counts) versus dissipation time (Δt) in hours.

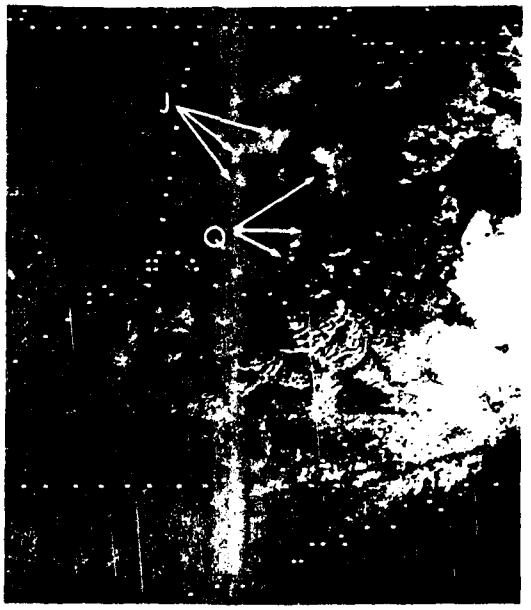

Fig. 8. GOES-1 1-km visible 1630 GMT, 20 Oct 77.

U.S. DEPARTMENT OF COMMERCE

National Weather Service/National Environmental Satellite Service
SATELLITE APPLICATIONS INFORMATION NOTE 78/5

EFFECT OF SNOW COVER ON DISSIPATION OF FOG AND STRATUS

Edward C. Johnston
SFSS, Kansas City, Missouri

During the pre-dawn hours of March 23, 1977, a band of fog and stratus developed behind a weak cold front which had been sagging southward through the Plains during the night. (See 12Z NMC surface analysis, Fig. 1.) At 15Z, this band stretched from western South Dakota to the Nebraska-Kansas Border (O-P, Fig. 3).

Going back to the day before (March 22, Fig. 2), we see that a portion of the ground over which this band later formed was covered with snow (S and T). This small area of snow in southern Nebraska was left from the previous weekend's storm that deposited up to 14 inches in places. This snow area (S) was faintly visible through the fog (Fig. 3) suggesting the fog/stratus layer was quite thin. However, this did not mean it would rapidly disappear, as illustrated in subsequent pictures.

As surface heating progressed at the periphery of the fog/stratus deck on the morning of the 23rd, the familiar pattern of dissipation from the outside edges inward occurred. The resulting pattern is clearly seen in the 17Z picture (Fig. 4). However, very little change in area coverage was noted over the snow cover in southern Nebraska.

Later in the day, as the surface ridge (Fig. 1) shifted eastward, the gradient winds veered around to the east and east-southeast. The air that had become heated over the adjacent bare ground to the east was advected over the snow-covered area. The fog then began to dissipate from the windward side (Fig. 5). The outlined area (F) in Figure 5 represents the fog-covered area at 19Z.

Grand Island (GRI), which had been "socked in" most of the day, finally cleared by 21Z. But a small patch of stratus still remained over the northwestern portion of the snow cover (Fig. 6) and over the bare ground just downstream.

A portion of the original fog/stratus band formed over the eastern fringe of the snow cover (T) in southern South Dakota (Fig. 3). But this area was under the influence of stronger southerly winds to the west of the surface ridge so the snow here was not as much of a factor.

This picture sequence vividly illustrates the effect that snow on the ground can have on the dissipation rate of fog and stratus. Only after surface winds increased and advected warmer outside air into the area did the fog break up. Even then, some persisted well into the afternoon.

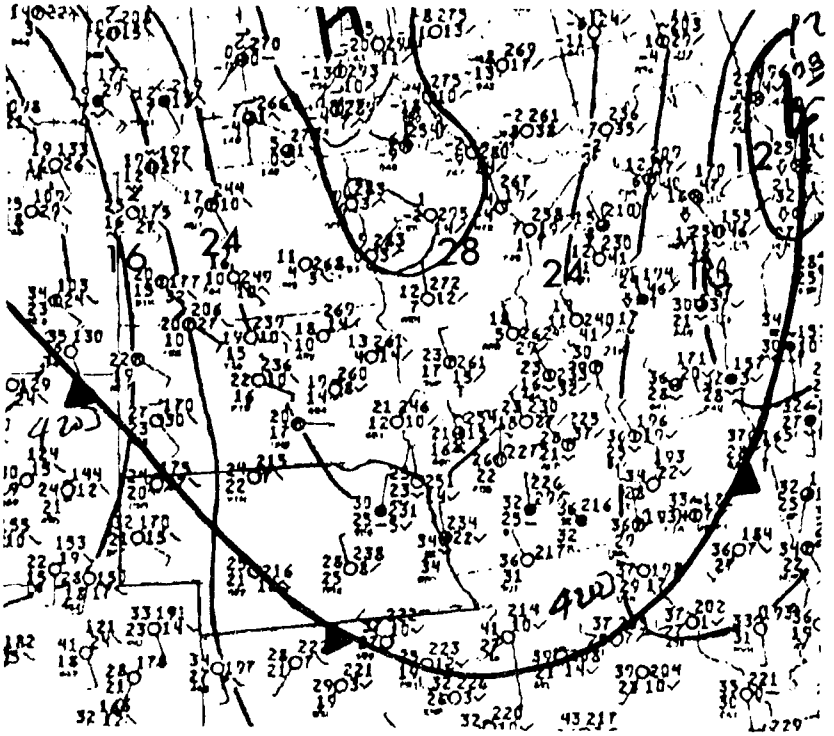

FIG 1 SURFACE ANALYSIS 1200 Z 23 MAR 77

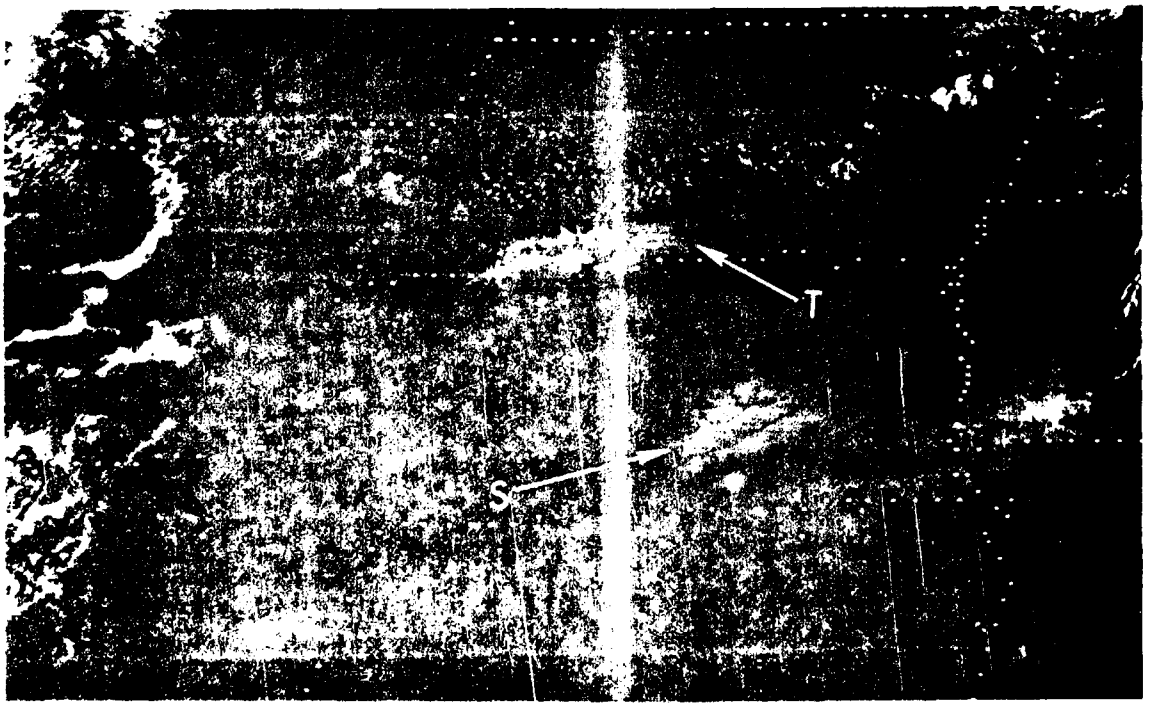

FIG 2 2230 Z 22 MAR 77

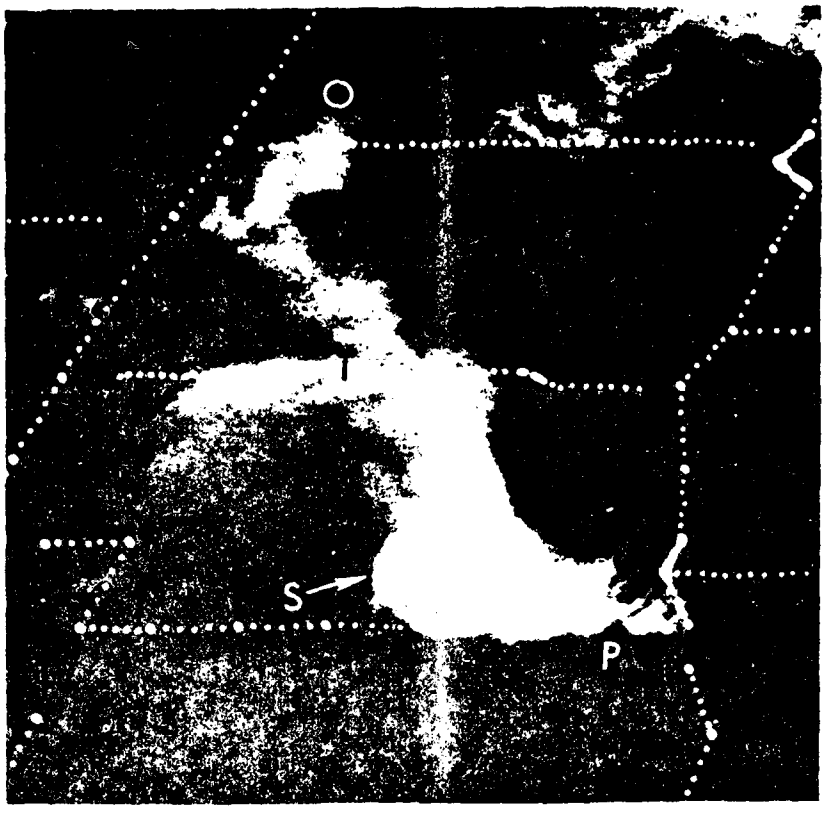

FIG 3 1500 Z 23 MAR 77

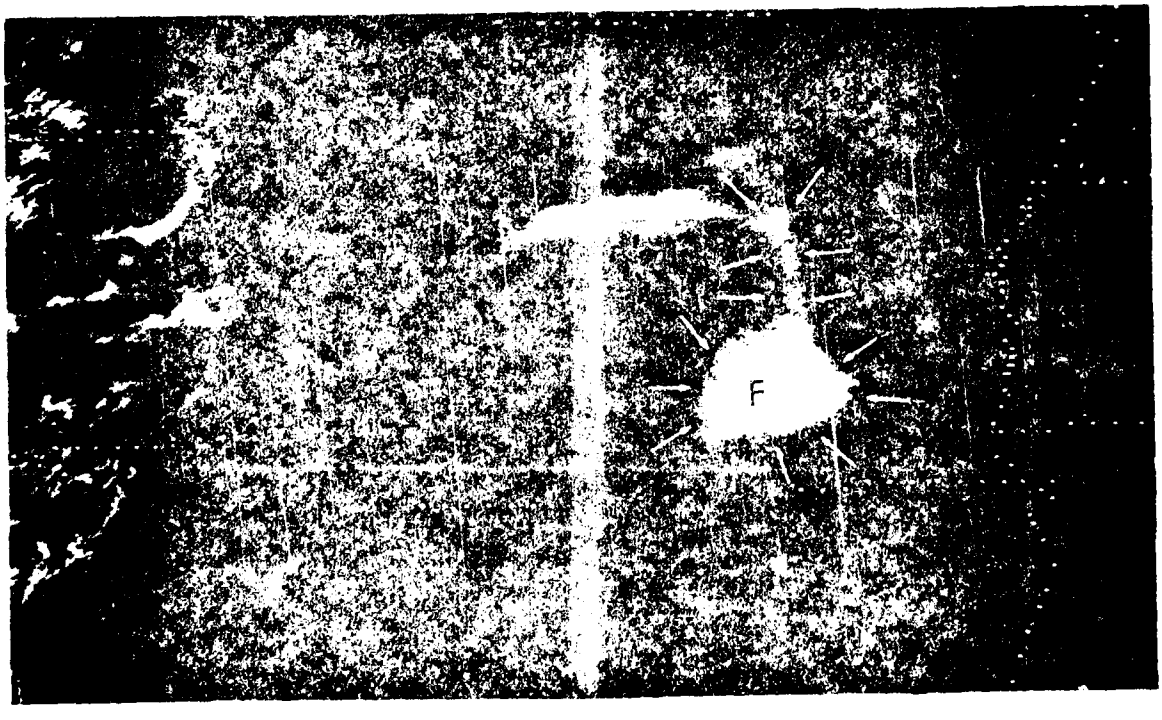

FIG 4 1709 Z 23 MAR 77

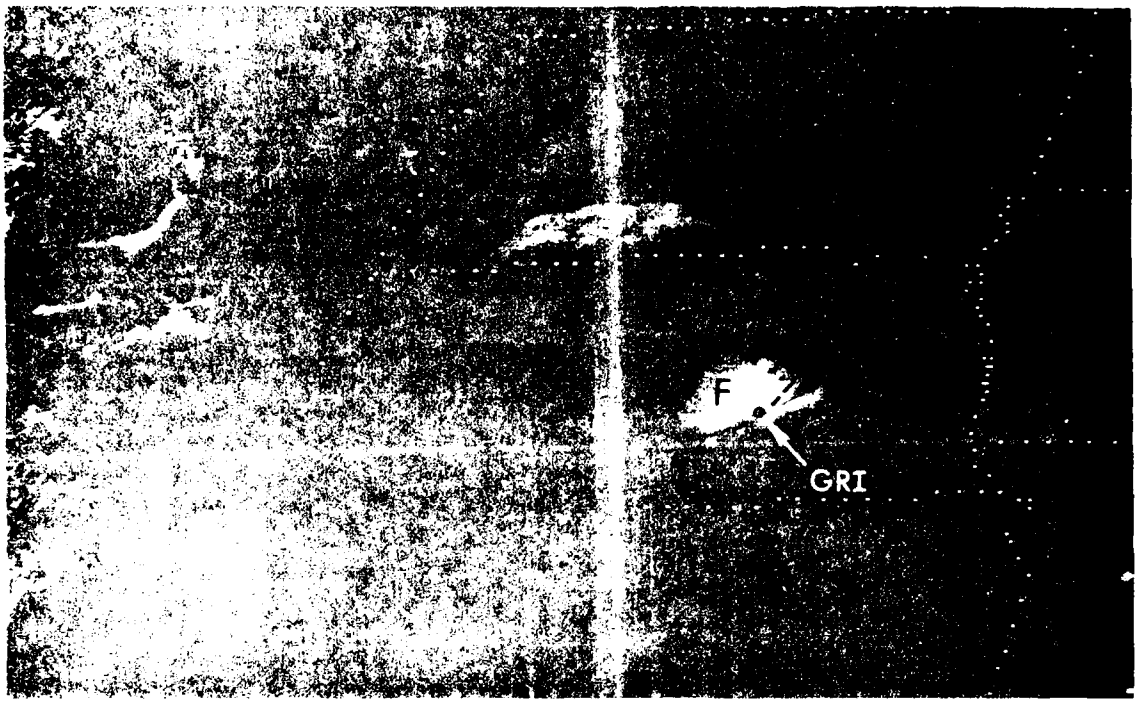

[illegible] MAR 77

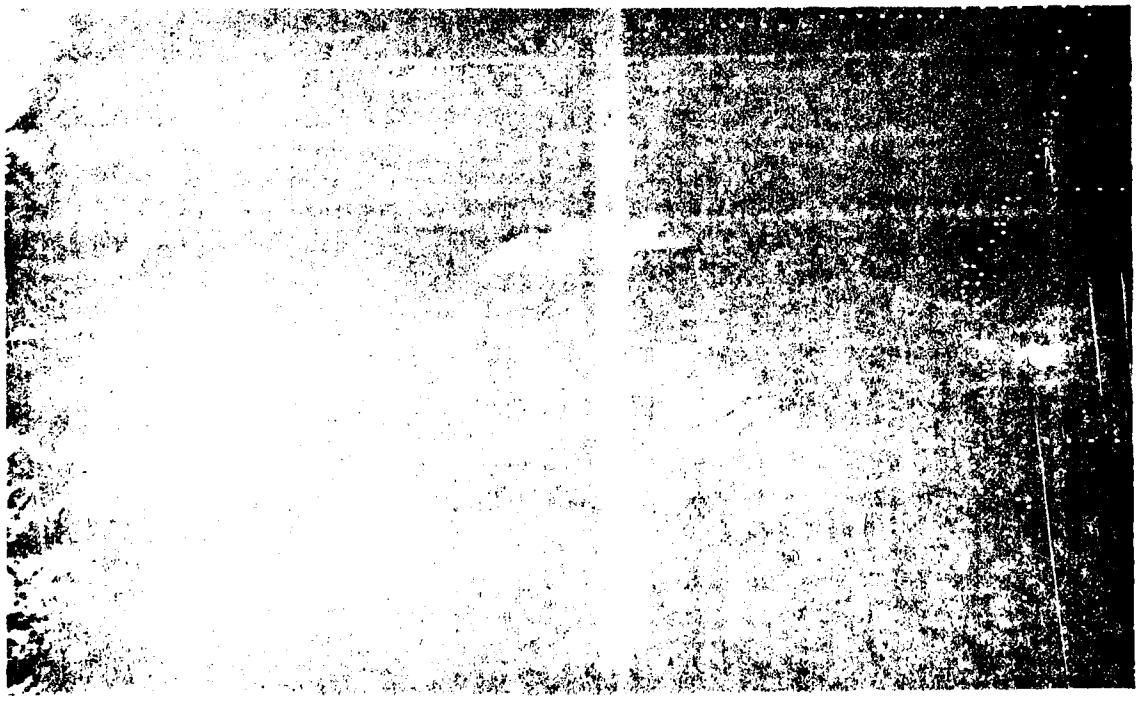

[illegible]

U.S. DEPARTMENT OF COMMERCE

National Weather Service/National Environmental Satellite Service
SATELLITE APPLICATIONS INFORMATION NOTE 78/6

COMPARISON OF SATELLITE CLOUD CIRCULATION CENTERS AND AIRCRAFT RECONNAISSANCE WIND CIRCULATION CENTERS

James B. Lushine
Satellite Field Services Station, Miami, Florida

What appears to be a well-defined cloud circulation center on satellite photos may not be the location of the wind circulation center. This fact has been pointed out by Weldon, 1975, using as an example a solid disc rotating and translating simultaneously. The center of rotation relative to the clouds is different than with respect to the ground in a translating system. For a northern hemisphere cyclone, the actual circulation center relative to the cloud center will be displaced to the left of the direction of motion and at a distance related to the ratio of the speed of translation (V_{Tr}) and the speed of rotation (V_R). A case study of a tropical cyclone in the Atlantic is presented which illustrates this displacement. The consequences of such a displacement on tropical storm positioning, and a method to eliminate the displacement are presented.

A subtropical cyclone formed in the eastern Atlantic in January 1978. The system moved generally westward, passing north of Puerto Rico. The system acquired characteristics of a tropical cyclone. Surface winds estimated from Air Force reconnaissance reached a maximum of 50 knots at a point 45 nmi east-northeast of the circulation center on 21 January 1978. For almost its entire lifetime, the cyclone's center was defined in satellite imagery by lines of cumulus clouds with tops near 2500 meters. The system had a forward speed that ranged from 8 to 15 knots with maximum surface wind speeds ranging from 15 to 50 knots. Three aircraft reconnaissance fixes during daylight hours on 21, 22, and 23 January 1978 gave good comparative data for the satellite location estimates which were made with 2-km resolution visible images from GOES-2. Figures 1, 2, and 3 are the GOES-2 images at 1930 GMT 21 January, 2030 GMT 22 January, and 1230 GMT 23 January with cloud centers as estimated from these single pictures marked by an "O".* Reconnaissance aircraft fixes at 1925 GMT 21 January, 2025 GMT 22 January, and 1230 GMT 23 January are marked on the picture by an "X". At these times, the ratio of V_{Tr} to V_R was 13/50, 10/30, and 10/15, respectively. The distances between the O's and X's are about 20 nmi, 30 nmi, and 40 nmi, respectively, showing that the greater the ratio V_{Tr}/V_R, the greater the distance from O to X. To determine the wind circulation center, it is necessary to know the details of the wind field. This can be accomplished using a satellite movie loop and measuring the cloud displacements to define a wind field. Since the cloud motions are

*A slight adjustment for a gridding error of the satellite pictures has been made.

subject to both V_{Tr} and V_R motion, the wind vectors derived from a movie loop will define the actual circulation center. This center will be at the level of the clouds being measured. If, as in this case, the clouds are at low levels, the wind center defined by the cloud motions will be in the low levels.

Figure 4 is the same satellite view as figure 2, but with a low cloud wind analysis made from a movie loop that covered the time span from 1830-2000 GMT 22 January 1978 superimposed upon it. After adjustment for the difference of 1 hour between the midpoint of the movie loop and the reconnaissance position, the centers derived from the satellite winds and that from the aircraft reconnaissance, X, were essentially coincident.

To illustrate the intensity of the tropical systems with which we might be dealing, the following information should be noted. For a developing tropical system in which a low cloud center is used for positioning, the maximum winds would normally be less than 50 knots. This is based on definitions of cloud features used in the Dvorak technique for estimating maximum winds from satellite pictures (Dvorak, 1975). For a weakening system, where the convective cloud mass is sheared off from the low level clouds, a maximum wind speed of 65 knots might occur. This is due to the time lag between cloud pattern weakening and actual wind speed reduction (Lushine, 1976). For tropical systems in which a low cloud center is not used in positioning, which is often the situation, the relationship between cloud center and wind center becomes more difficult to establish. Fortunately, in terms of tropical cyclone warnings, the greater the maximum winds become the smaller is the difference between cloud and wind center.

The two salient points in this discussion are: (1) when plotting positions from both satellite and reconnaissance, care should be taken in mixing these data, and (2) when possible, a satellite movie loop should be used to define low level centers of circulation.

References

Weldon, R. B. NWS Satellite Training Course Notes, Part 1, NESS April 1975.

Dvorak, V.F. "Tropical Cyclone Intensity Analysis and Forecasting from Satellite Imagery" Monthly Weather Review No. 103 (5-1975, pages 420-430).

Lushine, J.B. "A Relationship Between Weakening of Tropical Cyclone Cloud Pattern and Lessening of Wind Speed" NOAA Technical Memorandum NESS 85, March 1977.

272

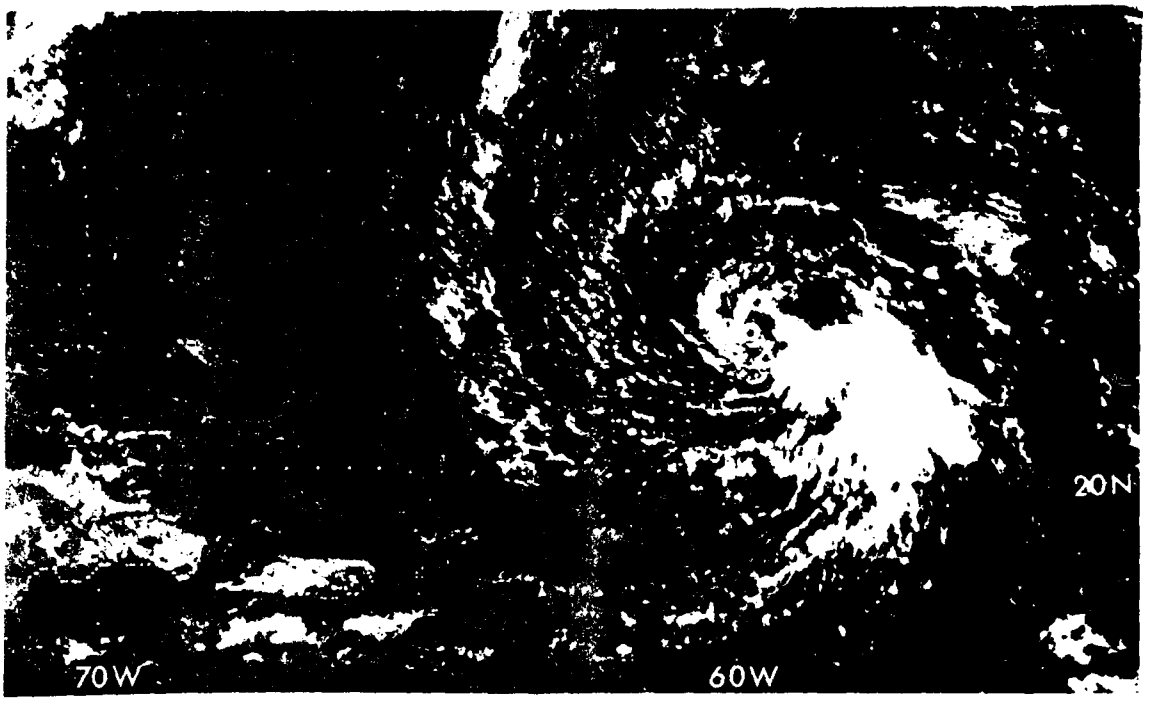

Figure 1. 1930 GMT 21 Jan 1978

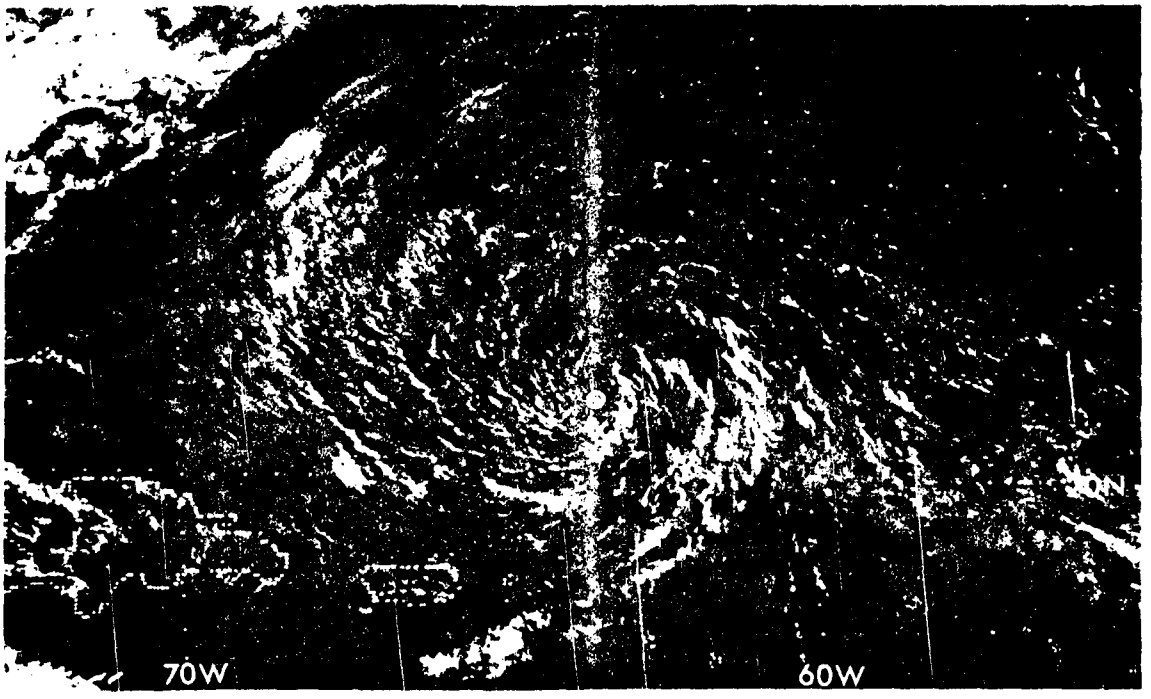

Figure 2. 2030 GMT 22 Jan 1978

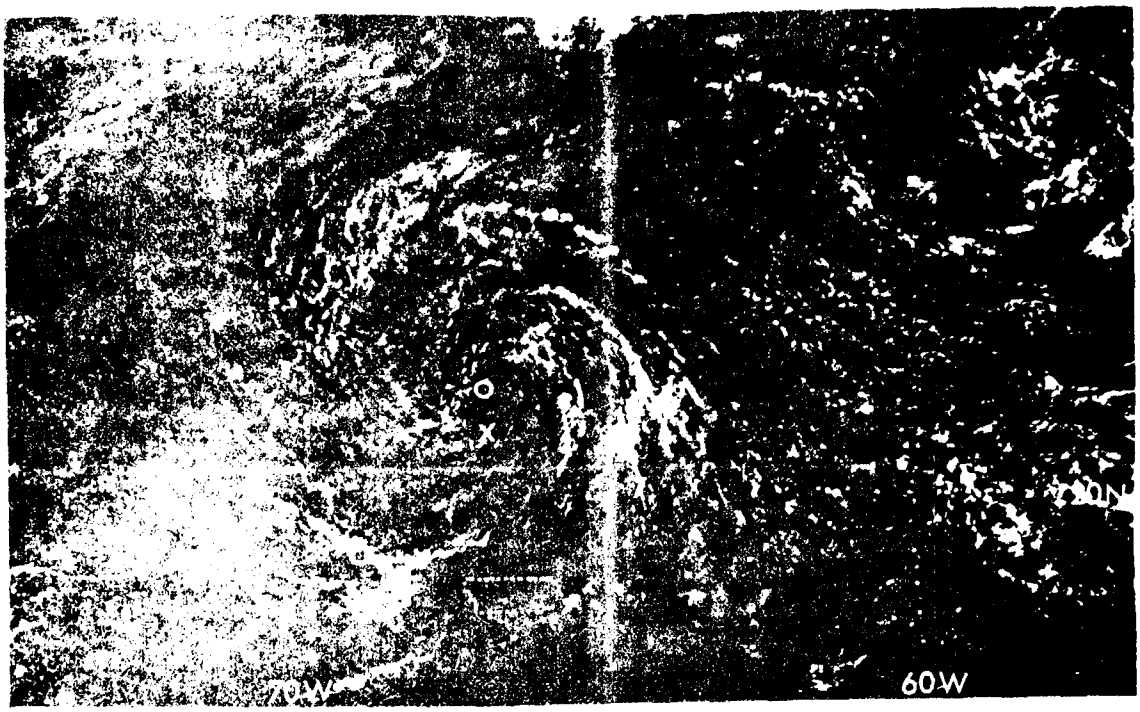

Figure [illegible] 1230 GMT 23 Jan 1978

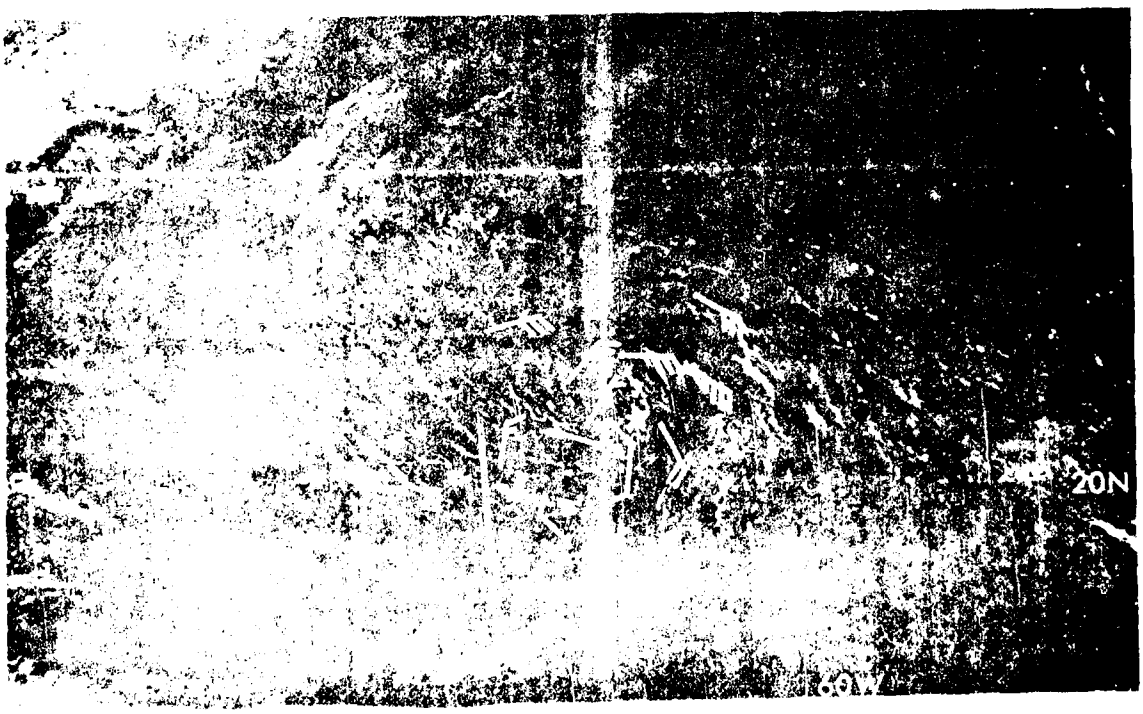

[illegible] GMT 23 Jan 1978

U.S. DEPARTMENT OF COMMERCE

National Weather Service/National Environmental Satellite Service
SATELLITE APPLICATIONS INFORMATION NOTE 78/7

RECORD TEXAS SNOWSTORM

Samuel K. Beckman
NESS, Satellite Field Services Station
Kansas City, MO

The purpose of this note is to show the relationship between a band of heavy (greater than 4 inches) snow that fell across the south central U.S. and the track of the 500 mb vorticity center. This study covers a 36-hour period from 0000 GMT, 17 February, to 1200 GMT, 18 February 1978. The area of heaviest snow will be compared to changes in the comma-shaped cloud pattern, associated with the vorticity center and synoptic scale features, depicted by conventional data.

The snow began to fall during the evening of the 16th in west Texas, accumulating more than 4 inches during the night in northern Texas and southeast Oklahoma. By sunrise, the snow had reached the Dallas-Fort Worth area. Snow continued to fall in southeast Oklahoma and Arkansas on the 17th before ending in northeast Arkansas on the morning of the 18th. A satellite view taken on the 19th (Fig. 1) shows the snow-covered ground surrounding the many lakes from north Texas to northeast Arkansas. In west Texas, clouds obscure the snow field. The area of snowfall totals of greater than 4 inches from this storm is depicted in Figure 2. Amounts exceeded 8 inches in the Lubbock-Plainview area and from Dallas-Fort Worth to near McAlester, Oklahoma. There was significantly less snowfall south of a line from Texarkana (TXK) to 30 nm northwest of Waco (ACT).

The initial analyses for the morning LFM and PE prog packages on February 16 (Fig. 3) show a vorticity center near Page, Arizona (PGA). Both progs indicated a southeast movement of 25 kts across New Mexico into west Texas and then to a position near Lubbock in 24 hours. Next, the progs moved the vorticity center eastward across northern Texas to near Texarkana by the next evening. The evening barotropic package progged the vorticity center eastward to southeast Oklahoma in 24 hours and then accelerated it northeast to the vicinity of Cincinnati, Ohio, in 36 hours. This track was about 60 nm north of that shown by the morning LFM and PE progs.

In Figure 4, a sequence of 2-mile (4 km) satellite images acquired at 6-hour intervals shows the progression of the vorticity center as it moved across the southern U.S. At 0000 GMT on the 17th (Fig. 4a), a well-defined comma cloud was evident over New Mexico with the vorticity center southwest of Albuquerque. The comma cloud moved into west Texas at 0600 GMT (Fig. 4b) with the leading edge of the clouds associated with positive vorticity advection (PVA) along a line from Wichita Falls (SPS) to Fort Stockton (FST). Lubbock reported a 7-inch snowfall between 0000 and 0600 GMT.

By 1200 GMT (Fig. 4c), a band of showers was forming along a cold front (Fig. 5) just east of a line from Dallas (DAL) to San Antonio (SAT). At this time, heavy snow was reported in the Dallas-Fort Worth area. The coldest cloud tops were near the intersection of the polar and low-level jets (Fig. 6) just east of Dallas. The radar summary chart at 1235 GMT (Fig. 7) depicted a broken area of echoes indicating snow with uniform tops to 15,000 feet within the comma cloud over Oklahoma and northern Texas. Snowfall amounts of 4 to 6 1/2 inches were reported in the Dallas-Fort Worth area by 1500 GMT.

At 1800 GMT (Fig. 4d), the comma cloud was becoming distorted with the thickest clouds (coldest tops) over Arkansas, western Louisiana, and extreme east Texas. A line of thunderstorms had developed along the cold front from southeast Texas into the Gulf of Mexico. Snowfall totals during the 6-hour period ending at 1800 GMT were 4 inches at McAlester, Oklahoma, and 6 inches at the Dallas-Fort Worth airport.

At 0000 GMT (Fig. 4e), a small area of enhanced clouds from east Oklahoma to southwest Missouri was located in advance of the vorticity center in southeast Oklahoma. Most of the higher and thicker clouds had moved east of the Mississippi River. Snowfall amounts had diminished to less than 4 inches since 1800 GMT. The area of enhanced clouds associated with the vorticity center continued to decrease during the subsequent 12 hours (Figs. 4f and 4g), and the vorticity center became less discernible in the satellite imagery.

Six hourly positions of the vorticity center as followed in satellite imagery are also shown in Figure 3. This path of the vorticity center was very close to the first 24 hours of the LFM and PE progs while the center was moving southeast. As the vorticity center curved toward the east, the barotropic prog verified best.

The following points can be made about the heavy snow associated with this storm:

1. The area of heavy snow (Fig. 2) was generally within 1.5 degrees of latitude either side of the track of the vorticity center (Fig. 3) and north of the polar jet (Fig. 6). There was no closed circulation at any level. At the surface, a cold front lay in an inverted trough that skirted around a large high centered in the central plains (Fig. 5). According to Goree and Younkin (1966), at upper air data time the most favorable location of heavy snow is 6.5 to 7 degrees of latitude downstream and 2.5 degrees of latitude to the left of the vorticity center. In all their cases, the system had a closed circulation and was deepening or occluding.

2. When the comma associated with the vorticity center was new and compact, the heaviest 6-hour snowfall was in the region of PVA within the tail of the comma. The 7 inches received at Lubbock fell between 0000 GMT and 0600 GMT (Figs. 4, 4a,and 4b). Only 1 additional inch of snow was reported at Lubbock after 0600 GMT when the colder and thicker clouds (Fig. 4b) in the comma tail had moved east of the station. Weinrich (1975) has also noted a strong correlation between the enhanced clouds associated with a vorticity comma and heavy snow.

3. As the comma cloud became less organized and the distance between the comma tail and the vorticity center increased, the snowfall intensity began to decrease (Fig. 4d). During the last 12 hours of the storm's life, the region of heaviest snowfall pulled back closer to the vorticity center in the colder air aloft (Figs. 4e and 4f).

4. Snowfall totals were greater than 8 inches in the Lubbock-Plainview area where low-level easterly winds were being lifted by an erosional escarpment that is usually referred to as the "Cap Rock". The large amount of snow (greater than 8 inches) in the Dallas-Fort Worth area was near the western edge of deeper low-level moisture in the vicinity of the intersection of the polar and low-level jets.

REFERENCES

Goree, P. A. and R. J. Younkin, 1966: Synoptic Climatology of Heavy Snowfall Over the Central and Eastern United States. Mon. Wea. Rev., 94, 663-668.

Weinrich, M. J., 1975: Infrared Satellite Data and Heavy Snow, Central Region Headquarters, Scientific Services Division. GOES Technical Attachment 75-G1.

277

AD-A167 989 SATELLITE APPLICATIONS INFORMATION NOTES OCTOBER 1975 - DECEMBER 1978(U) AIR WEATHER SERVICE SCOTT AFB IL AUG 79 AWS/TN-79/003 4/4

UNCLASSIFIED F/G 4/2 NL

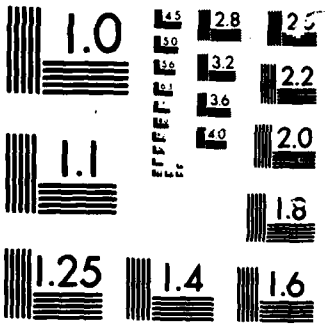

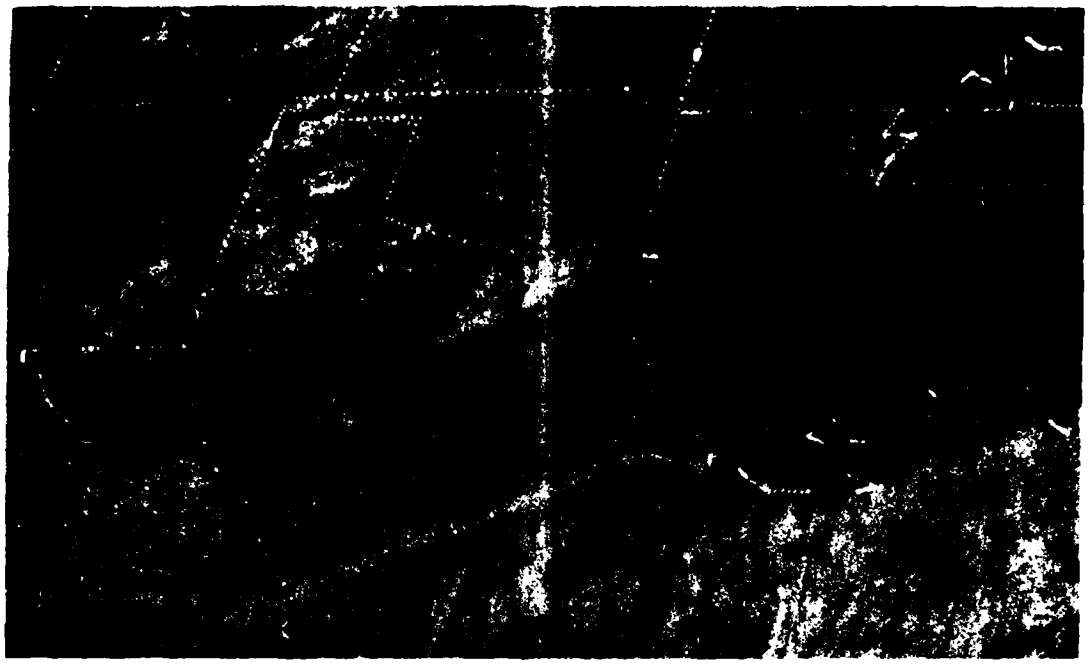

Figure 1. One-mile resolution visible imagery at 1600 GMT on 19 Feb 1978.

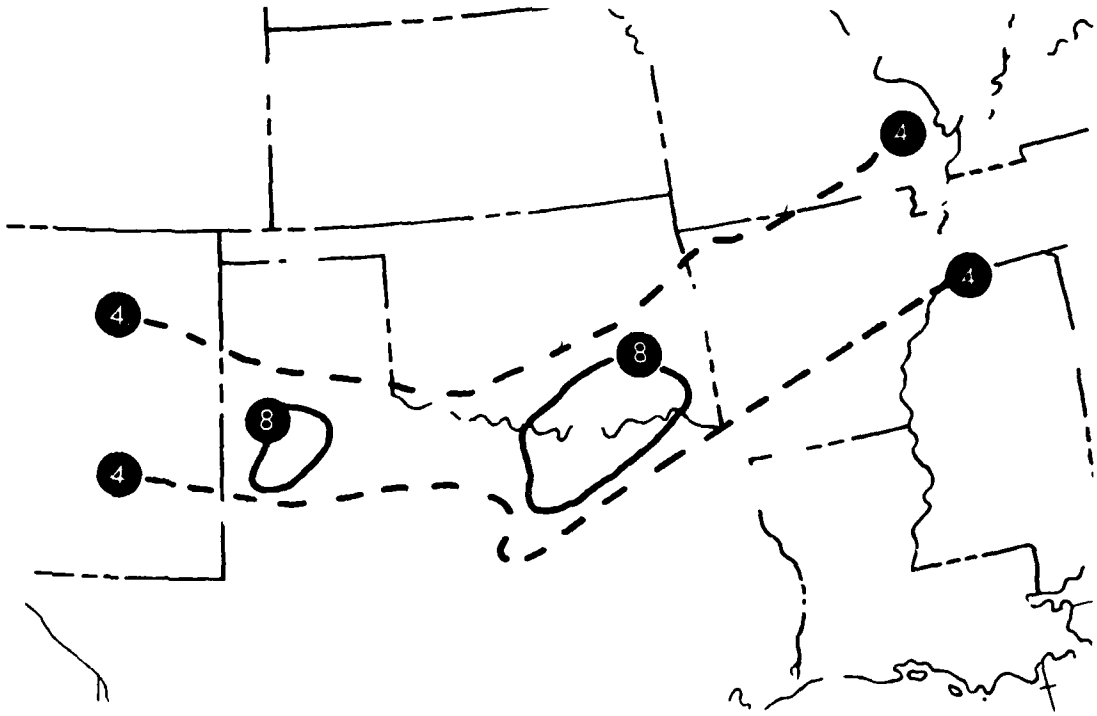

Figure 2. Snowfall totals of amounts greater than 4 inches (dashed lines) and 8 inches (solid lines) during 36-hr period 0000 GMT, 17 Feb to 1200 GMT, 18 Feb.

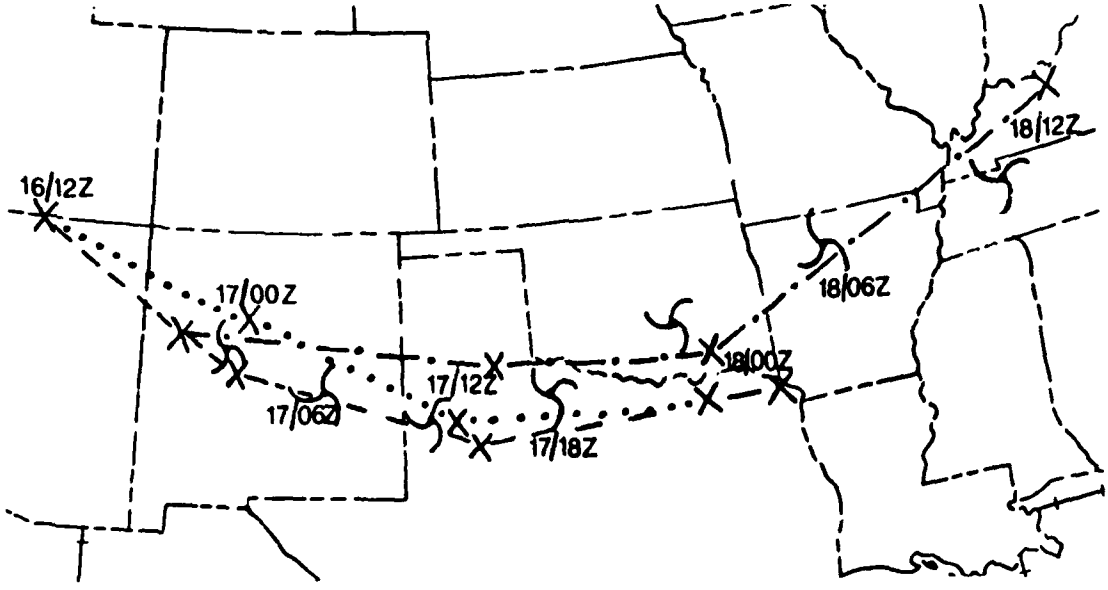

Figure 3. Initial and prog positions of the vorticity center according to the 1200 GMT, 16 Feb PE (dot), and LFM (dash), and the 0000 GMT, 17 Feb Barotropic (dash-dot). The vorticity center indicated by satellite is shown every 6 hours.

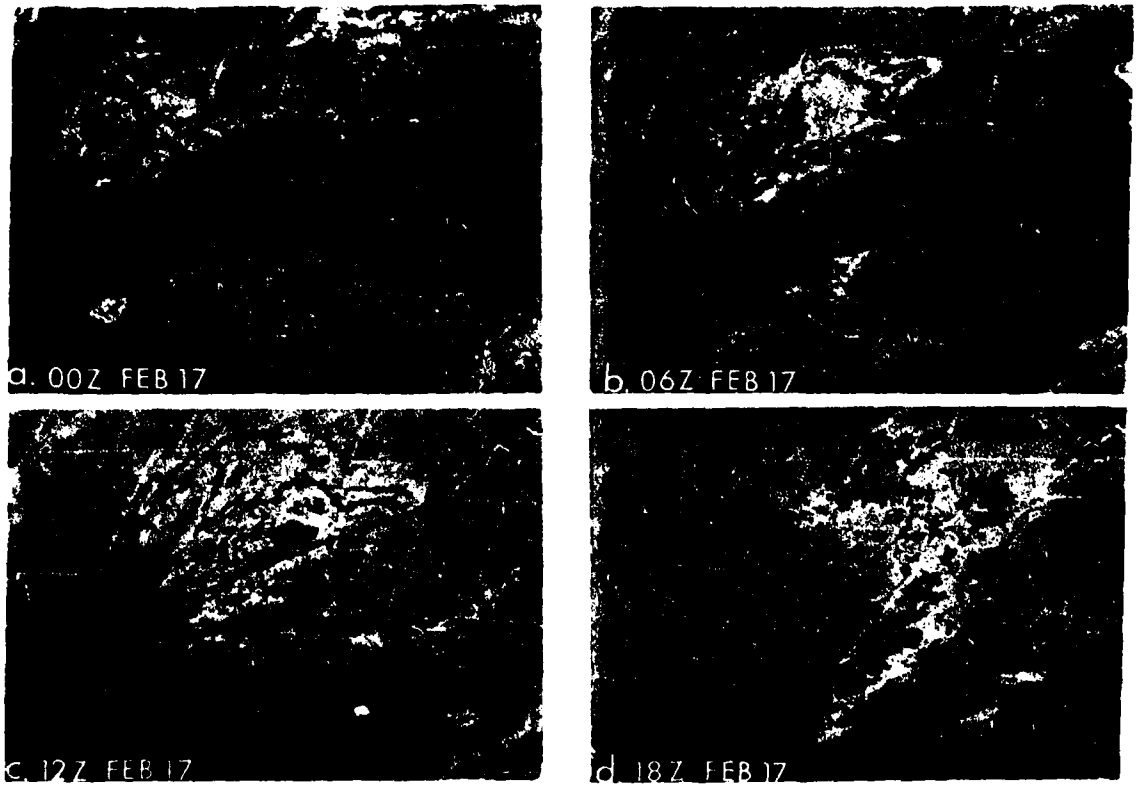

Figure 4. Sequence of 2-mi images acquired at 6-hr intervals from 0000 GMT, 17 Feb to 1200 GMT, 18 Feb 1978.

279

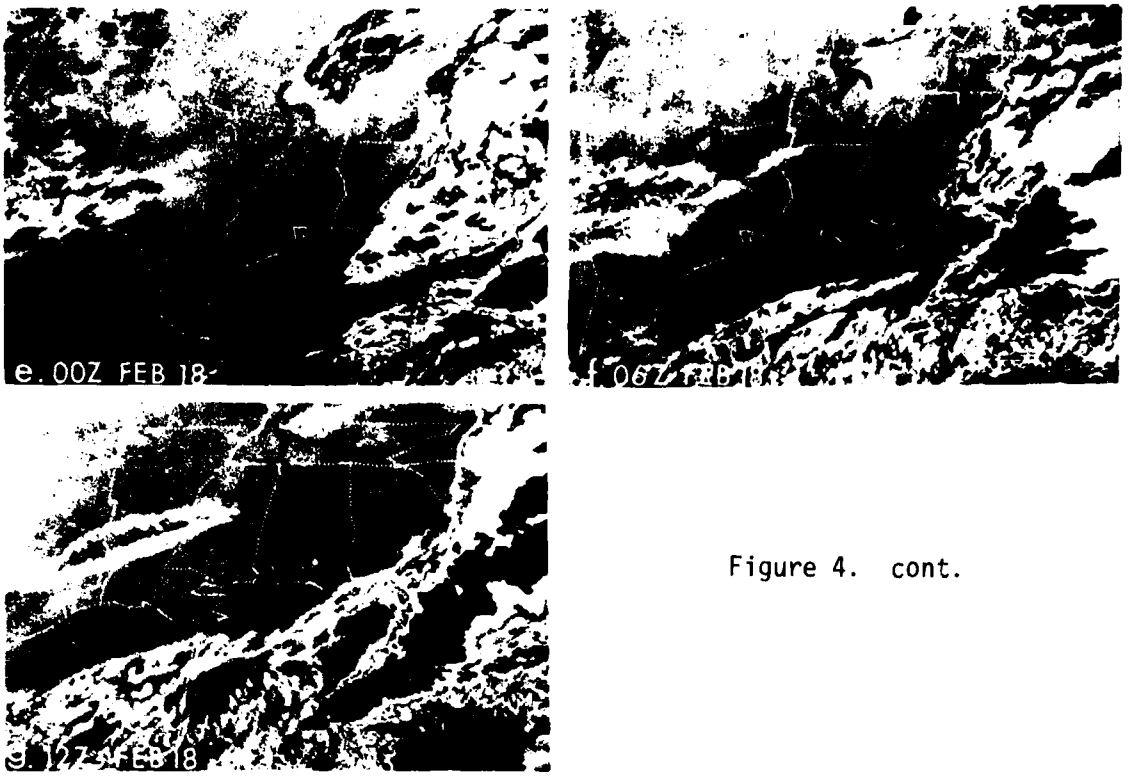

Figure 4. cont.

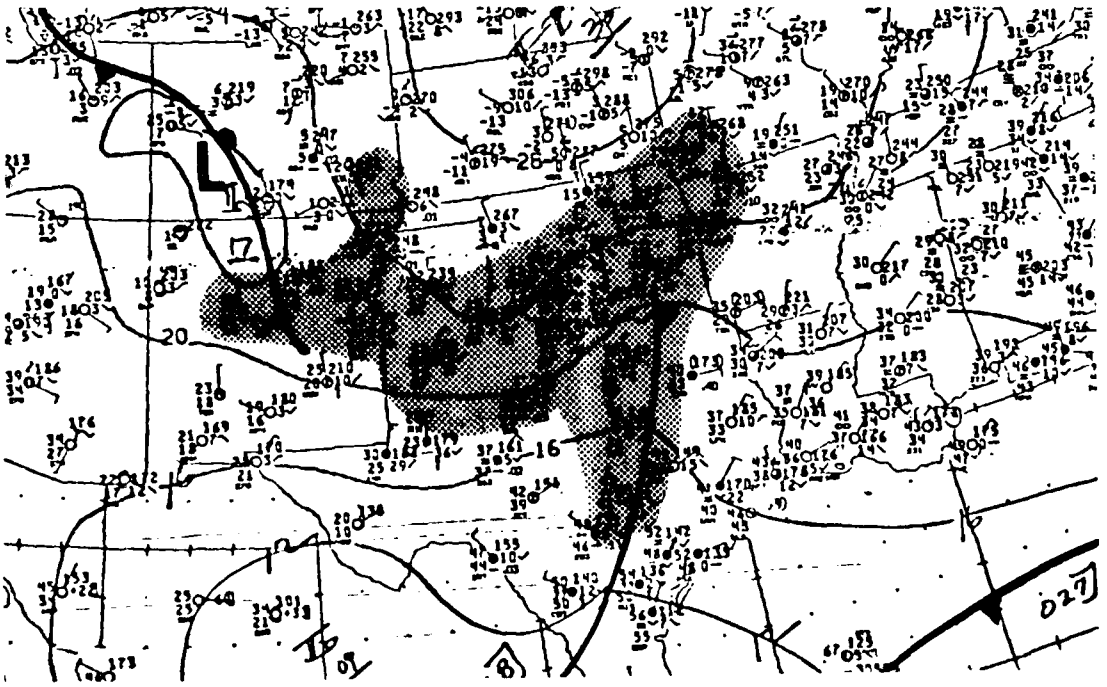

Figure 5. NMC surface analysis at 1200 GMT. Surface precipitation area is shaded.

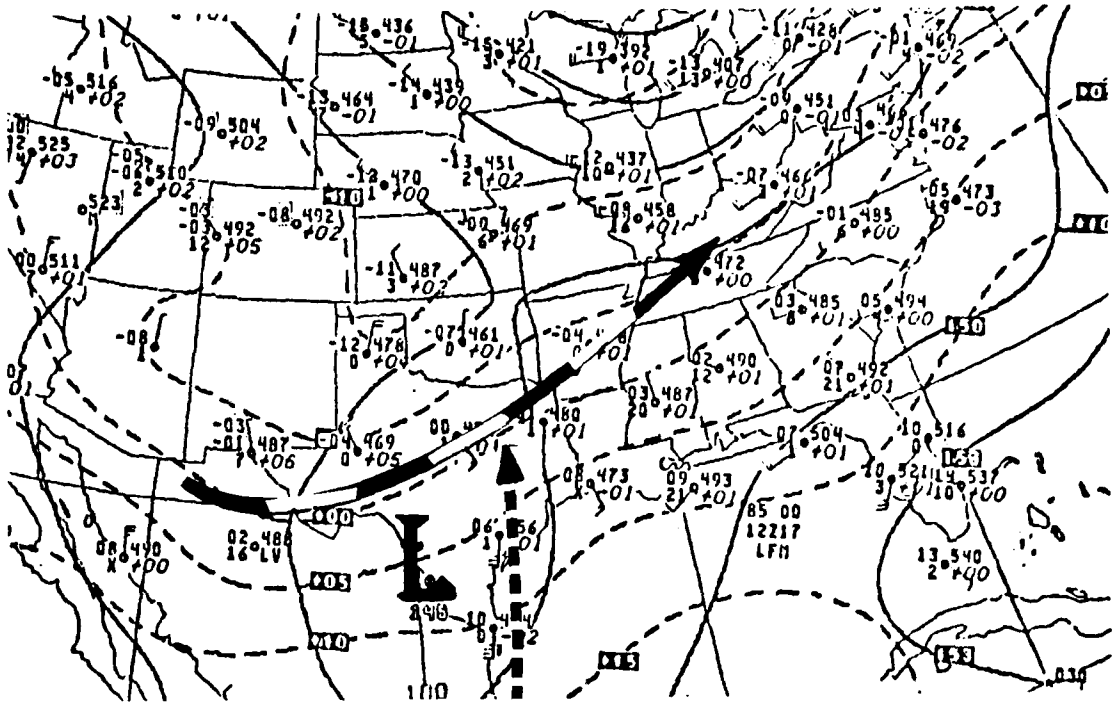

Figure 6. 850 mb analysis at 1200 GMT, Feb 17, with low-level jet (short dashes); polar jet position indicated by long dashes.

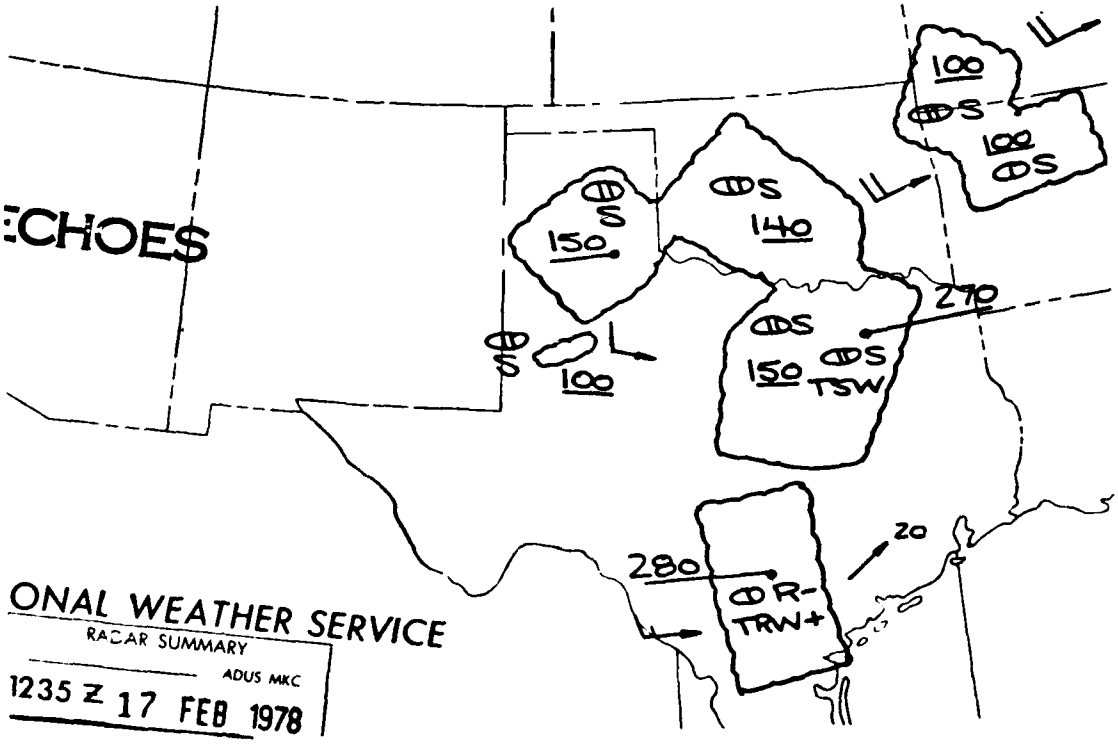

Figure 7. Radar Summary Chart at 1235 GMT.

U.S. DEPARTMENT OF COMMERCE

National Weather Service/National Environmental Satellite Service
SATELLITE APPLICATIONS INFORMATION NOTE 78/8

CLOUD-LOCATION CORRECTIONS NEAR THE HORIZON OF AN SMS IMAGE

Carl E. Weiss
Applications Division, NESS, Washington, D.C.

Cloud interpretation near the horizon of an SMS image is, in part, complicated by the fact that the earth's surface curves rapidly away from the satellite line-of-sight. For a cloud located precisely over the satellite subpoint, the apparent and actual cloud positions coincide, but the difference between the apparent and actual positions increases as the cloud's distance from the subpoint increases.

Figure 1 illustrates this problem. In order to accurately locate a cloud feature on an SMS image, a correction for the effect of the earth's curvature must be made in the direction of the satellite subpoint. Near the horizon, this correction will be large. This SAIN gives cloud location corrections for areas near the edge of the earth's disk.

Several authors have addressed this problem and have calculated cloud location corrections primarily for areas within 50° great circle arc of the satellite subpoint. Pike (1974) developed latitude/longitude component corrections for cloud tops of 40,000 feet over the Atlantic and Caribbean. National Weather Service Central Region Headquarters (1977) calculated location corrections over the U.S. and displayed them as concentric circles of equal correction centered on the satellite subpoint. Corrections were given for cloud tops of 20,000 feet, 40,000 feet, and 60,000 feet.

The cloud-location corrections developed in this note apply to areas of 50° great circle arc and farther from the satellite subpoint. Also, the corrections can be applied to cloud tops of any height. The dimensions used for determining the cloud corrections are shown in Figure 2. Here ϕs is the great circle arc from the satellite subpoint to a cloud's apparent location on an SMS image, h is the cloud height above the earth's surface, $\bar{R}$ is the mean earth radius, $\bar{R}_e$ is the mean equatorial earth radius, $\bar{A}$ is the mean SMS altitude, and d is the location correction[1]. A sample calculation for a cloud top at 10 km and appearing at 60° of arc is given in the appendix.

Cloud-location corrections were computed at 5° great circle arc intervals, starting at 50° of arc and ending at 70° of arc. At each arc interval, corrections were determined for cloud heights of 3 km, 10 km, and 15 km. These corrections are shown in Table 1. We see that for a cloud top at 5 km and appearing at 55°, the cloud position must be corrected by 9.67 km toward the satellite subpoint.

1. This correction represents a distance measured along the curved surface of the earth.

Now, by taking the ratios of the location corrections to the cloud heights (d/h) at a given ϕs, we find that the results are, for practical purposes, the same. The mean d/h ratio values or coefficients at each ϕs can be used to find corrections for clouds of any height. Multiplying the cloud height by the appropriate $\overline{d/h}$ value from Table 2 gives the distance by which the cloud's position must be corrected. Because the ratio values are dimensionless, they can be used with cloud heights given in any units. Remember, these location corrections are always applied radially toward the satellite subpoint.

Mean d/h values were plotted against the appropriate great circle arc (Figure 3). Then ϕs values were interpolated for each 0.5 interval of $\overline{d/h}$ coefficient. Each $\overline{d/h}$ coefficient was drawn on an SMS grid as a concentric circle corresponding to the appropriate great-circle arc (Figure 4). Radial lines converging at the subpoint indicate the direction of the correction.

As an example of using Figure 4, consider a cloud top at 10 km appearing over Anchorage (ANC). This position must be corrected by 30 km to the SSE to find the actual cloud location. Corrections for clouds appearing between circles can be estimated by interpolating the value of the correction coefficient between circles.

The correction coefficients provide a quick and easy method for determining cloud location corrections for cloud tops of any height. Nomograms such as Figure 4 can be drawn for various locations viewed by either SMS to give the user a handy means to accurately locate cloud features.

REFERENCES

NWS Central Regional Technical Attachment No. 77-G4, April 1977, Displacement Error of Satellite Cloud Tops.

Pike, A. C., 1974: A Short Routine for the Adjustment of Geostationary Satellite Cloud Positions Viewed Obliquely. Unpublished Paper, NWSS, Coral Gables, Fla., 8 pp.

283

APPENDIX

A sample cloud displacement calculation for a cloud top at 10 km and appearing at 60° of great circle arc from the SMS subpoint is shown below. Referring to Figure 2, the following information is known:

$\overline{R}$ = 6371 km

$\overline{R}_e$ = 6378 km

ϕs = 60°

$\overline{A}$ = 35,793 km

h = 10 km

For triangle $\gamma\beta\phi s$, we can write

(1) $$\tan 1/2(\beta - \gamma) = \frac{\overline{R} - (\overline{R}_e + \overline{A})}{\overline{R} + (\overline{R}_e + \overline{A})} \tan 1/2(\beta + \gamma).$$

However, substituting the given values into (1), we have

(2) $$\frac{\overline{R} - (\overline{R}_e + \overline{A})}{\overline{R} + (\overline{R}_e + \overline{A})} = -\frac{35800 \text{ km}}{48542 \text{ km}} = -0.737506.$$

Remembering that the sum of the interior angles of any triangle equals 180°, we have for triangle $\gamma\beta\phi s$

(3) $\beta + \gamma + \phi s = 180°$.

Solving for $\beta + \gamma$

(4) $\beta + \gamma = 180° - \phi s$.

Substituting (3) and (4) into (1), we can write

(5) $\tan 1/2(\beta - \gamma) = -0.737506 \tan 1/2(180° - \phi s)$.

We are given that $\phi s = 60°$, so

$$\tan 1/2(\beta - \gamma) = -0.737506 \tan 1/2(180° - 60°)$$

or,

$$\begin{aligned} \tan 1/2(\beta - \gamma) &= -0.737506 \tan 1/2(120°) \\ &= -0.737506 \tan 60° \\ &= (-0.737506)(1.732051) \end{aligned}$$

(6) $\tan 1/2(\beta - \gamma) = -1.277397$.

284

Evaluating (6) gives us

$$1/2(\beta - \gamma) = \text{Arctan } (-1.277397)$$
$$1/2(\beta - \gamma) = -51.944669°,$$

and

(7) $\beta - \gamma = -103.889338°.$

Now, from (4) we have

(8) $\beta + \gamma = 120°,$

and adding (8) to (7) gives

$$\begin{array}{l} \beta - \gamma = -103.889338° \\ \underline{\beta + \gamma = 120°} \\ 2\beta \quad = 16.110662°, \end{array}$$

(9) $\beta = 8.055331°.$

Solving (4) for γ, we have

(10) $\gamma = 180° - (\phi s + \beta).$

Substituting the given values into (10) gives

$$\gamma = 180° - (60° + 8.055331°)$$
$$= 180° - 68.055331°$$

(11) $\gamma = 111.944669°$

The law of sines gives us for triangle $\delta\gamma\eta$, Figure 2,

(12) $$\frac{h + \bar{R}}{\sin \gamma} = \frac{\bar{R}}{\sin \delta}$$

Solving (12) for sin δ, we have

(13) $$\sin \delta = \frac{\bar{R} \sin \delta}{h + \bar{R}}$$

Evaluating (13) gives

$$\sin \delta = \frac{(6371 \text{ km}) \sin(111.944669°)}{10 \text{ km} + 6371 \text{ km}}$$
$$= \frac{(6371 \text{ km})(0.927545)}{6381 \text{ km}}$$

$$\sin \delta = 0.926022,$$

and

(14) $\delta = \text{Arcsin } (0.926022) = 67.833535°.$

285

For triangle $\delta\gamma\eta$, summing the interior angles we have

(15) $\delta + \gamma + \eta = 180°$.

Solving (15) for η and evaluating gives

$$\begin{aligned}\eta &= 180° - (\delta + \gamma) \\ &= 180° - (67.833535° + 111.944669°) \\ &= 180° - 179.778204°\end{aligned}$$

(16) $\eta = 0.221796°$.

Finally, the arc length d is given by

(17) $d = \frac{\pi \bar{R} \eta}{180°}$.

Evaluating (17), we have

(18) $d = \frac{\pi(6371 \text{ km})(0.221796°)}{180°} = 24.662590 \text{ km}$.

Therefore, for a cloud top at 10 km and appearing at 60° of arc from the SMS subpoint, the displacement is 24.66 km toward the subpoint.

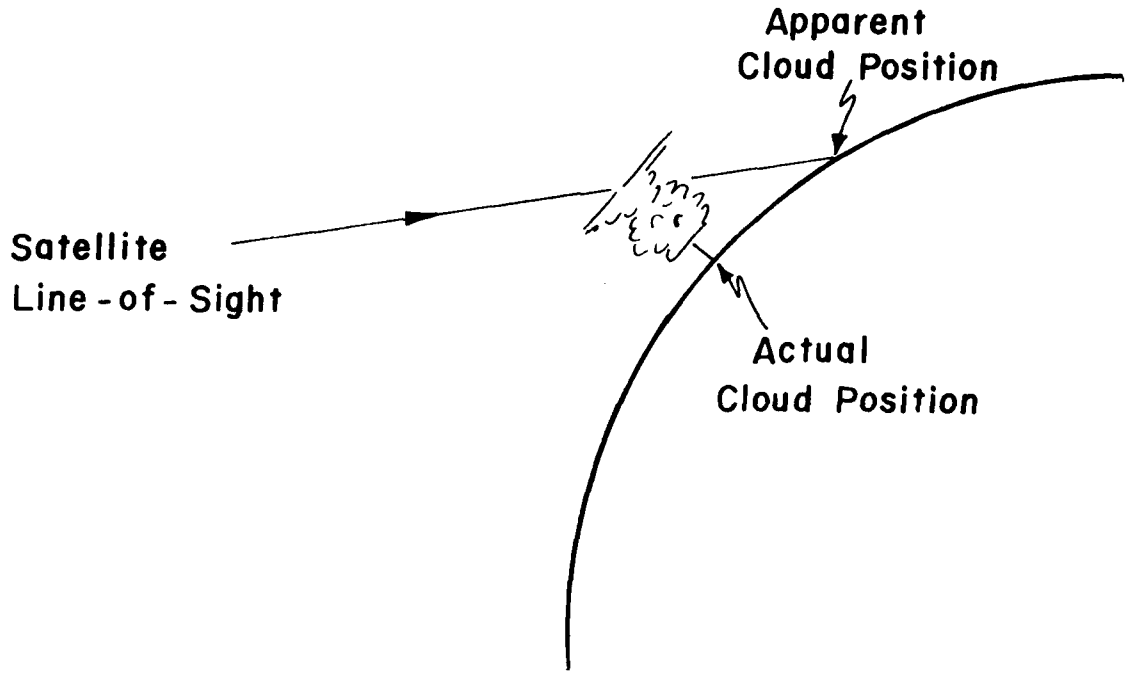

Figure 1. Diagram illustrating an actual vs. an apparent cloud location.

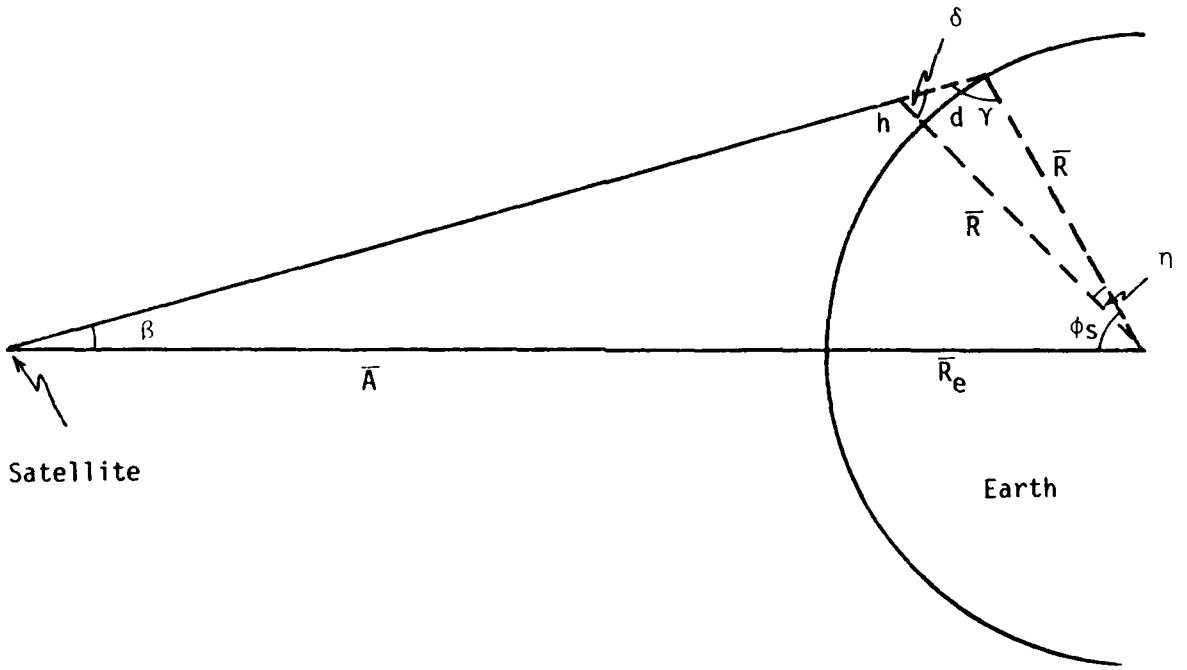

Figure 2. Dimensions used in calculating cloud location corrections.

287

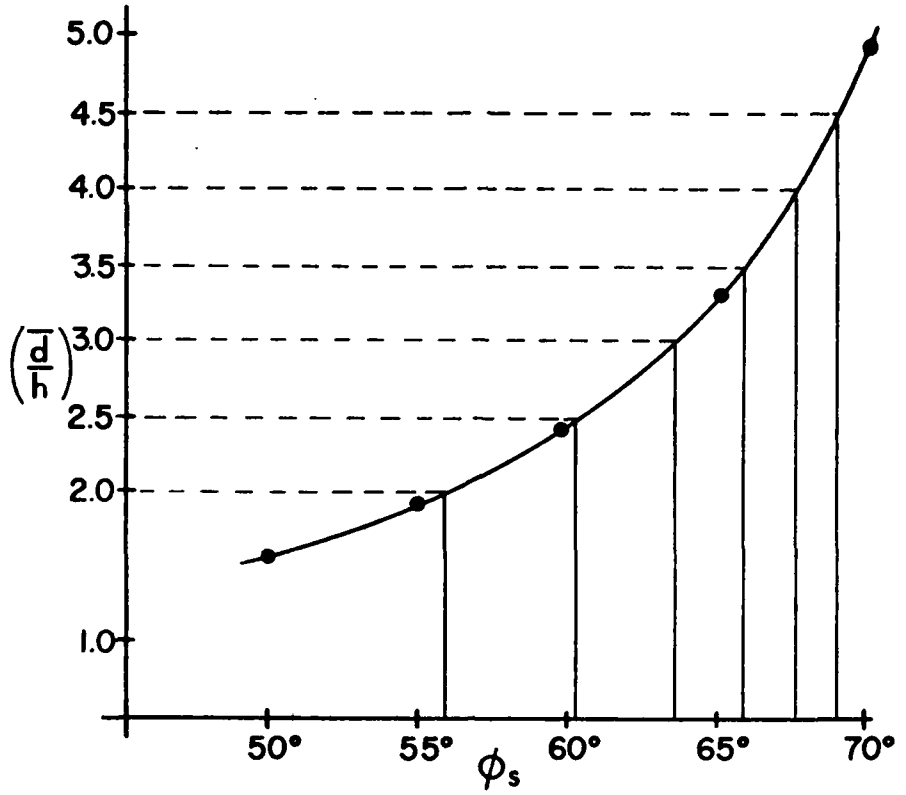

Figure 3. Mean correction coefficients, $(\frac{\bar{d}}{h})$, versus great-circle arcs, ϕs.

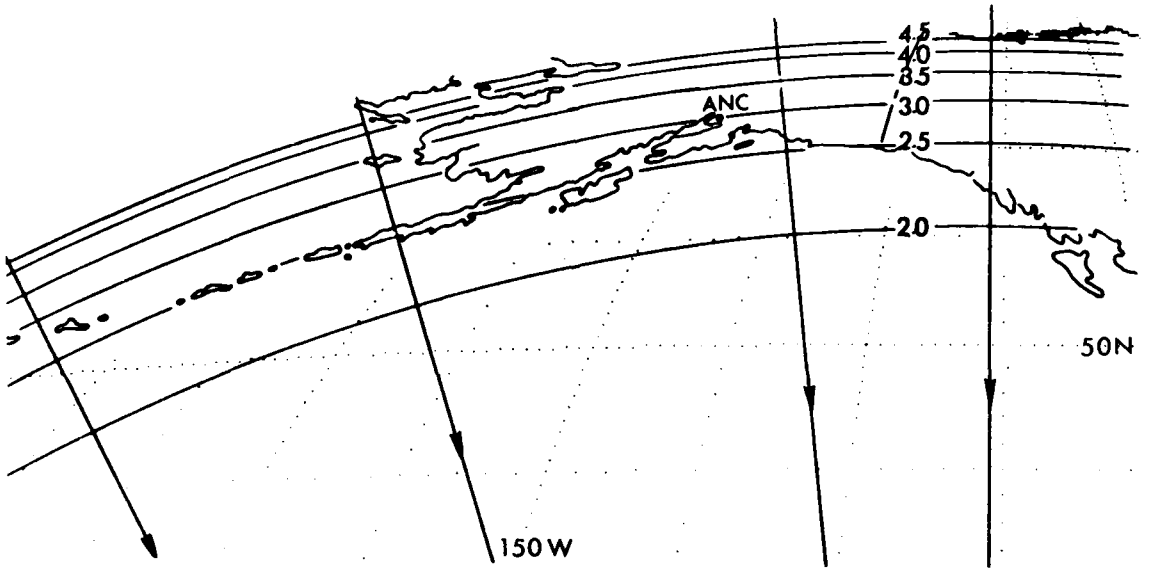

Figure 4. Mean correction coefficients, $(\frac{\bar{d}}{h})$, at 0.5 unit intervals plotted as concentric circles about the SMS-2 subpoint.

h \ φs	50°	55°	60°	65°	70°
3km	4.67	5.81	7.43	9.98	14.67
5km	7.78	9.67	12.37	16.60	24.36
10km	15.53	19.30	24.66	33.04	48.24
15km	23.25	28.89	36.88	49.31	71.66

Table 1. Cloud-location corrections (d) in kilometers for selected cloud heights at given φs values.

h \ φs	50°	55°	60°	65°	70°
3km	1.56	1.94	2.48	3.33	4.89
5km	1.56	1.93	2.47	3.32	4.87
10km	1.55	1.93	2.47	3.30	4.82
15km	1.55	1.93	2.46	3.29	4.78
$(\overline{\frac{d}{h}})$	1.55	1.93	2.47	3.31	4.84

Table 2. Correction coefficients (d/h) of cloud-location for selected cloud heights and average coefficients at given φs values.

U.S. GOVERNMENT PRINTING OFFICE: 1979 O-277-745

289

END

DTIC

6-86